Universidad Autónoma
de Madrid

UNIVERSIDAD AUTÓNOMA DE MADRID

Departamento de Bioquímica

Doctoral Thesis

Identification of new phaeochromocytoma and paraganglioma susceptibility genes

Laura Remacha Medina

Madrid, 2019

Universidad Autónoma
de Madrid

Departamento de Bioquímica
Facultad de Medicina
Universidad Autónoma de Madrid

Identification of new phaeochromocytoma and paraganglioma susceptibility genes

Tesis doctoral presentada por:

Laura Remacha Medina
Graduada en Biología Sanitaria por la Universidad de Alcalá (UAH)
Máster en Biomedicina Molecular por la Universidad Autónoma de Madrid (UAM)

Directores de la Tesis:

Dr. Alberto Cascón Soriano
Investigador del Grupo de Cáncer Endocrino Hereditario (CNIO)

Dra. Mercedes Robledo Batanero
Jefa del Grupo de Cáncer Endocrino Hereditario (CNIO)

Grupo de Cáncer Endocrino Hereditario
Programa de Genética del Cáncer Humano
Centro Nacional de Investigaciones Oncológicas (CNIO)

cnïo *stop cancer*

Dr. Alberto Cascón Soriano, Investigador del Grupo de Cáncer Endocrino Hereditario del Centro Nacional de Investigaciones Oncológicas (CNIO), como Codirector,

Dra. Mercedes Robledo Batanero, Jefa del Grupo de Cáncer Endocrino Hereditario del Centro Nacional de Investigaciones Oncológicas (CNIO), como Profesora Honoraria del Departamento Biología Molecular de la Universidad Autónoma de Madrid, como Codirectora y

Dra. Pilar Santisteban Sanz, Profesora de Investigación del Departamento de Biología del Cáncer del Instituto de Investigaciones Biomédicas "Alberto Sols" CSIC-UAM, como Tutora Académica de la UAM,

CERTIFICAN:

Que **Doña Laura Remacha Medina**, Graduada en Biología Sanitaria por la Universidad de Alcalá ha realizado la presente Tesis Doctoral **"Identification of new phaeochromocytoma and paraganglioma susceptibility genes"** y que a su juicio reúne plenamente todos los requisitos necesarios para optar al **Grado de Doctor**, a cuyos efectos será presentada en la Universidad Autónoma de Madrid, autorizando su presentación ante el Tribunal Calificador.

Y para que así conste se extiende el presente certificado,

Madrid, febrero 2019.

VºBº Codirector:	VºBº Codirectora:	VºBº Tutora:
Dr. Alberto Cascón Soriano	Dra. Mercedes Robledo Batanero	Dra. Pilar Santisteban Sanz

La presente Tesis Doctoral ha sido realizada en el Centro Nacional de Investigaciones Oncológicas (CNIO) de Madrid entre los años 2016 y 2018 bajo la supervisión del Dr. Alberto Cascón Soriano y la Dra. Mercedes Robledo Batanero.

Los siguientes proyectos han permitido la realización de esta Tesis Doctoral:

- Proyecto PI12/00236 de la Federación Española de Enfermedades Raras (FEDER) dirigido por el Dr. Alberto Cascón Soriano. Periodo: 2016-2017.

- Proyecto FP7/2007-2013 de European Network for the Study of Adrenal Tumors (ENS@T)- Seventh Framework Programme dirigido por la Dra. Mercedes Robledo Batanero. 2017.

- Proyecto PI14/00240 de la Federación Española de Enfermedades Raras (FEDER) dirigido por la Dra. Mercedes Robledo Batanero. 2018.

AGRADECIMIENTOS

Pese a haber sido una etapa breve, tengo mucho y muchos a los que agradecer.

Primero, a mis directores de tesis. A Meme, por darme la oportunidad de formar parte de su genial familia del CNIO, un laboratorio que ha sido mi segunda casa durante todo este tiempo. Y a Alberto, por ser el mejor guía que se pueda tener. Por tu positivismo, "Esta te la dan, Laura", por tu paciencia y maestría explicándome las cosas, por tu buen humor, y tu cercanía. Gracias infinitas por haber apostado por mí, haber luchado para que me quedara lo máximo posible y ponerme en bandeja esta tesis que es más tuya que mía.

A mi grupo de Endocrino. A la gente que estaba cuando llegué al laboratorio, la genial doctora Currás a mi izquierda y el crack de María Apellániz a la derecha; la linda y perfecta anfitriona Vero y el huracán Lara, que venía de visita de vez en cuando y que la he visto más en bares que en bata. A Rafa, que aún hoy me sigue escribiendo para ver qué tal voy. Y más especialmente, a la gente que está hoy y que han batallado conmigo en el día a día, ¡os voy a echar mucho de menos! A Roci, por ser el motor físico y psicológico del laboratorio, la "lab manager" que todo jefe querría tener. Gracias por tu sinceridad, las risas y también por las conversaciones serias. A Cris Montero, fuente de sabiduría y zen, siempre has tenido buenas y bonitas palabras para mí. A Cris Rodríguez, por tu simpatía y buen humor. A mis compis de faena: Bruna, mi companya de congresos y viajes al otro lado del mundo, hemos sobrevivido y no nos hemos matado en el intento, todo un logro. Gracias por el cachondeo y buenos ratos de cotilleos. Juanma, gracias por ayudarme siempre que lo he necesitado, por dejarme entero para mí el cajón grande y por ser un estupendo compañero de tesis. María, un remanso de paz y dulzura, siempre cariñosa y sonriente, y una gran curranta experta en paneles. Y a Alfonsi y a Javi, las nuevas incorporaciones, ¡qué vaya todo genial!

A Guille, por ser un manantial de conocimiento, por sus palmeras de chocolate y demás sobredosis de azúcar. Y a toda la gente de "los labos del pasillo", Roci, y las chicas y estudiantes del Cegen, Ana, Oriol, Fati, los chicos de Genética Humana... por compartir conmigo comidas, meriendas, botellones improvisados, muchas risas y como no, también algún que otro primer y protocolo.

A mi familia aluchense de elección. A mis chicas del Arcángel por tantos años de aventuras. A Raúl, por las llamadas de los viernes y por soportarme como nadie. A mi gran amigo en la distancia, Antoine. A miguelestu y pachancla, por darme dolores de cabeza en viajes increíbles. A Albi, por lo que tú y yo sabemos. Y a todos y cada uno del super grupo de WhatsApp "Remi_Lah_Chuli", porque me habéis acompañado en este viaje y algunos sois más importantes de lo que podáis pensar.

A mis hermanas, Mery y Andrea, juntas desde los 3 años e inseparables a los 26. Gracias, por vuestro cariño, apoyo incondicional y sobre todo por las fiestas, las risas y también por algún que otro llanto.

Y a Pablo, por aparecer en el momento preciso y apoyarme (y aguantarme) como nadie en la recta final.

A mis biosans, Andrea, Bárbara, Jelen, Lore y Sergio. Por esos preciosos años de vida universitaria en Alcalá-Mordor y por la amistad que salió de allí. Inmejorables compañeros de profesión y de viajes. ¡Lo que Pani unió que no lo separe la ciencia!

Y para el final el plato fuerte, mi familia. Cristina y Jorge son los mejores ejemplos que yo jamás desearía, espejos en los que ojalá me pueda reflejar dentro de 30 años. Me habéis enseñado los mejores valores de la vida, a ser honrada, generosa, curiosa, ecologista, lectora, menos cabezota y chillona, a luchar por las injusticias y a pelear y trabajar por lo que de verdad importa, y aunque quizá haya muchas otras cosas que por el momento no hayáis conseguido domar en mí, no desistáis, sé que no soy nada fácil. Prometo irme pronto de casa xD. A mi bro, por enseñarme tanto desde enana, por editar con mimo esta tesis, y por supuesto, por traer a mi familia el ser más noble que existe, Sombri. A mis tíos y primos, gatos y cántabros. Y a mis abuelos, por ser el pilar de la familia, por su infinito amor y sus buenas cenas, siempre preguntándome qué tal, preocupándose por mí. ¡Al final, lo he conseguido!

Aluche, 2019

Laura Remacha

RESUMEN/ABSTRACT

RESUMEN

Los feocromocitomas y paragangliomas (PPGLs) son tumores derivados de la cresta neural que se desarrollan a partir de las células cromafines de la médula adrenal (PCC) o de los paraganglios ubicados en la cabeza y cuello, abdomen y tórax (PGL). Aproximadamente un 75% de los PPGLs porta mutaciones mutuamente excluyentes, bien germinales (~40%) o somáticas (~30%), en al menos uno de 17 genes de susceptibilidad. El alto porcentaje de pacientes en el cual se ha identificado mutaciones germinales ha convertido a los PPGLs en los tumores humanos más hereditarios. Sin embargo, aún quedan casos de PPGLs con signos clínicos de heredabilidad, tales como tumores múltiples, edad temprana de aparición o historia familiar de la enfermedad, que no han sido diagnosticados genéticamente.

Por ello, el objetivo primordial de esta tesis fue la identificación de nuevos genes de susceptibilidad a desarrollar PPGL en pacientes sin mutaciones en los principales genes identificados hasta la fecha.

En el primer proyecto, se aplicó un panel de secuenciación exómica dirigida que incluía genes relacionados con el ciclo de los ácidos tricarboxílicos (TCA) a una serie seleccionada de PPGLs hipermetilados. De esta forma, se pudieron identificar mutaciones somáticas en genes de susceptibilidad ya conocidos, como *IDH1* y *SDHC*, así como alteraciones germinales en dos genes nuevos, *GOT2* e *IDH3B*. Este estudio permitió enfatizar la relevancia del ciclo TCA en el desarrollo de PPGL, así como la participación de otras enzimas con funciones de intercambio metabólico entre la mitocondria y el citosol.

Entre los tumores seleccionados en el primer proyecto y sin mutaciones en ninguno de los genes incluidos en el panel, se encontraba el de una paciente joven con múltiples PGLs pero sin historia familiar de la enfermedad. En el segundo proyecto, se llevó a cabo la secuenciación germinal del exoma completo de un trio probando-padres, descubriéndose así una mutación *de novo* activadora en el gen *DNMT3A* (c.896A>T, p.Lys299Ile). La presencia de un fenotipo metilador en diversos tejidos mutados, la identificación de mutaciones somáticas subclonales en seis PGLs adicionales y el descubrimiento de una segunda mutación germinal (c.952C>T, p.Arg318Trp) en una paciente con historia familiar de PPGL, respaldaron el rol patogénico de las alteraciones en *DNMT3A*.

Finalmente, tras ampliar la serie de pacientes analizados con el panel de genes relacionados con el ciclo TCA, identificamos cinco variantes germinales diferentes en el gen *DLST* en siete pacientes no relacionados con PPGL. Se pudo demostrar que una mutación heterocigota recurrente en *DLST* (c.1121G>A, p.Gly374Glu), hallada en cuatro pacientes diferentes, confería susceptibilidad a desarrollar PPGL múltiple. La ausencia de proteína DLST salvaje tanto en tumores como en células DLST-KO interrumpía la actividad del complejo OGDH, desencadenando la acumulación de metabolitos y un perfil homogéneo tanto de expresión como de metilación en los tumores con mutación en *DLST*.

ABSTRACT

Phaeochromocytomas and paragangliomas (PPGLs) are neural crest-derived tumours that arise from the chromaffin cells of the adrenal medulla (PCC) or from the paraganglia of the head and neck, abdominal or thoracic regions (PGL). Approximately 75% of PPGLs carry mutually exclusive germline (~40%) or somatic (~30%) mutations affecting one of at least 17 major susceptibility genes. The high percentage of patients for which germline mutations have been found has turned PPGLs into the most heritable of all human tumours. However, there are still PPGL cases with clinical signs of heritability, such as multiple tumours, early age at onset or family history of the disease, that are genetically undiagnosed.

Therefore, the principal aim of this thesis was the identification of new PPGL susceptibility genes in patients without mutations in any of the main driver genes identified so far.

In the first project, a targeted exome sequencing panel of tricarboxylic acid (TCA) cycle-related genes was applied to a selected series of hypermethylated PPGLs. In this way, it was possible to identify somatic mutations in already known PPGL susceptibility genes such as *IDH1* and *SDHC*, as well as germline alterations in two new genes, *GOT2* and *IDH3B*. This study further highlighted both the relevance of the TCA cycle in PPGL development, as well as the involvement of other metabolic enzymes with a role in metabolite exchange between the mitochondria and the cytosol.

Among the tumours selected in the first project without mutations in any of the genes included in the panel, there was one from a young patient with multiple PGLs but without family history of the disease. In the second project, whole-exome germline sequencing was applied to a parents-proband trio, uncovering a *de novo* germline gain-of-function mutation in the *DNMT3A* gene (c.896A>T, p.Lys299Ile). The presence of a methylator phenotype in several mutated tissues, the identification of subclonal somatic mutations in six additional PGLs and the finding of a second *DNMT3A* germline mutation (c.952C>T, p.Arg318Trp) in a patient with family history of PPGL, further supported the pathogenic role of alterations in this gene.

Finally, upon extension of the series of patients analysed with the TCA cycle-related genes panel, we identified five different germline *DLST* variants in seven unrelated PPGL patients. We demonstrated that a recurrent heterozygous *DLST* mutation (c.1121G>A, p.Gly374Glu) found in four different patients, conferred susceptibility to develop multiple PPGL. The absence of wild-type DLST both in tumours (by germline mutation and loss of heterozygosity due to uniparental disomy) and in DLST-KO cells, disrupted the activity of the OGDH complex, triggering the accumulation of metabolites and leading to a homogeneous expression and methylation profile in *DLST*-mutated tumours.

TABLE OF CONTENTS

ABBREVIATIONS

^{123}I-MIBG: iodine-123-metaiodobenzylguanidine

2HG: 2-hydrohyglutarate

αKG: α-ketoglutarate; also known as **2OG:** 2-oxoglutarate

A-PGL: abdominal paraganglioma

AML: acute myeloid leukaemia

ATRX: alpha thalassemia/mental retardation syndrome X-linked

ccRCC: clear cell renal cell carcinoma

CIMP: CpG island methylator phenotype

CSDE1: cold shock domain containing E1

CT: computed tomography

DNMT3A: DNA methyltransferase 3 alpha

DLD: dihydrolipoamide dehydrogenase

DLST: dihydrolipoamide S-succinyltransferase

DOPA: dihydroxyphenylalanine

EPAS1: endothelial PAS domain-containing protein 1

FH: fumarate hydratase

GIST: gastrointestinal stromal tumours

GOT2: glutamic-oxaloacetic transaminase 2

H3F3A: H3 histone family member 3A

HIF: hypoxia inducible factor

HN-PGL: head and neck paraganglioma

HR: homologous recombination

HRAS: Harvey rat sarcoma viral oncogene homolog

IDH1: isocitrate dehydrogenase 1

IHC: immunohistochemistry

JMJ: jumonji

KIF1B: kinesin family member 1B

LOH: loss of heterozygosity

M-PPGL: metastatic PPGL

MAX: MYC-associated factor X

MAML3: mastermind like transcriptional coactivator 3

MDH1/2: malate dehydrogenase 1/2

MEN2: multiple endocrine neoplasia type 2

NF1: neurofibromatosis type 1

NGS: next generation sequencing

OGDH: OG or αKG dehydrogenase

PCC: phaeochromocytoma

PET: positron emission tomography

PGL: paraganglioma

PHD: prolyl hydroxylase domain

PPGL: phaeochromocytoma and paraganglioma

RBP1: retinol binding protein 1

RET: re-arranged during transfection

SDH: succinate dehydrogenase

SLC25A11: solute carrier family 25 member 11

SPECT: single-photon emission computed tomography

SSTR: somatostatin receptors

TCA: tricarboxylic acid

TMEM127: transmembrane protein 127

UPD: uniparental disomy

VHL: von Hippel-Lindau

VUS: variant of unknown significance

WES: whole-exome sequencing

INTRODUCTION

1. GENERAL FEATURES OF PHAEOCHROMOCYTOMA AND PARAGANGLIOMA

1.1. DISEASE DEFINITION

Phaeochromocytomas (PCCs) and paragangliomas (PGLs), together known as PPGLs, are neuroendocrine tumours derived from chromaffin cells of the adrenal medulla and from neural crest progenitors of extra-adrenal paraganglia, respectively. Sympathetic PPGLs, including PCCs and thoracic and abdominal (A-PGL) PGLs, are predominantly catecholamine-producing tumours. Whereas masses derived from parasympathetic paraganglia, mainly located in the head and neck region (HN-PGL) and less frequently in the thorax, are principally non-secreting tumours[1–3].

1.2. EPIDEMIOLOGY

PPGL is considered a rare disease with an incidence between 2-8 patients per million per year (1000-2000 new cases diagnosed every year) in the US[3], from which 10-20% occur in paediatric cases[4]. However, it remains a fact that up to 25% of PPGLs are discovered as incidentalomas[5] and diagnosis may be even missed during life; finding undiagnosed tumours in 0.05–0.1% of patients post-mortem[6]. The prevalence of PPGL in hypertensive patients varies between 0.2 and 0.6%[7]. Despite they can appear at any age, they have a peak incidence between the third and fifth decade of life and it occurs equally in men and women[8].

1.3. CLINICAL PRESENTATION

The heterogeneous signs and symptoms of PPGLs are attributed to hemodynamic and metabolic actions of the catecholamines synthetized and released by these tumours including noradrenaline, adrenaline and dopamine[9]. Patients with a functional PPGL can present with hypertension and tachycardia, and a wide range of symptoms, both paroxysmal and sustained, that are indistinguishable from common stress disorders. The symptoms include the classic triad: palpitations, headaches, and sweating, as well as many others such as flushing, tremors, abdominal or chest pain, nausea, fatigue weight loss, heat intolerance, visual disturbance, dizziness, change in bowel habit, and neurological symptoms and an "impending sense of doom"[10]. Additionally, catecholamine release of functional PPGLs[7,11] may derive in cardiac complications such as stroke, aortic dissection, myocardial infarction, arrhythmias and heart failure[12,13]. Symptoms are also often absent, even in the face of significant elevations of catecholamines or their metabolites, and it is frequent an incidentally discovered adrenal mass in PPGL patients. PPGLs enlarge over time and specially HN-PGLs may cause mass effect symptoms such as pain and nerve paralysis by

encroaching upon or extending into adjacent tissues and organs[7].

Despite predominantly benign and cured by surgical removal, PPGLs present a significant morbidity and mortality, due to clinical aggressiveness of tumours with multiple recurrences and metastatic disease for which therapeutic options remain scarce[14]. Between 10% (PCC) to up to 40% (PGL) of patients develop metastases in distant non-chromaffin tissues[11,15] such as lymph nodes (80%), bones (71%), liver (50%), and lungs (50%)[16]. Metastases are rarely found in the pancreas, breast, central nervous system, or skin. As expected, metastatic PPGL (M-PPGL) patients present a shorter overall survival, with a heterogeneous 5-year survival rate between 40-95% in adults[17,18].

1.4. PREDICTORS OF OUTCOME

PPGL risk factors are limited and imprecise. Conventional approaches include histological techniques such as the proliferation Ki-67 index, and scoring systems as the PASS (PCC of the adrenal gland scaled score) and GAPP (grading system for PPGL); tumour size (>5cm) and location (PGL>PCC) together with plasma levels of 3-methoxytyramine[19] (dopamine secretion)[20]. Some of these predictors have been included into the new staging classification of PPGLs, TNM (primary tumour size, lymph node involvement, and distant metastasis), proposed by the American Joint Committee on Cancer[14].

The best known genetic predictor of M-PPGL is the presence of germline mutations in the *SDHB* gene. Indeed, more than one third of patients with M-PPGL carry a germline *SDHB* mutation and half of *SDHB*-mutated patients will ultimately develop metastatic disease, having a lower overall survival than other M-PPGL patients[21].

However, any of the before mentioned predictive factors could help in the differentiation of benign and metastatic tumours at early stages, something crucial according to the recommendations of the World Health Organization in order to diagnose and treat M-PPGLs beforehand[22].

Therefore, it is of high relevance a further understanding of the molecular pathogenesis of the disease that would provide new markers of malignancy and may offer effective therapeutic options for tumours with negative clinical outcomes.

2. DIAGNOSIS

Diagnosis of PPGL relies on biochemical evidence of catecholamine release, imaging studies,

histopathological classification of the tumours, and identification of genetic syndromes, all of which can be used as prognostic markers.

2.1. BIOCHEMICAL

Biochemical testing should be performed in symptomatic patients, patients diagnosed with an incidentaloma, and those who have hereditary predisposition (i.e. mutation carriers) or syndromic features suggesting hereditary PPGL. Catecholamines are converted into their inactive metabolites (metanephrine and normetanephrine) by the catechol-O-methyltransferase present in PPGL tumour cells, independently of the exocytotic catecholamine release, and are subsequently released into the plasma in a continuous way. Recommended optimal screening should include fractionated metanephrine (adrenergic), normetanephrine (noradrenergic), and 3-methoxytyramine (dopaminergic), measured in plasma and/or urine. Finally, chromogranin A can be used as an alternative biochemical parameter for silent PPGLs[23].

2.2. IMAGING

After confirming the diagnosis of PPGL biochemically, imaging studies are critical for primary tumour localization, detection of multifocality, and metastases, but there is not a 'gold-standard' imaging technique for all patients. Despite their cost and availability, a combination of both, anatomical and functional imaging has presented with the highest sensitivity for PPGL staging. First line anatomical imaging modalities include computed tomography (CT) and magnetic resonance imaging. They provide a high sensitivity that allow precise tumour delineation, which is critical for pre-surgical evaluation, but a low specificity (75-80%)[24,25].

In the current era, PPGL imaging has moved beyond towards functional characterization of tumours, which provides a higher specificity and it is particularly recommended for diagno¬sis of multi-focal or metastatic disease. Planar scintigraphy, single-photon emission computed tomography (SPECT) and positron emission tomography (PET) have improved the sensitivity and spatial resolution. Functional imaging takes advantage of radiotracers, ligands that target cell membrane transporters or the vesicular catecholamine transport system. For the time being, the choice of ligand should be personalized according to features such as tumour location, metastases and underlying genetic mutation, as it has been proposed by the Endocrine Society guidelines[7].

Norepinephrine membrane transporter

Iodine-123-metaiodobenzylguanidine (^{123}I-MIBG) is a guanidine analogue, similar to noradrenaline,

and it is the most frequently used and available ligand for PPGL localization with scintigraphy and SPECT. Its sensitivity for PCC detection is excellent (nearly 100%). ^{18}F-fluorodopamine PET/CT has the highest sensitivity and specificity across genetically different PGLs (tumours negative or with unknown SDHB genotype), and it is the preferred technique for the localization of the primary PGL and to rule out metastases, except in HN-PGLs[24,26].

Somatostatin receptors (SSTR)

Overexpression of SSTRs was recently shown in *SDH*-deficient PPGLs, and since then, the use of different radiolabelled somatostatin analogues have been re-examined not only for the diagnosis, but also for therapeutic uses[27]. ^{111}In pentetreotide (Octreoscan™) is used in combination with PET[28]. Preliminary data indicates that ^{68}Ga-DOTATATE shows sensitivities approaching 100% and very high and selective affinity for SSTR2, being able to give an excellent diagnostic accuracy, superior to all other functional and anatomical imaging modalities in the evaluation of sporadic and *SDHB*-mutated M-PPGL, and HN-PGLs[29–31].

Glucose membrane transporters

^{18}F-fluorodeoxyglucose (^{18}F-FDG) accumulates in proportion to the glycolytic cellular rate, providing an index of intracellular glucose metabolism, a constant feature in PPGL. Sensitivity of ^{18}F-FDG-PET is very high for patients with *SDHB*-related M-PPGL.

Amino acid transporter system

Dihydroxyphenylalanine (DOPA) is the precursor of all endogenous catecholamines, and PPGL cells can take it up through the amino acid transporter system. ^{18}F-FDOPA PET/CT is recommended for the localization of non-M-PPGL, especially in HN-PGLs[24].

2.3. IMMUNOHISTOCHEMISTRY

After surgery, immunohistochemistry (IHC) can give information on the occurrence of a mutation in certain genes but it also can provide a classification of variants of unknown significance (VUS). A negative SDHB staining indicates a defect in any of the SDH-related genes (SDHx) with high sensitivity and specificity, and it has become a rapid and inexpensive preliminary test for testing SDHx deficiency in tumour tissue[32]. In a complementary way, SDHA IHC is also used to detect tumours with *SDHA* mutations, as they are negative at IHC for both SDHB and SDHA.

There are other optimized IHC assays, such as the use of MAX antibody for the identification of truncating

MAX mutations, and S-(2-succinyl) cysteine staining for tumours deficient in FH. Additionally, tumours with mutations in any of the tricarboxylic acid (TCA) cycle genes show loss of 5-hydroxymethylcytosine (5-hmC) expression due to the epigenetic impairment of 5-mC hydroxylation[33].

2.4. GENETIC DIAGNOSIS

Preventive medicine has been dramatically improved by cancer genetics. The identification of susceptibility genes for hereditary forms of cancers in the past decades opened avenues for detection of second primary and recurrent tumours. Once a given germline mutation is detected, genotype-phenotype associations allow the risk stratification and screening of relatives, and thus the diagnosis of tumours in an asymptomatic stage in carriers becomes possible.

Taking into account the high frequency of germline mutations found in patients with apparently sporadic PPGL, current guidelines indicate consideration of genetic testing in all patients with PPGL independent of a clear family history[7]. Systematic screening of all PPGL-related genes (including many of them with low prevalence) has become a time- and resource-consuming process.

When facing a PPGL patient, genetic testing algorithms have been proposed in order to help the clinician in prioritizing one or a few genes that should be tested in first place[34,35]. Those algorithms take into consideration three levels of analysis: biochemical phenotype (catecholamines released by the tumour), immunohistochemical characterization, and clinical presentation[36,37]. Including the latter, age at onset, location and number of tumours, family history, presence of metastases, and whether the PPGL is part of a syndrome such as neurofibromatosis type 1 (*NF1*), multiple endocrine neoplasia type 2 (MEN2, caused by mutations in the *RET* gene), von Hippel-Lindau disease (*VHL*), hereditary PGL (SDHx), polycythaemia PGL syndrome (*EPAS1*) or Reed's syndrome (*FH*). In the end, genetic diagnostics in PPGLs is a multidisciplinary approach combining the expertise of geneticists, endocrinologists, clinical chemists, and pathologists[38].

Traditionally, genetic diagnosis of PPGL has been performed by PCR-based amplification followed by Sanger sequencing and multiplex ligation-dependent probe amplification (MLPA, MRC-Holland Inc.) for large gene rearrangements. However, due to the large number of driver genes identified so far, this single-gene testing technology is becoming unfeasible as it is laborious, costly and time consuming[37]. The use of high-throughput DNA sequencing technology or next generation sequencing (NGS), where simultaneously multiple genes could be tested, makes the detection of mutations in PPGL predisposing genes easier[39].

3. TREATMENT AND MANAGEMENT

Preoperative management of PPGLs requires the administration of α1-adrenergic blocking agents followed by β-blockers, both necessary to prevent catecholamine-mediated life-threatening complications[40]. Nevertheless, reports of high-dose toxicity and lack of effectiveness of these drugs makes often necessary the administration of additional anti-hypertensive drugs to PPGL patients[41].

3.1. SURGERY

The preferred treatment for localized primary PPGLs is early surgical resection by laparoscopic approach[42]. However, if metastases are suspected, open laparotomy is recommended in order to remove as much malignant tissue as possible and to prevent tumour rupture[43].

In the case of bilateral PCC, the classical outcome would be bilateral adrenalectomy with subsequent Addison's disease and lifelong depending on steroid replacement. Partial adrenalectomy sparing at least one of the adrenal cortices is a highly successful treatment option that should be the surgical approach of choice to prevent permanent hipercortisolism[7,44]. HN-PGLs are rarely resected, this is due to their generally benign and non-catecholamine production phenotype, the risk of intraoperative vascular accidents and postoperative low cranial nerve neuropathy[45].

After PPGL resection, follow-up, for at least 10 years, is crucial to detect metachronous PPGLs or recurrences as well as new events in carriers of germline mutations in PPGL susceptibility genes[3,46].

Patients with M-PPGL are rarely cured by surgery, facing a dismal prognosis. Although symptoms usually improve with the different therapies available such as chemotherapy, radiotherapy or with the molecular targeted options, it is unclear whether any of the therapies modifies the natural history of M-PPGL or prolongs patient survival. Therefore, it is considered an orphan disease for which curative chances are very limited[47].

3.2. CHEMOTHERAPY

After surgery, M-PPGL are treated with systemic chemotherapy with a combination of cyclophosphamide, vincristine and dacarbazine, although patients generally do not have a complete response[48]. Temozolamide (an oral alternative of dacarbazine) in combination with thalidomide, both acting as antiangiogenic agents, were effective for one of three M-PPGL patients in a phase II trial[49]. To note, it has been reported

that *SDHB* mutations are responsible for the association with partial response to temozolamide in M-PPGL patients[50].

3.3. RADIOTHERAPY

For unresectable tumours detected by ^{123}I-MIBG scintigraphy, radiotherapy with ^{131}I-MIBG is recommended[51]. ^{131}I-MIBG is taken up by the noradrenaline transporter, and inside the tumour cell, releases lethal radiation that induces DNA damage and cell death[52]. The use of histone deacetylase (HDAC) inhibitors increases ^{123}I-MIBG uptake, thus enhancing the therapeutic efficacy of the treatment[53]. A phase II clinical trial was performed (some others are ongoing) with the second-line MIBG, Ultratrace Iobenguane ^{131}I (AZEDRA®, Progenics Pharmaceuticals, Inc.), a highly specific radiopharmaceutical agent that delivers very high levels of radioactivity per dose. Almost all treated patients had a tumour response and lower rate of cardiovascular events[54]. Peptide receptor radionuclide therapies such as ^{90}Y-DOTATOC and ^{177}Lu-DOTATATE bind to somatostatin receptors and deliver lethal radiation, however, initial prospective studies have been disappointing[55,56]. Remarkably, toxicity associated with chemotherapy and radiopharmaceutical agents cannot be underestimated[57].

3.4. MOLECULAR TARGETED THERAPIES

Our increasing knowledge on the molecular biology of PPGLs is helping to extend the number of promising therapeutic options. Unfortunately, these potential drugs present a shortage of positive results as well as different adverse effects.

- Some anti-proliferative agents have been included in specific clinical trials such as everolimus (mTOR pathway inhibitor), showed modest efficacy[58], or tested only in preclinical models, AZD8055 (ATP-competitive dual mTORC1/2 inhibitor[59]), Indotecan/LMP-400 (topoisomerase 1 inhibitor)[60], and Hsp90 inhibitors (tanespimycin and ganetespib).

- Tyrosine kinase receptor (RTK) inhibitors prevent neoangiogenesis, cell growth, cell migration, development of resistance and may induce apoptosis[61–63]. Sunitinib is the first RTK inhibitor recognized as a potential treatment for patients with M-PPGL. It also has a direct cell effect, causing tumour size reduction, disease stabilization, and hypertension improvement in some patients[22]. In a retrospective review of a series of 17 patients treated with sunitinib, 47% experienced clinical benefit, being most of them carriers of *SDHB* mutations[57]. There are several phase II trials, already finished or still ongoing (www.clinicaltrials.gov), using multikinase inhibitors which endpoints are response rate and/or progression-free survival[14]: FIRSTMAPPP-sunitinib (recruiting), pazopanib (halted, only 1/7 patients had a partial response[64]), axitinib (active), lenvatinib (recruiting), cabozantinib (recruiting M-PPGL

mainly with bone metastasis), and dovitinib (active). Imatinib mesylate (Glivec), a selective inhibitor of c-ABL, and the PDGF and stem cell ligand (c-kit) RTKs exhibited no response in two cases[65].

- Proteasome inhibitors such as bortezomib in combination with salinosporamid A showed PPGL cell death[66].

- DNA methyltransferase inhibitor, Guadecitabine (SGI-110) has been included in a phase II clinical trial for the treatment of SDHx-mutated PPGL patients (those exhibiting a CpG island methylation phenotype, CIMP profile) (www.clinicaltrials.gov).

-Immunotherapy drugs that fight hypoxia/pseudohypoxia-derived immune system disarrangements[67] include interferon alpha-2b and octreotide analogues that have been already used routinely in the treatment of gastroenteropancreatic neuroendocrine tumours, melanoma, kidney cancer, and occasionally M-PPGLs[68]. A recent retrospective study showed promising results, indicating that immunotherapy could have a positive impact on patients with M-PPGL[69]. Moreover, a phase II clinical trial of the immune checkpoint inhibitor pembrolizumab is currently underway for M-PPGL patients.

- HIF2A (hypoxia inducible factor 2 alpha) pathway inhibitors have been tested in cancer patients with low success[22]. However, new potent HIF2A antagonists targeting the cavity of the protein (PT2385 and PT2977), are quite promising despite they have not been tested yet for M-PPGL[70,71].

- Preclinical studies in other cancers suggest that ATR inhibitors and Wnt antagonists could also have a benefit in M-PPGL patients, and therefore they should be explored in clinical trials[72].

- Recent findings in *SDH*- and *FH*-mutated PPGLs showed that the accumulation of succinate or fumarate compromises homologous recombination (HR) DNA repair in the tumours. Thus, those PPGL patients could benefit from the vulnerability of tumoural cells to synthetic-lethal targeting with poly(ADP)-ribose polymerase (PARP) inhibitors[73].

4. PPGL GENETIC SCENARIO

PPGLs are considered the tumours with one of the highest degrees of heritability amongst all human neoplasms. Approximately 40% of patients suffering from this highly genetically heterogeneous disease carry a germline mutation[36] in one of 17 different major susceptibility genes. This includes classic driver genes such as *RET, NF1, VHL, SDHD, SDHC*, and *SDHB* as well as the more recently identified *SDHA*, *SDHAF2, TMEM127, MAX, FH, MDH2, EGLN1, EGLN2, KIF1B, MET*, and *SLC25A11*[74,75] (Figure 1). Furthermore, somatic mutations in some of these driver genes (mainly *RET, VHL, NF1* and *MAX*) and in others (*EPAS1, HRAS, IDH1, CSDE1*[76], and *ATRX*[77] among others) can be detected in an additional 30%

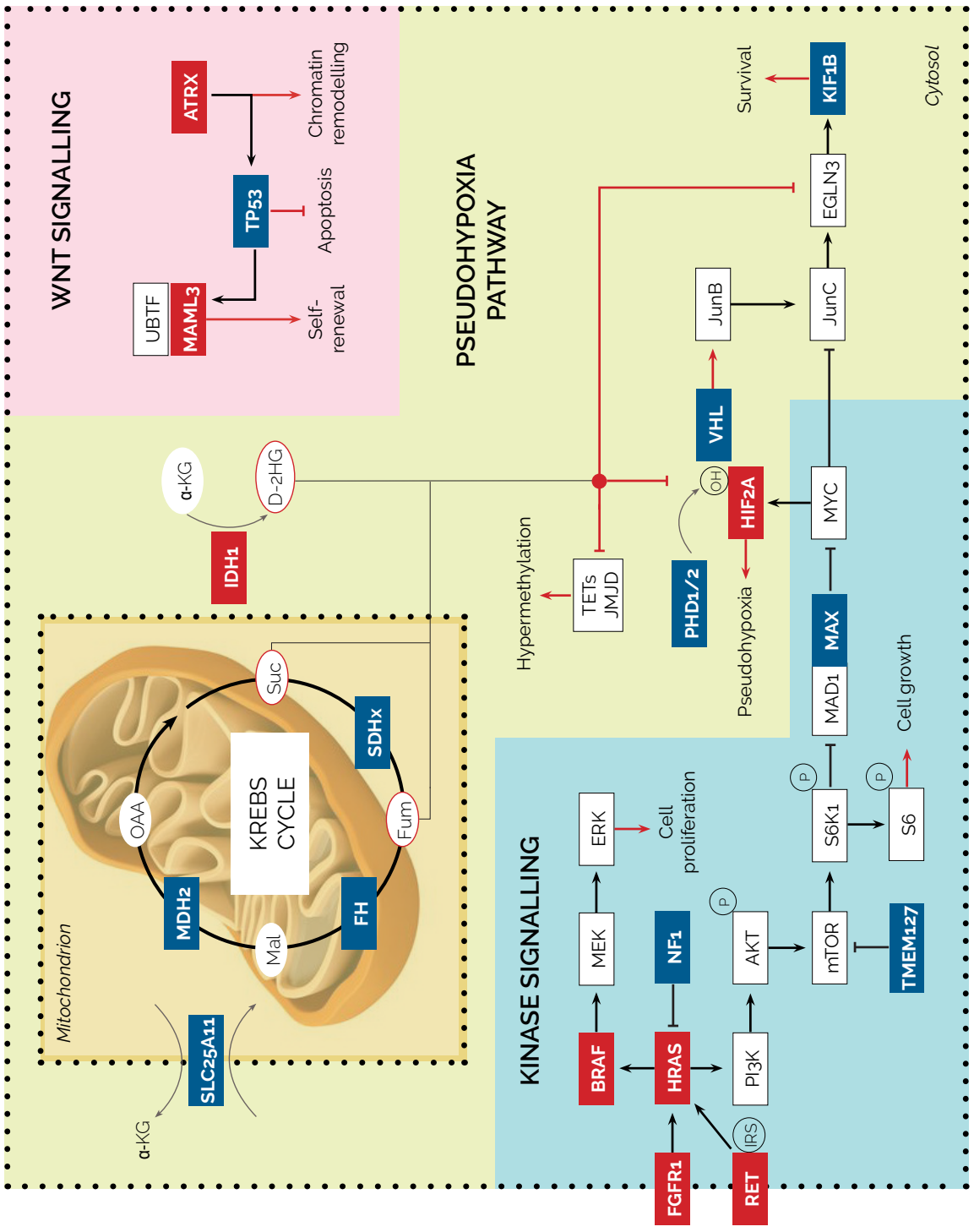

Figure 1. Canonical pathways recurrently altered in PPGL. Susceptibility genes found activated are denoted in red while those genes inactivated are represented in blue. Red lines indicate altered pathways due to mutated genes and metabolite accumulation is denoted by red circles.

of tumours[1]. Finally, there are also PPGL patients carrying somatic postzygotic mutations that occurs in early developmental stages (i.e. in *EPAS1*[78] and *H3F3A*[79]), and tumours affected by somatic gene fusions (i.e. *MAML3*[76]).

Except for the case of certain oncogenes such as *RET, EPAS1, H3F3A, MET, IDH1*, and *HRAS*, most PPGL susceptibility genes are tumour suppressor genes. Thus, patients carry an autosomal dominant heterozygous germline mutation in one of the PPGL tumour suppressor genes, and tumour development occurs following a somatic second hit or loss of the wild-type (WT) allele, that leads to loss of heterozygosity (LOH) and to the subsequent inactivation of the gene's function[36,80].

Based on multi-omics data (transcriptomic gene expression, copy number alterations, metabolomics signature, miRNA profiles and DNA methylation), PPGLs can be classified in different clusters according to their genetic background[81–83] (Figure 2).

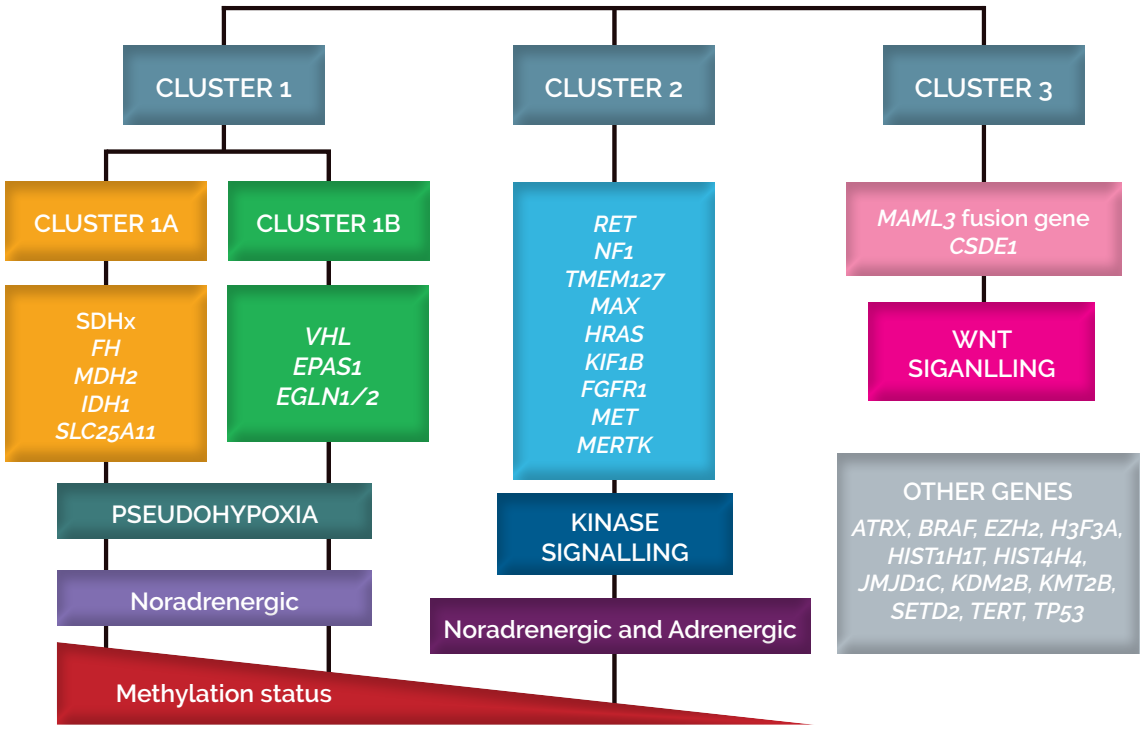

Figure 2. PPGL molecular signatures. Classification according to genotype, clinical and multi-omics data.

This omics-based classification of PPGLs have guided the discovery of novel susceptibility genes during the last years. The most studied are the transcriptional clusters (1, 2 and 3), and we will use them in this thesis to stratify the different PPGL susceptibility genes. Cluster 1 (hypoxic/angiogenic cluster, consisting in tumours with mutations in SDHx, *VHL, EPAS1* and *FH* genes) comprises tumours with features resembling the cellular response to hypoxia and a predominantly noradrenergic secretion. Cluster 2 (kinase-signalling cluster, which includes tumours carrying mutations in *RET, NF1, TMEM127*

and *MAX* genes, as well as most of the sporadic tumours) groups tumours, producing both adrenaline and noradrenaline, that display a profile of activated tyrosine kinase receptors and increased protein translation. Finally, Cluster 3 includes Wnt signalling-related tumours.

4.1. CLUSTER 1: PSEUDOHYPOXIA DRIVEN TUMOURS

A common feature for tumours carrying mutations in Cluster 1 genes, is the aberrant and constitutive activation of hypoxia inducible factors (HIFs) even under normal cellular oxygen levels, a condition known as pseudohypoxia. HIFs are heterodimeric transcription factors and their inducible components, the α-subunits (HIF-1α, -2α and -3α), are tightly regulated by hydroxylation by prolyl hydroxylase domain (PHD) proteins: PHD1, PHD2 and PHD3 (encoded by *EGLN2, EGLN1* and *EGLN3* genes, respectively)[84], enabling HIF recognition for proteasome-mediated degradation[1]. Upon pseudohypoxia, HIFs bind DNA at hypoxia response elements thereby activating not only the *EPO* gene but also a broad range of other genes that orchestrate adaptation to hypoxia and tumorigenesis when sustained (*VEGF, TGFα, GLUT1, CCD1, Oct4, CXCR4*, etc.). They are thought to have a key role in stimulating angiogenesis, cellular proliferation, reduced apoptosis, invasion and metastasis[84–86]. In these pseudohypoxic tumours, the Warburg effect causes downregulation of respiration that is substituted by aerobic glycolysis, resulting in increased glucose consumption for energy production[85]. Beyond genetics, prolonged exposure to hypoxia has been reported as an environmental risk factor for PPGL in people living at high altitude[87], as well as in patients with cyanotic congenital heart disease[88,89].

The Cluster 1 can be subdivided, in turn, into Cluster 1A and Cluster 1B.

4.1.1. CLUSTER 1A

This subcluster comprises tumours carrying mutations in genes encoding energy metabolism enzymes such as the succinate dehydrogenase (SDH) subunits (SDHx genes), fumarate hydratase or fumarase (*FH*), malate dehydrogenase 2 (*MDH2*), isocitrate dehydrogenase 1 (*IDH1*) or solute carrier family 25 member 11 (*SLC25A11*).

In addition to the metabolic re-wiring that occurs after the loss-of-function of TCA cycle enzymes, alterations in Cluster 1A genes also lead to the accumulation of "oncometabolites" such as succinate, fumarate, malate or 2-hydroxyglutarate (2HG). Among other functions[90], these oncometabolites act as competitors of αKG to broadly inhibit the activity of αKG-dependent dioxygenases, such as ten-eleven translocation DNA hydroxylases and Jumonji (JMJ) histones demethylases[91,92]. This causes a global hypermethylation with a characteristic CIMP profile in the tumours, leading to altered gene expression

and contributing to tumorigenesis, something already observed for glioblastomas[93] and clear cell renal cell carcinomas (ccRCC)[94] carrying metabolic alterations such as *IDH1/2* and *FH/SDHB* mutations, respectively. Recently, fumarate and succinate have been also found to suppress the HR DNA-repair pathway involved in the resolution of DNA double-strand breaks and the maintenance of genomic integrity[73].

- SDHx genes

The SDH enzyme complex is a heteroligomer that comprises four structural subunits: two hydrophilic catalytic subunits, SDHA and SDHB, and two hydrophobic subunits that anchor the catalytic ones to the inner mitochondrial membrane, SDHC and SDHD. The fifth SDH gene, *SDHAF2*, encodes a cofactor responsible for flavination of SDHA. The SDH complex catalyses the oxidative dehydrogenation of succinate to fumarate in the TCA cycle[95] and it is also functionally involved in the electron transport chain forming the mitochondrial complex II[96] (Figure 3). Germline mutations in the SDHx genes cause disassembly of the mitochondrial complex, with loss of SDH enzymatic activity and therefore triggering the accumulation of its substrate, succinate. Apart from the aforementioned CIMP profile, this accumulation competitively inhibits prolyl hydroxylases like PHDs, contributing to activation of the pseudohypoxic pathway[97,98]. Moreover, the accumulation of succinate also causes downregulation of the enzyme responsible for the conversion of norepinephrine to epinephrine, therefore inducing the characteristic noradrenergic phenotype of SDHx tumours[92].

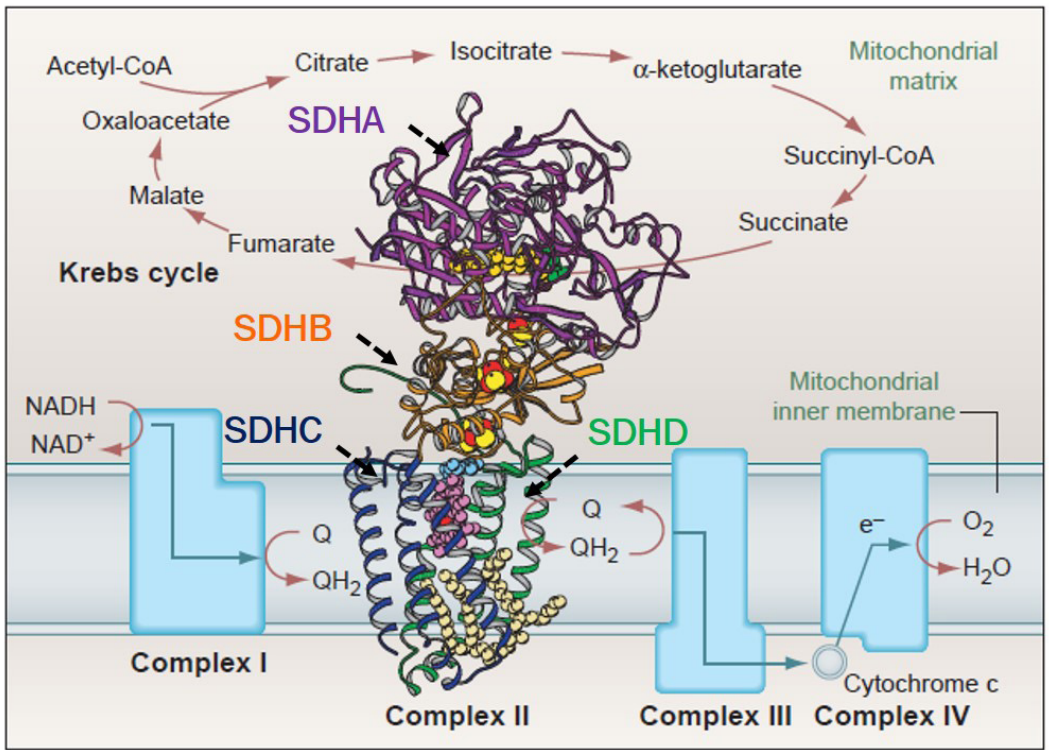

Figure 3. Structure of the succinate dehydrogenase enzyme. Adapted from *Hederstedt, Science 2003.*

Germline loss-of-function mutations in *SDHA, SDHAF2, SDHB, SDHC* and *SDHD* (together accounting for 20% of all PPGLs) cause the well-characterized familial PGL syndromes known as PGL5[99] (MIM: #614165), PGL2[100] (MIM: #601650), PGL4[101] (MIM: #115310), PGL3[102] (MIM: #605373) and PGL1[103] (MIM: #168000), respectively. Additional solid tumours such as gastrointestinal stromal tumours (GISTs)[104], ccRCCs[105] and pituitary adenomas[106] have been associated, although rarely, with these familial PGL syndromes[107]. Only 30% of SDHx-mutated cases have a family history of the disease mainly due to the incomplete penetrance of these syndromes[95].

SDHD became the first metabolic gene whose mutations were associated with the development of cancer[103]. Germline inactivating mutations in this gene show a high penetrance (43.2% at the age of 60 years[95]) with maternal genomic imprinting, and are the cause of multiple HN-PGLs, although rarely malignant[108]. On the contrary, *SDHB*-related tumours are usually diagnosed in patients with single PGLs, mutations in this gene show a low penetrance (21.8% by age 60 years[95]), and they present a high risk of malignancy (50%)[36] and ccRCC development (4.7% by age 60 years[95]). As previously mentioned, the presence of mutations in *SDHB* is the best biomarker of poor prognosis and malignancy in PGL syndromes[21,109]. Mutations in *SDHB* and *SDHD* account for the great majority (over 60%) of all SDHx-related PGL patients.

SDHC was the second SDHx gene identified as a cause of PPGLs, however its frequency is much lower than *SDHB*- and *SDHD*-related PPGLs, accounting for less than 1% of the patients. *SDHC* mutations result primarily in HN-PGLs but have also been identified in patients with sympathetic PGLs. Recently, postzygotic epimutations in *SDHC* promoter were identified in patients with PGLs[110], Carney triad (MIM: #604287) (GIST, pulmonary chondroma and PGLs)[111], and Carney-Stratakis syndrome (MIM: #606864) (co-occurrence of PGL and GIST)[112].

Familial PPGL related to mutations in *SDHA* shows a prevalence of 3%, and it has a very low penetrance and multifocality[113]. Finally, mutations in the SDHAF2 subunit have also been reported in HN-PGL with maternal imprinting[36], common multifocality[114], and very low prevalence (0.1%[113]).

- *FH*

FH catalyses the reaction that follows SDH complex activity in the TCA cycle, the conversion of fumarate to malate. Deficiency in FH activity results in the accumulation of the precursor metabolite, fumarate, which, as happens with succinate, affects the function of certain αKG-dependent enzymes[91]. But in this case, both JMJ demethylases inhibition and HIFα accumulation are reactive oxygen species (ROS)-dependent, with a ROS increased in *FH*-mutant cells and tumours[115]. Phenotype of *FH* affected patients (with a prevalence of ~1% in PPGL patients[11]) is characterized by multifocal PPGLs and a high frequency of metastatic disease[116]. FH deficiency is also linked to hereditary cutaneous and uterine leiomyomas (Reed's syndrome) and type 2 papillary renal carcinoma (MIM: #150800), being the appearance of PPGLs

in these patients exceptional[117].

- *MDH2*

MDH2 encodes malate dehydrogenase 2, which is essential for the reversible oxidation of malate to oxaloacetate in the TCA cycle. This tumour suppressor gene was first reported mutated, with an incomplete penetrance, in a single family with multiple malignant PGLs[118]. Very recently, the same mutation has been found in another patient with malignant PCC, and additional pathological variants have been also reported accounting for <1% of the patients[119].

- *IDH1/2*

Somatic mutations in the *IDH1* gene, frequently found in central nervous system tumours[120], have been also identified in PPGLs leading to a neomorphic production of D-2HG that finally causes the characteristic CIMP profile. However, they are low frequent events in PPGL (<1%)[76,112,121]. Very recently, a single HN-PGL carrying a somatic mutation in *IDH2* has also been reported[38].

- *SLC25A11*

Last year, germline mutations in the tumour suppressor gene *SLC25A11* have been identified in seven unrelated patients, many of them with metastatic A-PGLs. *SLC25A11*-mutated tumours showed a reduction of αKG levels with the pertinent accumulation of aspartate as a consequence of the malate-aspartate shuttle disruption. *SLC25A11* has been classified into Cluster 1A due to the SDHx-like molecular phenotype exhibited by the mutated tumours, including pseudohypoxia and a CIMP profile. *SLC25A11* gene mutations could account for 1% of all PPGL[75].

4.1.2. CLUSTER 1B

Cluster 1B genes such as *VHL* (encoding a HIF ubiquitin ligase), *EPAS1* (encoding HIF-2α itself) and *EGLN1/EGLN2* (encoding PHD proteins) are themselves constituents of the cellular response to hypoxia. Tumours carrying mutations in these "pseudohypoxic genes" show an intermediate methylation phenotype utterly different from Cluster 1A.

- *VHL*

The *VHL* (von Hippel-Lindau) gene encodes a member of an E3 ubiquitin ligase complex that addresses the α subunits of HIF-1 and HIF-2 proteins to proteasomal degradation under normoxia. Loss-of-function mutations in *VHL*, disrupt the process of HIF-1α degradation. Then, HIF-α molecules are stabilised leading to sustained expression of pro-tumorigenic hypoxic genes[122]. Additionally, in a HIF-independent manner, VHL can mediate tumorigenesis through regulation of the extracellular matrix, apoptosis, transcription, or stabilizing microtubules[123]. Germline (predominantly missense in PPGL[124]), mutations in the tumour suppressor gene *VHL*, occur in the setting of VHL syndrome (MIM: #193300)[125], where the most common associated tumours are hemangioblastomas of the brain, spinal cord, and retina, ccRCC, endolymphatic sac tumours, PPGLs (up to 20% of VHL patients), and pancreatic neuroendocrine tumours[126]. PPGLs tend to occur in younger patients and are frequently bilateral and occasionally multifocal, accounting for <10% of all PPGLs[127]. Somatic mutations of *VHL* are also frequently found in PPGLs (~10%)[128].

- *EPAS1*

The endothelial PAS domain-containing protein 1 gene (*EPAS1*), also known as *HIF2A*, encodes one of the members of the HIF family of transcriptional regulators involved in hypoxic response[129]. Gain-of-function somatic mutations (found in ~5% of sporadic PPGLs[130]) at *EPAS1* hydroxylation sites disrupt the recognition of EPAS1 by members of the PHD family, and therefore its hydroxylation and the following degradation by pVHL[1]. Stabilization and constitutive activation of EPAS1 leads to tumour growth *in vivo*, through a specific sensitivity of chromaffin cells to EPAS1 oncogenic properties such as the activation of the oncogene MYC[131]. Somatic mosaicism caused by postzygotic *EPAS1* mutations can lead to a non-inherited syndrome presenting with multiple and recurrent PGLs, somatostatinoma and congenital polycythaemia (also known as Pacak-Zhuang syndrome)[132,133]. Additionally, gain-of-function somatic mutations of *EPAS1* in PPGLs patients presenting with cyanotic congenital heart disease have been recently described[88].

- *EGLN1/2*

Germline mutations in Egl-9 Family Hypoxia Inducible Factors (*EGLN1*: n=2 and *EGLN2*: n=1; also known as PHD2 and PHD1, respectively) have been reported in three patients with PPGL-polycythaemia disorder[134,135]. Mutations in those genes cause substantial loss of protein stability of both PHD1 and PHD2, resulting in the upregulation of HIF-α target genes and therefore in the activation of hypoxic pathway[135].

4.2. CLUSTER 2: KINASE-SIGNALLING TUMOURS

Tumours from the second main transcription subgroup carry mutations in genes encoding the RET receptor, HRAS or its inhibitor NF1, TMEM127 and MAX, all of which led to hypomethylation and kinase signalling activation[74]. Thus, these mutations lead to the activation of RAS/RAF/MAPK, PI3K/AKT/mTOR or MYC-MAX intracellular pathways that are involved in cell growth, proliferation, survival and metastasis[136].

- *RET*

The *RET* (re-arranged during transfection) gene encodes a transmembrane tyrosine kinase receptor for members of the glial cell line-derived neurotropic factor family that is necessary for neural crest development[137]. Germline gain-of-function mutations in the oncogene *RET* (identified in 5-10% of PPGL patients), predispose to a rare autosomal dominant disorder named MEN2 syndromes (types 2A and B)[138]. MEN2A (MIM: #171400), also known as Sipple syndrome, causes medullary thyroid carcinoma, PCC and primary hyperparathyroidism, while MEN2B (MIM: #162300) is characterized by medullary thyroid carcinoma, PCC, Marfanoid habitus, intestinal and mucosal ganglioneuromatosis, being the latest rarer but also the most aggressive form of the disease[139]. Additionally, somatic *RET* mutations are detected in approximately 5% of sporadic PPGLs[128,140]. The study of this gene has provided a paradigm for heritable acti¬vated oncogenes in cancer predisposition syndromes. Its striking genotype-phenotype correlation leads to a better prediction of disease onset and prognosis, and genetic-based personalized medical care, for instance, early prophylactic thyroidectomy in MEN2B cases[141].

- NF1

The *NF1* (neurofibromin 1) gene encodes a GTPase-activating protein that functions as a tumour suppressor by promoting the conversion of the active GTP-bound RAS GTPase to the inactive GDP-bound RAS form, thereby acting as a RAS inhibitor. Germline loss-of-function mutations in *NF1* (with a prevalence lower than 3% in PPGL patients) predispose to neurofibromatosis type 1 (MIM: #162200), a frequently tumour-prone disorder with high penetrance and in which around 5% of patients develop PPGLs[142,143]. The most frequent clinical features of the syndrome are: café-au-lait spots, neurofibromas, axillary or inguinal freckling, optic glioma, bone lesion and/or Lisch nodules[144]. Somatic *NF1* mutations, most of them truncating, are present in 14% of cases, therefore considered as the foremost-inactivated gene in sporadic PPGLs[140,145].

- *TMEM127*

The transmembrane protein 127 (TMEM127) plays a role in endosomal signalling and it acts as a negative regulator of mTOR. Thus, loss-of-function mutations in *TMEM127* results in reduced inhibition of the mTOR pathway in a RAS/RAF/MAPK and PI3K/AKT independent manner. Germline mutations in this tumour suppressor gene (found in around 2% of all PPGLs)[113], mainly truncating, present low penetrance[136,146] and have been also reported in rare cases of ccRCC[147].

- *MAX*

MAX (MYC-associated factor X) mutations were discovered by WES applied to the germline of patients with hereditary PCC who lacked a mutation in other susceptibility genes[148]. MAX is a basic helix–loop–helix (bHLH) leucine zipper domain-containing protein that is involved in protein–protein interactions and DNA binding. MAX is predominantly found in complex with MXD1 and the MYC transcrip¬tion factor, a common oncogene in many human cancers[149]. MYC–MAX heterodimers bind to Ebox DNA recognition sequences in the promoters of many target genes that encode proteins involved in metabolism, growth and angiogenesis while MAX-MDX1 heterodimerization antagonizes this transcription. Upon MAX alterations affecting the bHLH domain, the ability of MAX to antagonize MYC-dependent cell transformation is destroyed, leading to tumour development[150]. Apart from PPGL, *MAX* have been found subsequently mutated in many other cancer types such as small cell lung cancer[151], GIST[152], endometrial cancer[153], and multiple myeloma[154] among others.

The second hit observed for *MAX*-mutated PCCs is the LOH either by paternal uniparental disomy (UPD) or by loss of chromosome 14q, which results in a unique transcriptomic signature. Germline mutations in this gene, which could also predispose to renal oncocytoma[155], appear with very low prevalence (0.8%) in patients with PPGL[148], though the prevalence amongst patients with bilateral PCC is much higher[113]. Additionally, somatic mutations in *MAX* have been also reported in an extensive patient cohort of sporadic tumours[156].

- *HRAS*

The *HRAS* (Harvey rat sarcoma viral oncogene homolog) gene encodes a small GTP-binding protein that affects multiple downstream pathways related to cell growth and homeostasis. It has been described as a common driver event in PPGL pathogenesis (prevalence of ~7%[157]), with exclusively somatic gain-of-function mutations in sporadic cases, mainly PCC[158,159].

- *KIF1B*

The *KIF1B* (kinesin family member 1B) gene has been found mutated, both somatically and germline, in different PPGL cases. It has been reported that *KIF1B* functions as a tumour suppressor and it is necessary and sufficient for neuronal apoptosis[160,161].

A small minority of PPGLs show potential driver mutations in other kinesins (apart from KIF1B) such as, *MERTK* germline mutations that may be related to rare *RET*-negative cases with MEN2-like clinical manifestations; germline and somatic mutations in *MET*; and a somatic oncogenic hotspot in *FGFR1*[79]. Tumours carrying mutations in these genes could probably be grouped with *RET*-mutated PPGLs in this Cluster 2.

Although Cluster 1 and 2 related genes are discussed separately, several of the pathways activated in these two major groups are linked. Thus, mTOR can activate HIF[162], and there are multiple levels of crosstalk between MYC and HIF-2α in oncogenesis[163].

4.3. CLUSTER 3: WNT SIGNALLING-RELATED TUMOURS

This recently defined cluster, related to genes not previously associated with PPGLs, comprises sporadic and probably more aggressive and hypomethylated tumours carrying mutations that trigger Wnt signalling activation.

This group includes PPGLs carrying somatic gene fusions affecting the *MAML3* (mastermind like transcriptional coactivator 3) transcription factor gene, with increased transcription levels of a chimeric MAML3. One of the fusions observed in PPGLs, *UBTF-MAML3*, leads to the activation of the Wnt target expression and Hedgehog signalling pathway, something similar as detected in neuroblastoma, a tumour with shared developmental origin with PPGLs. The first study describing MAML3 alterations in PPGL, carried out by The Cancer Genome Atlas project, also described somatic loss-of-function mutations in *CSDE1* (cold shock domain containing E1), that encodes an RNA-binding protein not hitherto associated with cancers[76].

Moreover, it has been suggested a fourth group that would comprise a minority of PPGLs displaying adrenocortical features. The identity of this cluster is less well defined, unlike the other three transcriptional groups, since they lack consistent driver mutations, copy number changes, or transcriptome and methylome patterns that would help to discern between PPGLs and other cortical tumours. It is currently under debate whether this represents a new biological entity or if it is an artefact from cortex tissue contamination[74,76].

4.4. OTHER GENES NOT CLEARLY ASSOCIATED TO ANY TRANSCRIPTIONAL CLUSTER

Recent publications have uncovered mutations in chromatin-remodelling genes, highlighting the relevance of epigenetic modifications in the development of PPGL. For instance, the presence of somatic loss-of-function mutations in *ATRX* (alpha thalassemia/mental retardation syndrome X-linked) in PPGLs was first described in 2015 mostly coexisting with SDHx mutations (and therefore associated to Cluster 1A). However, there are also cases without any further driver mutation which are related to the Cluster 3[76,164]. Mutations in *ATRX* have been associated with alternative lengthening of telomeres and clinically aggressive behaviour[80].

Postzygotic mosaic mutations in *H3F3A* (H3 histone family member 3A) cause PPGL together with giant cell tumour of the bone, and lead to the upregulation of MYCN oncoprotein[165]. H3F3A-mutated PPGLs have been proposed to be part of Cluster 2, although due to their function, those PPGLs may fit better into Cluster 1. Other chromatin-remodelling genes found mutated in PPGLs are: *EZH2*, *HIST1H1T*, *HIST4H4*, *JMJD1C*, *KDM2B*, *KMT2B*, or *SETD2*[82].

Additionally, commonly mutated genes in different cancer types (such as *TERT*, *TP53* and *BRAF*) have been also involved in PPGL pathogenesis[83,166]. However, the specific role of many of those genes in PPGL development needs to be further clarified.

Mutations in PPGL, either inherited or acquired, are mutually exclusive in the tumours. The presence of single driver events in PPGLs highlight the redundancy of the pathways affected[1]. In this respect, PPGLs are more similar to other Mendelian disorders, where a driver mutation can be related to a specific phenotype, than to most cancers. As aforementioned, an exception to this rule is the *ATRX* gene, which is mutated preferentially in tumours carrying a germline *SDHB* mutation[74]. There are, however, anecdotal examples of PPGLs with mutations in different driver genes (*NF1* together with *RET* o *VHL* mutations[167]) as well as double monoallelic mutations (EPAS1[168]).

Despite the past and present genetics/genomics efforts that have led to deciphering the driver causal event in around 60% of PPGL patients, there is still a percentage of patients with clinical features indicative of a hereditary condition (i.e. early age of onset, tumour multiplicity and/or family history of PPGL), but without mutations in any of the known PPGL susceptibility genes[74]. Therefore, identification of additional germline or mosaic disruptions in those genetically undiagnosed patients would have important implications in their management, and in the early diagnosis and treatment of at-risk individuals[20].

As established by the NGS in PPGL study group, WES is the preferred method for discovering the primary mutation in PPGLs without mutations among the PPGL susceptibility genes[37]. However, the

potential of targeted NGS approaches, which improve the efficiency and accuracy of the detection, is higher when there is a candidate list of genes. When planning a NGS-based project, one of the most critical steps is the adequate selection of cases that will be included in the study. This selection is usually based on the presence of similar phenotypes, distinctive molecular markers or particular clinical features. Regarding this, mutations in *MAX* were discovered thanks to the selection of PCCs showing a common and characteristic expression profile. In other example, the gene *NF1* was found somatically mutated in a surprising high number of PPGLs by selecting tumours with loss of chromosome 17. In this regard, previous studies identified that *RBP1* (retinol binding protein 1) was amongst the genes silenced by promoter hypermethylation not only in TCA cycle-mutated PPGLs (SDHx, *FH* and *MDH2*[92,118]), but also in gliomas related to IDH1 and IDH2 mutations[169]. Thus, downregulation of this gene constitutes a marker not only of a CIMP profile, but also of a TCA cycle alteration, and the assessment of its expression could be used for selection of PPGLs in order to uncover mutations in new candidate susceptibility genes implicated in this key metabolic pathway.

OBJECTIVES

The main objective of this thesis was:

1. To identify new PPGL susceptibility genes in selected patients without any mutation in the already known driver genes using NGS approaches. Once a new candidate PPGL susceptibility gene was identified we aimed:

a) To determine the pathogenicity of the variants found in the identified gene/s using omics data as well as *in vitro* and *in silico* models.

b) To assess the prevalence of mutations in the new gene/s applying targeted sequencing to larger series of PPGL patients, and establish, if any, the associated clinical presentation.

ARTICLES

ARTICLE 1: Targeted Exome Sequencing of Krebs Cycle Genes Reveals Candidate Cancer–Predisposing Mutations in Pheochromocytomas and Paragangliomas.

Authors: **Laura Remacha**, Iñaki Comino-Méndez, Susan Richter, Laura Contreras, Maria Currás-Freixes, Guillermo Pita, Rocío Letón, Antonio Galarreta, Rafael Torres-Pérez, Emiliano Honrado, Scherezade Jiménez, Lorena Maestre, Sebastián Morán, Manel Esteller, Jorgina Satrústegui, Graeme Eisenhofer, Mercedes Robledo, and Alberto Cascón

Published in *Clinical Cancer Research*, 2017 Oct 15;23(20):6315-6324

ABSTRACT

Mutations in phaeochromocytoma and paraganglioma (PPGL) predisposition genes encoding enzymes involved in the TCA cycle lead to a particular CpG island hypermethylation phenotype. In this study, we used selected tumours with this phenotype for targeted exome sequencing of a home designed panel of TCA cycle-related genes in order to find new PPGL susceptibility genes.

We identified for the first time a germline variant in the glutamic-oxaloacetic transaminase 2 gene (*GOT2*), a mitochondrial transporter, in a patient with multiple tumours (n=9) and metastasis. This variant increased GOT2 activity and expression, and caused alterations in TCA cycle metabolite ratios, both in tumours and in *GOT2* KD cells transfected with the variant, suggesting that *GOT2* is involved in PPGL predisposition. In addition, we found a truncating germline mutation in a new candidate susceptibility gene, the isocitrate dehydrogenase 3 (NAD+) Beta (*IDH3B*), in a patient with a single PGL showing an altered a-ketoglutarate/isocitrate ratio.

Finally, we also identified two extremely rare variants in already known cancer-predisposing genes; the third somatic mutation in *IDH1* reported until now was identified by sequencing the panel in one patient with PGL, and array methylation-based analysis uncovered a somatic epigenetic mutation in *SDHC* in a patient with multiple PGLs and GIST.

This study further attests to the relevance of the TCA cycle in the development of PPGL, some of which might be effectively treated with DNA-demethylating agents.

Personal contribution:

I participated in the development of methodology including knocking down of *GOT2* and *OGDHL* in HeLa cells and further transfection of the variants into the knocked-down cells for functional studies. Moreover, I collaborated in the targeted sequencing analysis of tumours for TCA cycle-associated genes as well as in the analysis of the novel variant found in *IDH3B*. I also took part in the drafting and revision of the paper.

Published OnlineFirst July 18, 2017; DOI: 10.1158/1078-0432.CCR-16-2250

Biology of Human Tumors

Clinical Cancer Research

Targeted Exome Sequencing of Krebs Cycle Genes Reveals Candidate Cancer–Predisposing Mutations in Pheochromocytomas and Paragangliomas

Laura Remacha[1], Iñaki Comino-Méndez[1], Susan Richter[2], Laura Contreras[3,4], María Currás-Freixes[1], Guillermo Pita[5], Rocío Letón[1], Antonio Galarreta[1], Rafael Torres-Pérez[1], Emiliano Honrado[6], Scherezade Jiménez[7], Lorena Maestre[7], Sebastian Moran[8], Manel Esteller[8], Jorgina Satrústegui[3,4], Graeme Eisenhofer[2], Mercedes Robledo[1,3], and Alberto Cascón[1,3]

Abstract

Purpose: Mutations in Krebs cycle genes are frequently found in patients with pheochromocytomas/paragangliomas. Disruption of SDH, FH or MDH2 enzymatic activities lead to accumulation of specific metabolites, which give rise to epigenetic changes in the genome that cause a characteristic hypermethylated phenotype. Tumors showing this phenotype, but no alterations in the known predisposing genes, could harbor mutations in other Krebs cycle genes.

Experimental Design: We used downregulation and methylation of *RBP1*, as a marker of a hypermethylation phenotype, to select eleven pheochromocytomas and paragangliomas for targeted exome sequencing of a panel of Krebs cycle-related genes. Methylation profiling, metabolite assessment and additional analyses were also performed in selected cases.

Results: One of the 11 tumors was found to carry a known cancer-predisposing somatic mutation in *IDH1*. A variant in *GOT2*, c.357A>T, found in a patient with multiple tumors, was associated with higher tumor mRNA and protein expression levels, increased GOT2 enzymatic activity in lymphoblastic cells, and altered metabolite ratios both in tumors and in GOT2 knockdown HeLa cells transfected with the variant. Array methylation-based analysis uncovered a somatic epigenetic mutation in *SDHC* in a patient with multiple pheochromocytomas and a gastrointestinal stromal tumor. Finally, a truncating germline *IDH3B* mutation was found in a patient with a single paraganglioma showing an altered α-ketoglutarate/isocitrate ratio.

Conclusions: This study further attests to the relevance of the Krebs cycle in the development of PCC and PGL, and points to a potential role of other metabolic enzymes involved in metabolite exchange between mitochondria and cytosol. *Clin Cancer Res; 1–10.* ©2017 AACR.

Introduction

Despite their low prevalence, pheochromocytomas (PCC) and paragangliomas (PGL) represent a paradigm for hereditary cancer due to the highest degree of heritability of these tumors among all human neoplasms (1). Up to 40% of individuals with PCC and/or PGL have a hereditary background due to germline mutations affecting one of 13 susceptibility genes (2–13). The mutations result in two broad groups of tumors characterized by either activation of hypoxia or kinase receptor signaling pathways (1). Furthermore, somatic mutations in several of these genes or in two other PCC/PGL predisposition genes, *HIF2A* and *HRAS* (14, 15), are found in an additional approximately 30% of tumors (16). Finally, the presence of features of heritability amongst some of the patients without germline mutations in the known susceptibility genes, strongly suggests the implication of additional genes in this multigenetic disease. Of note, more than half of the PCC/PGL predisposition genes encode enzymes involved in the Krebs cycle (*SDHA*, *SDHB*, *SDHC*, *SDHD*, *SDHAF2*, *FH*, and *MDH2*), which stresses the crucial role of this pathway in PCC/PGL development and suggests that alterations in other genes from this pathway could account for more patients. This is even more

[1]Hereditary Endocrine Cancer Group, Spanish National Cancer Research Centre (CNIO), Madrid, Spain. [2]Institute of Clinical Chemistry and Laboratory Medicine, University Hospital Carl Gustav Carus, Medical Faculty Carl Gustav Carus, Technische Universität Dresden, Dresden, Germany. [3]Centro de Investigación Biomédica en Red de Enfermedades Raras (CIBERER), Madrid, Spain. [4]Departamento de Biología Molecular, Centro de Biología Molecular Severo Ochoa UAM-CSIC, Universidad Autónoma de Madrid and Instituto de Investigación Sanitaria Fundación Jiménez Díaz (IIS-FJD), Madrid, Spain. [5]Human Genotyping Unit-CeGen, Human Cancer Genetics Program, Spanish National Cancer Research Centre (CNIO), Madrid, Spain. [6]Anatomical Pathology Service, Hospital de León, León, Spain. [7]Monoclonal Antibodies Unit, Biotechnology Program, Spanish National Cancer Research Centre (CNIO), Madrid, Spain. [8]Cancer Epigenetics and Biology Program (PEBC), Bellvitge Biomedical Research Institute (IDIBELL), L'Hospitalet, Barcelona, Spain.

Note: Supplementary data for this article are available at Clinical Cancer Research Online (http://clincancerres.aacrjournals.org/).

L. Remacha and I. Comino-Méndez contributed equally to this article.

Corresponding Author: Alberto Cascón, Spanish National Cancer Research Centre (CNIO) and ISCIII Center for Biomedical Research on Rare Diseases (CIBERER), Melchor Fernández Almagro 3, 28029 Madrid, Spain. Phone: 34-91-224-6947. Fax: 34-91-224-6923. E-mail: acascon@cnio.es

doi: 10.1158/1078-0432.CCR-16-2250

Published OnlineFirst July 18, 2017; DOI: 10.1158/1078-0432.CCR-16-2250

Translational Relevance

Mutations in pheochromocytoma (PCC)/paraganglioma (PGL) predisposition genes encoding enzymes involved in the Krebs cycle lead to a particular CpG island hypermethylation phenotype in these tumors. We used selected tumors with this phenotype for targeted exome sequencing of a panel of Krebs cycle-related genes to find new PCC/PGL susceptibility genes. Apart from known cancer-predisposing somatic alterations in *IDH1* and *SDHC*, we found a germline variant in *GOT2*. This variant increased GOT2 activity and expression, and caused alterations in Krebs cycle metabolite ratios, both in tumors and in GOT2 KD cells transfected with the variant, suggesting that *GOT2* is involved in PCC/PGL predisposition. In addition, we found a truncating germline *IDH3B* mutation in a patient with a PGL showing an altered α-ketoglutarate/isocitrate ratio. This study further attests to the relevance of the Krebs cycle in the development of PCC/PGL, some of which might be effectively treated with DNA-demethylating agents.

likely for cases showing a noradrenergic or dopaminergic phenotype, which is associated with the presence of mutations in the aforementioned Krebs cycle-related genes.

In recent years, the application of high-throughput "omics" technologies to PCC/PGL research has led to improved understanding of the biology of these tumors, and paved the way for discovery of new predisposing genes (7, 12, 17). It has been known for years that pseudo-hypoxic PCCs/PGLs, such as SDH- and VHL-mutated tumors, share a similar transcriptional profile (18) that can be further segregated into different gene expression signatures (19). More recently, high-throughput methylation studies performed in PCCs/PGLs have revealed a particular CpG island methylation phenotype (CIMP) associated with the presence of Krebs cycle gene (SDH, *FH*, or *MDH2*) mutations (11, 12). This CIMP profile is caused by impaired histone demethylation and 5-mC hydroxylation (5-hmC) due to the enzymatic inhibition of multiple α-KG–dependent dioxygenases by the accumulation of succinate and fumarate (20). In addition, mutations in other Krebs cycle-related genes (*IDH1* and *IDH2*) also lead to a similar CIMP in gliomas (21), caused in this case by the accumulation of D-2-hydroxyglutarate (22). *IDH1* has been also found to be somatically mutated in two PGLs (23, 24). Though the majority of genes that define the altered methylation profile in PCC/PGL and gliomas are different, a substantial percentage of them (~25%) are silenced in both neoplasias (12). That is the case for *RBP1*, which is consistently methylated and downregulated in both types of tumors carrying Krebs cycle mutations (11, 25). Tumors carrying mutations in other PCC/PGL susceptibility genes, such as *RET*, *NF1*, *MAX* or *TMEM127*, all belonging to the so-called expression cluster 2, do not exhibit methylation of *RBP1* (11).

In the present study, we use the low expression of *RBP1* as a marker of hypermethylation to select PCCs and PGLs as candidates for targeted exome sequencing of a panel of Krebs cycle-related genes to find new PCC/PGL predisposition genes.

Materials and Methods

Samples

Forty-nine tumors from patients showing noradrenergic or dopaminergic catecholamine phenotypes or no evidence of catecholamine production (when available), and testing negative for mutations in the major susceptibility genes (including all known PCC/PGL Krebs cycle-related genes: SDH, *FH* and *MDH2*), were included in the study. Immunostaining of SDHB was performed when formalin-fixed paraffin-embedded (FFPE) tissues were available, to rule out hidden mutations affecting the SDH genes, because negative SDHB immunohistochemistry is associated with the presence of SDH gene mutations in PCC/PGL (26, 27). The Instituto de Salud Carlos III (ISCIII) ethics committee approved the study, and all the patients provided written informed consent.

Quantitative real-time PCR

Total RNA was obtained from FFPE or from frozen material using the RNeasy FFPE (Qiagen) or TriReagent (MRC) Kit, respectively, according to the manufacturers' instructions. cDNA was prepared from 1 μg of total RNA using oligo (dT) primers and SuperScript III RT (Invitrogen). RBP1, SDHC and GOT2 mRNA levels were determined by quantitative PCR on a 7500 fast real-time PCR system (Applied Biosystems) using the Universal ProbeLibrary set (https://www.roche-applied-science.com), as described by the manufacturer. Relative mRNA levels were estimated by the $2\text{-}C_t$ method (28) and normalized using β-actin (ACTB) as housekeeping gene. The results are shown as mean + SD ($n \geq 3$). mRNA obtained from tumors carrying mutations in other known pheochromocytoma susceptibility genes were used as controls. Tumors with RBP1 expression below 15 relative units (RU; $n = 14$) were considered candidates for subsequent analyses.

Pyrosequencing

Specific primers were used for PCR amplification and sequencing using the PyroMark assay (design version 2.0.01.15) to interrogate the methylation status of CpG sites from *RBP1*, as previously described (11).

Targeted next-generation sequencing

DNA extracted from 11 selected tumor samples was sequenced for a set of genes involved in the Krebs cycle by TruSight sequencing technology (Illumina), which comprises oligo probes targeting the genes of interest. The makeup of the panel was planned to cover the complete coding region of 37 human genes found to be directly or indirectly involved in the Krebs cycle based on the KEGG (http://www.genome.jp/kegg/pathway.html) and Genecard (http://www.genecards.org/) databases (Supplementary Table S1). *Designstudio* software (Illumina) was used to design the 733 amplicons included in the panel (cumulative Target: 65525 bp and coverage of 99%). This tool avoids designing for amplification primers that include known polymorphisms. Once the library was prepared following the manufacturer's instructions, next-generation sequencing was performed using MiSeq desktop sequencer (Illumina) and sequence alignment was carried out using *MiSeq Reporter* and *Illumina VariantStudio* softwares (Illumina). Variant calling was performed using GATK and *Somatic Variant Caller,* and identified variants were filtered considering mapping quality, variant score, depth, strand bias and annotation quality. To establish a cutoff value to consider a nucleotide substitution reported in controls as a candidate pathogenic

Published OnlineFirst July 18, 2017; DOI: 10.1158/1078-0432.CCR-16-2250

variant, we used publically available data for *SDHB* germline mutations because they have the lowest penetrance amongst mutations in the known PCC/PGL susceptibility genes (29). The highest frequency for a known pathogenic *SDHB* mutation, found in the Genome Aggregation Consortium (gnomAD) database (http://gnomad.broadinstitute.org/), was 1.805×10^{-5}, which was therefore applied as the cutoff value. Targeted regions without appropriate coverage and quality or with low mappability were re-amplified by Sanger sequencing. The PredictSNP consensus classifier (30) was used to predict the effect of the substitutions that passed all filtering steps. Tumor DNA samples from a series of 63 unselected patients with PCC or PGL, and negative for germline mutations in the known susceptibility genes, were tested by targeted next-generation sequencing for the presence of mutations in TCA-related genes.

Methylation assay and data processing

DNA was extracted and purified from the 11 selected cases, and from five SDH gene-mutated controls (two *SDHB*, one *SDHA*, one SDHD, and one *SDHC*-mutated tumors), using the DNeasy Blood & Tissue Kit (Qiagen) according to manufacturer's recommendations. Bisulfite conversion of DNA was performed using the EZ DNA Methylation Kit (Zymo Research) and genome-wide DNA methylation was assayed using the Infinium HumanMethylation450 BeadChip (Illumina) at the *Centro Nacional de Genotipado* (CEGEN-ISCIII), as previously described (31). This BeadChip interrogates more than 485,000 methylation sites per sample. Beta values for each interrogated CpG were assigned using the Genome Studio Methylation module. Methylomes from the 19 tumors were profiled together with 13 additional controls (four non-SDH gene-mutated and nine SDH gene-mutated tumors) obtained from the GEO database (accession number GSE43298). We used the clustering average for linkage and City-block as the distance measure, and assumed a standard deviation of 0.22.

Immunohistochemistry

Immunohistochemical SDHB (HPA002868, Sigma) analysis of 3-μm formalin-fixed paraffin-embedded (FFPE) tissues was used for all cases, where tissue was available, to further rule out the presence of SDH gene mutations, as previously reported (26). Specific immunohistochemical staining of GOT2 (NBP1-80521, Novus) was performed using FFPE sections from the two available *GOT2*-mutated tumors, following standard procedures; five tumors carrying mutations in PCC susceptibility genes were used as controls. Finally, immunohistochemical staining of 5-hmc (Active Motif; 39770) was performed using 3-μm FFPE sections from the *IDH3B*-mutated tumors, following standard procedures.

Enzymatic activity analyses

Cytosolic and mitochondrial fractions were obtained after processing of lymphoblastoid cells obtained from the *GOT2*-mutation carrier and from three controls, as previously described (32). Protein concentration was determined using Bradford method with BSA as standard. The cytosolic and mitochondrial fractions were used to determine the enzymatic activity of GOT1 and GOT2, quantified as a decrease in NADH fluorescence, after the addition of aspartate, using a BMG plate reader, as previously described (33). Control and mutant *GOT* activity in cell fractions were measured in duplicate at different dilutions in 3 independent paired experiments. Lactate dehydrogenase (LDH, measured as the increase in NADH caused by lactate addition) and citrate synthase (CS, measured as the increase in absorption of 5,5′-dithiobis-2-nitrobenzoic acid after the addition of OAA) were assayed using standard procedures (33, 34). GOT2 activity was corrected by subtracting the estimated cytosolic contamination (% of LDH present) from the activity measured in the mitochondrial fraction.

Mutagenesis

GOT2 c.357A>T and c.223T>G variants and the *OGDHL* c.750G>T substitution were generated by mutagenesis using the QuikChange II Site-Directed Mutagenesis Kit (Stratagene), according to the manufacturer's instructions. Wild-type and mutagenized inserts were verified by sequencing both strands.

Cell cultures

Lymphocytes from the carrier of the c.357A>T *GOT2* mutation were immortalized using Epstein-Barr virus (EBV), as previously described (35). HeLa cell line (kindly provided by Flow Cytometry Core Unit, CNIO, Madrid) was authenticated by short tandem repeat profiling (GenePrint 10 System, Promega) and periodically confirmed to be *Mycoplasma* free by qPCR. HeLa cells, used within 10 passages after authentication, were cultured in Dulbecco's modified Eagle medium Gluta MAX (DMEM; Invitrogen), supplemented with 10% (v/v) FBS (PAA laboratories), 1% (v/v) penicillin/streptomycin, and 0.6% (v/v) Fungizone (Gibco), and maintained at 37°C in a humidified incubator with 5% CO_2. MISSION shRNA lentiviral transduction particles were used to specifically knockdown *GOT2* (TRCN0000034827; Sigma) and *OGDHL* (TRCN0000426732; Sigma). Stable gene knockdown (KD) was established by cellular resistance to puromycin (1 μg/mL). Scrambled non-target shRNA control vectors served as negative controls. HeLa (GOT2 or OGDHL) KD cells were seeded at 550,000 cells per well on 6-well plates for 24 hours. Each well was transiently transfected with 2 μg of pCMV6-AC plasmid containing the full cDNA sequence of *GOT2* (SC127269, Origene), or *OGDHL* (RC205225, Origene), or with 2 μg of pCMV6-AC plasmids carrying the corresponding variant (*GOT2* c.357A>T and c.223T>G, or *OGDHL* c.750G>T) using Lipofectamine 2000 (Invitrogen), according to the manufacturer's recommendations. pCMV6-AC empty vector (EV) was used as a control. In the proliferation assay, GOT2 KD HeLa cells were transfected with EV, GOT2-WT or GOT2-c.357A>T cDNA, and were seeded 24 hours post-transfection at 30,000 cells per well on 12-well plates. Then, cells were trypsinized and counted after 48, 72, and 96 hours post-transfection.

Western blot

To demonstrate the absence of full-length GOT2 or OGDHL proteins in KD HeLa cells, we performed Western blot analysis using polyclonal rabbit anti-GOT2 (NBP1-80521; Novus) and anti-OGDHL (NBP1-91486; Novus) antibodies. Proteins were separated by 10% SDS-PAGE and transferred to a polyvinylidene fluoride membrane. The membrane was blocked and then incubated with a 1:2,000 or a 1:1,000 dilution of GOT2 and OGDHL, respectively, following the manufacturer's instructions. Equal protein loading was assessed using a 1:12,000 dilution of monoclonal anti–β-actin mouse antibody (A5441, Sigma-Aldrich).

Published OnlineFirst July 18, 2017; DOI: 10.1158/1078-0432.CCR-16-2250

Liquid chromatographic tandem-mass spectrometric determination of metabolites

Fresh frozen or FFPE tumor tissue (5–10 mg) from available selected cases and from 15 controls, was immersed in 500 μL LC/MS grade methanol containing isotope-labeled internal standards and processes as previously described (11). For cell cultures, 500,000 cells were cultured, washed 4 times with PBS and extracted in methanol containing isotope-labeled internal standards. Analysis of metabolites was carried out using an AB Sciex 5500 QTRAP mass spectrometer coupled to an Acquity ultra–high-performance liquid chromatographic system (Waters), as previously described (11).

Results

Clinical and molecular features of cases showing downregulation and methylation of RBP1

Fourteen out of the 49 tumors analyzed by qPCR showed low (lower than 15 RU) or almost no RBP1 expression levels compared with the remaining 35 assessed tumors and 10 control tumors carrying mutations in PCC/PGL susceptibility genes (Supplementary Fig. S1A). Pyrosequencing analysis confirmed gene methylation as the cause of the *RBP1* downregulation in 11 out of the 14 tumors, and therefore further analysis were focused on these 11 cases. Five of the 11 patients had multiple PCCs/PGLs, one of them suffering also from a gastrointestinal stromal tumor (GIST), and one case showed distant metastases (Table 1). Nine cases showed a positive immunostaining for SDHB that ruled out the presence of SDH gene causal mutations in these patients. Only one H&N PGL developed by the patient who also suffered from GIST tested negative (Supplementary Fig. S1B), suggesting that a hidden SDH gene alteration could account for this patient.

Next-generation sequencing findings

Five missense variants, affecting four genes and detected in three samples, passed the filtering process after excluding variants found at a frequency $>2.471 \times 10^{-5}$ of controls in gnomAD (Table 1). Sanger sequencing was used to validate both the presence of the variants in the corresponding tumor (Fig. 1A), and the presence/absence of the variant in the germline of the patients. All variants were found in the germline of the corresponding patient, with the exception of the c.394C>T *IDH1* somatic mutation. Three variants were predicted to be deleterious and two neutral by PredictSNP (data not shown).

Seven variants (six missense and one frameshift), affecting four genes and found in seven samples, were detected and validated in the extended series of 63 tumors. When we applied the same filtering process to that used for the selected series of tumors, only a novel *IDH3B* truncating mutation remained (Fig. 1B). The variant was found in the germline of a patient with a single non-secreting jugular PGL at age 51 years.

Methylation profiling classified most tumors within the CIMP cluster

Methylomes from 16 tumors (11 selected cases and five SDH gene-mutated controls) were profiled together with methylomes from 13 additional genotyped PCCs/PGLs obtained from GEO. Ten RBP1-downregulated and methylated tumors showed a "CIMP-like" profile similar to that observed for PCC/PGLs carrying SDH gene mutations, whereas only one case clustered with hypomethylated tumors carrying mutations in *NF1*, *RET* or *MAX* (Fig. 1C). When we focused on the methylation status of the Krebs

Table 1. Clinical and genetic findings of studied cases

ID	Tumor_1	Tumor_2	Tumor_3	Tumor_4	Tumor_5	Tumor_6	Tumor_7	Tumor_8	Tumor_9	Tumor_10	Tumor_11
Gene(s) altered	*IDH1*	*GOT2*	*OGDHL*	*PCK2*	–	–	–	–	–	–	–
DNA variant	c.394C>T	c.223T>G	c.357A>T	c.750G>T	c.1742C>T	–	–	–	–	–	–
Protein change	p.Arg132 Cys	p.Tyr75 Asp	p.Glu119Asp	p.Arg250 Ser	p.Ala581 Val	–	–	–	–	–	–
Frequency in gnomAD	Not found	3/246192	2/277174	Not found	2/246224	–	–	–	–	–	–
Frequency in Spaniards[a]	0/816	0/816	0/816	0/816	0/816	–	–	–	–	–	–
PredictSNP	Del	Del	Neutral	Del	–	–	–	–	–	–	–
Methylation cluster	CIMP	CIMP	non-CIMP	CIMP	CIMP	CIMP	non-CIMP	CIMP	CIMP	CIMP	CIMP
SDHB IHC	Positive	Positive	Positive	Negative	Positive	Positive	Positive	Positive	NA	Positive	Positive
Metabolites	H	S/F	S/F	–	–	–	–	–	NA	–	–
Location	TAP	TAP	PCC	H&N	H&N	H&N	H&N	H&N	H&N	H&N	TAP
Biochemical Phenotype	NM	D	NM	NM, D	NS	NM	U	U	NS	NS	NM
Number of tumors	S	M ($n = 9$)	S	M ($n = 3$), GIST	M ($n = 2$)	M ($n = 5$)	S	S	S	S	M ($n = 3$)
Clinical behavior	B	Mg	B	B	B	B	U	B	U	B	B

Abbreviations: B, Benign; D, dopamine; Del, deleterious; GIST, gastrointestinal stromal tumor; H&N, head and neck PGL; H, high hydroxyglutarate levels; M, multiple; Mg, malignant; NA, not available; NM, normetanephrine; NS, predominant secretion not specified; PCC, pheochromocytoma; S/F, high succinate/fumarate ratio; S, single; TAP, thoracic-abdominal PGL; U, unknown.

[a]CIBERER Spanish exome database (http://csvs.babelomics.org/).

Published OnlineFirst July 18, 2017; DOI: 10.1158/1078-0432.CCR-16-2250

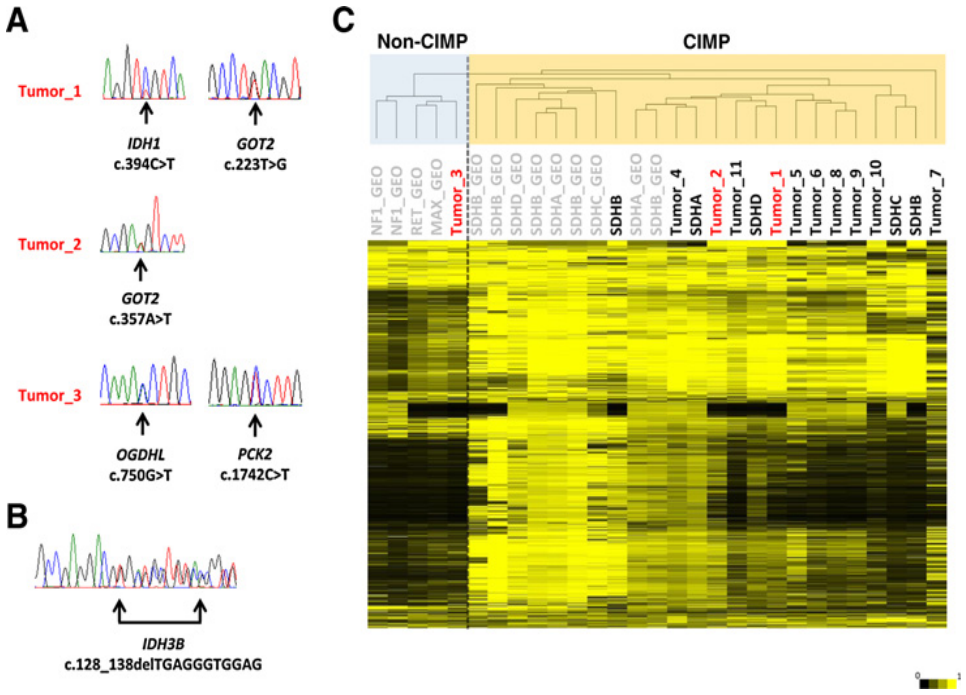

Figure 1.

A, Sanger sequencing validation (in tumor DNA) of targeted exome findings. **B,** Sanger sequencing validation (in tumor DNA) of the *IDH3B* mutation found in the extended series. **C,** Hierarchical clustering of the 11 pheochromocytomas/paragangliomas showing *RBP1* mRNA downregulation, as well as SDH gene-mutated and non-SDH gene-mutated controls. Tumors hybridized and analyzed in the present study are denoted in black letters, whereas tumors downloaded from GEO are denoted in gray. Two clusters were observed and named CIMP (including all SDH gene-mutated controls), and non-CIMP (including all non-SDH gene-mutated controls). Tumor_3: tumor carrying the *OGDHL* and *PCK2* variants; tumor_2: tumor carrying the c.357A>T *GOT2* variant and tumor_1: tumor carrying the *IDH1* and the c.223T>G *GOT2* variants.

cycle genes included in the panel, a tumor (Tumor_4 in Table 1) was found to show significantly higher methylation levels for 11 CpG targets encompassing the SDHC promoter region in 1q23.3 (Fig. 2A). To test for constitutional *SDHC* methylation in the patient, we analyzed DNA obtained from blood and found no silencing of the *SDHC* locus (Supplementary Fig. S1C). Absence of *SDHC* mRNA expression was demonstrated by qPCR for the tumor-exhibiting methylation of the *SDHC* promoter, compared to controls (Fig. 2B). Of note, and as mentioned above, the *SDHC*-methylated tumor was the only one from our series that showed negative SDHB immunohistochemistry. Finally, the methylome from the *IDH3B*-mutated tumor also showed a "CIMP-like" profile (data not shown), further supported by a negative 5-hmC immunohistochemistry (Supplementary Fig. S1D).

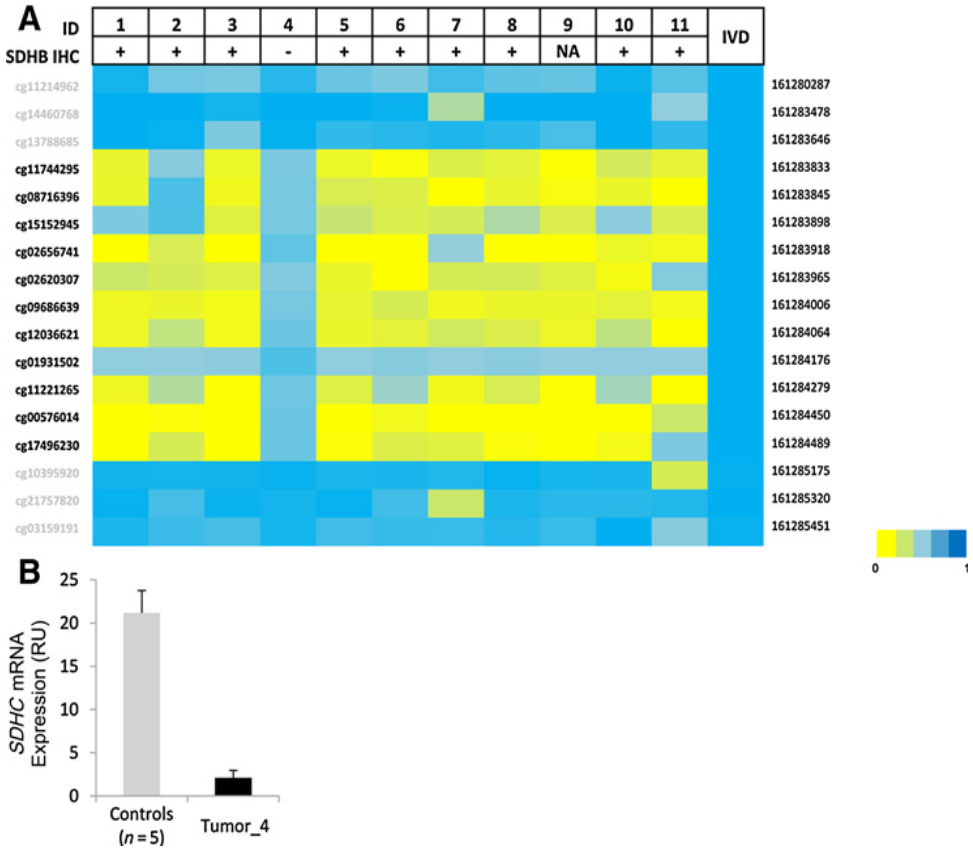

Figure 2.

A, DNA methylation (M_values) for 17 CpG island probes located within the *SDHC* locus in the 11 analyzed tumors, compared with IVD (*in vitro* methylated DNA). The results of the immunostaining for SDHB (SDHB IHC) are also represented. NA: not available. **B,** mRNA expression of *SDHC* in the *SDHC*-methylated tumor (tumor_4) compared with controls ($n = 5$). Error bars represent standard deviations.

Published OnlineFirst July 18, 2017; DOI: 10.1158/1078-0432.CCR-16-2250

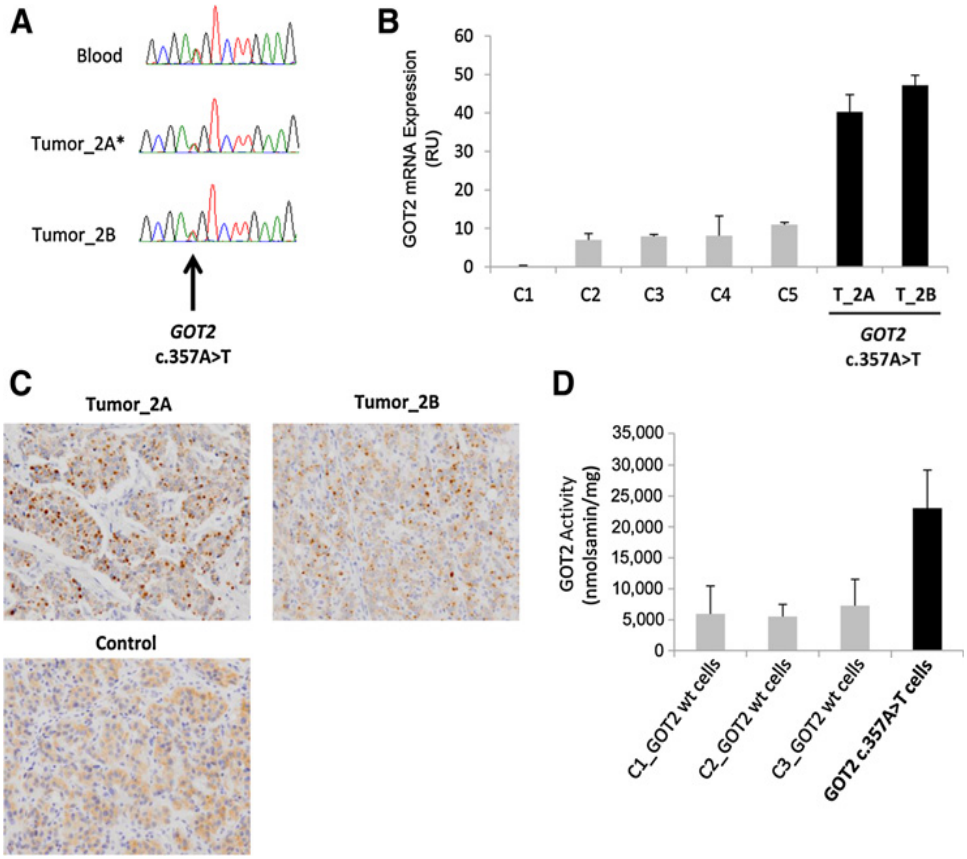

Figure 3.

A, *GOT2* c.357A>T variant in the germline and in two tumors from the patient revealed by Sanger sequencing. The asterisk marks the tumor subjected to exome sequencing. **B,** GOT2 mRNA expression in two tumors (tumor_2A and tumor_2B) carrying the *GOT2* c.357A>T variant, compared with controls (C1–C5). Expression level was normalized to β-actin (ACTB) and presented as mean and standard deviation ($n \geq 3$). Error bars represent standard deviations. **C,** Immunohistochemical staining of GOT2 in two tumors carrying the *GOT2* c.357A>T variant and in one control with WT-GOT2. Cytoplasmic aggregates were observed only in *GOT2*-mutated tumors. **D,** GOT2 activity measured in lymphoblastic *GOT2*-mutated (c.357A>T) and non-mutated cells (C1–C3).

Higher GOT2 expression and activity in tissues carrying the c.357A>T mutation

Because we found two different variants in *GOT2* in two different cases, and both tumors were grouped within the "CIMP-like" cluster, we assessed the expression of the gene in the tumors. Two available tumors from the patient carrying the *GOT2* c.357A>T variant (Fig. 3A) showed a significantly higher GOT2 mRNA expression (Fig. 3B), as well as a granular cytoplasmic differential immunostaining, compared with controls (Fig. 3C). Tumor_1 that carried the other *GOT2* variant, c.223T>G, showed normal GOT2 expression. EBV-immortalized lymphoblastoid cells carrying the c.357A>T GOT2 mutation exhibited significantly higher GOT2 enzymatic activity compared with three GOT2–wild-type lymphoblastoid cell lines (Fig. 3D).

Tumoral metabolite ratios

Liquid chromatographic tandem-mass spectrometric was applied to all available tissues to assess whether the tumors carrying the identified variants showed significant alterations in the metabolites of the Krebs cycle. Amongst the 10 cases tested (Tumor_9 could not be analyzed) only the tumors carrying the *GOT2* c.357A>T variant (Tumor_2) and the *OGDHL*/*PCK2* variations (Tumor_3), showed a high succinate/fumarate ratio (Fig. 4A) similar to that observed for SDH gene-mutated tumors. This abnormal succinate/fumarate ratio was not associated with SDH alterations in either of the two tumors, because they resulted positive for SDHB immunohistochemistry (Table 1). In addition, the tumor carrying the *IDH1* c.394C>T mutation, showed an elevated hydroxyglutarate/isocitrate ratio compared to controls ($n = 8$; Fig. 4B), which is consistent with the presence of pathological *IDH1/2* mutations. None of the other tumors (those not carrying these variants) had altered metabolite ratios. The *IDH3B*-mutated tumor showed an elevated α-ketoglutarate/isocitrate ratio compared to controls (Fig. 4C).

c.357A>T GOT2 introduction in GOT2 KD cells increased metabolite ratios

To demonstrate the relevance of the c.357A>T variant in GOT2 enzymatic activity, we first silenced GOT2 (GOT2 KD) by shRNA in HeLa cells (Supplementary Fig. S2A). Subsequent transient introduction of GOT2 cDNA carrying the variant c.357A>T in GOT2 KD cells triggered a slight increase in the succinate/fumarate ratio and a significant increase of α-ketoglutarate/citrate and aspartate/glutamate ratios, compared with GOT2 KD cells transfected with wild-type GOT2 cDNA (Fig. 4D and E). Moreover, the growth rate of GOT2 KD cells transfected with c.357A>T-GOT2 was higher (although not significantly so) than that observed for GOT2 KD cells transfected with WT-GOT2, and significantly higher than that observed for KD cells (Supplementary Fig. S2B). Furthermore, GOT2 KD cells transfected with the c.223T>G variant showed aspartate/glutamate ratios similar to the control (Supplementary Fig. S3A).

Depletion of OGDHL had no effect on metabolite ratios

No alteration in the succinate/fumarate ratio was observed after silencing *OGDHL* in HeLa cells by shRNA, or after transient introduction of the c.750G>T variant in KD cells (Supplementary Fig. S3B). Silencing *PCK2* in HeLa cells was not possible either by shRNA or CRISPR-Cas9 technologies (data not shown).

Published OnlineFirst July 18, 2017; DOI: 10.1158/1078-0432.CCR-16-2250

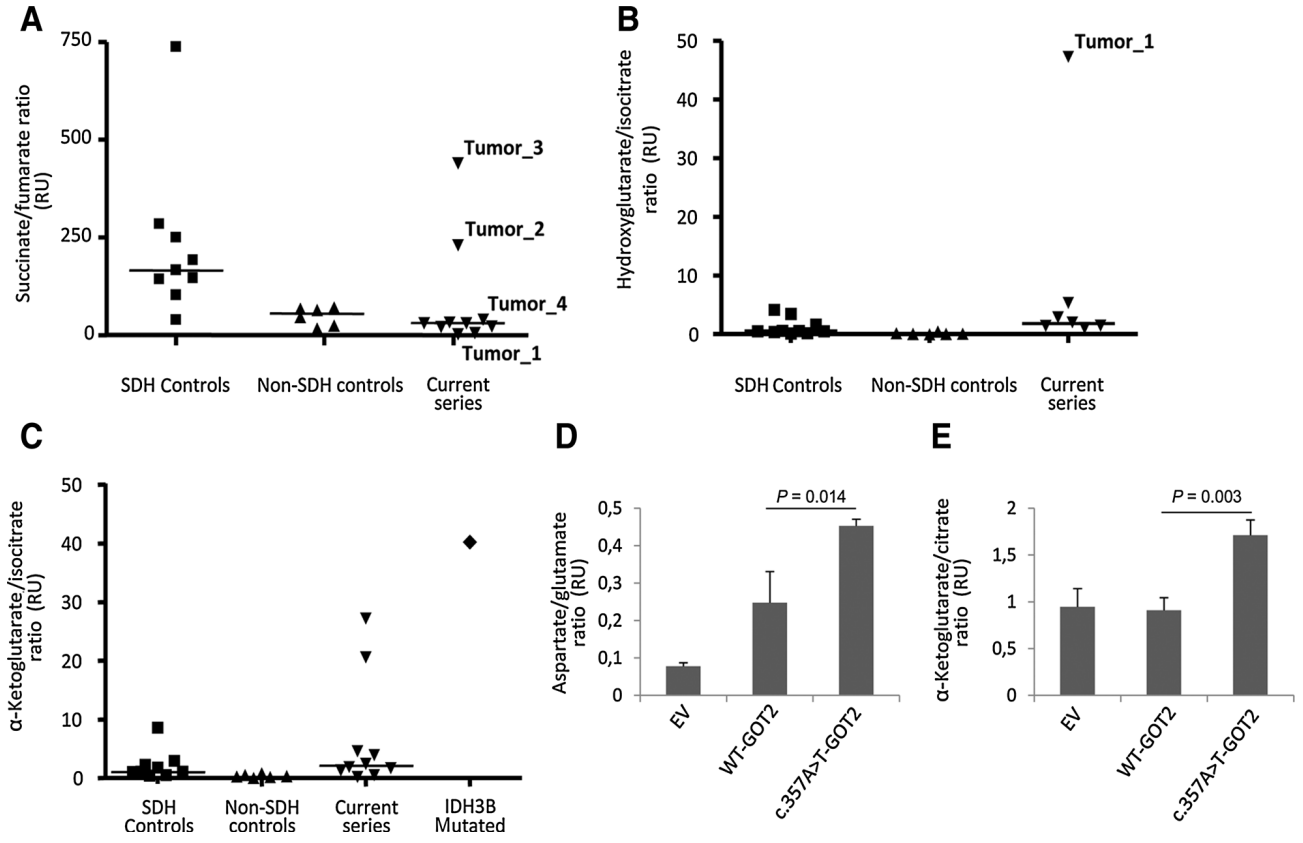

Figure 4.

A, Succinate/fumarate ratios assessed by liquid chromatographic tandem-mass spectrometry (LC/MS) in 13 tumors assayed in the present study compared with SDH gene-mutated ($n = 9$) and non-SDH gene-mutated controls ($n = 6$). Tumor_1: tumor carrying the IDH1 and the c.223T>G GOT2 variants; tumor_2: tumor carrying the c.357A>T GOT2 variant; tumor_3: tumor carrying the OGDHL and PCK2 variants; tumor_4: tumor showing DNA methylation of SDHC. The black lines represent medians. **B,** Hydroxyglutarate/isocitrate ratios assessed by LC/MS in nine tumors from the present study compared with SDH gene-mutated ($n = 9$) and non-SDH gene-mutated controls ($n = 6$). The IDH1-mutated tumor is indicated. The black lines represent medians. **C,** α-Ketoglutarate/isocitrate ratios assessed by LC/MS in the *IDH3B*-mutated tumor compared with 10 tumors from the present study, nine SDH gene-mutated cases and six non-SDH gene-mutated controls. The black lines represent medians. **D,** Aspartate/glutamate ratios assessed by LC-MS in GOT2 KD Hela cells transfected with empty vector (EV), GOT2 wild-type (WT) cDNA, and GOT2- c.357A>T cDNA. The ratios were reported as mean and standard deviation ($n = 3$). Error bars represent standard deviations. A *t* test was applied to test for differences between GOT WT and GOT2- c.357A>T-transfected cells. **E,** α-Ketoglutarate/citrate ratios assessed by LC-MS in GOT2 KD Hela cells transfected with EV, GOT2 WT cDNA, and GOT2- c.357A>T cDNA. The ratios were reported as mean and standard deviation ($n = 3$). Error bars represent standard deviations. A *t* test was applied to test for differences between GOT WT and GOT2- c.357A>T-transfected cells.

Discussion

PCC/PGL are paradigmatic for illustrating the importance of human genetics in cancer, not only because of the high degree of heritability of the tumors and involvement of a large number of genes (more than 13), but also because these tumors are the main manifestation of genetic alterations in *SDHD*. *SDHD* is a gene that went down in history as the first metabolic gene involved in the Krebs cycle and the respiratory chain whose mutations were associated with the development of cancer. Since then, mutations affecting six additional genes involved in the Krebs cycle energy pathway have been associated with the development of PCC/PGL and with a particular hypermethylator phenotype. Herein, we describe how the selection of samples based on the expression of a methylation marker, identifies PCCs/PGLs harboring candidate variants affecting other Krebs cycle-related genes. These results highlight both the relevance of this pathway in PCC/PGL development and the need for marker-based selection of samples for the discovery of cancer susceptibility genes to avoid genetic heterogeneity.

To date, only two studies have focused on the involvement of *IDH1/2* in PCC/PGL development, yielding 1/365 and 0/104 tumors carrying a pathogenic mutation affecting *IDH1* (23). Another *IDH1* mutation has also been identified in one PGL among 173 samples from The Cancer Genome Atlas (http://www.cbioportal.org/index.do; ref. 24), which further confirms the low frequency of alterations affecting this gene in PCC/PGL. The two mentioned *IDH1* mutations, as well as the one reported herein, affect the same amino acid (p.Arg132Cys) and were found in older patients (>61 years) with PGLs, which stresses the relevance of this cancer-prone alteration to extra-adrenal tumors. The accumulation of hydroxyglutarate observed in the tumor, and the absence of any other somatic or germline alteration in the known PCC/PGL susceptibility genes, confirmed the driver role of the *IDH1* mutation in this case and explains its CIMP profile.

Glutamic-oxaloacetic transaminase 2 (GOT2) is a mitochondrial enzyme that plays a role in amino acid metabolism and the urea and Krebs cycles. GOT2 converts oxaloacetate into aspartate by transamination, with the consequent conversion of glutamate

Published OnlineFirst July 18, 2017; DOI: 10.1158/1078-0432.CCR-16-2250

to α-ketoglutarate. In SDH-deficient cells, glutamine and glutamate are used to provide metabolic intermediates to the truncated Krebs cycle, after conversion to α-ketoglutarate by GOT2 or GLUD1 enzymes (36, 37). It has been recently described that lysine acetylation of GOT2 enhances the protein association between GOT2 and MDH2, stimulating the malate shuttle activity and thus promoting pancreatic cell proliferation and tumor growth *in vivo* (38). Mutant *KRAS* promotes the reprogramming of glutamine metabolism in pancreatic cancer through GOT1/GOT2-mediated transamination pathway (39).

Both the expression of GOT2 and its enzymatic activity found in c.357A>T-mutated tissues suggest an activating role of the mutation. Moreover, the high succinate/fumarate ratio observed in the *GOT2*-mutated tumor, as well as the slight increment of α-ketoglutarate compared to controls, could be explained by an excess of this latter metabolite due to the higher enzymatic activity of GOT2. Introduction of the mutated p.Glu119Asp variant, but not p.Tyr75Asp, in GOT2 KD HeLa cells recapitulates the accumulation of metabolites observed in tumors carrying the variant, and increases cell proliferation. Interestingly, GOT2 knockdown led to an accumulation of glutamate as well as to significantly lower levels of Krebs cycle metabolites fumarate and malate in melanoma cells (40). Thus, it seems plausible that a higher activity of GOT2 could lead to an increment of anaplerotic incorporation of α-ketoglutarate to the Krebs cycle, and hence to the oncogenic accumulation of succinate. The absence of *GOT2* variants in unselected cases suggests their prevalence is low in PCC/PGL patients, which has also reported for other TCA-related genes (11, 41).

The presence of aberrant hypermethylation of *SDHC* has been reported to be a novel mechanism of tumor development in Carney triad (PGL, GIST, and pulmonary chondroma) patients (42). Moreover, epimutations in *SDHC* have also been reported in hypermethylated SDH-deficient GISTs (43), mainly associated with Carney triad. Interestingly, in both studies the aberrant methylation of *SDHC* occurred exclusively in females. Recently, epigenetic mutation of the SDHC promoter has been found in another female with two PGLs (44). As far as we know, the case reported in the present study is the first example of a *SDHC* epimutation affecting a patient with Carney-Stratakis syndrome (co-occurrence of PGL and GIST). Regarding the mechanism involved in silencing *SDHC*, a potential role of sex chromosome or hormone biology has been proposed (43). The patient described herein is a female, and this explanation could also account for this case. The complete absence of SDHC expression in the tumor suggested that, in addition to the observed hemimethylation, a second hit affecting the gene was also present. High-density SNP genotyping performed in the tumor showing *SDHC* methylation revealed no alterations affecting chromosome 1, where *SDHC* is located (data not shown). Furthermore, the tumor had a normal DNA copy-number profile, which is consistent with previous findings describing that DNA copy-number changes are infrequent in parasympathetic PGLs (45). The absence of high succinate/fumarate ratio in this tumor could be due to the lower reliability of measurements of these metabolites in H&N PGLs (46), presumably due to a higher content of stromal cells diluting the signal from tumor cells. The absence of aberrant hypermethylation in known susceptibility genes in the other tumors analyzed (Supplementary Fig. S4) suggests that this mechanism is extremely rare in PCC/PGL.

The altered succinate/fumarate ratio observed in a tumor carrying two rare variants in *OGDHL* and *PCK2* suggested that either gene could be involved in the disease. Interestingly, the promoter of *OGDHL* is differentially methylated in different tissue types, and it is thought that inactivation of *OGDHL* can contribute to cervical tumorigenesis (47). On the other hand, the mitochondrial phosphoenolpyruvate carboxykinase (PCK2) is an enzyme involved in gluconeogenesis, converting oxaloacetate into phosphoenolpyruvate, which also has a cataplerotic function, maintaining metabolic flux through the Krebs cycle by removing excess oxaloacetate. It has been reported that PCK2 activation mediates an adaptive response to glucose depletion in lung cancer (48). Although we have ruled out a link between *OGDHL* depletion and an altered succinate/fumarate ratio, we were not able to demonstrate the relevance of *PCK2* in PCC/PGL development.

Homozygous loss-of-function mutations in *IDH3B* have been found in two families with retinitis pigmentosa (49), and somatic mutations in *IDH3B* have been recently found in acute myelogenous leukemia (50). *IDH3B* encodes the beta subunit of NAD-specific isocitrate dehydrogenase 3 (IDH3), which is involved in the oxidation of isocitrate to α-ketoglutarate in the Krebs cycle. It has been demonstrated that IDH3 activity in lysates from cells carrying heterozygous truncating *IDH3B* mutations was only 24% of that observed in normal controls (49). In addition, the altered α-ketoglutarate/isocitrate ratio detected in the tumor carrying the truncating mutation, and the associated CIMP-like profile further suggest a causative role for this variant in PGL development.

In summary, based on our selection of cases for exome sequencing of Krebs cycle genes and whole-genome DNA methylation assessment, we have identified rare pathological alterations in known PCC/PGL susceptibility genes (*SDHC* and *IDH1*), and two new candidate genes possibly involved in the hereditary predisposition (*GOT2* and *IDH3B*). This study further strengthens the evidence for the relevance of the Krebs cycle in the development of PCC and PGL, and points to other enzymes involved in metabolite exchange between mitochondria and cytosol.

Disclosure of Potential Conflicts of Interest

No potential conflicts of interest were disclosed.

Authors' Contributions

Conception and design: L. Remacha, M. Robledo, A. Cascón

Development of methodology: L. Remacha, I. Comino-Méndez, M. Currás-Freixes, R. Letón, R. Torres-Perez, S. Jiménez, L. Maestre, J. Satrústegui, G. Eisenhofer, A. Cascón

Acquisition of data (provided animals, acquired and managed patients, provided facilities, etc.): S. Richter, L. Contreras, A. Galarreta, E. Honrado, S. Moran, M. Esteller, G. Eisenhofer, M. Robledo

Analysis and interpretation of data (e.g., statistical analysis, biostatistics, computational analysis): I. Comino-Méndez, S. Richter, L. Contreras, G. Pita, A. Galarreta, R. Torres-Perez, M. Esteller, J. Satrústegui, G. Eisenhofer, A. Cascón

Writing, review, and/or revision of the manuscript: L. Remacha, S. Richter, G. Eisenhofer, M. Robledo, A. Cascón

Administrative, technical, or material support (i.e., reporting or organizing data, constructing databases): I. Comino-Méndez, M. Currás-Freixes, M. Robledo

Study supervision: A. Cascón

Grant Support

This work was supported by the Fondo de Investigaciones Sanitarias project PI15/00783, FEDER 2014-2020 (to A. Cascón) and the Deutsche Forschungsgemeinschaft (grant RI 2684/1-1; to S. Richter). CEGEN-PRB2-ISCIII is supported by grant PT13/0001, ISCIII-SGEFI/FEDER.

Received September 8, 2016; revised May 22, 2017; accepted July 12, 2017; published OnlineFirst July 18, 2017.

Published OnlineFirst July 18, 2017; DOI: 10.1158/1078-0432.CCR-16-2250

References

1. Dahia PL. Pheochromocytoma and paraganglioma pathogenesis: learning from genetic heterogeneity. Nat Rev Cancer 2014;14:108–19.
2. Astuti D, Latif F, Dallol A, Dahia PL, Douglas F, George E, et al. Gene mutations in the succinate dehydrogenase subunit SDHB cause susceptibility to familial pheochromocytoma and to familial paraganglioma. Am J Hum Genet 2001;69:49–54.
3. Burnichon N, Briere JJ, Libe R, Vescovo L, Riviere J, Tissier F, et al. SDHA is a tumor suppressor gene causing paraganglioma. Hum Mol Genet 2010;19: 3011–20.
4. Baysal BE, Ferrell RE, Willett-Brozick JE, Lawrence EC, Myssiorek D, Bosch A, et al. Mutations in SDHD, a mitochondrial complex II gene, in hereditary paraganglioma. Science 2000;287:848–51.
5. Latif F, Tory K, Gnarra J, Yao M, Duh FM, Orcutt ML, et al. Identification of the von Hippel-Lindau disease tumor suppressor gene. Science 1993; 260:1317–20.
6. Mulligan LM, Kwok JB, Healey CS, Elsdon MJ, Eng C, Gardner E, et al. Germ-line mutations of the RET proto-oncogene in multiple endocrine neoplasia type 2A. Nature 1993;363:458–60.
7. Qin Y, Yao L, King EE, Buddavarapu K, Lenci RE, Chocron ES, et al. Germline mutations in TMEM127 confer susceptibility to pheochromocytoma. Nat Genet 2010;42:229–33.
8. Niemann S, Muller U. Mutations in SDHC cause autosomal dominant paraganglioma, type 3. Nat Genet 2000;26:268–70.
9. Wallace MR, Marchuk DA, Andersen LB, Letcher R, Odeh HM, Saulino AM, et al. Type 1 neurofibromatosis gene: identification of a large transcript disrupted in three NF1 patients. Science 1990;249:181–6.
10. Hao HX, Khalimonchuk O, Schraders M, Dephoure N, Bayley JP, Kunst H, et al. SDH5, a gene required for flavination of succinate dehydrogenase, is mutated in paraganglioma. Science 2009;325:1139–42.
11. Cascon A, Comino-Mendez I, Curras-Freixes M, de Cubas AA, Contreras L, Richter S, et al. Whole-exome sequencing identifies MDH2 as a new familial paraganglioma gene. J Natl Cancer Inst 2015;107:pii: djv053.
12. Letouze E, Martinelli C, Loriot C, Burnichon N, Abermil N, Ottolenghi C, et al. SDH mutations establish a hypermethylator phenotype in paraganglioma. Cancer Cell 2013;23:739–52.
13. Yang C, Zhuang Z, Fliedner SM, Shankavaram U, Sun MG, Bullova P, et al. Germ-line PHD1 and PHD2 mutations detected in patients with pheochromocytoma/paraganglioma-polycythemia. J Mol Med 2015;93:93–104.
14. Crona J, Delgado Verdugo A, Maharjan R, Stalberg P, Granberg D, Hellman P, et al. Somatic mutations in H-RAS in sporadic pheochromocytoma and paraganglioma identified by exome sequencing. J Clin Endocrinol Metab 2013;98:E1266–71.
15. Zhuang Z, Yang C, Lorenzo F, Merino M, Fojo T, Kebebew E, et al. Somatic HIF2A gain-of-function mutations in paraganglioma with polycythemia. N Engl J Med 2012;367:922–30.
16. Curras-Freixes M, Inglada-Perez L, Mancikova V, Montero-Conde C, Leton R, Comino-Mendez I, et al. Recommendations for somatic and germline genetic testing of single pheochromocytoma and paraganglioma based on findings from a series of 329 patients. J Med Genet 2015;52:647–56.
17. Comino-Mendez I, Gracia-Aznarez FJ, Schiavi F, Landa I, Leandro-Garcia LJ, Leton R, et al. Exome sequencing identifies MAX mutations as a cause of hereditary pheochromocytoma. Nat Genet 2011;43:663–7.
18. Dahia PL, Ross KN, Wright ME, Hayashida CY, Santagata S, Barontini M, et al. A HIF1alpha regulatory loop links hypoxia and mitochondrial signals in pheochromocytomas. PLoS Genet 2005;1:72–80.
19. Lopez-Jimenez E, Gomez-Lopez G, Leandro-Garcia LJ, Munoz I, Schiavi F, Montero-Conde C, et al. Research resource: Transcriptional profiling reveals different pseudohypoxic signatures in SDHB and VHL-related pheochromocytomas. Mol Endocrinol 2010;24:2382–91.
20. Xiao M, Yang H, Xu W, Ma S, Lin H, Zhu H, et al. Inhibition of alpha-KG-dependent histone and DNA demethylases by fumarate and succinate that are accumulated in mutations of FH and SDH tumor suppressors. Genes Dev 2012;26:1326–38.
21. Turcan S, Rohle D, Goenka A, Walsh LA, Fang F, Yilmaz E, et al. IDH1 mutation is sufficient to establish the glioma hypermethylator phenotype. Nature 2012;483:479–83.
22. Dang L, White DW, Gross S, Bennett BD, Bittinger MA, Driggers EM, et al. Cancer-associated IDH1 mutations produce 2-hydroxyglutarate. Nature 2009;462:739–44.
23. Gaal J, Burnichon N, Korpershoek E, Roncelin I, Bertherat J, Plouin PF, et al. Isocitrate dehydrogenase mutations are rare in pheochromocytomas and paragangliomas. J Clin Endocrinol Metab 2010;95:1274–8.
24. Fishbein L, Leshchiner I, Walter V, Danilova L, Robertson AG, Johnson AR, et al. Comprehensive molecular characterization of pheochromocytoma and paraganglioma. Cancer Cell 2017;31:181–93.
25. Chou AP, Chowdhury R, Li S, Chen W, Kim AJ, Piccioni DE, et al. Identification of retinol binding protein 1 promoter hypermethylation in isocitrate dehydrogenase 1 and 2 mutant gliomas. J Natl Cancer Inst 2012;104:1458–69.
26. van Nederveen FH, Gaal J, Favier J, Korpershoek E, Oldenburg RA, de Bruyn EM, et al. An immunohistochemical procedure to detect patients with paraganglioma and phaeochromocytoma with germline SDHB, SDHC, or SDHD gene mutations: a retrospective and prospective analysis. Lancet Oncol 2009;10:764–71.
27. Gill AJ, Benn DE, Chou A, Clarkson A, Muljono A, Meyer-Rochow GY, et al. Immunohistochemistry for SDHB triages genetic testing of SDHB, SDHC, and SDHD in paraganglioma-pheochromocytoma syndromes. Hum Pathol 2010;41:805–14.
28. Livak KJ, Schmittgen TD. Analysis of relative gene expression data using real-time quantitative PCR and the 2(-Delta Delta C(T)) Method. Methods 2001;25:402–8.
29. Schiavi F, Milne RL, Anda E, Blay P, Castellano M, Opocher G, et al. Are we overestimating the penetrance of mutations in SDHB? Hum Mutat 2010;31:761–2.
30. Bendl J, Stourac J, Salanda O, Pavelka A, Wieben ED, Zendulka J, et al. PredictSNP: robust and accurate consensus classifier for prediction of disease-related mutations. PLoS Comput Biol 2014;10:e1003440.
31. Bibikova M, Le J, Barnes B, Saedinia-Melnyk S, Zhou L, Shen R, et al. Genome-wide DNA methylation profiling using Infinium(R) assay. Epigenomics 2009;1:177–200.
32. Trounce IA, Kim YL, Jun AS, Wallace DC. Assessment of mitochondrial oxidative phosphorylation in patient muscle biopsies, lymphoblasts, and transmitochondrial cell lines. Methods Enzymol 1996;264: 484–509.
33. Bergmeyer HU, Bergmeyer J, Grassl M. Methods of enzymatic analysis / V. 3, Enzymes 1 oxidoreductases, transferases. 3rd ed. Weinheim: Verlag Chemie; 1983.
34. Bergmeyer HU, Bergmeyer J, Grabl M. Methods of enzymatic analysis. IV, Enzymes 2,. Esterases, glycosidases, lyases, ligases. 3rd ed. Weinheim [etc.]: Verlagchemie; 1984.
35. Ausubel FM. Current protocols in molecular biology. New York: Greene Pub. Associates; Wiley-Interscience; 1988. p. v. (loose-leaf).
36. Saxena N, Maio N, Crooks DR, Ricketts CJ, Yang Y, Wei MH, et al. SDHB-deficient cancers: the role of mutations that impair iron sulfur cluster delivery. J Natl Cancer Inst 2016;108:djv287.
37. Lussey-Lepoutre C, Hollinshead KE, Ludwig C, Menara M, Morin A, Castro-Vega LJ, et al. Loss of succinate dehydrogenase activity results in dependency on pyruvate carboxylation for cellular anabolism. Nat Commun 2015;6:8784.
38. Yang H, Zhou L, Shi Q, Zhao Y, Lin H, Zhang M, et al. SIRT3-dependent GOT2 acetylation status affects the malate-aspartate NADH shuttle activity and pancreatic tumor growth. EMBO J 2015;34:1110–25.
39. Son J, Lyssiotis CA, Ying H, Wang X, Hua S, Ligorio M, et al. Glutamine supports pancreatic cancer growth through a KRAS-regulated metabolic pathway. Nature 2013;496:101–5.
40. Ratnikov B, Aza-Blanc P, Ronai ZA, Smith JW, Osterman AL, Scott DA. Glutamate and asparagine cataplerosis underlie glutamine addiction in melanoma. Oncotarget 2015;6:7379–89.
41. Bayley JP, Kunst HP, Cascon A, Sampietro ML, Gaal J, Korpershoek E, et al. SDHAF2 mutations in familial and sporadic paraganglioma and phaeochromocytoma. Lancet Oncol 2010;11:366–72.
42. Haller F, Moskalev EA, Faucz FR, Barthelmess S, Wiemann S, Bieg M, et al. Aberrant DNA hypermethylation of SDHC: a novel mechanism of tumor development in Carney triad. Endocr Relat Cancer 2014;21: 567–77.
43. Killian JK, Miettinen M, Walker RL, Wang Y, Zhu YJ, Waterfall JJ, et al. Recurrent epimutation of SDHC in gastrointestinal stromal tumors. Sci Transl Med 2014;6:268ra177.

Published OnlineFirst July 18, 2017; DOI: 10.1158/1078-0432.CCR-16-2250

44. Richter S, Klink B, Nacke B, deCubas AA, Mangelis A, Rapizzi E, et al. Epigenetic mutation of the succinate dehydrogenase C promoter in a patient with two paragangliomas. J Clin Endocrinol Metab 2016:101: 359–63.
45. Dannenberg H, de Krijger RR, Zhao J, Speel EJ, Saremaslani P, Dinjens WN, et al. Differential loss of chromosome 11q in familial and sporadic parasympathetic paragangliomas detected by comparative genomic hybridization. Am J Pathol 2001;158:1937–42.
46. Richter S, Peitzsch M, Rapizzi E, Lenders JW, Qin N, de Cubas AA, et al. Krebs cycle metabolite profiling for identification and stratification of pheochromocytomas/paragangliomas due to succinate dehydrogenase deficiency. J Clin Endocrinol Metab 2014;99:3903–11.
47. Sen T, Sen N, Noordhuis MG, Ravi R, Wu TC, Ha PK, et al. OGDHL is a modifier of AKT-dependent signaling and NF-kappaB function. PLoS One 2012;7:e48770.
48. Leithner K, Hrzenjak A, Trotzmuller M, Moustafa T, Kofeler HC, Wohlkoenig C, et al. PCK2 activation mediates an adaptive response to glucose depletion in lung cancer. Oncogene 2015;34:1044–50.
49. Hartong DT, Dange M, McGee TL, Berson EL, Dryja TP, Colman RF. Insights from retinitis pigmentosa into the roles of isocitrate dehydrogenases in the Krebs cycle. Nat Genet 2008;40:1230–4.
50. Garg M, Nagata Y, Kanojia D, Mayakonda A, Yoshida K, Haridas Keloth S, et al. Profiling of somatic mutations in acute myeloid leukemia with FLT3-ITD at diagnosis and relapse. Blood 2015;126:2491–501.

SUPPLEMENTARY DATA

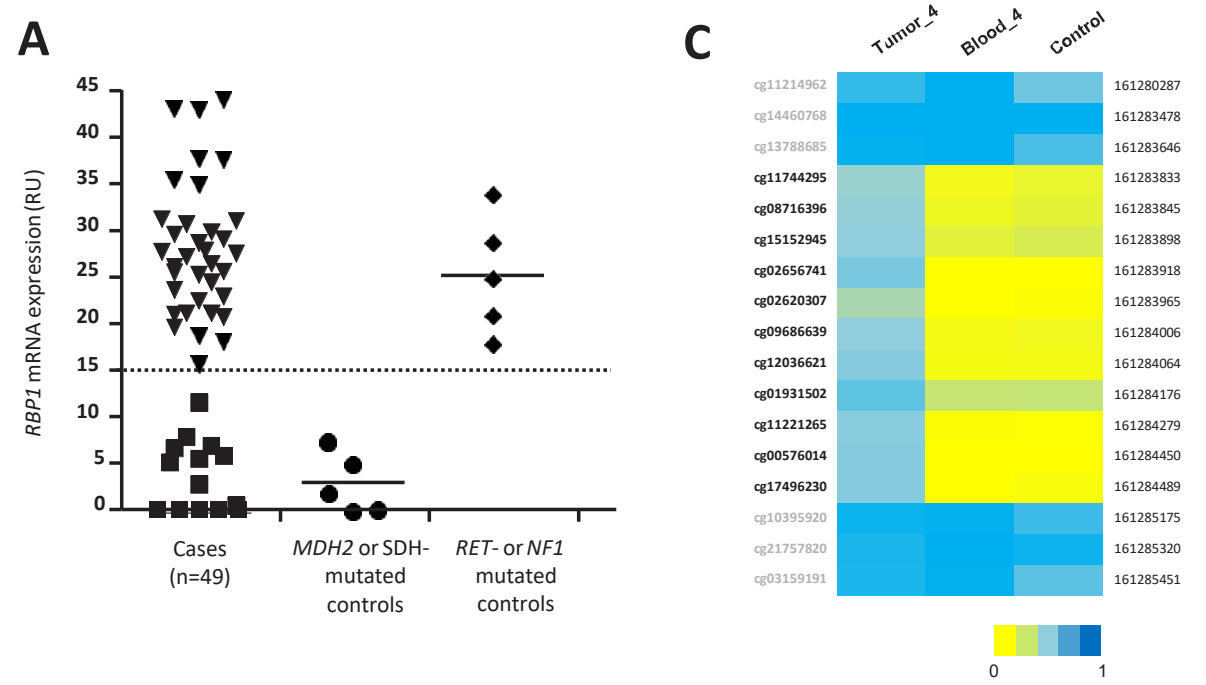

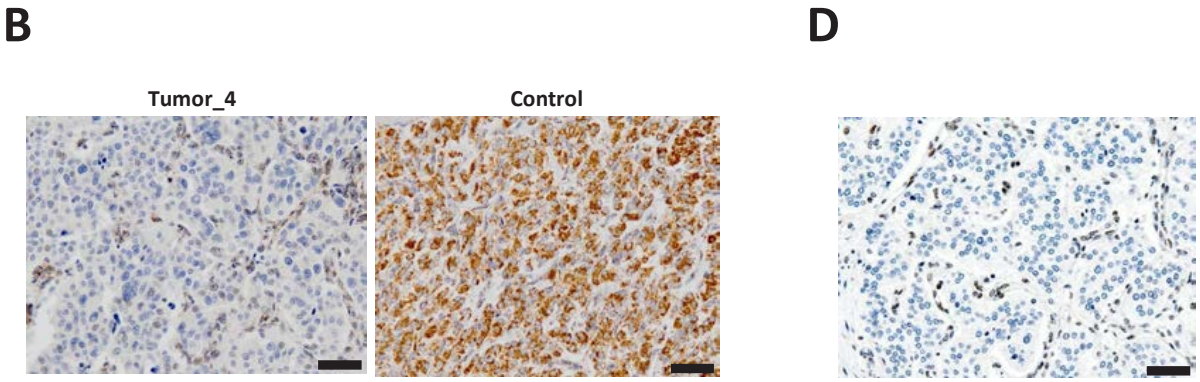

Supplementary Figure S1. (**A**) Quantitative PCR analysis of RBP1 expression of the 49 tumors included in the study compared to controls comprising five tumors carrying mutation in Krebs cycle genes and five cases carrying mutations in *RET* or *NF1*. RU: relative units. (**B**) SDHB immunohistochemistry of tumor_4 compared to a positive control tumor carrying a non-SDH mutation. The scale bars represent 50µm. (**C**) Representation of DNA methylation (M_values) of the CpG island probes located within the *SDHC* locus of tumor_4 compared to a blood sample from the same patient and a control DNA. (**D**) Immunohistochemical staining of 5-hmC in *IDH3B*-mutated tumor. Nuclear 5-hmC was observed only in sustentacular and some stromal cells. The scale bar represents 50µm.

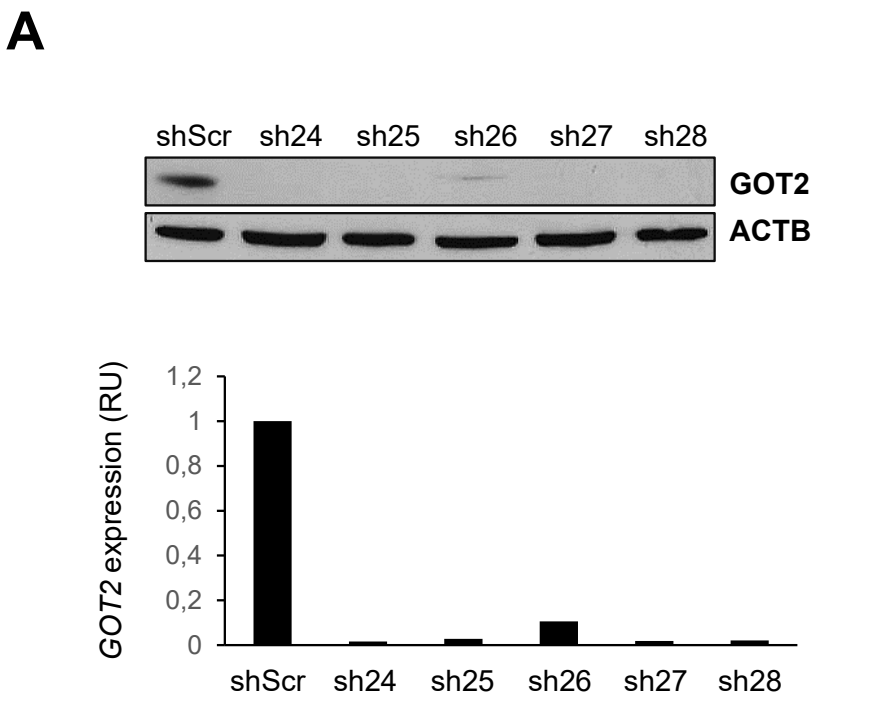

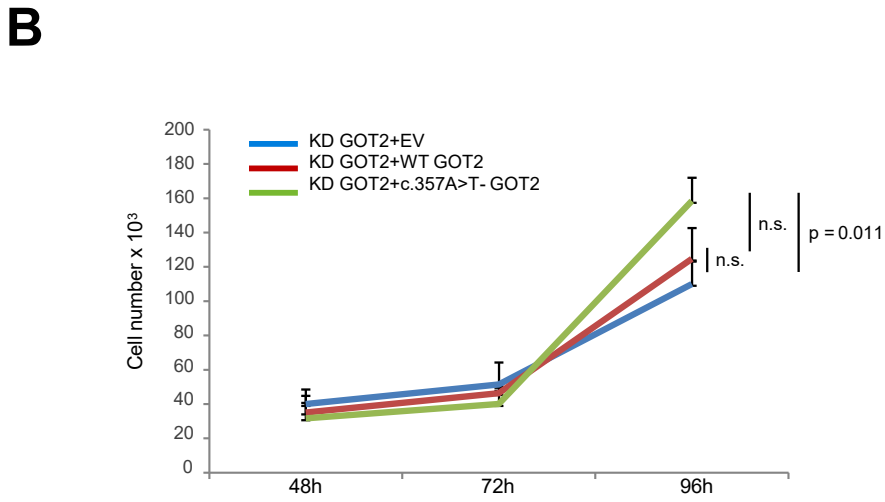

Supplementary Figure S2. (**A**) GOT2 western blot of HeLa cells stably silenced for GOT2 expression by shRNA transfection compared to non-silenced scrambled (Scr) control cells. β-actin was used as a loading control. (**B**) Number of GOT2 KD HeLa cells after transfection with empty vector (EV), GOT2- WT cDNA, and GOT2- c.357A>T. Cells were seeded into 12-well plates and incubated for various times, as indicated. The counts are reported as means (n=3). A t-test was applied to test for differences. n.s.: not significant.

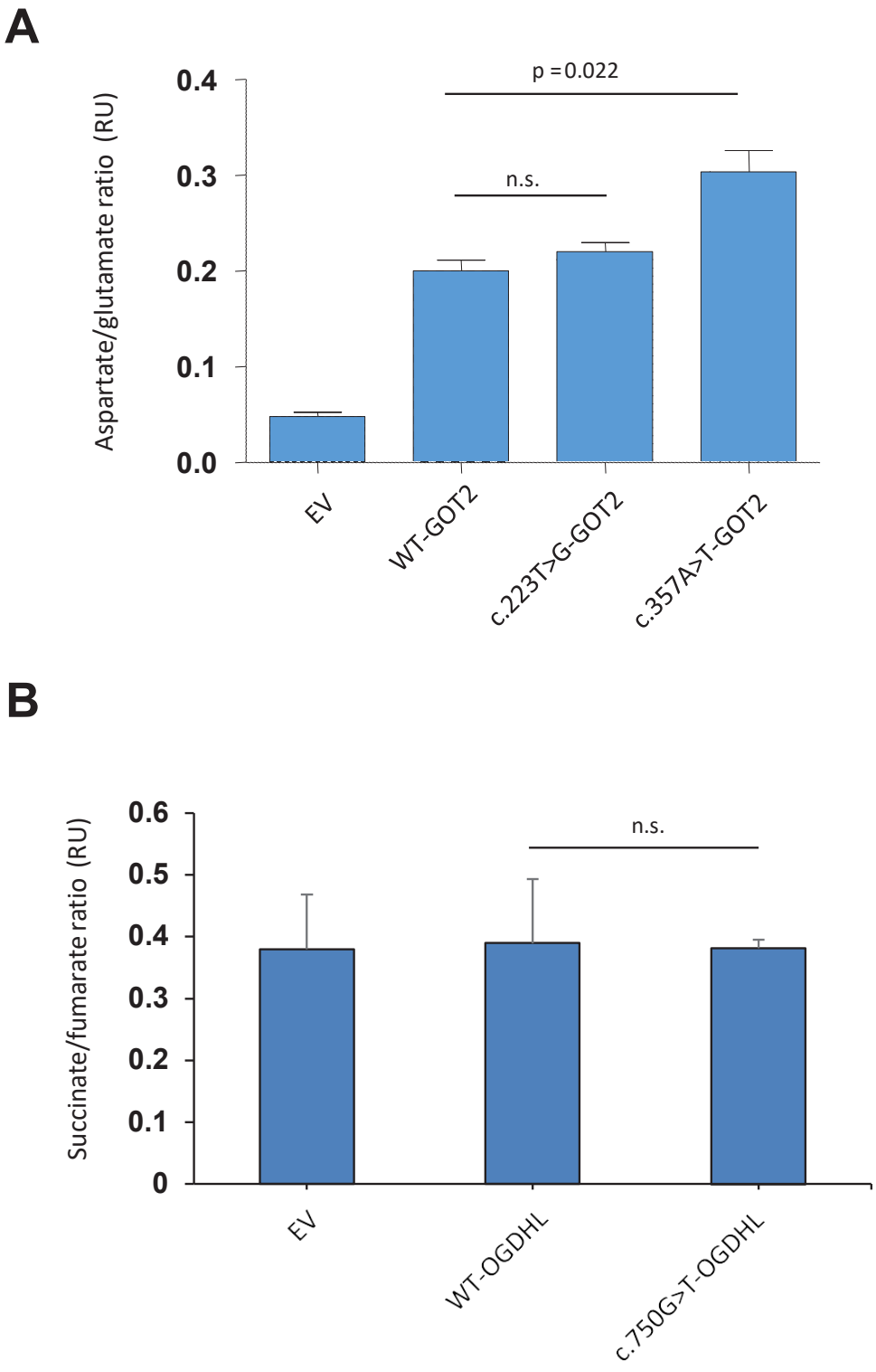

Supplementary Figure S3. (A) Aspartate/glutamate ratios assessed by LC-MS in GOT2 KD Hela cells transfected with empty vector (EV), GOT2 wild-type (WT) cDNA, GOT2- c.223T>G cDNA, and GOT2- c.357A>T cDNA. The ratios were reported as means (n=3). Error bars represent standard deviations. A t-test was applied to test for differences between GOT WT and GOT2- c.223T>G and - c.357A>T transfected cells. n.s.: not significant. **(B)** Succinate/fumarate ratios assessed by LC-MS in OGDHL KD Hela cells transfected with EV, OGDHL WT cDNA, and OGDHL- c.750G>T cDNA. The ratios were reported as means (n=3). Error bars represent standard deviations. A t-test was applied to test for differences. n.s.: not significant

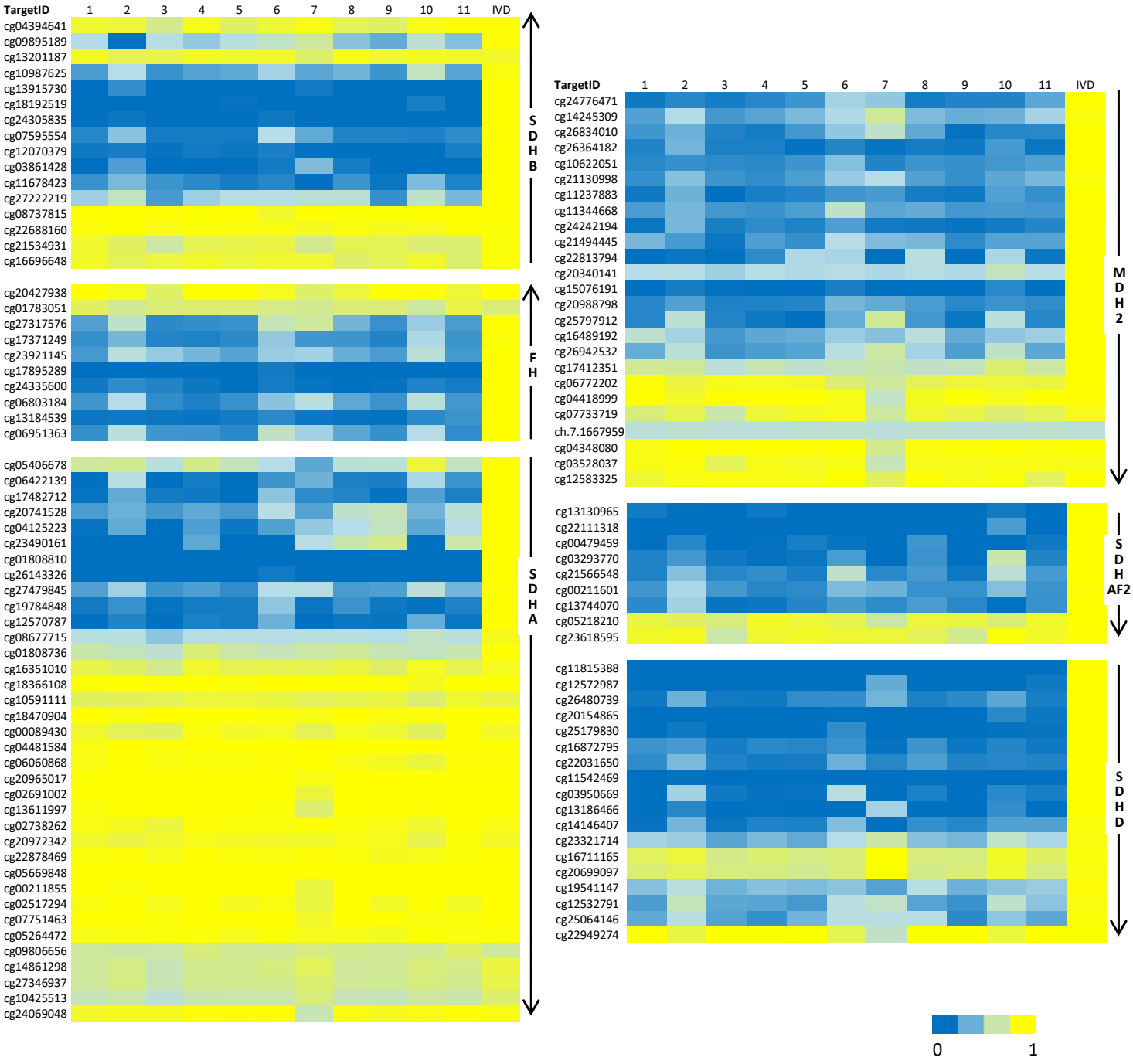

Supplementary Figure S4. DNA methylation (M-values) of the CpG island probes located within six PCC/PGL susceptibility genes encoding Krebs cycle enzymes (SDHA, SDHAF2, SDHB, SDHD, FH, and MDH2) in the 11 analyzed tumors, compared to in vitro methylated DNA (IVD).

Supplementary Table 1. Genes included in the targeted next-generation sequencing panel

ACO1
ACO2
CS
DLAT
DLD
DLST
GOT1
GOT2
IDH1
IDH2
IDH3A
IDH3B
IDH3G
MDH1
OGDH
OGDHL
PC
PCK1
PCK2
PDHA1
PDHA2
PDHB
SLC25A1
SLC25A10
SLC25A11
SLC25A13
SUCLA2
SUCLG1
SUCLG2
FH
MDH2
SDHA
SDHB
SDHC
SDHD
SDHAF1
SDHAF2

ARTICLE 2: Gain-of-function mutations in *DNMT3A* in patients with paraganglioma.

Authors: **Laura Remacha**, Maria Currás-Freixes, Raúl Torres-Ruiz, Francesca Schiavi, Rafael Torres-Pérez, Bruna Calsina, Rocío Letón, Iñaki Comino-Méndez, Juan M Roldán-Romero, Cristina Montero-Conde, María Santos, Lucía Inglada Pérez, Guillermo Pita, María R. Alonso, Emiliano Honrado, Susana Pedrinaci, Benedicto Crespo-Facorro, Antonio Percesepe, Maurizio Falcioni, Sandra Rodríguez-Perales, Esther Korpershoek, Santiago Ramón-Maiques, Giuseppe Opocher, Cristina Rodríguez-Antona, Mercedes Robledo, and Alberto Cascón

Published in *Genetics in Medicine*, 2018 Dec;20(12):1644–1651

ABSTRACT

The high percentage of patients carrying germline mutations makes phaeochromocytomas and paragangliomas (PPGL) the most heritable of all tumours. However, there are still PPGL cases that are not explained by mutations in the already known susceptibility genes. Therefore, in this study we aimed to identify the genetic cause in a selected patient strongly suspected of having hereditary PPGL due to the presence of multiple PGLs and early age at diagnosis, but without family history of the disease.

Whole-exome sequencing was applied to the germline DNA of the parents-proband trio identifying a single, novel *de novo* mutation in the DNA methyltransferase 3A gene (*DNMT3A*). This mutation (c.896A>T; p.Lys299Ile) was affecting a highly conserved residue of the protein located close to the aromatic cage that binds to trimethylated histone H3.

Upon genome-wide methylome analysis of *DNMT3A*-mutated tissues from the patient we could observe a characteristic CpG island methylator phenotype (CIMP) profile as well as a significant hypermethylation of homeobox-containing genes (FDR<0.15), suggesting an activating role of the mutation. CRISPR/Cas9 gene editing was used to reproduce the knock-in in HeLa cells. The *DNMT3A* mutation was leading to global changes in methylation in those cells, therefore providing evidence of the methyltransferase altered function. Additionally, an extension of the study applying targeted deep sequencing to a series of PPGL patients and tumours, revealed the presence of somatic subclonal mutations affecting the same residue in six additional PPGL cases, all of them paragangliomas. Finally, a second germline *DNMT3A* mutation (c.952C>T; p.Arg318Trp) was found in a patient with family history of PCC, and it also caused global tumour DNA hypermethylation similar to the one identified in the tumour from the c.896A>T mutation carrier.

The mutations described herein not only increases the number of paraganglioma susceptibility genes, but also represents, to the best of our knowledge, the first example of gain-of-function mutations affecting a DNA methyltransferase gene involved in cancer predisposition.

Personal contribution:

I participated in the conception and design of the study. I performed *in vitro* experiments using the CRISPR/Cas9 technology in HeLa cells as well as I collaborated in the identification and characterization of additional *DNMT3A*-mutated PPGL cases through targeted deep sequencing and DNA methylation analysis. I also took part in the drafting and the revision of the article.

ARTICLE | Genetics inMedicine

Gain-of-function mutations in *DNMT3A* in patients with paraganglioma

Laura Remacha, BS[1], Maria Currás-Freixes, MD, PhD[1], Raúl Torres-Ruiz, PhD[2], Francesca Schiavi, MD, PhD[3], Rafael Torres-Pérez, BS[1], Bruna Calsina, BS[1], Rocío Letón, BS[1], Iñaki Comino-Méndez, PhD[1], Juan M Roldán-Romero, BS[1], Cristina Montero-Conde, PhD[1], María Santos, BS[1], Lucía Inglada Pérez, PhD[1], Guillermo Pita, BS[4], María R. Alonso, BS[4], Emiliano Honrado, MD, PhD[5], Susana Pedrinaci, MD[6], Benedicto Crespo-Facorro, MD, PhD[7], Antonio Percesepe, MD[8], Maurizio Falcioni, MD[9], Sandra Rodríguez-Perales, PhD[2], Esther Korpershoek, PhD[10], Santiago Ramón-Maiques, PhD[11], Giuseppe Opocher, MD, PhD[3], Cristina Rodríguez-Antona, PhD[1,12], Mercedes Robledo, PhD[1,12] and Alberto Cascón, PhD[1,12]

Purpose: The high percentage of patients carrying germline mutations makes pheochromocytomas/paragangliomas the most heritable of all tumors. However, there are still cases unexplained by mutations in the known genes. We aimed to identify the genetic cause of disease in patients strongly suspected of having hereditary tumors.

Methods: Whole-exome sequencing was applied to the germlines of a parent–proband trio. Genome-wide methylome analysis, RNA-seq, CRISPR/Cas9 gene editing, and targeted sequencing were also performed.

Results: We identified a novel de novo germline mutation in *DNMT3A*, affecting a highly conserved residue located close to the aromatic cage that binds to trimethylated histone H3. *DNMT3A*-mutated tumors exhibited significant hypermethylation of homeobox-containing genes, suggesting an activating role of the mutation. CRISPR/Cas9-mediated knock-in in HeLa cells led to global changes in methylation, providing evidence of the DNMT3A-altered function. Targeted sequencing revealed subclonal somatic mutations in six additional paragangliomas. Finally, a second germline *DNMT3A* mutation, also causing global tumor DNA hypermethylation, was found in a patient with a family history of pheochromocytoma.

Conclusion: Our findings suggest that *DNMT3A* may be a susceptibility gene for paragangliomas and, if confirmed in future studies, would represent the first example of gain-of-function mutations affecting a DNA methyltransferase gene involved in cancer predisposition.

Genetics in Medicine (2018) https://doi.org/10.1038/s41436-018-0003-y

Keywords: *DNMT3A*; paraganglioma; exome sequencing; hypermethylation; CRISPR/Cas9 gene editing

INTRODUCTION

Approximately 75% of neural crest-derived pheochromocytomas (PCCs) and paragangliomas (PGLs) (OMIM 171300) carry mutually exclusive germline (~40%) or somatic (~35%) mutations affecting 1 of at least 20 genes.[1] The high percentage of patients for which germline mutations have been found in recent years has turned PCCs and PGLs into the most heritable of all tumors. In addition to the known hereditary cases, there is still a subset of PCC/PGL patients showing clinical features of heritability without germline mutations in the susceptibility genes identified so far. The presence of multiple tumors in some of these patients, in the absence of a family history of the disease, strongly suggests the presence of de novo alterations, recessive inheritance, imprinting, or somatic mosaicism involving precursor cells.

More than one-third of the PCC/PGL disease-causing genes (*SDHA*, *SDHB*, *SDHC*, *SDHD*, *SDHAF2*, *FH*, *MDH2* and *IDH1*) encode Krebs cycle enzymes. Recently, gene expression and methylation profiling have shown that tumors carrying mutations in Krebs cycle-related genes exhibit an identifiable CpG island methylator phenotype (CIMP), caused by the accumulation of specific metabolites.[2] These oncometabolites lead to inactivation of DNA demethylases such as TET2 and lysine demethylases, giving rise to epigenetic alterations in the genome that cause global gene expression changes similar to those found in glioblastomas carrying mutations in *IDH1* and *IDH2*.[3] In addition, mutations affecting chromatin

[1]Hereditary Endocrine Cancer Group, Spanish National Cancer Research Centre (CNIO), Madrid, Spain; [2]Molecular Cytogenetics Unit, Human Cancer Genetics Programme, Spanish National Cancer Research Centre (CNIO), Madrid, Spain; [3]Veneto Institute of Oncology, Istituto di Ricovero e Cura a Carattere Scientifico, Padua, Italy; [4]Human Genotyping Unit-CeGen, Human Cancer Genetics Programme, Spanish National Cancer Research Centre (CNIO), Madrid, Spain; [5]Anatomical Pathology Service, Hospital de León, León, Spain; [6]Department of Genetics, Hospital Universitario Virgen de las Nieves, Granada, Spain; [7]University of Cantabria and HU Marqués de Valdecilla-IDIVAL, CIBER Mental Health Santander, Santander, Spain; [8]Medical Genetics, Department of Medicine and Surgery, University of Parma, Parma, Italy; [9]Otolaryngology and Otoneurosurgery Department, Azienda Ospedaliero-Universitaria di Parma, Parma, Italy; [10]Department of Pathology, Erasmus Medical Center Cancer Institute, University Medical Center Rotterdam, Rotterdam, The Netherlands; [11]Structural Bases of Genome Integrity Group, Structural Biology and Biocomputing Programme, Spanish National Cancer Research Centre (CNIO), Madrid, Spain; [12]Centro de Investigación Biomédica en Red de Enfermedades Raras (CIBERER), Madrid, Spain. Correspondence: Alberto Cascón(acascon@cnio.es)

Submitted 14 August 2017; accepted: 20 March 2018
Published online: 08 May 2018

remodeling genes have recently been found either in the germline or in tumor cells of patients with PCC/PGL.[4] However, though global methylation changes are closely related to the development of a substantial subset of PCCs and PGLs, to date no alterations in DNA methyltransferase genes, which are frequently disrupted in cancer, have been reported in PCC/PGL.

In the present study, we identified a de novo germline mutation in the DNA (cytosine-5-)-methyltransferase 3 alpha (*DNMT3A*) gene in a patient with multiple ($n = 7$) PGLs. The same mutation was also found subclonally in six additional PGLs. A second germline mutation was identified in a patient with a family history of the disease. The altered methylation profile exhibited by *DNMT3A*-mutated tissues (both PGLs and lymphocytes) and HeLa cells carrying one of the mutations, and the location of the altered amino acids close to the aromatic cage responsible for binding trimethylated histone H3, together suggest a gain of alternative activities (referred to as gain-of-function) caused by these alterations.

MATERIALS AND METHODS

Index patient

Whole-exome sequencing was applied to DNA samples from a parent–proband trio. The index case, a 22-year-old woman, was referred to hospital because of persistent dysphonia for 3 years. Multiple laryngeal PGLs (T1) and a right carotid PGL (T2) were detected by single photon emission computed tomography (CT), magnetic resonance imaging (MRI), and octreoscan, and the patient underwent surgery at the age of 23 years. Four additional PGLs were diagnosed subsequently, two jugulotympanic, one in the left carotid, and one normetanephrine-producing paracardiac tumor presenting with impaired fasting glucose and high blood pressure. One jugulotympanic PGL was treated with radiosurgery at age 28 years, and the other was embolized, surgically removed (T3), and treated with radiosurgery at ages 29 and 30 years. The paracardiac and left carotid PGLs were treated with external radiation therapy at ages 30 and 32 years, respectively. The patient reported no family history of PCC or PGL.

Whole-exome sequencing analysis

Whole-exome sequencing was carried out at the National Centre for Genomic Analysis (CNAG) using germline DNA samples obtained from the patient and her parents using FlexiGene DNA kit (Qiagen). Briefly, the Covaris S2 System (Covaris) was used for DNA fragmentation. Exome capture was performed using the SureSelect XT HumanAllExon 50-Mb kit (Agilent Technologies). Exome sequencing at a mean coverage >50× was performed by 75-bp paired-end technology using a HiSeq2000 sequencer (Illumina). The GEM[5] and BFAST programs were used to align the reads against the whole human genome (hg19 assembly). To identify single-nucleotide substitutions and small insertions and deletions (indels) the SAMtools program was used (http://samtools.sourceforge.net). Filtering was applied to exclude noncoding substitutions and variants in genomic regions with low mappability, with low depth readings, with the alternative allele present in <20% of reads, or with the alternative allele present only in forward or reverse reads. Variants with genotype quality (GQ) lower than 90% in any of the three exomes were also excluded. The GQ for a variant is a measure, derived from the Phred quality scores, of the probability that the genotype is correct. The higher the GQ value (highest possible value = 99%), the more likely it is that the genotype is correct. Three inheritance models were assessed: de novo, recessive, and dominant with incomplete penetrance. Manual curation using Integrative Genomics Viewer (IGV) software was also applied in the de novo analysis to exclude variants present in at least one of the progenitors or caused by a sequencing artifact. The PredictSNP consensus classifier[6] was used to predict the effect of the only nucleotide substitution that passed all filtering steps.

Extended study of PCC/PGL patients

Sanger sequencing of the two exons (8 and 9) encompassing the complete proline–tryptophan–tryptophan–proline (PWWP) domain of *DNMT3A* was applied to screen for additional germline mutations in a selected series of patients (n=35) without germline alterations in known susceptibility genes and who were strongly suspected of having hereditary PCC/PGL due to the presence of multiple tumors and/or familial antecedents of the disease. The Instituto de Salud Carlos III (ISCIII) ethics committee approved the study, and all the patients provided written informed consent. Also studied for mutations within the PWWP domain of *DNMT3A* were 95 tumors (52 head and neck PGLs, 28 PCCs, and 15 thoracic–abdominal PGLs) that tested negative for mutations in the known PCC/PGL susceptibility genes and, when it could be assessed, positive for SDHB immunostaining (to rule out the presence of hidden mutations affecting the SDH genes). To test for subclonal *DNMT3A* mutations, targeted deep sequencing (Illumina) of an amplicon containing the c.896A>T mutation was applied to the 95 tumor DNA samples. Once the library was prepared following the manufacturer's instructions, next-generation sequencing was performed using the MiSeq desktop sequencer (Illumina). Sequence alignment was carried out using MiSeq Reporter and Illumina VariantStudio software (Illumina). Variant calling was performed using GATK[7] and Somatic Variant Caller (Illumina) and identified variants were filtered considering mapping quality, variant score, depth, strand bias, and annotation quality.

DNA methylation assay

DNA from peripheral blood leukocytes and formalin-fixed paraffin-embedded (FFPE) PCCs/PGLs was obtained using the DNeasy kit (Qiagen), following the manufacturer's instructions. Bisulfite conversion of DNA was performed using the EZ DNA Methylation Kit (Zymo Research) and genome-wide DNA methylation was assayed using the Infinium MethylationEPIC BeadChip (Illumina) at the *Centro Nacional de Genotipado*

(CEGEN-ISCIII) (www.cegen.org), as previously described.[8] This BeadChip interrogates over 850,000 methylation sites per sample. Beta values for interrogated CpGs were assigned using the Genome Studio Methylation module and transformed into *M* values by applying the formula: $\log_2$[Beta value/(1-Beta value)]. Negative *M* values indicate less than 50% methylation and positive *M* values indicate more than 50% methylation. *M* values were used for all statistical analyses. The Infinium MethylationEPIC BeadChip (Illumina) was also used to identify specific methylated probes related to the *DNMT3A* genetic alteration. Three c.896A>T *DNMT3A*-mutated PGLs (T1, T2, and T3) from the index patient were used for supervised analysis, along with 17 controls (5 *SDHB*-, 2 *HRAS*-, 1 *NF1*-, 1 *RET*-, 1 *VHL*-, and 1 *IDH3B*-mutated PCCs/PGLs, and 6 tumors without a known mutation). Differentially methylated probes were identified using a *t* test (limma) carried out as implemented in POMELO II.[9] To account for multiple hypothesis testing, the significance level (*P*) was adjusted using Benjamini's FDR correction.[10] Probes with an FDR < 0.05 were considered differentially methylated between classes. Gene functional annotation analysis was performed by applying the web-based applications DAVID (the Database for Annotation, Visualization, and Integrated Discovery).[11] and Enrichr.[12] to the genes annotated to significantly methylated probes obtained in the supervised analysis. After accounting for duplicate genes (i.e., various probes targeting the same gene), 1,285 individual human genes were recognized by DAVID and included in further analysis. Hierarchical clustering, performed using GeneCluster 2.0[13] on the 3,092 probes found to be significantly differentially methylated in the supervised analysis, was used to interrogate first the EPIC methylation data from the three *DNMT3A*-mutated tumors (T1–T3) from the index patient, the c.952C>T *DNMT3A*-mutated PGL plus the 17 control tumors previously described; and second, EPIC methylation data from lymphocyte DNAs from the c.896A>T *DNMT3A*-mutated carrier (average of two samples) and her parents (I1 and I2), the c.952C>T *DNMT3A*-mutated patient, and eight controls (C1–C8). Additionally, we used the same list of probes to interrogate Illumina 450k methylation data from 26 acute myeloid leukemia (AML) samples carrying *DNMT3A* mutations compared with 30 *DNMT3A* wild-type (WT) cases.[14] Finally, supervised analysis was performed to identify differentially methylated probes between HeLa knock-in (c.896A>T) and HeLa WT cells. The reliability of the clusters obtained with *DNMT3A*-mutated and no-mutated PCCs/PGLs was verified by consensus clustering, a method that obtains the consensus across multiple runs of a clustering algorithm and assess the stability of the discovered clusters by using resampling techniques.

Reverse-transcriptase PCR and qPCR

Total RNA was isolated from peripheral blood lymphocytes from both *DNMT3A*-mutation carriers and the parents of the index case using the TriReagent kit (MRC), following the manufacturer's instructions. First strand complementary DNA (cDNA) was synthesized from 1 µg of total RNA by oligo (dT) 14 primer reverse transcription using Superscript II Reverse Transcriptase (Invitrogen) following the manufacturer's instructions. Three genes, *HOXD13*, *IRX5*, and *NKX2-4*, were selected for messenger RNA (mRNA) quantification because several CpGs annotated to them were found amongst the differentially methylated in *DNMT3A*-mutated tumors. HOXD13, IRX5, and NKX2-4 mRNA levels were determined by quantitative polymerase chain reaction (PCR) on a 7500 fast real-time PCR system (Applied Biosystems) using the Universal ProbeLibrary set (https://www.roche-applied-science.com), as described by the manufacturer. Relative mRNA levels were estimated using the 2-CT method[15] and normalized using β-glucuronidase (GUS) and β-actin (ACTB) as housekeeping genes. The results are shown as mean ± s.d. ($n \geq 2$).

CRISPR/Cas9

A HeLa cell line (provided by Flow Cytometry Core Unit, CNIO, Madrid) was authenticated by short tandem repeat profiling (GenePrint 10 System, Promega) and periodically confirmed to be mycoplasma-free by qPCR. HeLa cells were cultured in Dulbecco's modified Eagle medium Gluta MAX (DMEM; Invitrogen); supplemented with 10% (v/v) fetal bovine serum (FBS, PAA Laboratories), 1% (v/v) penicillin/streptomycin, and 0.6% (v/v) Fungizone (Gibco); and maintained at 37 °C in a humidified incubator with 5% CO_2. Recombinant Cas9 protein and two single-guide RNAs (sgRNAs) (sgRNA-1: AACTGCGGGGCTTCTCCTGGTGG; sgRNA-2: CTGGTGTGGGGGAAACTGCGGGG) were used as previously described.[16] Briefly, sgRNAs were designed using the CRISPR MIT software tool (http://crispr.mit.edu) and transcribed in vitro through runoff reactions by T7 RNA polymerase using the HiScribe T7 high-yield RNA synthesis kit (NEB). Transcribed sgRNAs were purified with a column purification kit (RNeasy mini kit, Qiagen, Hilden, Germany), quantified, and quality-checked by denaturing RNA gel electrophoresis. RNP complexes were generate by premixing Cas9 protein (1–8 µg, Integrated DNA Technologies, CA) with in vitro transcribed sgRNA (0.5–8 µg) for 10 min at room temperature. A single-stranded oligodeoxynucleotide with the nucleotide change c.896A>T was purchased from IDT as an ultramer oligo (available upon request). For electroporation, we employed the Neon Transfection System (ThermoFisher Scientific, Waltham, MA). Confluent HeLa cells were trypsinized and washed twice with DPBS, counted, and resuspended in 10 µl Buffer T (ThermoFisher Scientific) per well. In each reaction approximately 100,000 cells were electroporated under the following conditions: 2 pulses of 35-ms width and 1,005 V. Cells were then seeded in a 96-well plate with prewarmed medium. The following day the media was replaced with fresh DMEM. After culture expansion, cells were sorted to a 96-well plate to establish single-cell clones. Detection of knock-in cell clones was performed using Sanger sequencing. Genomic DNA extraction, PCR amplification, and purification of PCR product were performed following standard procedures.

RNA sequencing (RNA-seq)

PolyA+ fraction from total RNA samples was purified and randomly fragmented, converted to double-stranded cDNA, and processed using the TruSeq Stranded mRNA Library Prep Kit (Illumina). Adapter-ligated library was completed by PCR and the resulting purified cDNA library was applied to a flow cell for cluster generation and sequenced on a HiSeq 2500 instrument, following manufacturer protocols. Image analysis, basecalling, and quality score assignment was performed with Real Time Analysis software (Illumina), and Illumina2bam tool, BamToFastq (Bedtools), and SAMtools (http://samtools.sourceforge.net/) were used to convert the files to BAM, FASTQ, and SAM format, respectively. FASTQ files containing the Illumina reads (length = 50) of the samples were submitted to the Nextpresso v.1.8 pipeline using the default parameters. Clustering average for linkage and Euclidean as the distance measure were applied in the hierarchical clustering using Genecluster 2.0, and a standard deviation of 0.5 was assumed.

Immunohistochemistry

An automated immunostaining platform was used (Ventana Discovery XT, Roche) for immunohistochemistry of H3(K9) in 3-µm FFPE sections from the *DNMT3A*-mutated tumors. Antigen retrieval was first performed with RiboCC (pH6) and endogenous peroxidase was blocked (peroxide hydrogen at 3%). Then, slides were incubated with rabbit polyclonal anti-H3(K9) (1/500; Abcam, ab8898) and following with the corresponding visualization system (OmniMap antirabbit, Ventana, Roche) conjugated with horseradish peroxidase. Immunohistochemical reaction was developed using 3,30-diaminobenzidine tetrahydrochloride (DAB) (ChromoMap DAB, Ventana, Roche). Nuclei were counterstained with Carazzi's hematoxylin. Finally, the slides was dehydrated, cleared, and mounted with a permanent mounting medium for microscopic evaluation.

RESULTS

Exome sequencing findings

First, we focused on heterozygous gene-coding single-nucleotide substitutions and small insertions and deletions that were present in blood DNA from the patient but absent

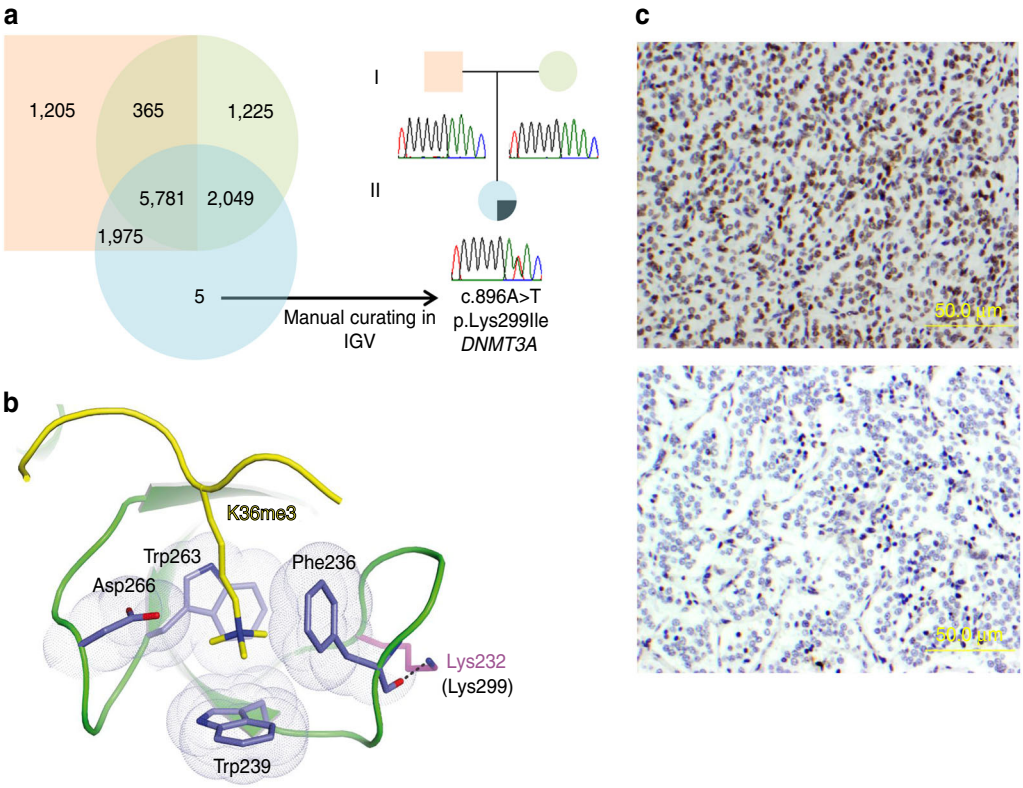

Fig. 1 Exome sequencing findings, trimethylated histone H3 interactions, and immunohistochemical staining. (**a**) Schematic representation of the coding variants passing all filtering steps (with a genotype quality ≥90) that were found in the father (orange square), the mother (green circle), and the patient (blue circle) exomes. Manual curating by the integrative genomic viewer (IGV) excluded 4 of the 5 variants because they were either found in at least one of the progenitors or because they were probably the result of a sequencing artifact. The single de novo variant found (c.896A>T in *DNMT3A*) was confirmed by Sanger sequencing. (**b**) PyMOL representation of the interactions between the PWWP domain of DNMT3B and trimethylated K36 in histone H3 (structure deposited in the Protein Data Base with accession code 5CIU). The histone peptide is shown in yellow and the aromatic cage residues in blue. The represented residues are fully conserved in DNMT3A. The lysine residue 232 is equivalent to lysine 299 in DNMT3A and is represented in magenta. The dashed line depicts a hydrogen bond interaction between Lys232 and the carbonyl oxygen of a phenylalanine within the same loop. (**c**) Highly positive immunohistochemical staining for H3K9me3 in one representative c.896A>T *DNMT3A*-mutated tumor from the de novo patient (upper panel) compared to a *DNMT3A* wild-type tumor staining negative (lower panel). The scale bars represent 50 µm

in germline DNA from both of her parents, following a de novo model. The filtering process applied uncovered a single de novo missense variant (c.896A>T; p.Lys299Ile) in *DNMT3A*, which was subsequently validated by Sanger sequencing (Fig. **1a**). The substitution was not found in the >120,000 exomes in the gnomAD database (http://gnomad.broadinstitute.org/), 570 population-matched unrelated Spanish exomes from the CIBERER Spanish Variant Server (http://csvs.babelomics.org/), or the database of Epigenetic Modifiers (dbEM; http://crdd.osdd.net/raghava/dbem/). The lysine residue affected by the mutation (Lys299) is located within the highly conserved PWWP domain of the protein (Fig. **1b**), and all in silico algorithms predict the change to be deleterious (Supplementary Figure S1). In addition, high levels of H3K9me3 were observed in the c.896A>T *DNMT3A*-mutated tumor compared with controls (Fig. **1c**). Though recessive and autosomal dominant with incomplete penetrance models of inheritance were also considered, we gave priority to the de novo model because we found a single mutation in a gene previously associated with various cancers.

Extended study of PCC/PGL patients and tumors

Considering the recurrence of activating mutations affecting oncogenes, Sanger sequencing–based screening for germline mutations was performed on the sequence encompassing the PWWP domain of *DNMT3A*. A missense mutation (c.952C>T; p.Arg318Trp) (Supplementary Figure S2A) affecting a highly conserved residue was identified in germline DNA from a woman (54 yr) with two head and neck PGLs and a family history of the disease (her mother was diagnosed with bilateral head and neck PGL). The arginine 318 amino acid is highly conserved, and the mutation (predicted to be deleterious) (Supplementary Figure S2B) introduces a tryptophan that could alter the binding of DNMT3A to trimethylated histone H3 (Fig. **2a**). Further study of the PWWP domain in a series of 94 tumors identified three cases with a small mutation peak affecting the same nucleotide as that mutated in the original patient (Table **1**). Subsequent analysis by targeted deep sequencing showed a clonal effect, ranging between 14 and 36% of reads, in all three cases, and identified three additional carriers that hadn't been detected by Sanger sequencing. All c.896A>T *DNMT3A* mutations were found in head and neck PGLs. The analysis of the corresponding germline DNA showed in all available cases that the mutation was somatic. All available *DNMT3A*-mutated PGLs showed high immunostaining of H3K9me3.

Methylation and expression profiles of *DNMT3A*-mutated tissues

Supervised DNA methylation analyses revealed 3,092 probes differentially methylated (FDR <0.05) in tumors carrying the c.896A>T *DNMT3A* mutation, compared with controls. Amongst the differentially methylated probes, an enrichment of homeobox-containing genes ($n = 90$), dopaminergic neurogenesis, neural crest differentiation, and pattern specification and embryonic morphogenesis processes (Supplementary Table S1), was observed. Probes from 26 Hox genes were amongst those methylated in c.896A>T *DNMT3A*-mutated tumors. Twenty-one probes targeting the *HOXD9-13*locus, nine of them targeting *HOXD13*, were significantly more methylated (Supplementary Figure S3). Downregulation of three of the differentially methylated homeobox-containing genes (*HOXD13*, *NKX2-4*, and *IRX5*) was found by qPCR in c.896A>T *DNMT3A*-mutated lymphocytes compared with controls (Supplementary Figure S4A). Hierarchical clustering, using data from the 3,092 probes significantly differentially methylated, grouped all the tumors carrying *DNMT3A* mutations together; the three c.896A>T-mutated tumors, previously used in the supervised comparison, and the tumor carrying the c.952C>T mutation (Fig. **2b**). Additionally, following a similar profiling, lymphocyte DNAs from the two *DNMT3A* mutation carriers were also clustered together and separated from different controls (Supplementary Figure S4B). Moreover, a different global expression profile was observed in c.896A>T *DNMT3A*-mutated lymphocytes compared with controls by RNA-seq (Supplementary Figure S4C). On the whole, these results demonstrate that both *DNMT3A* mutations led to a similar and characteristic methylation profile, being independent of the tissue of origin. Finally, based on the same list of differentially methylated probes, all but two AML samples carrying the recurrent *DNMT3A* mutation affecting p.Arg882 (Supplementary Figure S5A) clustered together. This result suggests that either c.896A>T or c.952C>T and p.Arg882 *DNMT3A* mutations cause opposite effects on DNA methylation in PCC/PGL and AML, respectively.

The p.Lys299Ile mutation increases *DNMT3A* DNA methylation capabilities in HeLa cells

CRISPR/Cas9-mediated knock-in introduction of the *DNMT3A* p.Lys299Ile mutation in HeLa cells caused genome-wide alterations in DNA methylation. Thus, more than 16,000 probes, targeting more than 6,000 different genes, were found differentially methylated (FDR <0.05; fold change >|3.5|) in HeLa cells carrying the mutation compared with WT controls (represented in Supplementary Figure S5B). Amongst probes that were differentially hypermethylated upon the introduction of the mutation, an enrichment of those targeting homeobox-containing genes ($n = 52$), nervous system development, neuronal system, and signaling genes was observed compared to WT HeLa cells (adjusted $p < 0.05$) (Supplementary Table S2).

DISCUSSION

DNMT3A encodes one of the two de novo DNA methyltransferases, DNMT3A and DNMT3B, that establish DNA methylation patterns during embryonic development and gametogenesis in mammals.[17] Somatic inactivating mutations in *DNMT3A* were first described causing global hypomethylation in acute myeloid leukemia (AML),[18] and later most types of hematological malignancies.[19] Other recurrent somatic alterations affecting genes involved in epigenetic

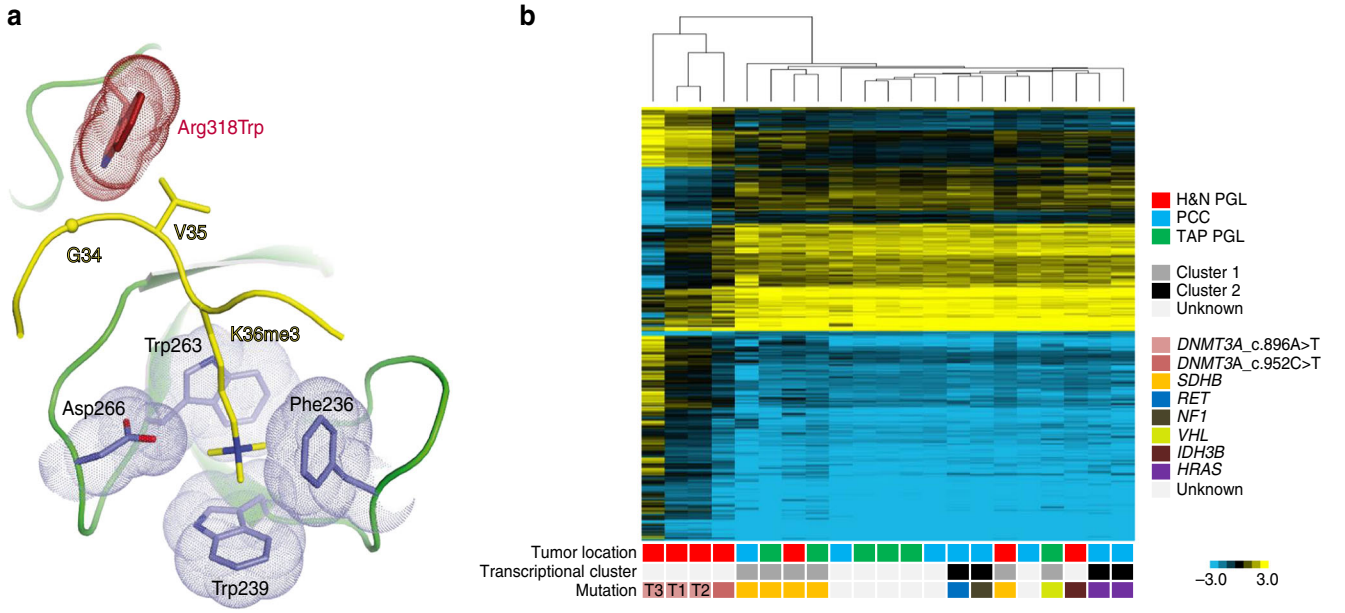

Fig. 2 Arg318 location in a DNMT3A 3D structural model and methylation profile for *DNMT3A*-mutated tumors. (**a**) PyMOL representation of the interactions between the PWWP domain of DNMT3B and trimethylated K36 in histone H3 (similar to the one depicted in Fig. 2a). The histone peptide is shown in yellow and the aromatic cage residues in blue. The tryptophan that substitutes the arginine 318 amino acid (equivalent to lysine 251 in DNMT3B) in the mutated Arg318Trp-DNMT3A sample is represented in dark red. (**b**) Hierarchical clustering using methylation data from the 3,092 probes significantly differentially methylated (FDR <0.05) between c.896A>T *DNMT3A*-mutated and nonmutated tumors. T1–T3: c.896A>T *DNMT3A*-mutated PGLs. *H&N* head and neck, *PGL* paraganglioma, *PCC* pheochromocytoma, TAP thoracic, abdominal or pelvic

regulation are common in myeloid malignancies.[20] In fact, the crosstalk between genomic alterations and deregulation of epigenetic pathways is a well-known cause of cancer that is not limited to hematologic malignancies. Thus, alterations in genome-wide gene expression caused by somatic disruption of epigenetic modifying genes lead to the development of several solid tumors, including PCC/PGL.[4] However, to date no constitutional alteration of an epigenetic regulator has been reported as a cause of hereditary cancer. As far as we know, the case described herein might be the first example of a Mendelian disorder caused by an alteration of the epigenetic machinery involved exclusively in cancer predisposition. In addition, our finding of subclonal somatic mutations in a substantial number of cases points to the importance of *DNMT3A* alterations in PGL, especially for tumors located in the head and neck region. However, due to the low allele frequencies of the *DNMT3A* mutation, it is unlikely that this mutation is the cancer initiating event in these sporadic cases.

Variant p.Lys299Ile affects a highly conserved residue within the PWWP motif of DNMT3A that is involved in both DNA binding and targeting the protein to trimethyl lysine marks (on lysine 36 and 9) in histone H3 (H3K36me3 and H3K9me3, respectively).[21,22] The lysine 299 residue is one of the most conserved amino acids within the PWWP domain.[23] It is part of the positively charged surface of the protein that interacts with DNA[22] It also interacts with the aromatic cage of DNMT3A involved in binding methyllysine histones,[22,23] presumably through a hydrogen bond with one of the amino acids. NMR perturbation experiments performed on histone-binding PWWP motifs of two proteins, Pdp1 and BRPF1, showed a high chemical shift for the equivalent lysine residue in both.[24,25] The specific methylation of homeobox-containing genes observed in c.896A>T *DNMT3A*–mutated tissues (PGLs and blood from the patient), further suggests that, instead of a loss of function, the p.Lys299Ile variation is associated with different DNMT3A-related DNA methylation capabilities. The high level of H3K9me3 observed in *DNMT3A*-mutated tumors, something also found in SDH- and *FH*-mutated PCC/PGL,[26] provides further evidence for the transcriptional repression role of the mutation. The effect on DNA methylation caused by the introduction of the p.Lys299Ile mutation in HeLa cells supports the role of this mutation in changing DNMT3A function, which is consistent with the hypermethylated profile observed in PCC/PGL.

Germline de novo loss-of-function mutations in *DNMT3A* cause overgrowth syndrome with intellectual disability,[27] while inherited compound heterozygous or homozygous mutations in *DNMT3B* are the most common cause of the ICF (immunodeficiency, centrosome instability, and facial anomalies) syndrome in humans.[28] The patient described herein did not have any clinical feature related to the overgrowth or ICF syndromes. Overgrowth syndromes are also caused by constitutional mutations in two well-known AML-related genes that encode important histone methyltransferases: *EZH2* (Weaver syndrome)[29] and *NSD1* (Sotos syndrome and Beckwith–Wiedemann syndrome).[30] Moreover, germline de novo inactivating mutations in *ASXL1*, which are frequently found in myelodysplastic syndromes and in AML, also cause a growth disorder called

Table 1 Clinical and genetic features of patients carrying the c.896A>T *DNMT3A* mutation analyzed by targeted deep sequencing

ID	Sex	Age at onset	Tumor location	Mutation type	Reads carrying the mutation (%)
T1	F	23	mH&N PGL[a]	Germline	52
14T148	F	38	Thyroid PGL	Somatic	36
X27	F	33	Thyroid PGL	Somatic	25
X191	F	54	Jugulotympanic PGL	Undetermined	14
X78	F	58	Jugulotympanic PGL	Undetermined	6.5
X88	F	44	Jugulotympanic PGL	Undetermined	7.9
X98	M	46	Carotid PGL	Somatic	6.8

The ID of the tumor from the index patient is shown in bold
H&N head and neck, *m* multiple, *PGL* paraganglioma
[a]Larynx, carotid, jugulotympanic, juxtavagal, and mediastinum

Bohring–Opitz syndrome.[31] In all cases of these syndromes, genome-wide hypomethylation was observed and no cancer development was reported. Taken together, our data suggest that, unlike constitutional inactivation of DNMT3A, *DNMT3A* gain-of-function might be associated with PCC/PGL development. Interestingly, both gain-of-function and loss-of-function *EZH2* mutations occur in cancers with distinct subtypes,[32] including PCC.[4]

Several Hox family genes, which encode crucial players during embryogenesis, neural crest patterning, and hematopoietic development, are hypomethylated and upregulated in hematological malignancies carrying somatic *DNMT3A* mutations,[33,34] and have been proposed as targets for *DNMT3A*-dependent methylation. However, Hox genes could be important for both oncogenesis and tumor suppression, depending on the context. Thus, hypermethylation of several Hox genes has been widely found in breast, lung, prostate, urothelial, and ovarian tumors,[35] and methylation of *HOXA9* has been found in both neuroblastoma and PCC.[36] The presence of methylation of 26 Hox genes in *DNMT3A*-mutated tumors suggests that these transcription factors may have a tumor suppressor role in PCC/PGL. Our results are also suggestive of a critical role of methylation of homeobox-containing genes in PCC/PGL development. So far, ~300 homeobox genes have been identified in the human genome and the aberrant expression of several members of this superfamily of transcription factors has been implicated in tumor initiation and metastasis in many human tumors.[37] Both losses and gains of homeobox gene expression are related to tumorigenesis, and *DNMT3A* mutations are known to be associated with altered expression of homeobox-containing genes.[38] Of note, this latter is also observed in our model of HeLa cells carrying the *DNMT3A* p.Lys299Ile mutation. Interestingly, 65 differentially methylated homeobox-containing genes found in c.896A>T *DNMT3A*-mutated tumors were found differentially methylated in FLT3-ITD/*DNMT3A*-mutated compared with FLT3-ITD/*DNMT3A*-WT AMLs.[38] The methylation described herein in *DNMT3A*-mutated PGLs and blood samples of mammalian key neural crest determination genes, such as *PAX3*, *FOXD3*, *WT1*, and the ZIC genes, stresses the relevance of repression of autonomic lineage cell differentiation in PCC/PGL, which is also observed in *HIF2A*-mutated PCCs.[39]

In summary, we describe herein the first example of gain-of-function mutations affecting a DNA methyl transferase gene potentially involved in cancer predisposition. More cases and further studies, such as mutation segregation analysis and additional functional assays, are necessary to more precisely determine the role of *DNMT3A* alterations in PCC/PGL susceptibility.

ELECTRONIC SUPPLEMENTARY MATERIAL

The online version of this article (https://doi.org/10.1038/s41436-018-0003-y) contains supplementary material, which is available to authorized users.

ACKNOWLEDGEMENTS

This work was supported by the Instituto de Salud Carlos III (ISCIII), through the "Acción Estratégica en Salud" (AES) (projects PI15/00783 to A.C., PI14/00240 to M.R., and PI14/01884 to S.R.-P., cofounded by the European Regional Development Fund (ERDF)). M.C.-F. is a predoctoral fellow of the Severo Ochoa Program. We thank Antonio Galarreta for his help with the validation of the exome sequencing findings. We thank Maria Jesús Artiga and Manuel Morente for their help in obtaining tumor samples, collected from Spanish hospitals through the Spanish National Tumor Bank Network (CNIO).

CONFLICT OF INTEREST

The authors declare no conflicts of interest.

REFERENCES

1. Dahia PL. Pheochromocytoma and paraganglioma pathogenesis: learning from genetic heterogeneity. *Nat Rev Cancer.* 2014;14:108–19.
2. Letouze E, Martinelli C, Loriot C, et al. SDH mutations establish a hypermethylator phenotype in paraganglioma. *Cancer Cell.* 2013;23:739–52.
3. Noushmehr H, Weisenberger DJ, Diefes K, et al. Identification of a CpG island methylator phenotype that defines a distinct subgroup of glioma. *Cancer Cell.* 2010;17:510–22.
4. Toledo RA, Qin Y, Cheng ZM, et al. Recurrent mutations of chromatin-remodeling genes and kinase receptors in pheochromocytomas and paragangliomas. *Clin Cancer Res.* 2016;22:2301–10.

5. Marco-Sola S, Sammeth M, Guigo R, Ribeca P. The GEM mapper: fast, accurate and versatile alignment by filtration. *Nat Methods.* 2012;9:1185–8.
6. Bendl J, Stourac J, Salanda O, et al. PredictSNP: robust and accurate consensus classifier for prediction of disease-related mutations. *PLoS Comput Biol.* 2014;10:e1003440.
7. McKenna A, Hanna M, Banks E, et al. The Genome Analysis Toolkit: a MapReduce framework for analyzing next-generation DNA sequencing data. *Genome Res.* 2010;20:1297–303.
8. Bibikova M, Le J, Barnes B, et al. Genome-wide DNA methylation profiling using Infinium(R) assay. *Epigenomics.* 2009;1:177–200.
9. Morrissey ER, Diaz-Uriarte R. Pomelo II: finding differentially expressed genes. *Nucleic Acids Res.* 2009;37:W581–586.
10. Benjamini Y, Drai D, Elmer G, Kafkafi N, Golani I. Controlling the false discovery rate in behavior genetics research. *Behav Brain Res.* 2001;125:279–84.
11. Huang da W, Sherman BT, Lempicki RA. Systematic and integrative analysis of large gene lists using DAVID bioinformatics resources. *Nat Protoc.* 2009;4:44–57.
12. Chen EY, Tan CM, Kou Y, et al. Enrichr: interactive and collaborative HTML5 gene list enrichment analysis tool. *BMC Bioinformatics.* 2013;14:128.
13. Reich M, Ohm K, Angelo M, Tamayo P, Mesirov JP. GeneCluster 2.0: an advanced toolset for bioarray analysis. *Bioinformatics.* 2004;20:1797–8.
14. Ley TJ, Miller C, Ding L, et al. Genomic and epigenomic landscapes of adult de novo acute myeloid leukemia. *N Engl J Med.* 2013;368:2059–74.
15. Livak KJ, Schmittgen TD. Analysis of relative gene expression data using real-time quantitative PCR and the 2(-Delta Delta C(T)) method. *Methods.* 2001;25:402–8.
16. Torres-Ruiz R, Martinez-Lage M, Martin MC, et al. Efficient recreation of t (11;22) EWSR1-FLI1+in human stem cells using CRISPR/Cas9. *Stem Cell Rep.* 2017;8:1408–20.
17. Bestor TH. The DNA methyltransferases of mammals. *Hum Mol Genet.* 2000;9:2395–402.
18. Ley TJ, Ding L, Walter MJ, et al. DNMT3A mutations in acute myeloid leukemia. *N Engl J Med.* 2010;363:2424–33.
19. Yang L, Rau R, Goodell MA. DNMT3A in haematological malignancies. *Nat Rev Cancer.* 2015;15:152–65.
20. Shih AH, Abdel-Wahab O, Patel JP, Levine RL. The role of mutations in epigenetic regulators in myeloid malignancies. *Nat Rev Cancer.* 2012;12:599–612.
21. Dhayalan A, Rajavelu A, Rathert P, et al. The Dnmt3a PWWP domain reads histone 3 lysine 36 trimethylation and guides DNA methylation. *J Biol Chem.* 2010;285:26114–20.
22. Rondelet G, Dal Maso T, Willems L, Wouters J. Structural basis for recognition of histone H3K36me3 nucleosome by human de novo DNA methyltransferases 3A and 3B. *J Struct Biol.* 2016;194:357–67.
23. Wu H, Zeng H, Lam R, et al. Structural and histone binding ability characterizations of human PWWP domains. *PLoS ONE.* 2011;6:e18919.
24. Vezzoli A, Bonadies N, Allen MD, et al. Molecular basis of histone H3K36me3 recognition by the PWWP domain of Brpf1. *Nat Struct Mol Biol.* 2010;17:617–9.
25. Qiu Y, Zhang W, Zhao C, et al. Solution structure of the Pdp1 PWWP domain reveals its unique binding sites for methylated H4K20 and DNA. *Biochem J.* 2012;442:527–38.
26. Hoekstra AS, de Graaff MA, Briaire-de Bruijn IH, et al. Inactivation of SDH and FH cause loss of 5hmC and increased H3K9me3 in paraganglioma/pheochromocytoma and smooth muscle tumors. *Oncotarget.* 2015;6:38777–88.
27. Tatton-Brown K, Seal S, Ruark E, et al. Mutations in the DNA methyltransferase gene DNMT3A cause an overgrowth syndrome with intellectual disability. *Nat Genet.* 2014;46:385–8.
28. Hansen RS, Wijmenga C, Luo P, et al. The DNMT3B DNA methyltransferase gene is mutated in the ICF immunodeficiency syndrome. *Proc Natl Acad Sci U S A.* 1999;96:14412–7.
29. Tatton-Brown K, Hanks S, Ruark E, et al. Germline mutations in the oncogene EZH2 cause Weaver syndrome and increased human height. *Oncotarget.* 2011;2:1127–33.
30. Baujat G, Rio M, Rossignol S, et al. Paradoxical NSD1 mutations in Beckwith-Wiedemann syndrome and 11p15 anomalies in Sotos syndrome. *Am J Hum Genet.* 2004;74:715–20.
31. Hoischen A, van Bon BW, Rodriguez-Santiago B, et al. De novo nonsense mutations in ASXL1 cause Bohring-Opitz syndrome. *Nat Genet.* 2011;43:729–31.
32. Kim KH, Roberts CW. Targeting EZH2 in cancer. Nat Med. 2016;22:128–34.
33. Yan XJ, Xu J, Gu ZH, et al. Exome sequencing identifies somatic mutations of DNA methyltransferase gene DNMT3A in acute monocytic leukemia. *Nat Genet.* 2011;43:309–15.
34. Qu Y, Lennartsson A, Gaidzik VI, et al. Differential methylation in CN-AML preferentially targets non-CGI regions and is dictated by DNMT3A mutational status and associated with predominant hypomethylation of HOX genes. *Epigenetics.* 2014;9:1108–19.
35. Shah N, Sukumar S. The Hox genes and their roles in oncogenesis. Nat Rev Cancer. 2010;10:361–71.
36. Margetts CD, Morris M, Astuti D, et al. Evaluation of a functional epigenetic approach to identify promoter region methylation in phaeochromocytoma and neuroblastoma. *Endocr Relat Cancer.* 2008;15:777–86.
37. Abate-Shen C. Homeobox genes and cancer: new OCTaves for an old tune. *Cancer Cell.* 2003;4:329–30.
38. Meyer SE, Qin T, Muench DE, et al. Dnmt3a haploinsufficiency transforms Flt3-ITD myeloproliferative disease into a rapid, spontaneous, and fully-penetrant acute myeloid leukemia. *Cancer Discov.* 2016;6:501–15.
39. Toledo RA, Qin Y, Srikantan S, et al. In vivo and in vitro oncogenic effects of HIF2A mutations in pheochromocytomas and paragangliomas. *Endocr Relat Cancer.* 2013;20:349–59.

Supplementary Information

A

B

neutral	deleterious	% expected accuracy					
Mutation	PredictSNP	MAPP	PhD-SNP	PolyPhen-1	PolyPhen-2	SIFT	SNAP
p.Lys299Ile	**87%**	77%	88%	74%	81%	79%	56%

Supplementary Fig. 1. (**A**) Multiple sequence alignment of twenty-two PWWP domains. Invariant Lys299 is shown in red. (**B**) Deleterious PredictSNP results for the p.Lys299Ile variant.

A

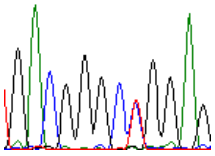

c.952C>T
p.Arg318Trp
DNMT3A

B

neutral deleterious % expected accuracy

Mutation	PredictSNP	MAPP	PhD-SNP	PolyPhen-1	PolyPhen-2	SIFT	SNAP
p.Arg318Trp	**87%**	59%	68%	74%	81%	79%	72%

Supplementary Fig. 2. (**A**) Sanger sequencing chromatogram showing the c.952C>T *DNMT3A* variant found in the germline of a paraganglioma patient with family history of PGL. (**B**) Deleterious PredictSNP results for the p.Arg318Trp variant.

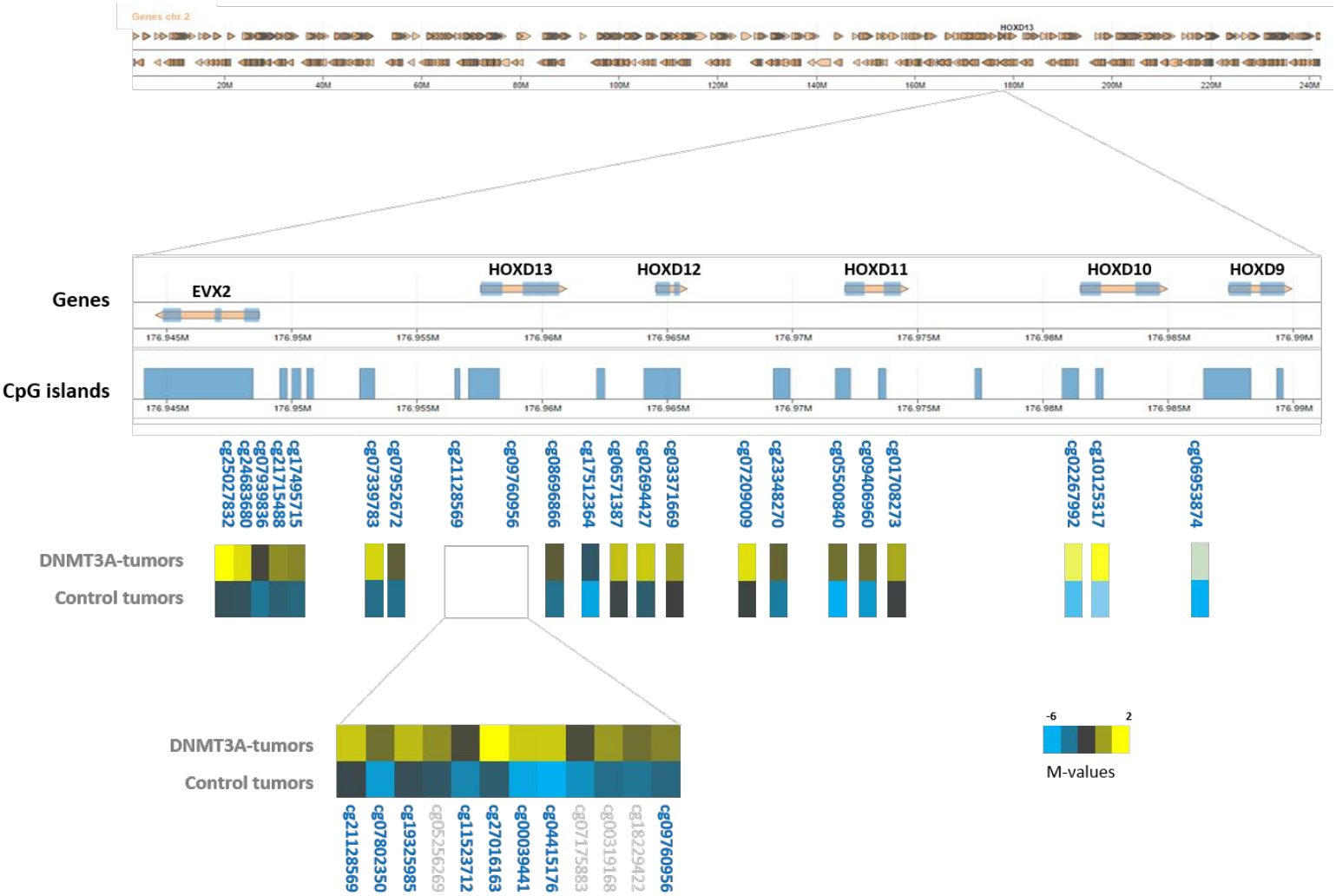

Supplementary Fig. 3. Epiviz visualization of the HOXD genes *locus* on chromosome 2. Significantly differentially methylated EPIC-array probes in *DNMT3A*-mutated PGLs are shown in blue. Additional, non-significant *HOXD13* probes are shown in grey. Mean M-values for *DNMT3A*-mutated tumors (n=3) and controls (n=17) are shown for each probe.

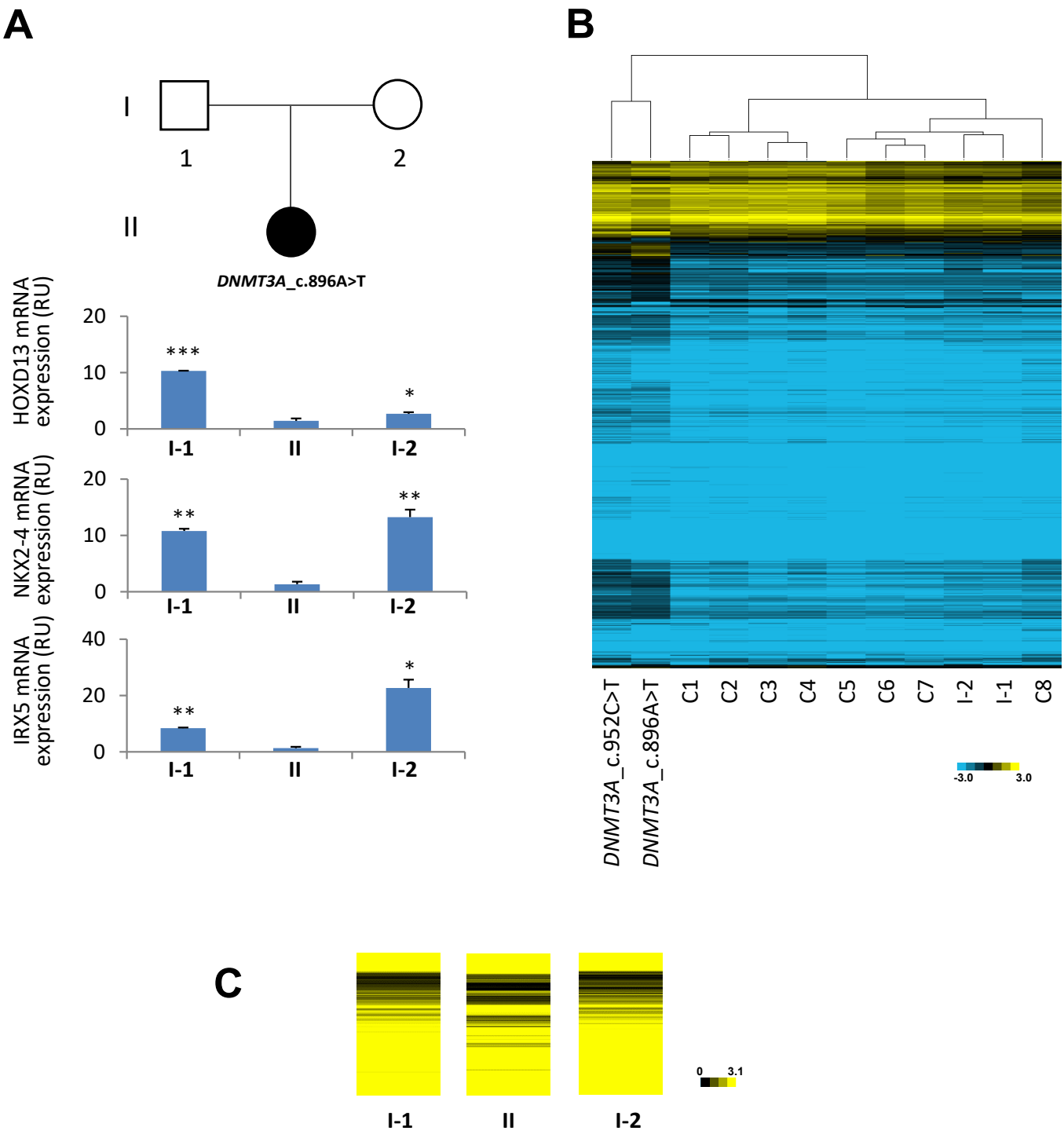

Supplementary Fig. 4. (**A**) HOXD13, NKX2-4 and IRX5 mRNA expression in *DNMT3A*-mutated (proband, II) and non-mutated (parents, I-1 and I-2) lymphocytes. Expression level was normalized to β-actin (ACTB) and presented as mean and standard deviation (n≥2). RU: relative units. Error bars represent standard deviation. A t test was applied to test for differences between the proband and both of her parents. *P<0.05, **P<0.01, ***P<0.001. (**B**) Hierarchical clustering of c.896A>T and c.952C>T *DNMT3A*-mutated lymphocyte samples and ten controls using DNA methylation data from the 3,092 probes significantly differentially methylated between *DNMT3A*-mutated and non-mutated tumors. I-1 and I-2 correspond to lymphocyte samples from the father and the mother, respectively, of the proband carrying the c.896A>T mutation. (**C**) Unsupervised clustering using RNA-seq data from *DNMT3A*-mutated (proband, II) and non-mutated (parents, I-1 and I-2) lymphocytes. Clustering average for linkage and euclidean were used as the distance measure using Genecluster 2.0, and a standard deviation of 0.5 was assumed.

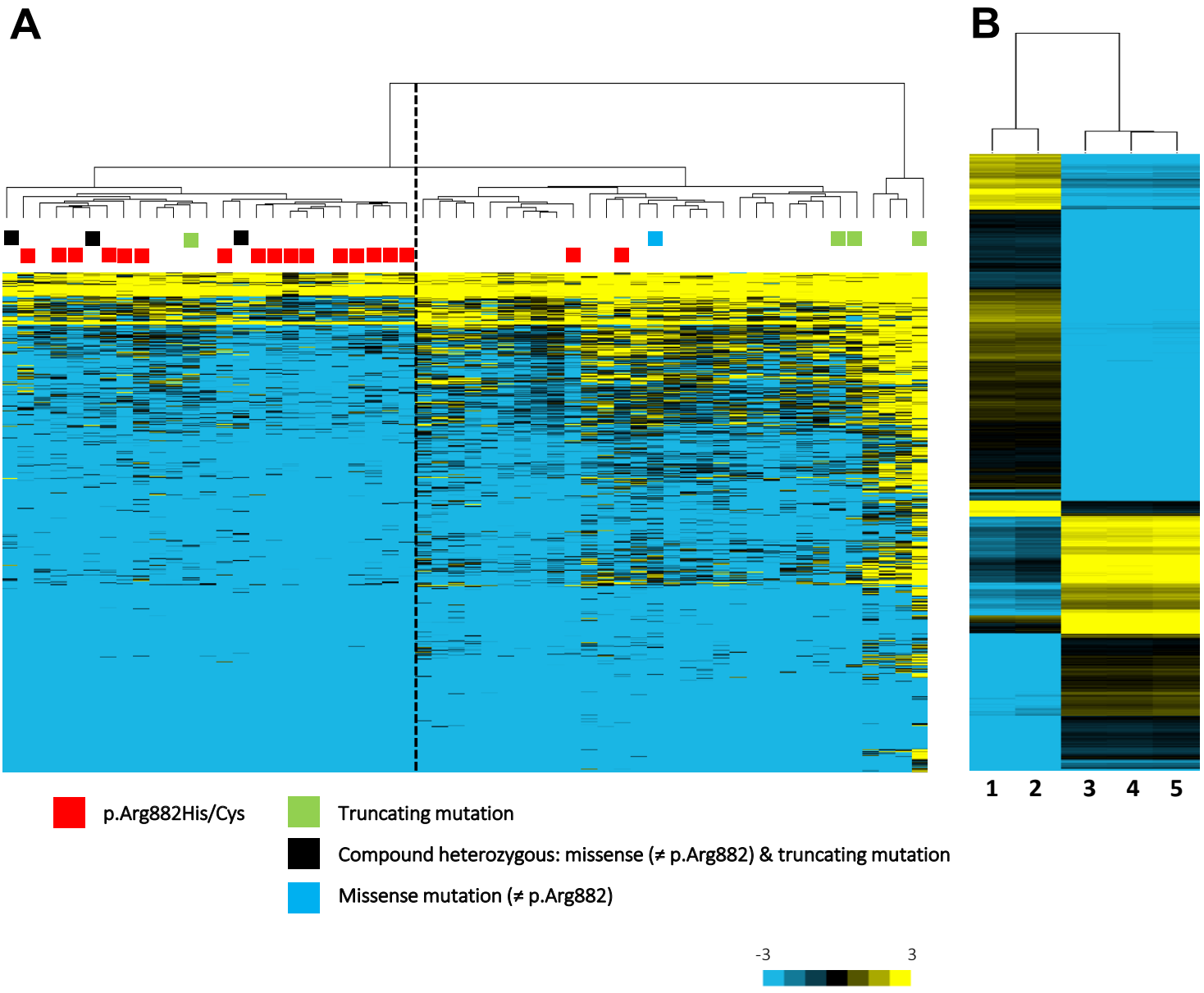

Supplementary Fig. 5. (**A**) Hierarchical clustering of 26 AML samples carrying *DNMT3A* mutations (denoted with color boxes) and 30 *DNMT3A* wild-type AML tumors using DNA methylation data from the 3,092 probes significantly differentially methylated between *DNMT3A*-mutated and non-mutated PGLs. (**B**) Hierarchical clustering performed using DNA methylation data from 16,811 probes significantly differentially methylated (fold-change >|3|) between HeLa WT (two [1, 2] technical replicates) cells and HeLa knock-in cells (c.896A>T) (three [3-5] technical replicates).

Supplementary Table S1. Enrichment for the 3092 probes (1378 genes) differentially methylated in *DNMT3A* -mutated tumors

Enrichr-based enrichment for 1378 input gene IDs

WikiPathway (Homo sapiens)*	**P-value**	**Adjusted p-value**
Dopaminergic Neurogenesis_Homo sapiens_WP2855	2.95E-08	4.96E-06
Neural Crest Differentiation_Homo sapiens_WP2064	6.50E-08	7.27E-06
Endoderm Differentiation_Homo sapiens_WP2853	1.02E-06	6.85E-05
Heart Development_Homo sapiens_WP1591	2.01E-06	1.13E-04
Focal Adhesion_Homo sapiens_WP306	1.22E-04	3.73E-03

*Only the top 5 significant WikiPathways are shown

GO Biological Process (2015)#	**P-value**	**Adjusted p-value**
pattern specification process (GO:0007389)	2.781E-34	1.164E-30
embryonic morphogenesis (GO:0048598)	9.636E-32	2.017E-28
regionalization (GO:0003002)	1.07E-30	1.493E-27
organ morphogenesis (GO:0009887)	5.527E-25	5.785E-22
anterior/posterior pattern specification (GO:0009952)	3.849E-20	2.686E-17
embryonic organ morphogenesis (GO:0048562)	4.582E-21	3.837E-18
neuron differentiation (GO:0030182)	6.008E-20	3.428E-17
tissue morphogenesis (GO:0048729)	5.414E-19	2.267E-16
cell fate commitment (GO:0045165)	6.55E-20	3.428E-17
regulation of neuron differentiation (GO:0045664)	5.892E-18	2.243E-15

#Only the top 10 significant Biological processes are shown

Supplementary Table S2. Enrichr-based enrichment for the 3,094 genes with probes differentially methylated in *DNMT3A* knock-in HeLa cells

GO Biological Process	**P-value**	**Adjusted p-value**
nervous system development (GO:0007399)	2.07E-11	4.93E-08
chemical synaptic transmission (GO:0007268)	4.16E-06	2.53E-03
retina layer formation (GO:0010842)	4.25E-06	2.53E-03
synapse assembly (GO:0007416)	6.22E-06	2.96E-03
membrane depolarization during action potential (GO:0086010)	3.36E-06	2.53E-03
branching involved in ureteric bud morphogenesis (GO:0001658)	1.32E-05	5.22E-03
positive regulation of dendrite extension (GO:1903861)	2.52E-05	8.56E-03
neuronal action potential (GO:0019228)	4.65E-05	1.38E-02
Reactome*		
Neuronal System Homo sapiens R-HSA-112316	6.57E-06	6.05E-03
Cardiac conduction Homo sapiens R-HSA-5576891	9.25E-06	6.05E-03
112315	9.14E-05	2.39E-02
Ion channel transport Homo sapiens R-HSA-983712	6.01E-05	1.96E-02
Phase 0 - rapid depolarisation Homo sapiens R-HSA-5576892	4.34E-05	1.89E-02
445095	1.66E-04	2.76E-02
Transmission In The Postsynaptic Cell Homo sapiens R-HSA-	1.74E-04	2.76E-02
Muscle contraction Homo sapiens R-HSA-397014	1.77E-04	2.76E-02

ARTICLE 3: Recurrent germline *DLST* mutations in individuals with multiple pheochromocytomas and paragangliomas.

Authors: **Laura Remacha**, David Pirman, Christopher E. Mahoney, Javier Coloma, Maria Currás-Freixes, Bruna Calsina, Rocío Letón, Rafael Torres-Pérez, Susan Richter, Guillermo Pita, Belén Herráez, Giovanni Cianchetta, Emiliano Honrado, Lorena Maestre, Miguel Urioste, Javier Aller, Óscar García Uriarte, María Ángeles Gálvez, Raúl M. Luque, Marcos Lahera, Cristina Moreno-Rengel, Graeme Eisenhofer, Cristina Montero-Conde, Cristina Rodríguez-Antona, Óscar Llorca, Gromoslaw A. Smolen, Mercedes Robledo, and Alberto Cascón

Accepted in *American Journal of Human Genetics*, February 2019.

ABSTRACT

Hereditary phaeochromocytoma and paraganglioma (PPGL) is a genetically heterogeneous disease caused by germline mutations affecting one of seventeen major susceptibility genes, many of which encode enzymes involved in the tricarboxylic acid (TCA) cycle. Therefore, in this study we aimed to identify novel disease-related TCA cycle genes that could explain additional patients without mutations in any of the known susceptibility genes.

For that, we applied targeted sequencing of several TCA cycle-related genes to genetically undiagnosed patients' samples. This way, we identified five germline variants affecting the dihydrolipoamide S-succinyltransferase (*DLST*) gene in seven unrelated patients, all except one diagnosed with multiple PPGLs. A recurrent mutation (c.1121G>A; p.Gly374Glu) was found to disrupt the TCA cycle triggering the accumulation of 2-hydroxyglutarate, both in tumours and in a cell-based $^{13}C_5$-glutamate labelling assay. In addition, p.Gly374Glu-DLST tumours exhibited loss of heterozygosity (by means of uniparental disomy), as well as homogeneous expression and methylation patterns.

We also found DLST IHC as a useful tool for identifying tumours carrying alterations not only in *DLST* but also in any of the other TCA cycle-associated genes.

Together, these findings not only unravel *DLST* as a new PPGL susceptibility gene, but they also further strengthen the relevance of the TCA cycle in disease development.

Personal contribution:

I participated in the conception of the study as well as I performed experiments such as targeted sequencing, RT-qPCRs and DLST immunofluorescence in DLST-KO cells. I also collaborated in the analysis of data coming from the SNP, genome-wide methylome and gene expression arrays. I finally took part in the figures' conception, writing of the original draft and its revision.

TITLE: Recurrent germline *DLST* mutations in individuals with multiple pheochromocytomas and paragangliomas

Laura Remacha,[1] David Pirman,[2] Christopher E. Mahoney,[2] Javier Coloma,[3] Bruna Calsina,[1] Maria Currás-Freixes,[1] Rocío Letón,[1] Rafael Torres-Pérez,[1] Susan Richter,[4] Guillermo Pita,[5] Belén Herráez,[5] Giovanni Cianchetta,[2] Emiliano Honrado,[6] Lorena Maestre,[7] Miguel Urioste,[8] Javier Aller,[9] Óscar García Uriarte,[10] María Ángeles Gálvez,[11] Raúl M. Luque,[12] Marcos Lahera,[13] Cristina Moreno-Rengel[14], Graeme Eisenhofer,[4] Cristina Montero-Conde,[1] Cristina Rodríguez-Antona,[1,15] Óscar Llorca,[3] Gromoslaw A. Smolen,[2] Mercedes Robledo,[1,15] and Alberto Cascón,[1,15,*]

Affiliations:

[1]Hereditary Endocrine Cancer Group, Spanish National Cancer Research Centre (CNIO), Madrid, Madrid, 28029, Spain

[2]Agios Pharmaceuticals, 88 Sidney Street, Cambridge, MA 02139, USA

[3]Structural Biology Programme, Spanish National Cancer Research Centre (CNIO), Madrid, Madrid, 28029, Spain

[4]Institute of Clinical Chemistry and Laboratory Medicine, University Hospital Carl Gustav Carus, Medical Faculty Carl Gustav Carus, Technische Universität Dresden, Dresden, Freistaat Sachsen, 01069, Germany

[5]Human Genotyping Unit-CeGen, Human Cancer Genetics Programme, Spanish National Cancer Research Centre (CNIO), Madrid, Madrid, 28029, Spain

[6]Anatomical Pathology Service, Hospital of León, León, Castilla y León, 24071, Spain

[7]Monoclonal Antibodies Unit, Biotechnology Programme, Spanish National Cancer Research Centre (CNIO), Madrid, Madrid, 28029, Spain

[8]Familial Cancer Clinical Unit, Spanish National Cancer Research Centre (CNIO), Madrid, Madrid, 28029, Spain

[9]Department of Endocrinology, University Hospital Puerta de Hierro, Majadahonda, Madrid, 28222, Spain

[10]Nephrology Department, University Hospital of Araba (HUA), Vitoria, País Vasco, 01009, Spain

[11]Service of Endocrinology and Nutrition, University Hospital Reina Sofía (HURS); Maimónides Institute of Biomedical Research of Cordoba (IMIBIC), Córdoba, Andalucía, 14004, Spain

[12]Hormones and Cancer Group. Maimónides Institute of Biomedical Research of Córdoba (IMIBIC), Córdoba, Andalucía, 14004, Spain

[13]Endocrinology and Nutrition Department, La Princesa University Hospital, Madrid, Madrid, 28006, Spain

[14]Department of Endocrinology and Nutrition, University Hospital of Basurto, Bilbao, Spain

[15]Centro de Investigación Biomédica en Red de Enfermedades Raras (CIBERER), Madrid, Madrid, 28029, Spain

*Correspondence: acascon@cnio.es

Abstract

Pheochromocytomas and paragangliomas (PPGLs) provide some of the clearest genetic evidence for the critical role of metabolism in the tumorigenesis process. Approximately 40% of PPGLs are caused by driver germline mutations in 16 known susceptibility genes, and approximately half of these encode members of the tricarboxylic acid (TCA) cycle. Taking as a starting point the involvement of the TCA cycle in PPGL development, we aimed to identify unreported mutations in genes involved in this key metabolic pathway that could explain additional individuals lacking mutations in known susceptibility genes. For that, targeted sequencing of thirty-seven TCA cycle-related genes was applied to DNA from 104 PPGL individuals with no mutations in the major known predisposing genes. Omics-based analyses, TCA-related metabolite determination and $^{13}C_5$-glutamate labeling assays were also performed. We identified five germline variants affecting *DLST* in eight unrelated individuals (~7%), all except one diagnosed with multiple PPGLs. A recurrent variant, p.Gly374Glu, found in four of the eight individuals, triggered accumulation of 2-hydroxyglutarate, both in tumors and in a heterologous cell-based assay designed to functionally evaluate DLST variants. p.Gly374Glu-DLST tumors exhibited loss of heterozygosity and consistent methylation and expression profiles similarly to *EPAS1*-mutated PPGLs, suggesting a link between DLST disruption and pseudohypoxia. Moreover, we found positive DLST immunostaining exclusively in tumors carrying TCA cycle mutations and in cases with *EPAS1* mutations. In summary, this study reveals *DLST* as a PPGL susceptibility gene, and further strengthens the relevance of the TCA cycle in PPGL development.

Introduction

Pheochromocytomas and paragangliomas, together called PPGLs (MIM: 171300), are rare neuroendocrine tumors derived from chromaffin cells of the adrenal medulla and extra-adrenal paraganglia, respectively. PPGLs have one of the highest heritability rates of all neoplasms in humans. Approximately 40% of individuals with this genetically heterogeneous disease carry a germline mutation in one of 16 different susceptibility genes (*FH* [MIM: 136850]*, KIF1B* [MIM: 605995]*, MAX* [MIM: 154950]*, MDH2* [MIM: 154100], *NF1* [MIM: 613113]*, EGLN2* [MIM: 606424]*, EGLN1* [MIM: 606425]*, RET* [MIM: 164761]*, SDHA* [MIM: 600857], *SDHAF2* [MIM: 613019]*, SDHB* [MIM: 185470], *SDHC* [MIM: 602413], *SDHD* [MIM: 602690], *SLC25A11* [MIM: 604165]*, TMEM127* [MIM: 613403] and *VHL* [MIM: 608537]).[1,2] However, there is still an important fraction of individuals with clinical features indicative of a hereditary condition, such as a family history of PPGL, multifocal tumors, or an early age of onset, without mutations in any of the known PPGL susceptibility genes.

Based on many expression and methylation profiling studies (for a review, see[3]), PPGLs can be classified into two main clusters; one of them (cluster 1) is enriched in tumors carrying mutations in genes encoding tricarboxylic acid (TCA) cycle enzymes, such as the SDH genes, *FH, MDH2* and *IDH1* [MIM: 147700]. These alterations lead to disruption of the TCA cycle, which results in the accumulation of "oncometabolites" like succinate, fumarate and 2-hydroxyglutarate (2HG). These oncometabolites contribute to PPGL tumorigenesis through abrogating the function of α-ketoglutarate (αKG)-dependent dioxygenases such as Tet methylcytosine dioxygenase 2 or histone N-methyl-lysine demethylases. This leads to a hypermethylation signature, also known as the CpG island methylator phenotype (CIMP) profile, similar to the ones observed in glioblastomas[4] and renal cell carcinomas[5,6] carrying metabolic alterations such as gain-of-function *IDH1*/*2* and loss-of-function (LoF) *FH*/*SDHB* mutations, respectively. Interestingly, there are still PPGLs that exhibit a CIMP-like profile, but have no alteration in any of the known TCA cycle-related susceptibility genes.[7]

Most PPGLs are benign, but 10-20% of PPGL individuals develop metastases in distant non-chromaffin tissues like the liver, bones, lymph nodes and lungs.[8,9] Despite limited knowledge of markers of malignancy, it is known that PPGLs carrying mutations in TCA cycle-related genes, such as *SDHB* or *FH*, show particularly high rates of malignancy and lower survival rates.[10] Therefore, a better understanding of the molecular pathogenesis of this disease may determine the appropriate management of affected individuals or the treatment strategy.

Considering the relevance of the TCA cycle in PPGL development, we hypothesized that other genes involved in this metabolic pathway could be responsible for the disease in genetically as yet uncharacterized cases. In the present study, we identified a PPGL susceptibility gene by sequencing thirty-seven TCA cycle-related genes in a series of affected individuals without known mutations. We found four different missense mutations and one splice-site variant in the dihydrolipoamide S-succinyltransferase (*DLST* [MIM: 126063])

gene in eight unrelated individuals, suggesting a pathogenic role of the disruption of the αKG dehydrogenase (OGDH) complex activity. The characteristic methylation profile and the accumulation of 2HG found in tumors and cells carrying the recurrent variant p.Gly374Glu suggest that *DLST* may be a PPGL susceptibility gene, and further supports the importance of TCA cycle alterations in PPGL development.

Material and Methods

Research subjects

One hundred and four index affected individuals, without mutations in known PPGL susceptibility genes (*RET*, *VHL*, *NF1*, *MAX*, *TMEM127*, *SDHA*, *SDHB*, *SDHC*, *SDHD*, *SDHAF2*, *MDH2*, *FH*, *EPAS1* [MIM: 603349], and *HRAS* [MIM: 190020]), were included in the study. A summary of the clinical data of the affected individuals is shown in Table S1. Immunostaining of SDHB was performed when formalin-fixed paraffin-embedded (FFPE) tumor tissues were available, in order to rule out hidden mutations affecting the SDH genes.[11] Genomic DNA was extracted from peripheral blood leukocytes using the Maxwell® 16 Blood DNA purification system (Promega). Tumor DNA was obtained using the DNeasy Blood and Tissue kit (Qiagen) for frozen tissues, and the Covaris S2 System (Covaris) for FFPE tissues, following the manufacturers' instructions. The Instituto de Salud Carlos III (ISCIII) ethics committee (Spain) approved the study, and all individuals provided written informed consent to participate in this study.

Targeted next-generation sequencing (NGS)

DNA extracted from the selected samples was sequenced for a set of thirty-seven genes involved in the TCA cycle (Table S2) by TruSight sequencing technology using a previously reported NGS panel.[7] In brief, the NGS panel was designed using Designstudio software (Illumina) and DNA samples were sequenced using a MiSeq desktop sequencer, as previously described.[7] Identified coding and splice-site variants were filtered considering mapping quality, variant score, depth, strand bias, annotation quality, and predicted effect. The cutoff applied to consider a nucleotide substitution as a candidate pathogenic variant was 1.805×10^{-5}, which is the highest frequency of a known pathogenic *SDHB* mutation in the Genome Aggregation Consortium (gnomAD) database. The PredictSNP consensus classifier[12] was used to predict the effects of the substitutions that passed all filtering steps, and Multalin software was used to study and visualize the conservation of specific residues in multiple aligned sequences from different species.

Structural modeling of DLST catalytic domain and predictions on variants

The full-length amino acid sequence of h*DLST* was submitted to the Phyre2 server for structure prediction.[13] Fourteen templates were selected to model the protein based on heuristics to maximize confidence,

percentage identity and alignment coverage. Of these, 13 templates were used to model the biotin/lipoyl attachment domain. The *E. coli* dihydrolipoamide succinyltransferase structure (PDB ID 1SCZ, 60% identity, 74% similarity) was used to model the catalytic domain. Nine residues were modeled *ab initio*. The final model of the protein had 98% of its sequence modeled at >90% confidence. The hDLST protein has been shown to be active as a trimer *in vivo*.[14] The trimeric structure was generated using the *E. coli* dihydrolipoamide succinyltransferase structure crystallized in a trigonal space group (PDB ID 1C4T) as a template. The steric clashes generated during modeling and trimerization were removed using the program Chiron.[15] The active site of the catalytic domain was localized using the known catalytic residues (His424 and Ser372). The binding site of the substrate was predicted using the dihydrolipoyl transacetylase structure of *A. vinelandii* crystallized in the presence of 6,8-dimercapto-octanoid acid amide and coenzyme A (PDB ID 1EAB). Images were generated using PyMOL.[16]

Loss of heterozygosity (LOH) and SNP array analyses

LOH analysis of the *DLST* locus was performed on samples for which tumor DNA was available. Sanger sequencing of tumor DNA using specific primers that amplified *DLST* regions containing the mutations identified was performed in eight tumor samples from five individuals. To characterize the mechanism of LOH, high-density SNP-array analysis was performed on DNA of sufficient quality from two tumors (#4 and #5a). A genome-wide scan was conducted on 250 ng of tumor DNA using the Illumina Human610-Quad BeadChip (Illumina) according to the manufacturer's specifications. Image data was analyzed using the Chromosome Viewer tool contained in GenomeStudio 2010.2 (Illumina). The metric used was the log-R ratio, which is the binary logarithm of the ratio of the observed to expected normalized R values for a given SNP.[17] In addition, the allele frequency was estimated for all SNPs. Microsatellite analysis was carried out on DNA from an additional case (#3). Primers for three polymorphic markers located in chromosome 14 and chromosome 2 (used as control) were designed and labeled (5' 6-FAM). Genomic and tumor DNA were amplified separately by means of a multiplex PCR kit (Qiagen, GmbH, Hilden, Germany), and PCR amplification products were used for fragment analysis on an ABI PRISMTM 310 capillary sequencer (Applied Biosystems, Foster City, CA, USA), and analyzed using Peak Scanner™ Software v1.0 (Applied Biosystems), as previously described.[18]

Lentiviral constructs and techniques

Overexpression of cDNA constructs were made in the pLVX-EF1a-IRES-neo vector, which was derived from the pLVX-EF1a-IRES-puro vector (631988, Clontech) by exchanging the selection cassettes. All *DLST* cDNA

constructs were untagged. All constructs were confirmed by sequencing. A catalytically dead DLST mutant was designed based on the crystal structure of the *E.coli* DLST ortholog (PDB ID: 1SCZ), and His375 was selected as critical for the deprotonation of the thiol group of coenzyme A. The corresponding human residue, His424, was selected for mutagenesis. Lentivirus-based constructs were made using the standard protocol of The RNAi Consortium from the Broad Institute. In order to evaluate the role of DLST variants, we used H838 DLST-KO cells previously generated by CRISPR/Cas9 technology[19]. To infect, H838 DLST-KO cells were centrifuged for 1 hour in the presence of the viruses and 8 μgg/ml Polybrene (H9268, Sigma). Media was replaced after the spin, and drug selection was started 24 hours later. Selection was carried out until all uninfected control cells were dead.

$^{13}C_5$ -glutamate labeling studies in DLST-KO cancer cells

Labeling studies and liquid chromatography-mass spectrometry (LC-MS) methods were conducted as previously described.[19] Briefly, cells were plated at 60%–70% confluency in triplicate in fresh RPMI-1640 media and incubated overnight. The next day, media was replaced with media containing 2 mM $^{13}C_5$-glutamate. Labeling was done for 3 hours, after which the cells were washed three times with PBS (pH 7.4) and metabolites were extracted by the addition of ice-cold 80% methanol. Cell debris was removed by centrifugation and samples were dried under a stream of nitrogen. Internal standard (L-Glutamic acid-$^{13}C_5$, ^{15}N,2,3,3,4,4-d_5, 749850, Sigma-Aldrich) was added at 1 mg/mL during the extraction step. In all labeling studies, the reported amounts of labeled species were corrected for natural isotope abundance.

Immunoblotting

Immunoblotting was conducted as previously described.[19] Briefly, cells were harvested in 1X RIPA buffer (BP-115, Boston BioProducts) containing a phosphatase and protease inhibitor cocktail (5872S, Cell Signaling Technology). Adherent cells were scraped into lysis buffer and sonicated briefly to solubilize. Cell lysates were cleared by centrifugation for 10 min at 4^{o}C. Protein quantification was done using the Pierce BCA Assay Kit (23225, Life Technologies). Primary antibodies used were anti-DLST (HPA003010; rabbit polyclonal 1:1000, Sigma) and anti-GAPDH (97166, 1:10,000, Cell Signaling Technology). Results were visualized using the Odyssey imaging system (LI-COR) and the following secondary antibodies: IRDye 680RD Donkey anti-Rabbit (926-68073, LI-COR) and IRDye 800CW Donkey anti-Mouse (926-32212, LI-COR).

Liquid chromatographic-tandem mass spectrometric determination of TCA-related metabolites

Fresh frozen or FFPE tumor tissue (5-10 mg) from four available cases (#1, #3a,b,c, #4, and #5a,b) (Table 1) and from 51 controls (*DLST*-WT PPGLs), were immersed in 500 µl LC-MS/MS-grade methanol containing isotope-labeled internal standards and processed as previously described.[20] Analysis of metabolites was carried out using an AB Sciex 5500 QTRAP mass spectrometer coupled to an Acquity ultra-high performance liquid chromatographic system (Waters), as previously described.[20]

DNA methylation array

Bisulfite conversion of DNA was performed using the EZ DNA Methylation Kit (Zymo Research) and genome-wide DNA methylation was assayed using the Infinium MethylationEPIC BeadChip Kit (Illumina) at the Centro Nacional de Genotipado (CEGEN-ISCIII), as previously described.[21] This BeadChip interrogates over 850,000 methylation sites per sample at single-nucleotide resolution. Beta values for interrogated CpGs were assigned using the Genome Studio Methylation module and transformed into M values by applying the formula: log2[beta value/(1-beta value)]. Negative M values indicate less than 50% methylation and positive M values indicate more than 50% methylation.[22] M-values were used for statistical analyses. Hierarchical clustering of methylation data from three unrelated *DLST*-mutated tumors and 13 PPGLs carrying known mutations in major susceptibility genes (four *SDHB*-, two *DNMT3A*-, two *HRAS*-, one *NF1*-, two *MAX*-, one *EPAS1*-, and one *RET*- mutated tumors) was performed using GeneCluster 2.0.[23]. A second unsupervised analysis was performed using a list of 125,112 probes corresponding to 4,662 genes with CpG sites reported as significantly hypermethylated in SDHx-mutated (M1) PPGLs.[24] We used the complete linkage as clustering method and the city-block metric as the distance measure in the unsupervised comparisons. The methylomes used in the analysis have been deposited in the National Center for Biotechnology Information GEO database, under accession numbers GSE111336 and GSE123185.

Gene expression array

The Agilent Whole Human Genome platform (4x44K) was used for competitive hybridization of labeled and amplified cDNAs obtained from Universal Human Reference RNA (Stratagene, La Jolla, CA, USA) and from RNAs extracted from PPGL tumor samples, as previously described.[25] To identify a transcriptional profile related to *DLST* alteration, we used gene expression data from two available *DLST*-mutated tumors and from 67 controls harboring mutations in other PPGL susceptibility genes (GEO database accession number GSE19422). Tumor samples were grouped according to their expression profiles by unsupervised clustering, and a supervised analysis was used to identify specific transcripts related to the presence of *DLST* mutations. For the hierarchical

clustering, we used expression data from a previously reported list of 451 genes (572 probes) differentially expressed in SDHx-, *VHL*- and *RET*/*NF1*/*TMEM127*-mutated PPGLs.[26] Differentially expressed genes were identified by a t-test (limma) carried out using POMELO II software.[27] To account for multiple hypothesis testing, the estimated significance level (P) was adjusted using the Benjamini false discovery rate (FDR) correction.[28] Genes with an FDR<0.05 were considered to be differentially expressed between tumor classes. The transcriptome from tumor #5a (data from tumor #4 are already included in GSE19422) has been deposited in GEO, under accession number GSE123344.

Quantitative real-time PCR

Total RNA was obtained from FFPE or frozen material using the RNeasy FFPE (Qiagen) or TriReagent (MRC) kit, respectively, according to the manufacturers' instructions. cDNA was prepared from 1 µg of total RNA using a mix of oligo-dT and random primers and qScript™ cDNA Synthesis Kit (#95047-100, Quanta Biosciences). mRNA levels from genes of interest were determined by quantitative PCR on a 7500 fast real-time PCR system (Applied Biosystems) using the Universal ProbeLibrary set; each sample was analyzed in triplicate. Relative mRNA levels were estimated by the ΔΔCt method[29] and normalized using β-actin (ACTB) as housekeeping gene. The results are shown as mean±SD. mRNAs obtained from frozen/FFPE tumors carrying mutations in other known PPGL susceptibility genes were used as controls.

Immunohistochemistry

Immunohistochemical (IHC) staining of DLST (11954; rabbit monoclonal 1:150, Cell Signaling Technology) was performed using 3 µm FFPE sections from six *DLST*-mutated tumor samples available, following standard procedures. Eighty-two tumors carrying mutations in other PPGL susceptibility genes were used as controls.

Results

TCA-targeted NGS findings

In order to identify additional genes mutated in PPGL affected individuals, we applied targeted sequencing of thirty-seven TCA cycle-related genes to individuals with PPGL and without mutations in the major known predisposing genes. Targeted NGS identified nine germline LoF and non-synonymous coding variants, affecting five different genes in thirteen unrelated affected individuals from the 104 cases analyzed (Table S3). All substitutions were validated by Sanger sequencing. One of the variants was found in a recently reported PPGL susceptibility gene (*SLC25A11;* GenBank: NM_003562 [MIM: 604165])[2], and the remaining changes affected genes that encode different subunits of TCA cycle enzymes (*DLST* and *SUCLG1;* GenBank*:* NM_001933 [MIM: 126063] and NM_003849 [MIM: 611224], respectively), a cytosolic TCA cycle-related protein (*IDH1;* GenBank: NM_001282387 [MIM: 147700]), and a mitochondrial carrier (*SLC25A10*: GenBank: NM_012140 [MIM: 606794]). The only recurrently mutated gene was *DLST*, in which we found five different variants in seven unrelated individuals (Table 1). In addition, upon revisiting 14 whole exomes from PPGL individuals, we found another person carrying a germline *DLST* mutation (#6). We therefore focused our further research on the role of this gene in PPGL development.

DLST is recurrently mutated in individuals with multiple PPGLs

The five different *DLST* variants consisted of four missense mutations (c.1121G>A, p.Gly374Glu [in four individuals]; c.692G>A, p.Arg231Gln; c.910G>A, p.Asp304Asn; and c.1265A>G, p.Tyr422Cys) and one intronic splice site variant (c.1060-3T>A) (Figure 1A and Table 1). None of the individuals with a *DLST* mutation had a family history of the disease and two of them also had non-PPGL tumors. Seven of the eight individuals carrying *DLST* mutations presented with tumors in multiple locations (significantly higher than 21/97 non-*DLST*-mutated cases; $p<0.001$), especially in the thoracic-abdominal region ($p<0.001$). One of the affected individuals developed distant metastasis, and all functional tumors produced normetanephrine (Table 1). Three of the four *DLST* missense substitutions were predicted as deleterious by PredictSNP (Figure S1A) and affected highly-conserved protein residues located close to amino acids predicted to be critical for protein functions (Figure 1B): Gly374 and Tyr422 are part of a pocket where the succinyl group fits in *E. coli*, and Tyr422 is close to the active site of the protein (Figure 1C).[30] All *DLST* variants were absent or found in at most 3 controls in gnomAD (out of more than 122,000 individuals) (Table S3), and two of them (p.Asp304Asn and p.Gly374Glu) were found as somatic variants in other cancers (Figure S1B). The number of heterozygous LoF

mutations per coding nucleotide found in gnomAD for *DLST* (n=12) was significantly lower ($p<0.05$) than that observed for *SDHB* (n=25), and similar to that observed for *FH* (n=18). Assuming that disease-causing genes are more intolerant of rare LoF variants,[31] this suggests that the presence of heterozygous *DLST* LoF variants could have phenotypic consequences.

The *DLST* variants locate in a region critical for functional activity

Structural analysis revealed that all missense variants detected map in regions of DLST involved in its catalytic activity. A structural model of human DLST was generated based on a comparison with available crystal structures from prokaryotic homologs. The structures of the N- and C-terminal domains were predicted with significant confidence due to their high conservation, but the spatial relationship between the two domains cannot be predicted accurately since there seems to be a poorly structured region connecting both domains. There is evidence of flexibility from the structures of related complexes,[14] which would be allowed by the linker connecting the catalytic and Biotin/Lipoyl attachment domains. The family of dehydrogenase multienzyme complexes that includes DLST functions as trimeric complexes with the catalytic domain formed by residues from two adjacent subunits.[32] Gly374 locates within the pocket where the succinyl group fits, but also in the region of interaction between two monomers. The recurrent p.Gly374Glu substitution introduces a large and negatively-charged side chain, compared to the Gly-containing structure, which could interfere with either binding to the succinyl group and/or oligomerization (Figure 1C).

p.Gly374Glu-DLST tumors show LOH due to uniparental disomy

Sanger sequencing revealed LOH of the WT *DLST* allele in six tumors from three independent individuals, all of them carrying the p.Gly374Glu variant (Table 1 and Figure S2A). Genome-wide SNP array and microsatellite analysis revealed that uniparental disomy (UPD) of chromosome 14q, on which *DLST* is located, caused LOH in tumors from three available individuals carrying the p.Gly374Glu variant (Figure 2). One of the tumors also showed loss of chromosomes 11 and 3q. The other two showed clonal gains in chromosomes 6p, 7p, and 22 and no chromosomal alterations in PPGL-predisposing loci (i.e. loss of chromosomes 1p, 11 and 3, and gain of chromosome 2p). In addition, a paternal origin of the UPD was determined in the three individuals carrying the p.Gly374Glu variant based on the methylation status (data obtained from the methylation arrays) of a maternally expressed imprinted gene, *MEG3*, which is located at the distal part of chromosome 14q (Figure 2). Collectively, the observed pattern of genetic changes at this locus suggests a tumor suppressor role for

DLST. Two additional *DLST*-mutated tumors, carrying substitutions different from the recurrent p.Gly374Glu variant, showed no LOH (Table 1).

Functional evaluation of DLST variants

To assess the impact of the missense variants on DLST function, we conducted $^{13}C_5$-glutamate labeling studies to trace the carbon flow in the TCA cycle (Figure 3A). The individual DLST mutants (see Table 1), along with the corresponding WT DLST control, were introduced in H838 DLST-KO cells. These cells do not demonstrate dramatic DLST-associated growth defects probably due to significant activity of compensatory metabolic pathways [19]. The complete inhibition of oxidative TCA in these cells, demonstrated by loss of $^{13}C_4$-succinate, $^{13}C_4$-fumarate and $^{13}C_4$-malate fractions, provides a robust assay for the evaluation of DLST variants. We also included a predicted catalytically-dead DLST mutant, p.His424Ala. The prediction was based on homology modeling of the *E.coli* DLST ortholog (PDB: 1SCZ) and the critical role this histidine plays in deprotonation of the coenzyme A thiol group. An equivalent protein level was achieved for all DLST constructs (Figure 3B).

As expected, DLST-KO cells displayed a significant block in carbon flow in the TCA cycle as evidenced by negligible levels of labeled downstream metabolites, such as $^{13}C_4$-succinate, $^{13}C_4$-fumarate, $^{13}C_4$-malate, and $^{13}C_4$-aspartate (Figure 3C). Reintroduction of WT DLST was able to effectively rescue this metabolic phenotype and the predicted catalytically-dead mutant, p.His424Ala, had dramatically diminished activity. Of the four variants identified in our PPGLs, only p.Gly374Glu showed partially compromised activity as compared to WT DLST. Importantly, all cells displayed equivalent levels of precursor labeling, as evidenced by $^{13}C_5$-glutamate and $^{13}C_5$-αKG levels. Confirmatory results were obtained using the $^{13}C_5$-2HG readout, where DLST-KO cells displayed significant levels of 2HG accumulation (L-2HG/D-2HG>25) that was decreased by reintroduction of WT DLST. Only two mutants, p.His424Ala and p.Gly374Glu, showed a behavior consistent with diminished enzymatic activity (Figure 3D). Collectively, these results indicate that the p.Gly374Glu variant results in a functionally compromised DLST protein. Considering this result, and due to tissue limitations, we focused our further research on the p.Gly374Glu-DLST- tumors.

p.Gly374Glu-DLST tumors accumulate αKG and 2HG

Liquid chromatography tandem-mass spectrometry revealed a significantly higher αKG/fumarate ratio (21.48±23.65; n=5) in p.Gly374Glu-DLST tumors as compared to WT-DLST tumors (2.27±4.99; n=51, $p<0.001$) (Figure 4A). Additionally, p.Gly374Glu-DLST tumors presented a significantly higher 2HG/fumarate ratio

(24.64±21.40; n=5) than PPGLs due to other mutations (1.97±0.87; n=6) ($p<0.05$) (Figure 4B). The levels of L-2HG, the 2HG enantiomer generated from αKG by promiscuous activity of lactate and malate dehydrogenases, were >2.3 times higher than D-2HG levels in three p.Gly374Glu-DLST tumors available for the measurement (data not shown). Since this ratio reflects normally found proportions of L-2HG to D-2HG and since *IDH1/2* mutations are associated with a complete reversal to many fold higher D-2HG to L-2HG concentrations[33], the data suggest that the increase in 2HG was not related to *IDH1/2* neomorphic mutations. All this data suggests that disruption of the TCA cycle in p.Gly374Glu-DLST tumors leads to aberrantly elevated αKG/fumarate and 2HG/fumarate ratios.

p.Gly374Glu-DLST tumors show a characteristic methylation profile

To understand the impact of *DLST* mutations on the global methylation patterns in PPGLs tumors, we profiled three tumors from unrelated individuals carrying the p.Gly374Glu-DLST variant and 14 tumors harboring known mutations in other PPGL susceptibility genes. The three DLST-mutated cases consistently clustered together within the non-CIMP methylation cluster, together with tumors with *EPAS1* and *MAX* mutations, close to tumors carrying *RET*/*NF1*/*HRAS* mutations, and separated from tumors carrying SDHx and *DNMT3A* mutations (Figure S2B). This relatively uniform methylation profile further supports the relevance of the p.Gly374Glu DLST variant, and is in agreement with previous studies that showed the importance of the driver mutation on PPGL methylation profiles. Hierarchical clustering using methylation data from 125,112 probes corresponding to 4,662 genes reported as significantly hypermethylated in SDHx-mutated tumors, grouped the four *SDHB*- and the two *DNMT3A*-mutated tumors together in a CIMP cluster, while *HRAS*-, *NF1*-, *RET*- and *MAX*-mutated cases and the only *EPAS1*-mutated tumor clustered in the non-CIMP cluster (Figure S2C). This unsupervised analysis clustered the three p.Gly374Glu-DLST tumors together and within the non-CIMP cluster. Thus, despite a very homogeneous methylation profile, p.Gly374Glu-DLST tumors do not show the CIMP profile associated with other TCA-cycle related mutations. Rather, *DLST*-mutated tumors clustered with the only M2 tumor (i.e. PPGLs showing an intermediate methylation phenotype) included in the analysis, which questions the role of the observed accumulation of metabolites as the mediators of tumorigenesis in *DSLT*-mutated PPGLs.

HIF3A is overexpressed in *DLST*-mutated tumors

Hierarchical clustering of whole gene expression data from 69 frozen tumors grouped the two (#4 and #5a) p.Gly374Glu-DLST tumors together, suggesting a common transcriptional profile. A second unsupervised

clustering using a list of 451 genes differentially expressed in PPGLs with different genetic backgrounds grouped all *VHL*- and SDHx-mutated tumors in cluster 1, and all tumors carrying mutations in *TMEM127*/*MAX*/*NF1*/*HRAS* genes in cluster 2. Interestingly, the two p.Gly374Glu-DLST cases (#4 and #5a) were grouped in cluster 1 together with all, except one, tumors carrying mutations in *EPAS1* (Figure 4C). This result suggests a consistent impact of the potential driver mutation on gene expression, and a link between p.Gly374Glu-DLST variant and pseudohypoxia. The supervised analysis revealed 132 probes significantly differentially expressed in *DLST*-mutated tumors compared to tumors carrying known mutations in other PPGL susceptibility genes (Table S4). The most representative probes targeted signal transduction and hematopoiesis genes such as *JAK3* [MIM: 600173], *ERBB4* [MIM: 600543] or *LEPR* [MIM: 601007], neural proteins like *MAP7D1*, *SPTBN5* [MIM: 605916]*, GABRA4* [MIM: 137141]*, ZIC4* [MIM: 608948] and *FRMD7* [MIM: 300628], and seven nucleosome genes. Moreover, four different probes targeting *HIF3A* [MIM: 609976] were found differentially overexpressed and were ranked amongst the five most significant ones. mRNA expression of *HIF3A,* measured by RT-qPCR, showed an overexpression of *HIF3A* in p.Gly374Glu-DLST tumors (#3a,c; #4 and #5a) when compared to controls (n=18) (Figure 4D), which further suggests a link between DLST disruption and pseudohypoxia.

DLST- and TCA cycle-mutated PPGLs show positive DLST immunostaining

Immunohistochemical (IHC) staining of DLST in all available *DLST*-mutated tumors revealed that this enzyme was more abundant in these samples as compared to *DLST*-WT PPGLs (Figure 5A). A strong staining was also observed in all tumors carrying mutations in genes encoding TCA cycle enzymes (n=33) compared with control PPGLs carrying mutations in other PPGL susceptibility genes ($p<0.001$) (Figure 5B). Four of the control tumors without TCA cycle mutations showed an intense IHC staining (IHC score=3), and two of them carried a mutation in *EPAS1*. Therefore, we extended the IHC study to six additional *EPAS1*-mutated tumors and found a positive staining in all of them (Figure 5B). This data suggests DLST immunohistochemistry as a useful tool to identify tumors from the pseudohypoxic cluster 1 carrying alterations either in TCA cycle-related genes or in *EPAS1*.

Discussion

The identification of heterozygous germline mutations in more than ten genes that are directly or indirectly involved in the TCA cycle point to this metabolic pathway as one of the main drivers for the development of PPGLs. Thus, the assessment of TCA cycle status has become a routine part of the genetic diagnosis of PPGL and has fueled intense interest in this pathway to identify therapeutic targets. In the present study, we have found variants affecting *DLST* in more than 6% of affected individuals (most of them with multiple tumors) without mutations in other PPGL-related genes. Moreover, we have demonstrated the deleterious effect for DLST function of one recurrently mutated residue (found in ~3% of the whole series of affected individuals) and therefore propose *DLST* as a PPGL susceptibility gene.

DLST encodes the E2 subunit of the mitochondrial αKG dehydrogenase (OGDH) complex, which has two additional subunits: E1 (encoded by *OGDH* [MIM: 613022]) and E3 (encoded by *DLD* [MIM: 238331]). The OGDH complex catalyzes the overall conversion of αKG to succinyl-CoA and CO_2. Depletion of any of the OGDH complex subunits leads to impaired enzymatic activity and αKG accumulation, and it has been demonstrated that DLST is a non-redundant member of the OGDH complex.[34] *Dlst* KO mice are embryonically lethal and while some DLST-KO cells can grow, they exhibit a complete disruption of the oxidative TCA cycle.[19,35] Any condition causing even a modest variation in the cytosolic levels of αKG may affect different pathways, promoting either oncogenic or tumor suppressive responses: increase of fatty acid biosynthesis or promotion of aberrant mammalian target of rapamycin 1 (mTORC1) activation (Figure S3). [36–38]. In addition, *DLST* mutation causing loss of OGDH complex nuclear translocation capacity, may lead to altered overall gene expression (Figure S3). [39] The increased αKG to fumarate ratio in p.Gly374Glu-mutated tumors suggests that this variant leads to a disruption of OGDH complex activity. Moreover, the accumulation of significant levels of L-2HG in DLST-KO cells reconstituted with p.Gly374Glu-DLST mutant protein further suggests a functional impairment of this mutant DLST, since an increase in L-2HG has been previously noted in other experimental models upon OGDH complex disruption.[34]

In contrast to D-2HG, which can be generated by neomorphic mutations in *IDH1* or *IDH2* [MIM: 147650],[40] the stereospecific production of L-2HG is driven by the reduction of mitochondrial αKG by both malate dehydrogenases (MDH1 and MDH2) and mainly by lactate dehydrogenase A (LDHA)[42], which specific inhibition prevents the accumulation of L-2HG in OGDH null cells. [34] This promiscuous substrate usage of αKG occurs specifically under conditions of increased αKG as a result of TCA cycle dysfunction, increased mitochondrial reducing potential, or oxygen limitation.[34,41,42] The labeling studies with $^{13}C_5$-glutamate revealed that the p.Gly374Glu-DLST variant is functionally compromised, as it was not able to reconstitute WT-DLST function in the context of DLST-KO cells. The location of Gly374 close to Ser372, an amino acid described to be essential for catalysis,[32] reinforces the hypothesis that distortion introduced by the Gly to Glu substitution

could interfere with the catalytic activity of DLST. The remaining substitutions, although two of them affect residues that are highly conserved and were predicted to be deleterious, displayed similar behavior to WT-DLST in our cellular model. Moreover, Tyr422 is very close to the critical residue of the active site (His424) of the protein. It is important to note that we cannot exclude the possibility that these variants affect other less-explored DLST functions, such as the biogenesis of the respiratory chain,[43] or that they manifest defects in a more physiologically relevant context not recapitulated by our heterologous system.

The presence of multiple tumors in most of the individuals with *DLST* mutations, similar to other hereditary cancer syndromes, supports the pathological role of *DLST* germline variants. On the other hand, the lack of family history of the disease in these particular individuals (Figure S4) points to a *de novo* or low penetrance inheritance; this latter mechanism is frequently observed in PPGL.[20,44] It is interesting to note that one of the individuals also harbored a pituitary adenoma, a pathology that has been described to co-occur in some persons with PPGL.[45] However, given the singularity of this observation, further studies in a larger number of affected individuals will be needed to elucidate the functional contribution of *DLST*.

To the best of our knowledge, there are no *DLST* or OGDH complex germline mutations reported in individuals with cancer. However, mutations in *DLD* result in an atypical form of αKG dehydrogenase deficiency,[46] and recessive variants in *DHTKD1* [MIM: 614984] and *OGDHL* [MIM: 617513], encoding proteins similar to subunits of the OGDH complex, have been found in individuals with neurodegenerative phenotypes,[38,47] and a decline in OGDH complex activity has also been associated with neurodegeneration.[48] Moreover, it is well known that homozygous or compound heterozygous mutations in TCA cycle-related genes (e.g. *SDH* genes, *FH*, *MDH2*, *ACO2* [MIM: 100850], *IDH3A* [MIM: 601149] or *SLC25A10*), lead to encephalopathy and neurodegeneration.[49–53] Thus, taking into account the evidences linking intermediary metabolism, tumorigenesis and neurodegeneration, it is not surprising to find mutations in *DLST* leading to cancer.

LOH of chromosomal regions is crucial in tumor progression and has been successfully used to map the locations of tumor suppressor genes. Since disease-causing genes appear to be more intolerant of rare LoF variants,[31] the presence of heterozygous *DLST* LoF variants could have phenotypic consequences. On the other hand, six tumors carrying the recurrent p.Gly374Glu variant showed LOH, suggesting a tumor suppressor role for *DLST.* Moreover, we were able to demonstrate in all individuals carrying the p.Gly374Glu-DLST variant that the chromosomal loss observed in their tumors was due to a paternal chromosome 14q UPD, a second-hit mechanism previously reported in PPGLs carrying mutations in the susceptibility gene *MAX*.[18] Interestingly, hierarchical genome-wide expression analysis of two *DLST*-mutated tumors showed that they had similar expression patterns that were also alike to *MAX*-mutated PPGLs. We studied these tumors in more detail and were able to rule out the presence of rare promoter or deep intronic *MAX* mutations (data not shown). The existence of a particular MAX-like expression profile has been previously reported in PPGL,[54] and it was suggested that certain unknown genes could phenocopy *MAX*-mutant tumors. Our findings suggest that *DLST*

may be one of these genes and that the gene expression alterations caused by paternal chromosome 14q UPD is the cause of this characteristic expression profile, underscoring the relevance of this mechanism for PPGL pathogenesis. Finally, the absence of somatic rearrangements in other PPGL susceptibility loci, and the finding of 14q UPD as the only common chromosomal alteration in p.Gly374Glu-DLST mutated tumors further supports the role of DLST in tumor development.

Previous methylome analyses on PPGLs identified stable clusters associated with distinct clinical features and mutational status.[22,24,55] The homogeneous methylation profile exhibited by the PPGLs carrying the p.Gly374Glu-DLST variant rules out a CIMP profile, and it further points to a driver role of this *DLST* mutation in these tumors. Moreover, the expression profile shared by *DLST*-mutated tumors further suggests that they carry a similar driver genetic alteration. Depletion of DLST leads to increased endogenous *HIF1A* [MIM: 603348] levels by L-2HG-mediated inhibition of enzymatic prolyl hydroxylase activities.[34] The expression profile similar to that of *EPAS1*-mutated tumors and the consistent upregulation of *HIF3A* mRNA observed in p.Gly374Glu-DLST tumors further strengthen the connection of tumors harboring TCA mutations to the induction of a pseudo-hypoxic state. [25,56] Moreover, it is known that *HIF3A* overexpression in pancreatic cancer tissues is correlated with a shorter survival time and increased local invasion and distant metastasis.[57] Further studies of *HIF3A* in this context are warranted.

Finally, the strong DLST immunostaining observed in *DLST*-mutated tumors may suggest that, as occurs with *SDHD* and the SDH complex,[58] the presence of mutations in *DLST* disrupt OGDH complex assembly and make the DLST epitope more accessible. This could also explain the high intensity of DLST immunostaining found in PPGLs carrying other mutations in TCA cycle-related genes, since these mutations also lead to disruption of the cycle. The positive DLST staining observed in *EPAS1*-mutated tumors suggests that the activation of this pseudohypoxic pathway could also provoke changes in the assembly of TCA cycle enzymes. This is in agreement with the proposed regulatory network between the TCA cycle and the hypoxia response in which each of the pathways reciprocally affects the other. [56] Although the mechanism remains unexplained, our data suggests that DLST immunohistochemistry may be useful to help in the classification of variants of unknown significance in genes related to the TCA cycle.

In summary, we have identified a recurrent germline variant (p.Gly374Glu) that functionally compromises DLST function. Tumors harboring this alteration display altered methylation and transcriptional profiles similar to the ones observed in *EPAS1*-mutated tumors, suggesting a connection between DLST functional abrogation and pseudohypoxia. Therefore, we propose *DLST* as a PPGL susceptibility gene.

Accession Numbers

The transcriptome from tumor #5a and the methylomes used in the analysis have been deposited in the National Center for Biotechnology Information GEO database under the accession numbers GSE123344 GSE111336 and GSE123185.

Supplemental Data

Supplemental data include five figures and four tables.

Declaration of interests

David Pirman, Christopher E. Mahoney, Giovanni Cianchetta and Gromoslaw A. Smolen are employees of and have ownership interest in Agios Pharmaceuticals. The other authors declare no competing interests.

Acknowledgments

This work was supported by the Instituto de Salud Carlos III (ISCIII), through the “Acción Estratégica en Salud” (AES) (projects PI15/00783 and PI17/01796, to A.C. and M.R., respectively, cofounded by the European Regional Development Fund (ERDF)), and the Deutsche Forschungsgemeinschaft (DFG RI2684/1-1 to S.R.). The Human Genotyping Unit is a member of CeGen, PRB3 and is supported by grant PT17/0019, of the PE I+D+i 2013-2016, funded by ISCIII and ERDF.

Web resources

Centro Nacional de Genotipado (CEGEN-ISCIII): www.cegen.org.

Genome Aggregation Consortium database: http://gnomad.broadinstitute.org.

Multalin software: http://multalin.toulouse.inra.fr.

National Center for Biotechnology Information GEO database: https://www.ncbi.nlm.nih.gov/geo/.

Online Mendelian Inheritance in Man: http://www.omim.org.

Phyre2 server: http://www.sbg.bio.ic.ac.uk/phyre2.

RNAi Consortium from the Broad Institute: http://portals.broadinstitute.org/gpp/public/resources/protocols.

Universal ProbeLibrary set: https://www.roche-applied-science.com.

References

1. Toledo, R. a., Burnichon, N., Cascon, A., Benn, D.E., Bayley, J.-P., Welander, J., Tops, C.M., Firth, H., Dwight, T., Ercolino, T., et al. (2017). Consensus Statement on next-generation-sequencing-based diagnostic testing of hereditary phaeochromocytomas and paragangliomas. Nat. Rev. Endocrinol. *13*, 233–247.

2. Buffet, A., Morin, A., Castro-Vega, L.-J., Habarou, F., Lussey-Lepoutre, C., Letouzé, E., Lefebvre, H., Guilhem, I., Magalie, H., Raingeard, I., et al. (2018). Germline mutations in the mitochondrial 2-oxoglutarate/malate carrier SLC25A11 gene confer a predisposition to metastatic paragangliomas. Cancer Res. *78*, 1914–1922.

3. Dahia, P.L.M. (2014). Pheochromocytoma and paraganglioma pathogenesis: Learning from genetic heterogeneity. Nat. Rev. Cancer *14*, 108–119.

4. Turcan, S., Rohle, D., Goenka, A., Walsh, L. a., Fang, F., Yilmaz, E., Campos, C., Fabius, A.W.M., Lu, C., Ward, P.S., et al. (2012). IDH1 mutation is sufficient to establish the glioma hypermethylator phenotype. Nature *483*, 479–483.

5. The Cancer Genome Atlas Research Network (2016). Comprehensive Molecular Characterization of Papillary Renal-Cell Carcinoma. N. Engl. J. Med. *374*, 135–145.

6. Ricketts, C., Killian, J.K., Vocke, C.D., Sourbier, C., Yang, Y., Merino, M.J., Meltzer, P.S., and Linehan., W.M. (2016). Abstract 2660: A renal CpG island methylator phenotype (R-CIMP) in kidney tumors associated with germline mutations of FH and SDHB. Cancer Res. *76*,.

7. Remacha, L., Comino-Méndez, I., Richter, S., Contreras, L., Currás-Freixes, M., Pita, G., Letón, R., Galarreta, A., Torres-Pérez, R., Honrado, E., et al. (2017). Targeted Exome Sequencing of Krebs Cycle Genes Reveals Candidate Cancer–Predisposing Mutations in Pheochromocytomas and Paragangliomas. Clin. Cancer Res. *23*, 6315–6324.

8. Björklund, P., Pacak, K., and Crona, J. (2016). Precision medicine in pheochromocytoma and paraganglioma: current and future concepts. J. Intern. Med. *280*, 559–573.

9. Lussey-Lepoutre, C., Buffet, A., Gimenez-Roqueplo, A.P., and Favier, J. (2017). Mitochondrial deficiencies in the predisposition to paraganglioma. Metabolites *7*, 1–13.

10. Amar, L., Baudin, E., Burnichon, N., Peyrard, S., Silvera, S., Bertherat, J., Bertagna, X., Schlumberger, M., Jeunemaitre, X., Gimenez-Roqueplo, A.-P., et al. (2007). Succinate dehydrogenase B gene mutations predict survival in patients with malignant pheochromocytomas or paragangliomas. J. Clin. Endocrinol. Metab. *92*, 3822–3828.

11. van Nederveen, F.H., Gaal, J., Favier, J., Korpershoek, E., Oldenburg, R. a., de Bruyn, E.M., Sleddens, H.F., Derkx, P., Rivière, J., Dannenberg, H., et al. (2009). An immunohistochemical procedure to detect patients with paraganglioma and phaeochromocytoma with germline SDHB, SDHC, or SDHD gene mutations: a retrospective and prospective analysis. Lancet Oncol. *10*, 764–771.

12. Bendl, J., Stourac, J., Salanda, O., Pavelka, A., Wieben, E.D., Zendulka, J., Brezovsky, J., and Damborsky, J. (2014). PredictSNP: Robust and Accurate Consensus Classifier for Prediction of Disease-Related Mutations. PLoS Comput. Biol. *10*, 1–11.

13. Kelley, L. a, Mezulis, S., Yates, C.M., Wass, M.N., and Sternberg, M.J.E. (2015). Europe PMC Funders Group The Phyre2 web portal for protein modelling , prediction and analysis. Nat. Protoc. *10*, 845–858.

14. Zhou, Z.H., McCarthy, D.B., O'Connor, C.M., Reed, L.J., and Stoops, J.K. (2001). The remarkable structural and functional organization of the eukaryotic pyruvate dehydrogenase complexes. Pnas *98*, 14802–14807.

15. Ramachandran, S., Kota, P., Ding, F., and Dokholyan, N. V. (2011). Automated minimization of steric clashes in protein structures. Proteins Struct. Funct. Bioinforma. *79*, 261–270.

16. The PyMOL Molecular Graphics System, Version 2.0 Schrödinger, LLC.

17. Simon-Sanchez, J., Scholz, S., Fung, H.C., Matarin, M., Hernandez, D., Gibbs, J.R., Britton, A., de Vrieze,

F.W., Peckham, E., Gwinn-Hardy, K., et al. (2007). Genome-wide SNP assay reveals structural genomic variation, extended homozygosity and cell-line induced alterations in normal individuals. Hum. Mol. Genet. *16*, 1–14.

18. Comino-Méndez, I., Gracia-aznárez, F.J., Schiavi, F., Landa, I., Leandro-garcía, L.J., Letón, R., Honrado, E., Ramos-medina, R., Caronia, D., Pita, G., et al. (2011). Exome sequencing identifies MAX mutations as a cause of hereditary pheochromocytoma. Nat. Genet. *43*, 663–667.

19. Allen, E.L., Ulanet, D.B., Pirman, D., Mahoney, C.E., Coco, J., Si, Y., Chen, Y., Huang, L., Ren, J., Choe, S., et al. (2016). Differential Aspartate Usage Identifies a Subset of Cancer Cells Particularly Dependent on OGDH. Cell Rep. *17*, 876–890.

20. Cascón, A., Comino-Méndez, I., Currás-Freixes, M., De Cubas, A. a., Contreras, L., Richter, S., Peitzsch, M., Mancikova, V., Inglada-Pérez, L., Pérez-Barrios, A., et al. (2015). Whole-exome sequencing identifies MDH2 as a new familial paraganglioma gene. J. Natl. Cancer Inst. *107*, 1–5.

21. Bibikova, M., Le, J., Barnes, B., Saedinia-Melnyk, S., Zhou, L., Shen, R., and Gunderson, K.L. (2009). Genome-wide DNA methylation profiling using Infinium® assay. Epigenomics *1*, 177–200.

22. De Cubas, A. a., Korpershoek, E., Inglada-Pérez, L., Letouzé, E., Currás-Freixes, M., Fernández, A.F., Comino-Méndez, I., Schiavi, F., Mancikova, V., Eisenhofer, G., et al. (2015). DNA methylation profiling in pheochromocytoma and paraganglioma reveals diagnostic and prognostic markers. Clin. Cancer Res. *21*, 3020–3030.

23. Reich, M., Ohm, K., Angelo, M., Tamayo, P., and Mesirov, J.P. (2004). GeneCluster 2.0: An advanced toolset for bioarray analysis. Bioinformatics *20*, 1797–1798.

24. Letouzé, E., Martinelli, C., Loriot, C., Burnichon, N., Abermil, N., Ottolenghi, C., Janin, M., Menara, M., Nguyen, A., Benit, P., et al. (2013). SDH Mutations Establish a Hypermethylator Phenotype in Paraganglioma. Cancer Cell *23*, 739–752.

25. López-Jiménez, E., Gómez-López, G., Leandro-García, L.J., Muñoz, I., Schiavi, F., Montero-Conde, C., de Cubas, A. a., Ramires, R., Landa, I., Leskelä, S., et al. (2010). Research Resource: Transcriptional Profiling Reveals Different Pseudohypoxic Signatures in SDHB and VHL-Related Pheochromocytomas. Mol. Endocrinol. *24*, 2382–2391.

26. Burnichon, N., Vescovo, L., Amar, L., Libé, R., de Reynies, A., Venisse, A., Jouanno, E., Laurendeau, I., Parfait, B., Bertherat, J., et al. (2011). Integrative genomic analysis reveals somatic mutations in pheochromocytoma and paraganglioma. Hum. Mol. Genet. *20*, 3974–3985.

27. Morrissey, E.R., and Diaz-Uriarte, R. (2009). Pomelo II: Finding differentially expressed genes. Nucleic Acids Res. *37*,.

28. Benjamini, Y., Drai, D., Elmer, G., Kafkafi, N., and Golani, I. (2001). Controlling the false discovery rate in behavior genetics research. Behav. Brain Res. *125*, 279–284.

29. Livak, K.J., and Schmittgen, T.D. (2001). Analysis of relative gene expression data using real-time quantitative PCR and. Methods *25*, 402–408.

30. Knapp, J.E., Mitchell, D.T., Yazdi, M. a, Ernst, S.R., Reed, L.J., and Hackert, M.L. (1998). Crystal structure of the truncated cubic core component of the Escherichia coli 2-oxoglutarate dehydrogenase multienzyme complex. J. Mol. Biol. *280*, 655–668.

31. Ruderfer, D.M., Hamamsy, T., Lek, M., Karczewski, K.J., Kavanagh, D., Samocha, K.E., Daly, M.J., Macarthur, D.G., Fromer, M., and Purcell, S.M. (2016). Patterns of genic intolerance of rare copy number variation in 59,898 human exomes. Nat. Genet. *48*, 1107–1111.

32. Wang, J., Nemeria, N.S., Chandrasekhar, K., Kumaran, S., Arjunan, P., Reynolds, S., Calero, G., Brukh, R., Kakalis, L., Furey, W., et al. (2014). Structure and function of the catalytic domain of the dihydrolipoyl acetyltransferase component in Escherichia coli pyruvate dehydrogenase complex. J. Biol. Chem. *289*, 15215–15230.

33. Richter, S., Gieldon, L., Pang, Y., Peitzsch, M., Huynh, T., Leton, R., Viana, B., Ercolino, T., Mangelis, A., Rapizzi, E., et al. (2018). Metabolome-guided genomics to identify pathogenic variants in isocitrate dehydrogenase, fumarate hydratase, and succinate dehydrogenase genes in pheochromocytoma and paraganglioma. Genet. Med. *0*,.

34. Burr, S.P., Costa, A.S.H., Grice, G.L., Timms, R.T., Lobb, I.T., Freisinger, P., Dodd, R.B., Dougan, G., Lehner, P.J., Frezza, C., et al. (2016). Mitochondrial Protein Lipoylation and the 2-Oxoglutarate Dehydrogenase Complex Controls HIF1α Stability in Aerobic Conditions. Cell Metab. *24*, 740–752.

35. Yang, L., Shi, Q., Ho, D.J., Starkov, A. a., Wille, E.J., Xu, H., Chen, H.L., Zhang, S., Stack, C.M., Calingasan, N.Y., et al. (2009). Mice deficient in dihydrolipoyl succinyl transferase show increased vulnerability to mitochondrial toxins. Neurobiol. Dis. *36*, 320–330.

36. Suzuki, J., Yamada, T., Inoue, K., Nabe, S., Kuwahara, M., Takemori, N., Takemori, A., Matsuda, S., Kanoh, M., Imai, Y., et al. (2018). The tumor suppressor menin prevents effector CD8 T-cell dysfunction by targeting mTORC1-dependent metabolic activation. Nat. Commun. *9*,.

37. Vatrinet, R., Leone, G., De Luise, M., Girolimetti, G., Vidone, M., Gasparre, G., and Porcelli, A.M. (2017). The α-ketoglutarate dehydrogenase complex in cancer metabolic plasticity. Cancer Metab. *5*, 3.

38. Yoon, W.H., Sandoval, H., Nagarkar-Jaiswal, S., Jaiswal, M., Yamamoto, S., Haelterman, N.A., Putluri, N., Putluri, V., Sreekumar, A., Tos, T., et al. (2017). Loss of Nardilysin, a Mitochondrial Co-chaperone for α-Ketoglutarate Dehydrogenase, Promotes mTORC1 Activation and Neurodegeneration. Neuron *93*, 115–131.

39. Wang, Y., Guo, Y.R., Liu, K., Yin, Z., Liu, R., Xia, Y., Tan, L., Yang, P., Lee, J.H., Li, X.J., et al. (2017). KAT2A coupled with the α-KGDH complex acts as a histone H3 succinyltransferase. Nature *552*, 273–277.

40. Dang, L., White, D.W., Gross, S., Bennett, B.D., Bittinger, M. a., Driggers, E.M., Fantin, V.R., Jang, H.G., Jin, S., Keenan, M.C., et al. (2009). Cancer-associated IDH1 mutations produce 2-hydroxyglutarate. Nature *462*, 739–744.

41. Oldham, W.M., Clish, C.B., Yang, Y., and Loscalzo, J. (2015). Hypoxia-Mediated Increases in l-2-hydroxyglutarate Coordinate the Metabolic Response to Reductive Stress. Cell Metab. *22*, 291–303.

42. Intlekofer, A.M., Wang, B., Liu, H., Shah, H., Carmona-Fontaine, C., Rustenburg, A.S., Salah, S., Gunner, M.R., Chodera, J.D., Cross, J.R., et al. (2017). L-2-Hydroxyglutarate production arises from noncanonical enzyme function at acidic pH. Nat. Chem. Biol. *13*, 494–500.

43. Kanamori, T., Nishimaki, K., Asoh, S., Ishibashi, Y., Takata, I., Kuwabara, T., Taira, K., Yamaguchi, H., Sugihara, S., Yamazaki, T., et al. (2003). Truncated product of the bifunctional DLST gene involved in biogenesis of the respiratory chain. EMBO J. *22*, 2913–2923.

44. Schiavi, F., Milne, R.L., Anda, E., Blay, P., Castellano, M., Opocher, G., Robledo, M., and Casc??n, A. (2010). Are we overestimating the penetrance of mutations in SDHB? Hum. Mutat. *31*, 761–762.

45. Dénes, J., Swords, F., Rattenberry, E., Stals, K., Owens, M., Cranston, T., Xekouki, P., Moran, L., Kumar, A., Wassif, C., et al. (2015). Heterogeneous genetic background of the association of pheochromocytoma/paraganglioma and pituitary adenoma: Results from a large patient cohort. J. Clin. Endocrinol. Metab. *100*, E531–E541.

46. Odièvre, M.-H., Chretien, D., Munnich, A., Robinson, B.H., Dumoulin, R., Masmoudi, S., Kadhom, N., Rötig, A., Rustin, P., and Bonnefont, J.-P. (2005). A novel mutation in the dihydrolipoamide dehydrogenase E3 subunit gene (DLD) resulting in an atypical form of α-ketoglutarate dehydrogenase deficiency. Hum. Mutat. *25*, 323–324.

47. Danhauser, K., Sauer, S.W., Haack, T.B., Wieland, T., Staufner, C., Graf, E., Zschocke, J., Strom, T.M., Traub, T., Okun, J.G., et al. (2012). DHTKD1 mutations cause 2-aminoadipic and 2-oxoadipic aciduria. Am. J. Hum. Genet. *91*, 1082–1087.

48. Gibson, G.E., Hirsch, J. a., Cirio, R.T., Jordan, B.D., Fonzetti, P., and Elder, J. (2013). Abnormal thiamine-dependent processes in Alzheimer's Disease. Lessons from diabetes. Mol. Cell. Neurosci. *55*, 17–25.

49. Bourgeron, T., Chretien, D., Poggi-Bach, J., Doonan, S., Rabier, D., Letouzé, P., Munnich, a., Rötig, a., Landrieu, P., and Rustin, P. (1994). Mutation of the fumarase gene in two siblings with progressive encephalopathy and fumarase deficiency. J. Clin. Invest. *93*, 2514–2518.

50. Bourgeron, T., Rustin, P., Chretien, D., Birch-Machin, M., Bourgeois, M., Viegas-Péquignot, E., Munnich, a, and Rötig, a (1995). Mutation of a nuclear succinate dehydrogenase gene results in mitochondrial respiratory chain deficiency. Nat. Genet. *11*, 144–149.

51. Fattal-Valevski, A., Eliyahu, H., Fraenkel, N.I.D., Elmaliach, G., Hausman-Kedem, M., Shaag, A., Mandel, D., Pines, O., and Elpeleg, O. (2017). Homozygous mutation, p.Pro304His, in IDH3A, encoding isocitrate dehydrogenase subunit is associated with severe encephalopathy in infancy. Neurogenetics *18*, 57–61.

52. Spiegel, R., Pines, O., Ta-Shma, A., Burak, E., Shaag, A., Halvardson, J., Edvardson, S., Mahajna, M., Zenvirt, S., Saada, A., et al. (2012). Infantile cerebellar-retinal degeneration associated with a mutation in mitochondrial aconitase, ACO2. Am. J. Hum. Genet. *90*, 518–523.

53. Punzi, G., Porcelli, V., Ruggiu, M., Hossain, M.F., Menga, A., Scarcia, P., Castegna, A., Gorgoglione, R., Pierri, C.L., Laera, L., et al. (2017). SLC25A10 biallelic mutations in intractable epileptic encephalopathy with complex I deficiency. Hum. Mol. Genet.

54. Flynn, A., Benn, D., Clifton-Bligh, R., Robinson, B., Trainer, A.H., James, P., Hogg, A., Waldeck, K., George, J., Li, J., et al. (2015). The genomic landscape of phaeochromocytoma. J. Pathol. *236*, 78–89.

55. Fishbein, L., Leshchiner, I., Walter, V., Danilova, L., Robertson, A.G., Johnson, A.R., Lichtenberg, T.M., Murray, B.A., Ghayee, H.K., Else, T., et al. (2017). Comprehensive Molecular Characterization of Pheochromocytoma and Paraganglioma. Cancer Cell *31*, 181–193.

56. Raimundo, N., Baysal, B.E., and Shadel, G.S. (2011). Revisiting the TCA cycle: Signaling to tumor formation. Trends Mol. Med. *17*, 641–649.

57. Zhou, X., Guo, X., Chen, M., Xie, C., and Jiang, J. (2018). HIF-3α Promotes Metastatic Phenotypes in Pancreatic Cancer by Transcriptional Regulation of the RhoC–ROCK1 Signaling Pathway. Mol. Cancer Res. *16*, 124–134.

58. Menara, M., Oudijk, L., Badoual, C., Bertherat, J., Lepoutre-Lussey, C., Amar, L., Iturrioz, X., Sibony, M., Zinzindohoué, F., De Krijger, R., et al. (2015). SDHD immunohistochemistry: A new tool to validate SDHx mutations in pheochromocytoma/paraganglioma. J. Clin. Endocrinol. Metab. *100*, E287–E291.

Table 1. Clinical data of the individuals with *DLST* mutations

ID	Tumors analyzed	Gender	Age (yr.)	Tumors	Other tumors	Biochemical Phenotype	Behavior	cDNA variant	Protein change	PredictSNP	LOH	DLST IHC
#1	#1	M	45	PCC	-	NM	Mg	c.692G>A	p.Arg231Gln	Deleterious	No	+
#2	-	F	63	H&N (n=2)	-	NS	Bg	c.910G>A	p.Asp304Asn	Neutral	NA	NA
#3	#3a,b,c	F	27	TAP (n=7)	Uterine endometrioid carcinoma	NM	Bg	c.1121G>A	p.Gly374Glu	Deleterious	Yes (UPD)	+++
#4	#4	M	38	TAP (n=3)	-	NM	Bg	c.1121G>A	p.Gly374Glu	Deleterious	Yes (UPD)	+++
#5	#5a,b	F	24	TAP, PCC	-	NM	Bg	c.1121G>A	p.Gly374Glu	Deleterious	Yes (UPD)	NA
#6[a]	-	M	29	TAP (n=4)	-	NM	Bg	c.1121G>A	p.Gly374Glu	Deleterious	NA	NA
#7	-	M	29	TAP (n=3)	-	NM	Bg	c.1265A>G	p.Tyr422Cys	Deleterious	NA	NA
#8	#8	M	54	PCC (n=2)	Pituitary adenoma (PRL)	NM	Bg	c.1060-3T>A	-	-	No	+++

Bg: benign; F: female; H&N: head and neck PGL; IHC: immunohistochemistry; LOH: loss of heterozygosity; M: male; Mg: malignant, MTC: medullary thyroid carcinoma; NA: not available; NM: normetanephrine; NS: non-secretory; PCC: pheochromocytoma; PRL: prolactinoma; TAP: thoracic-abdominal-pelvic PGL; UPD: uniparental disomy; + = weak immunostaining; +++ = strong immunostaining. [a]: individual studied by exome sequencing. *DLST* cDNA mutations are numbered according to human cDNA reference sequence NM_001933.

FIGURES

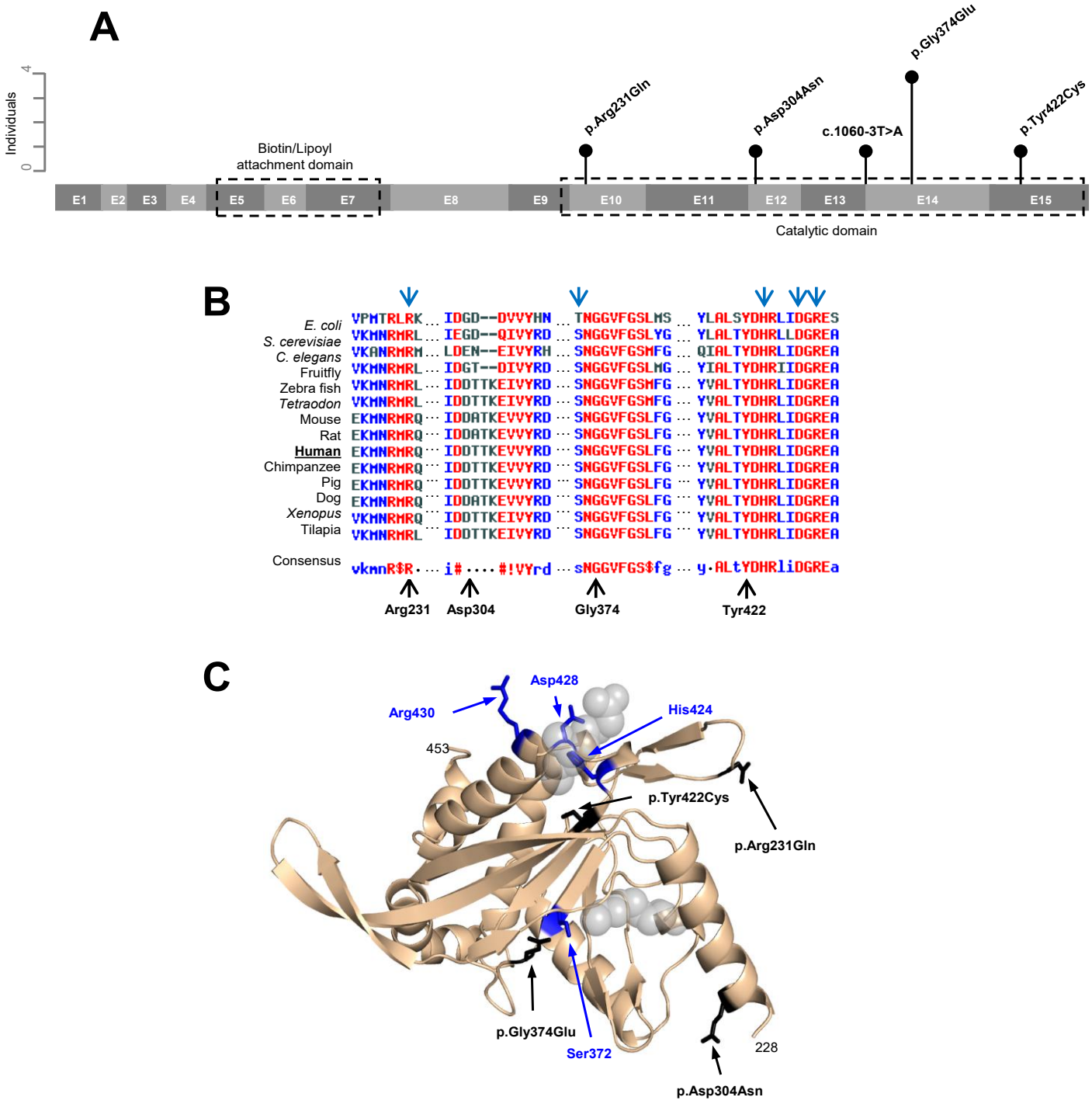

Figure 1. DLST protein structure. **(A)** Schematic representation of the DLST protein (15 exons) indicating the main active sites and all variants found in this study. Vertical bars represent the number of individuals carrying each variant. **(B)** Multiple sequence alignment and DLST residue conservation across different species using MultAlin software; high consensus in red, neutral in black and low consensus in blue. Blue arrows: predicted active sites in *E. coli* DLST. Black arrows indicate the different amino acids found mutated in our affected individuals. **(C)** Predicted structural model of the DLST catalytic domain. The catalytic residues are colored blue and indicated by blue arrows. The variants found in this study have been modeled, colored black and indicated by black arrows. The position of the putative substrate binding site is indicated with gray spheres for clarity.

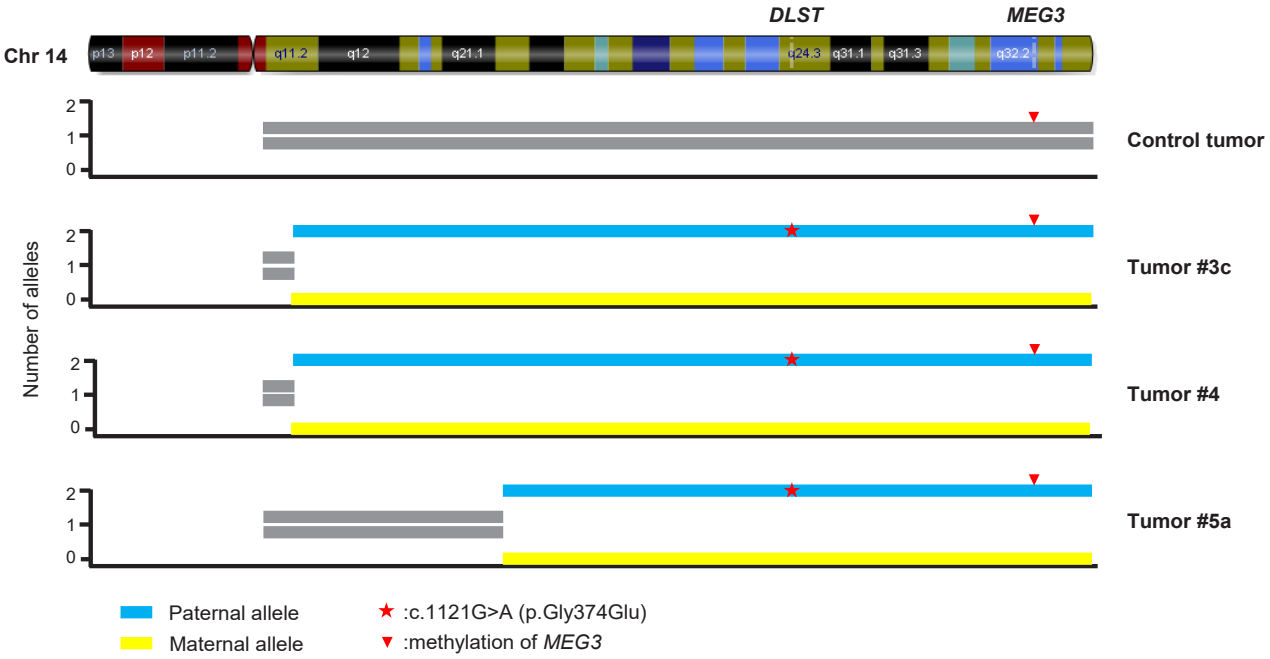

Figure 2. LOH analysis of p.Gly374Glu-DLST tumors. Schematic representation of chromosome 14 showing the uniparental disomy (UPD) identified by SNP array analysis in three PPGLs (#3c, #4 and #5a) carrying the p.Gly374Glu-DLST variant (indicated by a red asterisk) compared to a control tumor. Yellow bars represent the alleles with the lowest copy number (n=0), and blue bars represent the alleles with the highest copy number (n=2). *MEG3*, a maternally expressed imprinted gene, was used to determine the origin of the observed UPD. The presence in the three tumors of only the methylated allele of *MEG3* (indicated by a red arrowhead) indicates that the UPD has a paternal origin.

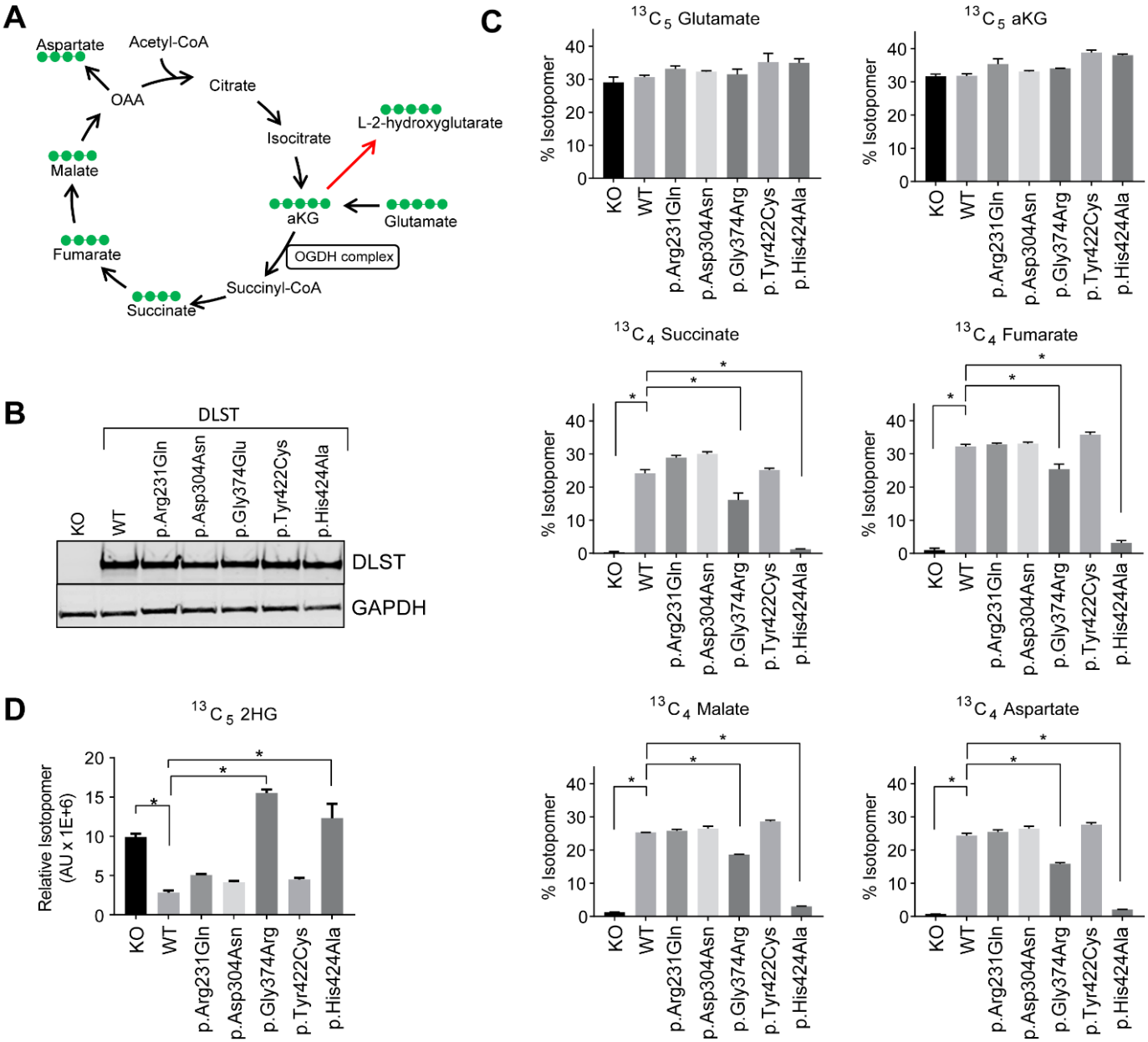

Figure 3. Functional analysis of DLST variants. **(A)** Schematic illustration of the TCA cycle. Carbon-13 is denoted by green dots in the context of a $^{13}C_5$–glutamate labeling experiment. The red arrow pointing at 2-hydroxyglutarate (2HG) represents the collective action of malate and lactate dehydrogenases. **(B)** Immunoblot analysis showing equivalent protein levels of WT and mutant DLST in DLST-KO cells. **(C)** Labeling patterns of TCA intermediates after $^{13}C_5$–glutamate labeling. **(D)** Pattern of $^{13}C_5$–2HG labeling after $^{13}C_5$–glutamate labeling. **(C-D)** Error bars represent the SD from a representative experiment. *p < 0.05 (Student's t-test; n = 3).

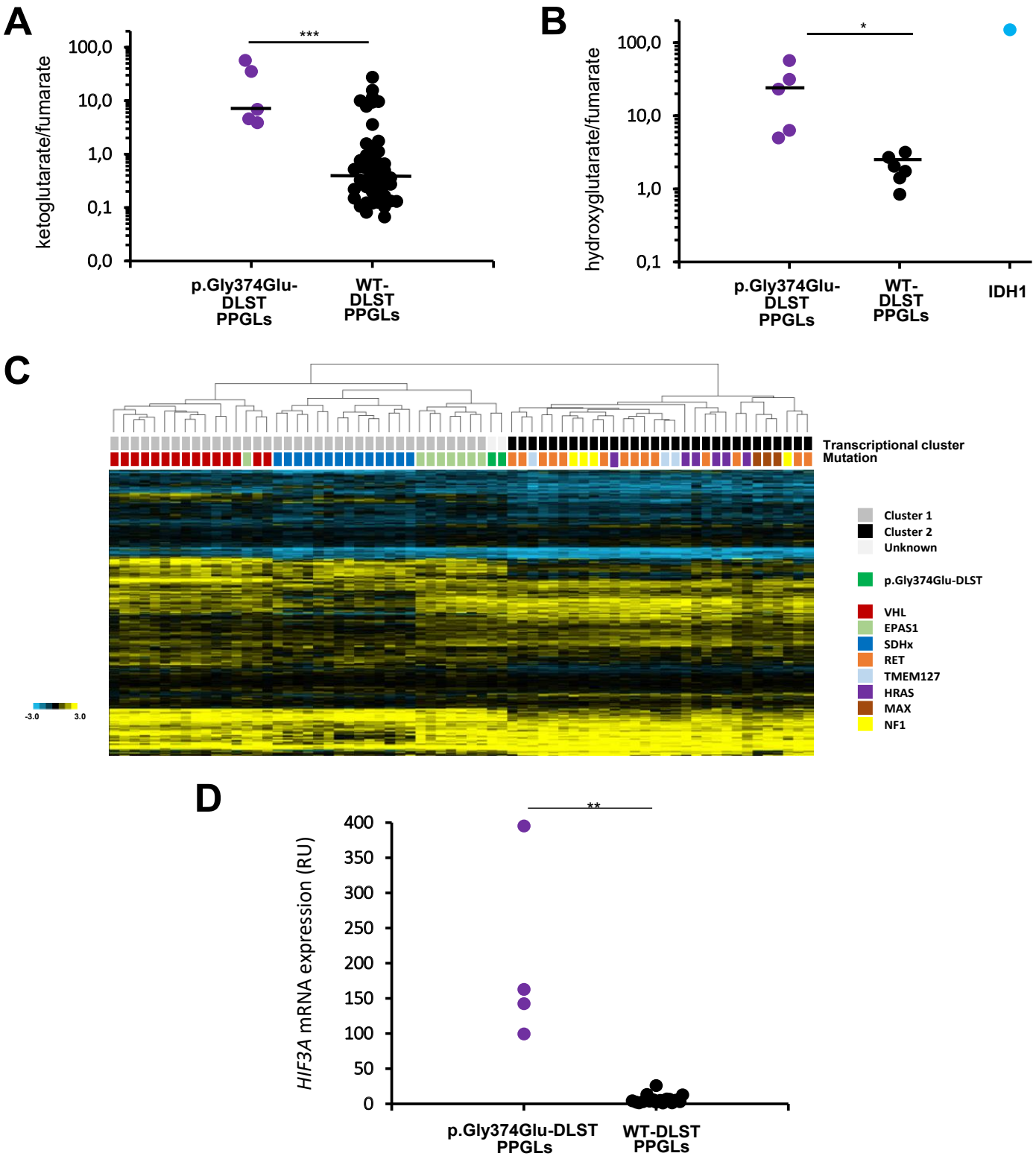

Figure 4. Metabolite assessment and gene expression profiling of p.Gly374Glu-DLST tumors. **(A)** α-ketoglutarate/fumarate ratios assessed by liquid chromatography-tandem mass spectrometry (LC-MS/MS) in p.Gly374Glu-DLST tumors (n=5) compared with WT-DLST control PPGLs (n=51). Black lines represent medians. A t-test was applied to test for differences between means; ***p<0.001. **(B)** 2-Hydroxyglutarate/fumarate ratios assessed by LC-MS/MS in p.Gly374Glu-DLST tumors (n=5) compared to WT-DLST control PPGLs (n=6). The ratio of these metabolites in an *IDH1*-mutated tumor was included as a positive control of 2HG accumulation. Black lines represent medians. A t-test was applied to test for differences between means; *p<0.05. **(C)** Hierarchical clustering of 69 mutated tumors based on expression data for 451 genes reported as differentially expressed in PPGL-mutated samples[26]. Control tumors (denoted with different colors depending on the gene mutated) were split up between the two main transcriptional clusters of PPGLs: cluster 1 (denoted in grey) which included *VHL*- (n=12), SDHx- (n=15) and *EPAS1*- (n=8) mutated tumors, and cluster 2 (denoted in black) which included *RET*- (n=14), *HRAS*- (n=6), *NF1*- (n=4), *TMEM127*- (n=3), and *MAX*- (n=3), mutated PPGLs. Two tumors carrying the p.Gly374Glu-DLST variant (#4 and #5a) were clustered within cluster 1 and grouped with *EPAS1*-mutated cases. City Block/uncentered and complete linkage characteristics were used for the analyses. **(D)** *HIF3A* mRNA expression in p.Gly374Glu-DLST PPGLs (n=4) vs WT-DLST control PPGLs (n=18) by RT-qPCR. Expression level was normalized to β-actin (ACTB) and presented as mean (n=3). Significance was determined by a Mann-Whitney U non-parametric test; **p<0.01.

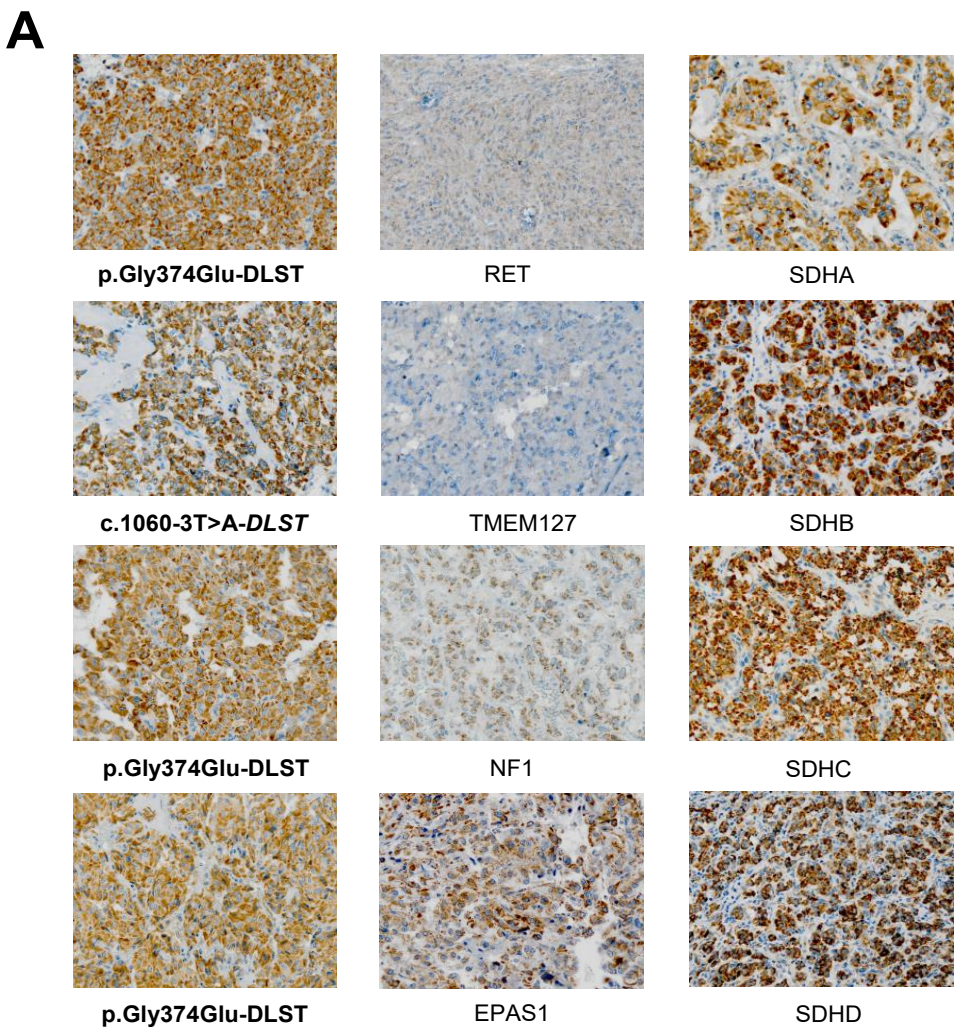

Figure 5. Immunohistochemistry of DLST in different tumors. (A) Positive immunostaining (x20) with cytoplasmic aggregates was assessed in *DLST*- and TCA cycle-mutated tumors (left and right columns, respectively) and compared to control tumors (middle column). **(B)** Representation of DLST IHC score (ranging from 0 to 3) for 88 tumors analyzed, including tumors carrying mutations in TCA cycle-related genes (n=33; *SDHA* (1), *SDHB* (11), *SDHC* (1), *SDHD* (6), *SDHAF2* (1), *GOT2* (2), *MDH2* (3), *IDH1* (1), *IDH3B* (1), *DLST* (6)), tumors carrying *EPAS1* mutations (n=9), and tumors carrying other mutations as controls (n=46; RET (24), VHL (11), HRAS (1), NF1 (7), MAX (2), TMEM127 (1)). Significance was determined by a Fisher's exact test; ***p<0.001.

SUPPLEMENTAL DATA

A

neutral	deleterious	% expected accuracy				
Mutation	PredictSNP	MAPP	PhD-SNP	PolyPhen-1	PolyPhen-2	SIFT	SNAP
p.Arg231Asn	**87%**	72%	59%	74%	81%	79%	81%
p.Asp304Asn	**75%**	78%	68%	67%	41%	90%	77%
p.Gly374Glu	**87%**	91%	68%	74%	81%	79%	89%
p.Tyr422Cys	**72%**	74%	61%	74%	81%	79%	89%

B

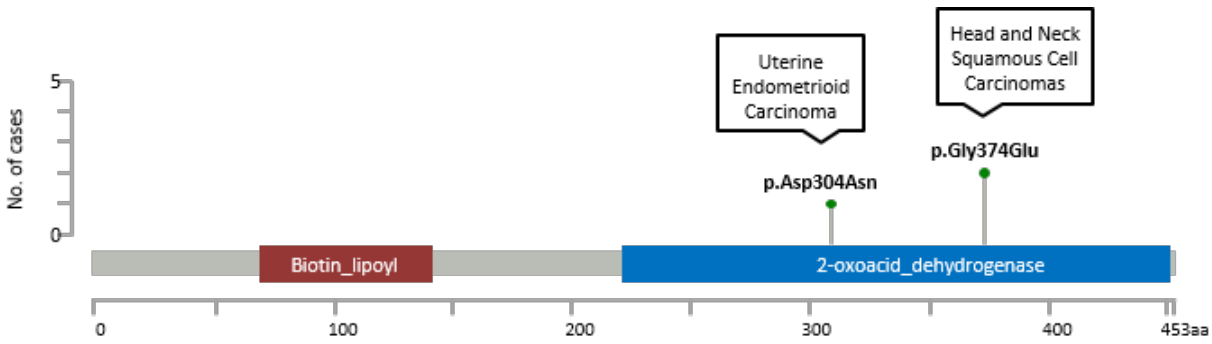

Figure S1. (A) Prediction of the effects of the different DLST substitutions by seven consensus classifiers using PredictSNP. **(B)** Previously reported DLST variants found in endometrioid carcinoma (p.Asp304Asn) and upper aerodigestive tract squamous cell carcinoma (p.Gly374Glu). Data are from cBioPortal. The number of cases of each variant is represented by vertical bars.

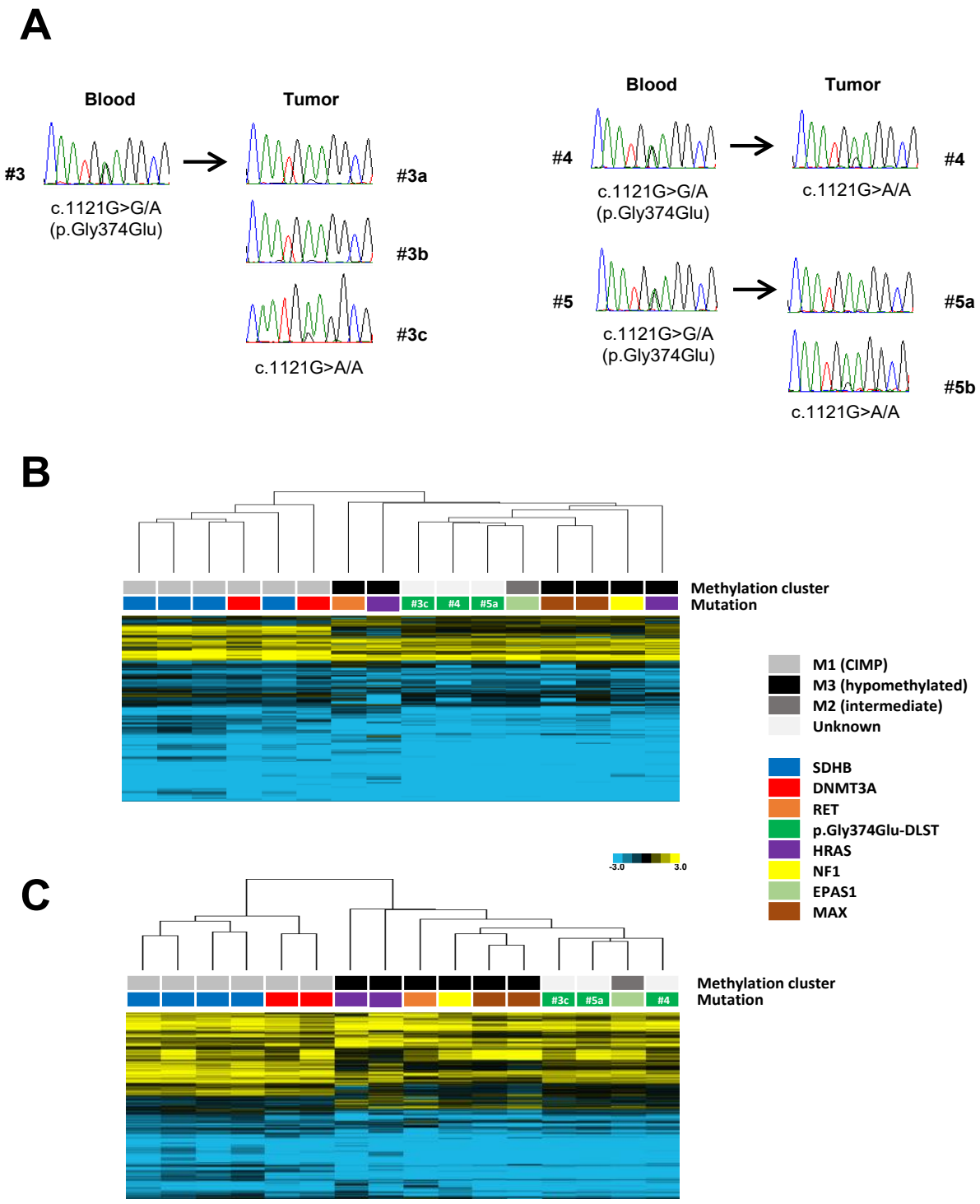

Figure S2. (A) Sanger sequencing of six tumors from three unrelated individuals (p.Gly374Glu) showing LOH of the wild-type *DLST* allele. **(B)** Hierarchical clustering of methylation data from p.Gly374Glu-DLST tumors (n=3; #3c, #4, #5a) compared to controls (n=13; 2 *DNMT3A*, 4 *SDHB*, 1 *EPAS1*, 2 *MAX*, 2 *HRAS*, 1 *RET* and 1 *NF1*-mutated tumors). Tumors (denoted with different colors depending on the gene mutated) were split up between different methylation clusters of PPGLs[30]: cluster M1 (denoted in light grey) which included SDHB- (n=4) and *DNMT3A*- (n=2) mutated tumors, cluster M2 (denoted in dark grey) which included one *EPAS1*-mutated tumor, and cluster M3 (denoted in black) which included *RET*- (n=1), *HRAS*- (n=2), *NF1*- (n=1), and *MAX*- (n=2) mutated PPGLs. City Block (SD=1.4) and complete linkage characteristics were used for the analysis. **(C)** Hierarchical clustering of the 16 mutated tumors from panel (B) based on methylation data for 125,112 probes corresponding to 4,662 genes with CpG sites reported as significantly hypermethylated in M1 (SDHx-mutated) PPGLs. The three tumors carrying the p.Gly374Glu-DLST variant (#3c, #4 and #5a), were clustered together and separated from cluster M1 samples. Uncentered correlation (SD=1.5) and complete linkage characteristics were used for the analysis.

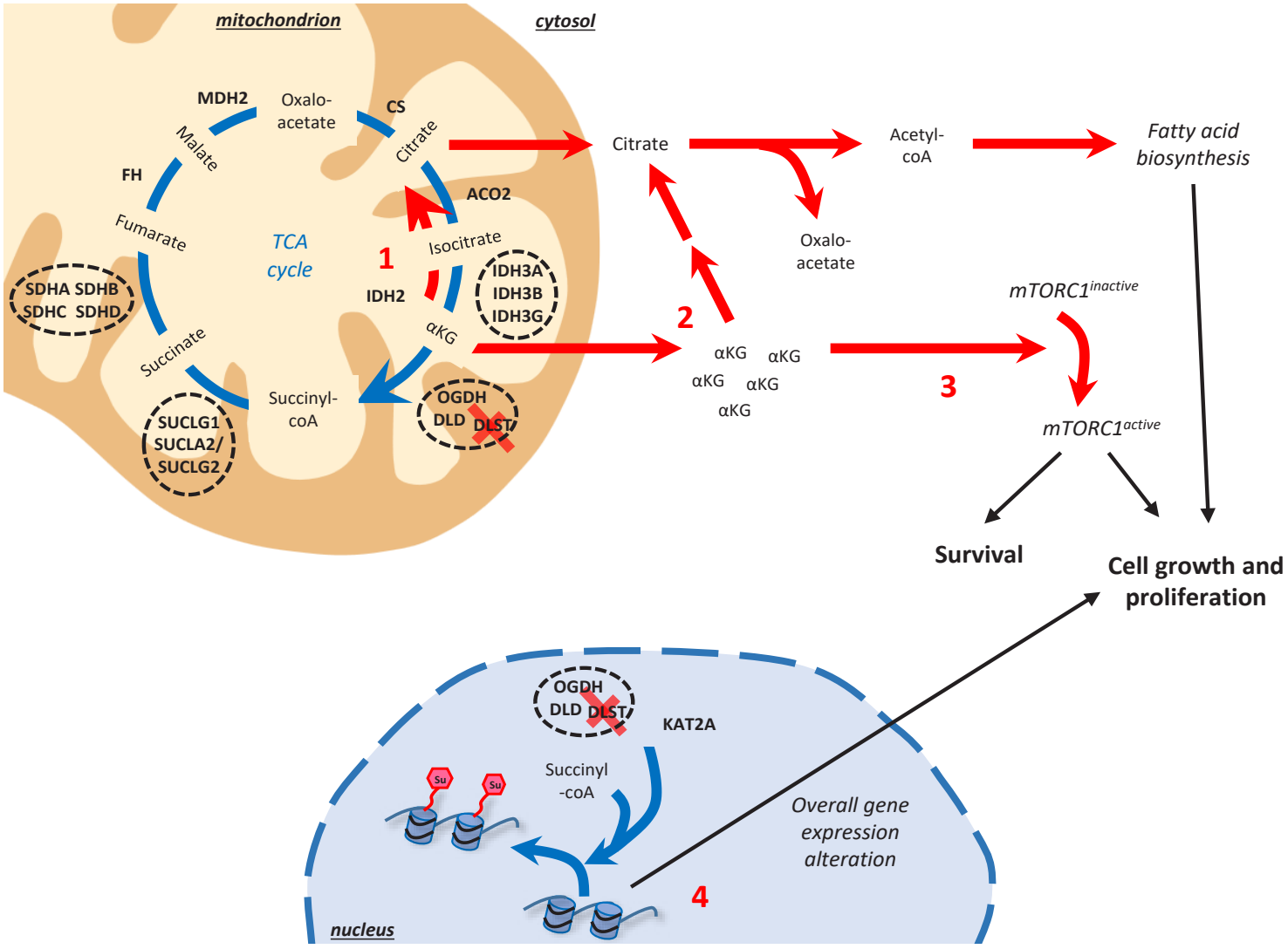

Figure S3. Schematic representation of theoretical extra-mitochondrial consequences due to αKG accumulation upon inactivation of OGDH-complex DLST subunit (denoted by a red cross). 1) Loss of activity of the OGDH complex and the unbalance of the αKG/citrate ratio can lead to a TCA cycle functioning in a reverse mode, ultimately supporting *de novo* fatty acid synthesis and favoring tumor growth. 2) In addition, perturbations of the αKG pool affect the cytoplasmic level of acetyl-CoA by its conversion to citrate, increasing fatty acid biosynthesis. 3) High cytosolic levels of αKG may also promote aberrant mammalian target of rapamycin complex 1 (mTORC1) activation, which might be beneficial for cancer cells by promoting survival and proliferation. 4) Finally, the OGDH complex, associated with KAT2A in gene promoter regions, plays an instrumental role in the regulation of gene expression by histone succinylation. Therefore, loss of OGDH activity by *DLST* mutation may lead to altered overall gene expression and tumor cell proliferation. Blue arrows denote the cellular processes in which the wild-type OGDH complex is involved, and red arrows indicate alternative pathways activated upon loss of OGDH activity.

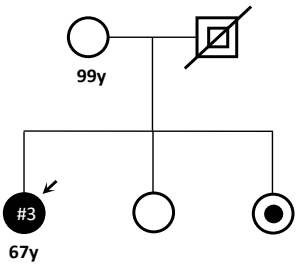

#3 PGL para-aortic (27y) + PGL renal and PGL pelvic (35y) + PGL pre-sacrum (41y) + PGL Zuckerkandl (49y) + PGL para-aortic and PGL iliac (53y, operated with 66y) + uterine endometrioid carcinoma (66y) - p.Gly374Glu

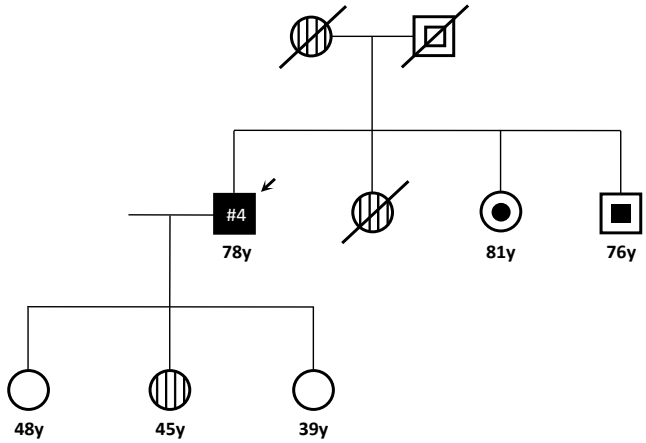

#4 PGL para-adrenal (38y) + PGL para-aortic (62y) + PGL para-vertebral (69y) - p.Gly374Glu

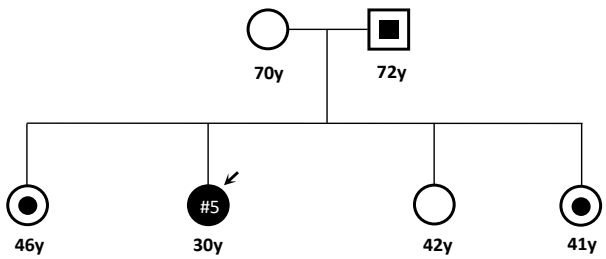

#5 PGL para-adrenal + PGL retroperitoneal (24y) + PGL para-adrenal *vs* recidivation (29y) - p.Gly374Glu

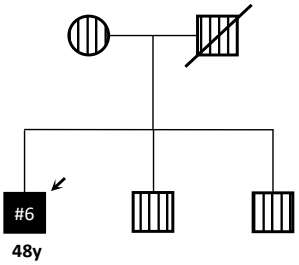

#6 PGL pre-sacrum + two PGLs para-aortic + PGL renal (29y) - p.Gly374Glu

Figure S4. Pedigrees of individuals #3, #4, #5 and #6. The proband of each pedigree is indicated by a black arrowhead; striped symbols indicate individuals in which no genetic test was performed; internal filled symbols indicate asymptomatic (no clinical surveillance performed) individuals carrying the p.Gly374Glu variant; internal empty symbols indicate individuals predicted to carry the p.Gly374Glu variant.

Table S1. Clinical data of the PPGL patients included in the study

Number of cases	*Gender*	*Median age at onset (range)*	*Patients with single (S) or multiple (M) tumors*	*Location of tumors*	*Catecholamine phenotype*	*Metastatic cases*
104	m: **43** f: **59** U: **2**	**49y** (8-82)	S: **77** M: **27**	PCC: **57** TAP: **22** H&N: **14** Misc: **9** U: **2**	NORA: **34** ADR: **17** NF: **14** DOPA: **8**	**11**

m: male; f: female; U: unknown; PCC: pheochromocytoma; TAP: thoracic-abdominal-pelvic paraganglioma; H&N: head and neck paraganglioma; Misc: miscellaneous; NORA: noradrenergic; ADR: adrenergic; NF= non functional, DOPA: dopaminergic

Table S2. Genes included in the targeted next-generation sequencing panel

ACO1
ACO2
CS
DLAT
DLD
DLST
GOT1
GOT2
IDH1
IDH2
IDH3A
IDH3B
IDH3G
MDH1
OGDH
OGDHL
PC
PCK1
PCK2
PDHA1
PDHA2
PDHB
SLC25A1
SLC25A10
SLC25A11
SLC25A13
SUCLA2
SUCLG1
SUCLG2
FH
MDH2
SDHA
SDHB
SDHC
SDHD
SDHAF1
SDHAF2

Table S3. Targeted NGS variants identified

Gene symbol	Description	Nucleotide variant	Chr	Coordinate	Consequence	SIFT	PolyPhen	cDNA variant	Protein variant	GnomAD (carriers:total individuals)
DLST GenBank: NM_001933	Dihydrolipoamide S-Succinyltransferase	G>G/A	14	75361034	Missense variant	deleterious	probably_damaging	c.692G>A	p.Arg231Gln	2:123,099
		G>G/A	14	75366634	Missense variant	tolerated	probably_damaging	c.910G>A	p.Asp304Asn	-
		G>A/A	14	75367830	Missense variant	deleterious	probably_damaging	c.1121G>A	p.Gly374Glu	2:123,121
		A>A/G	14	75368936	Missense variant	deleterious	probably_damaging	c.1265A>G	p.Tyr422Cys	3:137,372
		T>T/A	14	75367766	Splice region variant	-	-	c.1060-3T>A	-	1:122,641
IDH1 GenBank: NM_001282387	Isocitrate Dehydrogenase (NADP(+)) 1, Cytosolic	T>T/A	2	209113206	Missense variant	deleterious	probably_damaging	c.301A>T	p.Asn101Tyr	1:123,132
SLC25A10 GenBank: NM_012140	Solute Carrier Family 25 Member 10	C>C/T	17	79682747	Missense variant	deleterious	probably_damaging	c.353C>T	p.Thr118Met	-
SLC25A11 GenBank: NM_003562	Solute Carrier Family 25 Member 11	C>C/T	17	4841465	Missense variant	deleterious	probably_damaging	c.721G>A	p.Asp241Asn	1:123,042
SUCLG1 GenBank NM_003849	Succinate-CoA Ligase Alpha Subunit	G>G/T	2	84660523	Missense variant	deleterious	probably_damaging	c.626C>A	p.Ala209Glu	4:123,001

Chr: chromosome; SIFT: 'Sorting Intolerant From Tolerant' algorithm prediction; PolyPhen: 'Polymorphism Phenotyping' algorithm prediction; GnomAD: frequency of the variant in the gnomAD database

Table S4. Genes differentially expressed in p.Gly374Glu DLST tumors and PPGLs carrying other mutations

	Gene Name	unadj.p	FDR_indep	Obs_stat
1	A_23_P338534_HIF3A	< 0.0000001	< 0.0000001	11,895879
2	A_23_P374339_HIF3A	< 0.0000001	< 0.0000001	11,361279
3	A_23_P423853_ERBB4	< 0.0000001	< 0.0000001	9,223138
4	A_24_P188037_HIF3A	< 0.0000001	< 0.0000001	10,153642
5	A_23_P142187_HIF3A	< 0.0000001	< 0.0000001	9,056168
6	A_24_P252895_TSPAN32	< 0.0000001	1,00E-06	7,73081
7	A_24_P229638_ENST00000373295	< 0.0000001	1,00E-06	7,67991
8	A_32_P125542_THC2384778	< 0.0000001	1,10E-06	7,628959
9	A_24_P308096_JAK3	< 0.0000001	5,60E-06	7,178493
10	A_23_P152082_SPTBN5	< 0.0000001	1,81E-05	6,854214
11	A_23_P98671_C11orf21	< 0.0000001	3,91E-05	6,632856
12	A_23_P255298_GUP1	< 0.0000001	4,51E-05	6,560255
13	A_23_P56855_ENST00000343518	< 0.0000001	4,51E-05	-6,553498
14	A_23_P119337_ATF5	< 0.0000001	5,36E-05	6,49
15	A_32_P163306_KIAA1822	< 0.0000001	0,0001973	6,136795
16	A_23_P5301_TFCP2L1	< 0.0000001	0,0002109	6,102869
17	A_32_P126222_AW302758	1,00E-07	0,0003477	5,957344
18	A_23_P56883_GABRA4	2,00E-07	0,000349	5,94149
19	A_32_P234414_THC2441719	3,00E-07	0,0005559	5,805845
20	A_23_P42322_COL11A2	3,00E-07	0,0006285	5,760247
21	A_23_P363174_HIST1H2AL	4,00E-07	0,0008435	-5,670126
22	A_24_P217834_HIST1H3D	5,00E-07	0,0008452	-5,657366
23	A_24_P305050_CD300LG	8,00E-07	0,0013812	5,515835
24	A_24_P66780_FAM83B	9,00E-07	0,0014752	-5,487073
25	A_23_P250385_HIST1H1B	1,20E-06	0,0019022	-5,408592
26	A_32_P394951_LOC126147	1,30E-06	0,0019881	5,386356
27	A_23_P164057_MFAP4	1,50E-06	0,0020354	5,342249
28	A_24_P751492_C9orf128	1,50E-06	0,0020354	5,338875
29	A_23_P334857_ZNF533	1,40E-06	0,0020354	5,349056
30	A_24_P380311_CAMK2A	1,40E-06	0,0020354	5,364493
31	A_32_P86533_AF038185	1,50E-06	0,0020354	-5,333054
32	A_24_P217306_ZIC4	1,80E-06	0,0022184	5,285947
33	A_23_P145514_IL20RA	1,80E-06	0,0022184	-5,285214
34	A_23_P311818_GHRH	1,70E-06	0,0022184	5,299217
35	A_32_P919718_TMEM105	1,90E-06	0,002251	5,273515
36	A_24_P943301_ENST00000292357	2,10E-06	0,0023956	5,249219
37	A_23_P60627_ALOX15B	2,30E-06	0,0025415	5,225927
38	A_23_P501722_TSPAN32	2,90E-06	0,0030667	5,161023
39	A_24_P148026_AK024190	2,90E-06	0,0030667	5,163282
40	A_32_P170397_ENST00000309874	3,30E-06	0,0033812	5,127741
41	A_24_P934975_A_24_P934975	3,70E-06	0,0037187	5,095233
42	A_23_P168130_IHPK3	4,00E-06	0,0039241	5,074075
43	A_24_P758010_AJ318805	4,40E-06	0,0042372	5,046776
44	A_23_P126658_PRAMEF8	4,60E-06	0,004254	-5,039431
45	A_32_P129669_FRMPD3	5,20E-06	0,0046159	5,005025
46	A_23_P257263_ODZ1	5,10E-06	0,0046159	5,009052

47	A_24_P230948_PER3	6,20E-06	0,005374	4,957521
48	A_23_P75024_MSMB	6,80E-06	0,0057918	-4,931205
49	A_24_P942404_THC2412411	7,60E-06	0,0062365	4,899641
50	A_32_P14253_AW950828	7,50E-06	0,0062365	4,904229
51	A_24_P617427_AF339787	7,90E-06	0,0063173	4,89064
52	A_23_P394836_C14orf173	8,30E-06	0,0065346	4,87597
53	A_24_P920851_DKFZp667G2110	9,00E-06	0,0069743	4,852739
54	A_24_P174924_HIST1H3B	9,60E-06	0,0073094	-4,834599
55	A_24_P38572_NOL6	9,80E-06	0,0073368	4,828487
56	A_23_P161135_LEPR	1,11E-05	0,0081176	4,79547
57	A_24_P299469_GPR116	1,20E-05	0,0086071	4,773048
58	A_24_P76512_FLJ30064	1,22E-05	0,0086071	4,769459
59	A_24_P15834_TNXB	1,48E-05	0,0102808	4,715188
60	A_23_P333484_HIST1H3H	1,56E-05	0,0106304	-4,701148
61	A_23_P321935_OSBP2	1,76E-05	0,0114627	4,666383
62	A_23_P34376_TCEA3	1,75E-05	0,0114627	4,667707
63	A_24_P924920_ABHD2	1,72E-05	0,0114627	4,673638
64	A_24_P159548_HCP1	1,82E-05	0,0116609	4,657156
65	A_24_P372643_SLC22A18AS	1,92E-05	0,0121094	4,642206
66	A_24_P76313_FAM43B	1,96E-05	0,0121715	4,636477
67	A_23_P421483_CEACAM6	2,08E-05	0,0123123	-4,61913
68	A_24_P146683_MSMB	2,07E-05	0,0123123	-4,620543
69	A_24_P332314_FAM111B	2,04E-05	0,0123123	-4,624571
70	A_24_P3627_A_24_P3627	2,10E-05	0,0123123	4,616689
71	A_24_P258235_OR5L2	2,23E-05	0,012849	4,600669
72	A_23_P58407_UGT2B15	2,33E-05	0,0132591	-4,587858
73	A_24_P209389_MLXIPL	2,38E-05	0,0133918	4,581151
74	A_23_P215435_POM121	2,44E-05	0,0135422	4,574151
75	A_23_P1029_MFAP2	2,89E-05	0,0158164	4,526379
76	A_23_P30799_HIST1H3F	2,94E-05	0,015871	-4,521641
77	A_23_P79769_BIRC7	3,13E-05	0,0166818	4,503764
78	A_23_P309250_FLJ30719	3,35E-05	0,0175864	4,485057
79	A_24_P37253_MGC52057	3,52E-05	0,0181442	4,470179
80	A_24_P136905_AF116713	3,63E-05	0,0181442	-4,461909
81	A_24_P925490_AF086115	3,63E-05	0,0181442	-4,461885
82	A_32_P498899_KIAA1244	3,61E-05	0,0181442	4,463654
83	A_24_P154914_ZNF588	3,95E-05	0,0195169	-4,437569
84	A_32_P73151_AK124778	4,08E-05	0,0199111	4,428413
85	A_23_P151297_TENC1	4,41E-05	0,0212642	4,406164
86	A_23_P352226_MAPKBP1	4,48E-05	0,021323	4,401412
87	A_23_P51639_KIAA0467	4,52E-05	0,021323	4,398692
88	A_24_P8116_CCDC80	4,59E-05	0,0213987	4,39439
89	A_24_P172600_AK091555	4,71E-05	0,0216847	4,387322
90	A_23_P24555_PHLDB1	4,91E-05	0,0223809	4,375012
91	A_23_P71810_BAAT	5,28E-05	0,0237887	-4,354242
92	A_23_P129334_CLCN7	5,45E-05	0,024198	4,345077
93	A_23_P500010_KLK12	5,49E-05	0,024198	-4,343038
94	A_23_P166779_LOH3CR2A	5,89E-05	0,0256795	4,32276
95	A_23_P501754_CSF3	6,15E-05	0,0265373	4,310176
96	A_23_P331908_PRDM11	6,46E-05	0,0272858	4,296064

97	A_23_P368154_PODN	6,44E-05	0,0272858	4,296722
98	A_32_P59792_THC2444579	6,53E-05	0,0273035	4,292898
99	A_23_P416821_MGC42090	6,67E-05	0,0275859	4,286618
100	A_24_P248079_BC031319	6,73E-05	0,0275859	4,284039
101	A_24_P384469_A_24_P384469	7,66E-05	0,0302033	4,246218
102	A_23_P104275_SLC16A12	7,65E-05	0,0302033	4,246693
103	A_24_P945165_ENST00000371316	7,52E-05	0,0302033	4,25183
104	A_32_P79351_THC2440217	7,50E-05	0,0302033	4,252519
105	A_23_P115762_ECD	7,87E-05	0,0306682	-4,238417
106	A_23_P149075_RPRC1	7,93E-05	0,0306682	4,236196
107	A_32_P75867_THC2376729	8,28E-05	0,0317259	-4,223539
108	A_24_P934008_AY358789	8,90E-05	0,0334761	4,202389
109	A_32_P22401_RPRC1	8,84E-05	0,0334761	4,204285
110	A_32_P74391_SIRPD	8,98E-05	0,033482	-4,19966
111	A_32_P204740_BC065754	9,07E-05	0,0334911	4,196926
112	A_32_P336776_RP6-213H19.2	9,42E-05	0,034181	4,185698
113	A_23_P350396_CDSN	9,39E-05	0,034181	-4,186754
114	A_32_P221799_HIST1H2AM	9,68E-05	0,0347974	-4,177857
115	A_24_P15898_C1orf145	0,0001002	0,0357083	4,167687
116	A_32_P195793_THC2369621	0,0001026	0,0362757	4,160496
117	A_24_P943026_EPB41L4A	0,0001036	0,0363045	4,157734
118	A_23_P41021_NISCH	0,0001047	0,0363784	4,154626
119	A_23_P157338_UNQ739	0,0001141	0,0393221	4,129168
120	A_24_P119685_OBSCN	0,0001216	0,0415474	4,110403
121	A_23_P11644_SPRR2D	0,0001258	0,0419311	-4,10036
122	A_24_P393644_GYPB	0,000125	0,0419311	-4,102142
123	A_32_P223017_MAP3K6	0,0001255	0,0419311	4,101081
124	A_24_P353905_MXRA8	0,0001302	0,0430352	4,090245
125	A_23_P254254_SGSH	0,0001318	0,0432246	4,086556
126	A_32_P183765_AK126298	0,0001346	0,0434618	4,080213
127	A_24_P367864_BC038983	0,0001346	0,0434618	4,080324
128	A_24_P548297_AF086154	0,0001427	0,0450205	4,062782
129	A_23_P343927_HIST2H2AB	0,0001417	0,0450205	-4,065075
130	A_24_P94222_FBLIM1	0,0001415	0,0450205	4,065455
131	A_23_P159893_CHRDL1	0,0001501	0,0469876	4,047748
132	A_32_P144072_THC2305770	0,0001605	0,0498402	4,02787
133	A_23_P215431_POM121	0,0001627	0,0501653	4,023667
134	A_32_P215621_AK094991	0,000169	0,0516257	4,012276
135	A_23_P125435_GABRB1	0,00017	0,0516257	4,010603
136	A_32_P210622_THC2440737	0,0001724	0,0519612	4,006449
137	A_23_P134991_C9orf38	0,0001807	0,0540776	3,992269
138	A_23_P66432_TTYH2	0,0001853	0,0550448	3,984756
139	A_23_P131801_SGK2	0,0001892	0,0558163	3,978399
140	A_23_P133694_SLC29A1	0,0001921	0,056248	3,973922
141	A_23_P10077_PNPLA2	0,0002011	0,0584663	3,960123
142	A_23_P425990_KIAA0774	0,0002029	0,0585914	3,957347
143	A_23_P80752_PLXND1	0,0002049	0,0587555	3,954386
144	A_24_P153215_AL601841	0,0002076	0,0590969	3,950534
145	A_23_P151895_CILP	0,000211	0,059666	3,94555
146	A_24_P9321_HIST1H3I	0,0002146	0,0602608	-3,940475

147	A_23_P23191_HSPG2	0,0002166	0,0604167	3,93763
148	A_23_P89589_PER1	0,0002182	0,0604368	3,935479
149	A_23_P208340_SLC44A2	0,0002285	0,0628684	3,921499
150	A_23_P141946_LTBP4	0,0002311	0,0630143	3,918031
151	A_24_P933458_NAV2	0,0002321	0,0630143	3,916755
152	A_23_P140454_A_23_P140454	0,0002366	0,0638235	3,910883
153	A_23_P342641_SLC44A5	0,0002429	0,0650875	3,902939
154	A_24_P151032_MYL4	0,0002464	0,0656046	-3,898555
155	A_23_P89529_A_23_P89529	0,0002499	0,066109	3,89426
156	A_23_P83579_ARNT2	0,0002522	0,0662936	-3,891456
157	A_24_P489695_ENST00000340455	0,0002554	0,0666886	3,887705
158	A_24_P489690_FLJ46111	0,0002572	0,0667508	3,885488
159	A_23_P166336_DKFZp434N035	0,0002608	0,0672617	-3,881246
160	A_23_P112564_KCND2	0,0002676	0,0673074	3,873489
161	A_23_P312840_SEMA6A	0,0002692	0,0673074	3,871603
162	A_23_P351342_PLEKHM2	0,0002689	0,0673074	3,871973
163	A_32_P135385_CTB-1048E9.5	0,0002653	0,0673074	-3,876046
164	A_32_P41153_BM929882	0,0002676	0,0673074	3,873492
165	A_32_P142960_CR618217	0,000272	0,0675886	3,868477
166	A_23_P42198_HIST1H3G	0,0002839	0,0701163	-3,855422
167	A_23_P78888_FBL	0,0002938	0,072142	-3,844876
168	A_23_P218884_DVL3	0,0002969	0,0721833	3,841737
169	A_23_P397208_GSTM2	0,0002975	0,0721833	3,841057
170	A_24_P228978_C1QTNF3	0,0003117	0,0751822	3,826775
171	A_23_P43079_INTS8	0,0003217	0,0767445	-3,817135
172	A_24_P320796_FKBP9L	0,0003226	0,0767445	3,816286
173	A_24_P394510_HIST1H2AJ	0,0003238	0,0767445	-3,815092
174	A_23_P500034_GLI2	0,0003306	0,0770164	3,808721
175	A_24_P76158_DOCK11	0,0003274	0,0770164	3,811764
176	A_32_P104063_AF275804	0,0003289	0,0770164	-3,810324
177	A_23_P204721_AQP2	0,0003328	0,0770881	3,806692
178	A_23_P200999_ST3GAL3	0,0003392	0,0777033	3,800789
179	A_32_P204101_THC2439736	0,0003382	0,0777033	3,801746
180	A_23_P85783_PHGDH	0,000343	0,0778084	3,797385
181	A_24_P293192_FXYD3	0,0003469	0,0778084	-3,793902
182	A_24_P347310_P11	0,0003438	0,0778084	3,796661
183	A_24_P928217_AK026155	0,0003473	0,0778084	3,793568
184	A_24_P664939_AK021693	0,0003628	0,0808308	3,780136
185	A_23_P26154_PLIN	0,0003666	0,0812498	3,776866
186	A_24_P143301_KAAG1	0,0003725	0,0821024	3,771977
187	A_23_P126241_EIF4G3	0,0003752	0,0822691	3,769692
188	A_23_P119390_EHD2	0,0003786	0,0825633	3,76694
189	A_23_P10172_TSP50	0,0003829	0,0826363	3,763394
190	A_23_P57474_OSBP2	0,0003829	0,0826363	3,763414
191	A_23_P152344_GTF3C1	0,0003871	0,0830885	3,760081
192	A_23_P207967_KIAA0427	0,0003909	0,0834721	3,757039
193	A_24_P252130_PPARD	0,0003948	0,0838628	3,753984
194	A_23_P139260_SLC22A18	0,0004075	0,0852371	3,744165
195	A_23_P153767_AKAP8L	0,0004071	0,0852371	3,744463
196	A_32_P198325_LOC388886	0,0004052	0,0852371	3,745867

197	A_24_P922631_LOC133874	0,0004138	0,0861144	3,739409
198	A_24_P225339_MOBKL2C	0,0004298	0,0890031	3,727587
199	A_23_P85460_CDKN2C	0,000439	0,0899867	-3,721042
200	A_23_P86164_ZUBR1	0,000437	0,0899867	3,722437
201	A_24_P7021_KRT8P19	0,0004495	0,091689	3,713655
202	A_24_P384239_A_24_P384239	0,0004523	0,0918134	3,711687
203	A_24_P350683_SLC9A1	0,0004558	0,0920612	3,709308
204	A_32_P59516_BC041979	0,0004619	0,0928409	3,705147
205	A_23_P91970_AADACL2	0,0004749	0,0945177	3,696517
206	A_24_P383850_EIF4G3	0,0004745	0,0945177	3,696744
207	A_24_P375728_LOC92154	0,0004947	0,0952371	3,683744
208	A_23_P103310_S100A7	0,0004851	0,0952371	-3,68987
209	A_23_P215459_ELN	0,0004897	0,0952371	3,686944
210	A_23_P81640_KIAA1909	0,0004948	0,0952371	-3,683704
211	A_24_P255628_PACS2	0,0004939	0,0952371	3,684281
212	A_24_P257579_EPB41L4A	0,000494	0,0952371	3,684213
213	A_32_P114535_THC2288392	0,0004897	0,0952371	3,686898
214	A_23_P212854_GYPB	0,0005103	0,0977647	-3,674038
215	A_24_P409230_OR10A2	0,0005342	0,098209	3,6597
216	A_23_P121813_ENPP6	0,0005334	0,098209	3,660147
217	A_23_P98369_GRIA4	0,0005269	0,098209	3,664008
218	A_24_P120147_LOC284948	0,0005258	0,098209	3,664629
219	A_24_P226508_HS3ST5	0,0005325	0,098209	3,660687
220	A_24_P393449_DAPK1	0,0005286	0,098209	3,663011
221	A_24_P671875_THC2428713	0,0005318	0,098209	3,661062
222	A_24_P683917_FLNB	0,0005163	0,098209	3,670385
223	A_32_P231346_THC2458855	0,0005289	0,098209	3,662801
224	A_32_P184448_C18orf34	0,0005584	0,1022038	3,645767
225	A_23_P340338_LCE3E	0,0005676	0,1034289	3,640616
226	A_23_P208369_ITPKC	0,0005715	0,1036803	3,638456
227	A_23_P106371_GOLGA	0,0005803	0,1044194	3,633653
228	A_23_P84910_ZNF157	0,0005825	0,1044194	3,632433
229	A_24_P217520_EREG	0,0005832	0,1044194	-3,632065
230	A_23_P207125_NLGN2	0,0005895	0,1050766	3,628714
231	A_24_P105733_TNS1	0,0006033	0,1061715	3,621375
232	A_24_P113815_SLC35E2	0,0006034	0,1061715	3,621356
233	A_24_P264031_AK126415	0,0006033	0,1061715	3,621373
234	A_32_P179910_THC2315966	0,0006069	0,1063416	3,619499
235	A_23_P114381_STK23	0,0006104	0,1064947	3,617698
236	A_23_P68487_BMP7	0,0006177	0,107317	-3,613927
237	A_23_P317200_ATXN7L2	0,0006276	0,1085721	3,608915
238	A_23_P95359_DNAJC6	0,000635	0,1093941	3,605198
239	A_23_P18123_NLGN1	0,0006377	0,1094021	-3,603848
240	A_23_P203053_AK054929	0,0006414	0,1095648	3,602019
241	A_24_P43826_EBF2	0,000644	0,1095648	3,60074
242	A_23_P110266_FLJ23191	0,0006488	0,1099134	3,598423
243	A_23_P93258_HIST1H3B	0,000662	0,110339	-3,592004
244	A_24_P348265_FCAR	0,0006594	0,110339	3,593281
245	A_24_P407645_SPN	0,0006615	0,110339	-3,592265
246	A_32_P75299_AK125697	0,0006569	0,110339	-3,594492

247	A_32_P124887_A_32_P124887	0,0006658	0,1105195	-3,5902
248	A_32_P16989_A_32_P16989	0,0006705	0,1108493	3,587974
249	A_24_P307599_AF210649	0,0006836	0,1113555	3,581857
250	A_23_P118894_ATAD4	0,0006871	0,1113555	-3,580193
251	A_23_P157109_ADCYAP1R1	0,0006861	0,1113555	3,580692
252	A_23_P68327_CCDC104	0,000685	0,1113555	-3,581176
253	A_24_P358976_TMEM19	0,000687	0,1113555	-3,580258
254	A_23_P167389_CENTD3	0,000698	0,1126708	3,57521
255	A_24_P45651_HIST2H3A	0,000722	0,1156298	-3,56447
256	A_24_P942600_ENST00000349097	0,0007207	0,1156298	3,565048
257	A_23_P121945_SNCB	0,0007394	0,1179658	3,556859
258	A_23_P218442_CEACAM6	0,0007484	0,1184712	-3,553025
259	A_23_P427075_CTNS	0,0007476	0,1184712	3,553356
260	A_23_P406478_FLJ32784	0,0007557	0,1190867	3,549913
261	A_23_P82000_TEAD3	0,0007581	0,1190867	3,548919
262	A_23_P124335_LOC642299	0,0007746	0,1210102	-3,542027
263	A_23_P84952_TFE3	0,0007762	0,1210102	3,541367
264	A_32_P150382_VWF	0,00078	0,121139	3,539815
265	A_23_P12423_ATP13A2	0,0008041	0,1221739	3,530098
266	A_23_P13425_CD81	0,0008143	0,1221739	3,526057
267	A_23_P201596_AMPD2	0,0008116	0,1221739	3,527102
268	A_23_P412476_GREB1	0,0008091	0,1221739	-3,528105
269	A_23_P46639_C8A	0,0008078	0,1221739	-3,528619
270	A_23_P71867_IL11RA	0,0008125	0,1221739	3,526752
271	A_24_P140621_CCNJL	0,0008107	0,1221739	3,527459
272	A_24_P164505_FAM106A	0,0008165	0,1221739	3,525202
273	A_24_P276983_STK25	0,0008138	0,1221739	3,526251
274	A_32_P9816_AI857589	0,0008145	0,1221739	-3,525998
275	A_23_P367899_EPOR	0,0008255	0,1230766	3,521678
276	A_23_P128967_ALDH6A1	0,0008331	0,1233125	3,518742
277	A_24_P228667_MRPL40	0,0008305	0,1233125	-3,519753
278	A_23_P121783_SRD5A2L	0,000866	0,1263981	-3,506317
279	A_23_P200598_C1orf166	0,0008604	0,1263981	3,508421
280	A_23_P24414_EFEMP2	0,0008689	0,1263981	3,505233
281	A_23_P351295_HS3ST5	0,0008604	0,1263981	3,508386
282	A_32_P225768_A_32_P225768	0,0008694	0,1263981	3,505072
283	A_23_P136196_TBC1D19	0,0008774	0,1271151	-3,502117
284	A_23_P404045_MTHFR	0,0008856	0,1274089	3,499112
285	A_32_P215676_AL049990	0,000885	0,1274089	3,499331
286	A_23_P143981_FBLN2	0,0008899	0,127578	3,497559
287	A_23_P150979_SBEM	0,0009138	0,1300911	-3,48904
288	A_23_P73097_RGS20	0,0009134	0,1300911	3,489197
289	A_23_P101434_NALP12	0,0009204	0,1305777	3,486721
290	A_24_P161973_ATP11A	0,0009305	0,1315534	3,483209
291	A_23_P373598_MAFK	0,0009415	0,1326575	3,479405
292	A_23_P396800_NEGR1	0,0009499	0,1329834	3,476552
293	A_24_P254965_HDAC8	0,0009503	0,1329834	-3,476404
294	A_24_P269624_ENST00000381854	0,0009541	0,1330533	-3,475135
295	A_23_P66827_FAM106A	0,0009818	0,1364593	3,465876
296	A_23_P34375_TCEA3	0,0009945	0,1377525	3,461733

297	A_23_P104876_SPA17	0,0010199	0,137967	-3,453582
298	A_23_P107116_ZNF179	0,0010137	0,137967	3,455551
299	A_23_P126008_MAST2	0,0010191	0,137967	3,453843
300	A_23_P156953_IGF2R	0,0010247	0,137967	3,452049
301	A_23_P30805_HIST1H4J	0,0010216	0,137967	-3,453048
302	A_24_P410610_DPYD	0,0010238	0,137967	3,452349
303	A_24_P630640_CENTB1	0,0010216	0,137967	3,453042
304	A_32_P146382_BG181407	0,0010007	0,137967	-3,459715
305	A_32_P32923_A_32_P32923	0,0010263	0,137967	-3,451535
306	A_23_P47546_A_23_P47546	0,0010329	0,1383988	3,449463
307	A_32_P71675_ENST00000378266	0,001038	0,1386291	3,447866
308	A_24_P186936_ELN	0,0010523	0,1400787	3,44344
309	A_23_P121702_OCIAD2	0,0010668	0,1415467	-3,439005
310	A_24_P938508_AK022228	0,0010777	0,1425338	3,4357
311	A_23_P300484_BC061909	0,0010927	0,1439584	3,431217
312	A_32_P173955_A_32_P173955	0,0010955	0,1439584	-3,430381
313	A_32_P71571_FAM19A4	0,0011143	0,1459655	3,424838
314	A_32_P175198_ACTG1	0,0011302	0,1475676	3,420248
315	A_23_P252653_STK25	0,0011435	0,148059	3,416432
316	A_23_P78762_DHRS10	0,0011447	0,148059	3,416069
317	A_24_P127063_A_24_P127063	0,0011384	0,148059	-3,417894

DISCUSSION

PPGLs are paradigmatic for illustrating the importance of genetics in cancer development. These tumours show a high degree of heritability, around 40% carry a germline mutation, and they exhibit a great genetic heterogeneity with seventeen major susceptibility genes identified so far involved in the disease. Amongst them, *SDHD* was defined as the earliest metabolic gene involved in the TCA cycle and the respiratory chain whose mutations led to cancer development[103]. Since then, mutations in nine additional metabolic genes, all of them directly or indirectly related to the TCA cycle (*SDHA*, *SDHAF2*, *SDHB*, *SDHC*, *FH*, *MDH2*, *IDH1*, *IDH2*, and *SLC25A11*), have been reported to cause PPGL development with a characteristic CIMP profile, highlighting the relevance of this pathway in the disease. Despite recent genetic findings, there is still a percentage of hereditary PPGL cases that do not have a mutation in any of the known susceptibility genes, and for whom we were eager to get a genetic diagnosis.

Therefore, the overall purpose of this thesis was to implement NGS (WES and targeted gene panels) in genetically undiagnosed PPGL cases to identify new susceptibility genes. In order to avoid problems of data interpretation related to the aforementioned genetic heterogeneity, a proper selection of the patients to be included in the study was crucial. Thus, PPGL patients were classified according to molecular markers, like a CIMP profile, or based on relevant clinical features, such as tumour location and multiplicity.

- **ARTICLE 1: Candidate Cancer–Predisposing Mutations in TCA cycle genes.**

In this first study, we performed a selection of genetically undiagnosed PPGL cases according to the low expression and methylation of *RBP1*, a strategy for avoiding genetic heterogeneity that allowed us to focus exclusively on tumours with a CIMP profile, and therefore candidates to harbour genetic alterations in a TCA cycle-related gene. After the sampling phase, we applied to the selected series of cases a targeted exome sequencing panel that included 37 genes directly or indirectly involved in the TCA cycle. In addition, we carried out high-throughput DNA methylation profiling of selected tumours. Following this rational, we were able to identify various PPGL samples harbouring candidate variants affecting several genes TCA-related.

Firstly, we found mutations that although rare are already in the literature, such as the third reported pathogenic mutation in *IDH1* (c.394C>T; p.Arg132Cys) that affects mainly older patients (>61 years) with extra-adrenal PGLs[76,121]. In our study, we confirmed this cancer-prone alteration as the driver event in one PGL, diagnosed in a 78 years-old woman, by showing an accumulation of the oncometabolite 2HG in the mutated tumour that it is known to cause the inhibition of αKG-dependent dioxygenases, and therefore a characteristic CIMP profile. This finding further confirms a more predominant role of *IDH1* in PPGL pathogenesis than previously expected[170]. Additionally, although aberrant hypermethylation of the *SDHC* promoter has been reported in PGLs[110], GIST[171], and Carney triad patients[111], the case described in our study was the first example of a *SDHC* epimutation affecting a patient with Carney-Stratakis syndrome. These two examples of rare genetic events leading to PPGL development highlight

the need to apply well designed and comprehensive NGS panels and omics analysis for genetic testing in this multi-genetic disease, since diagnostic algorithms do not include the analysis of these low prevalent variants by conventional methods.

Secondly, we identified two new candidate genes (*GOT2* and *IDH3B*) involved in the hereditary predisposition to PPGL. GOT2 is a mitochondrial enzyme implicated in the malate-aspartate shuttle, the amino acid metabolism and the urea cycle. It also plays a role in the TCA cycle by converting oxaloacetate to aspartate and consequently glutamate to αKG, thus providing metabolic intermediates that are lacking due to the truncation of the TCA cycle, for instance in *SDH*-deficient cells[172]. The increase in GOT2 expression and the enhanced enzymatic activity found in the tissues carrying the c.357A>T (p.Glu119Asp) mutation suggested an activating role of this variant, fact that was supported by the increment of αKG levels and the following oncogenic accumulation of succinate observed in the *GOT2*-mutated tumour. The finding of a mutation affecting *GOT2*, a gene involved in the malate-aspartate shuttle and therefore in anaplerotic reactions, extended the PPGL susceptibility genes spectrum towards other genes not directly involved in the TCA cycle. Interestingly, the recent finding of mutations in *SLC25A11*, encoding a mitochondrial membrane carrier of αKG, points to the special relevance of the malate–aspartate shuttle in PPGL development[173] (Figure 4).

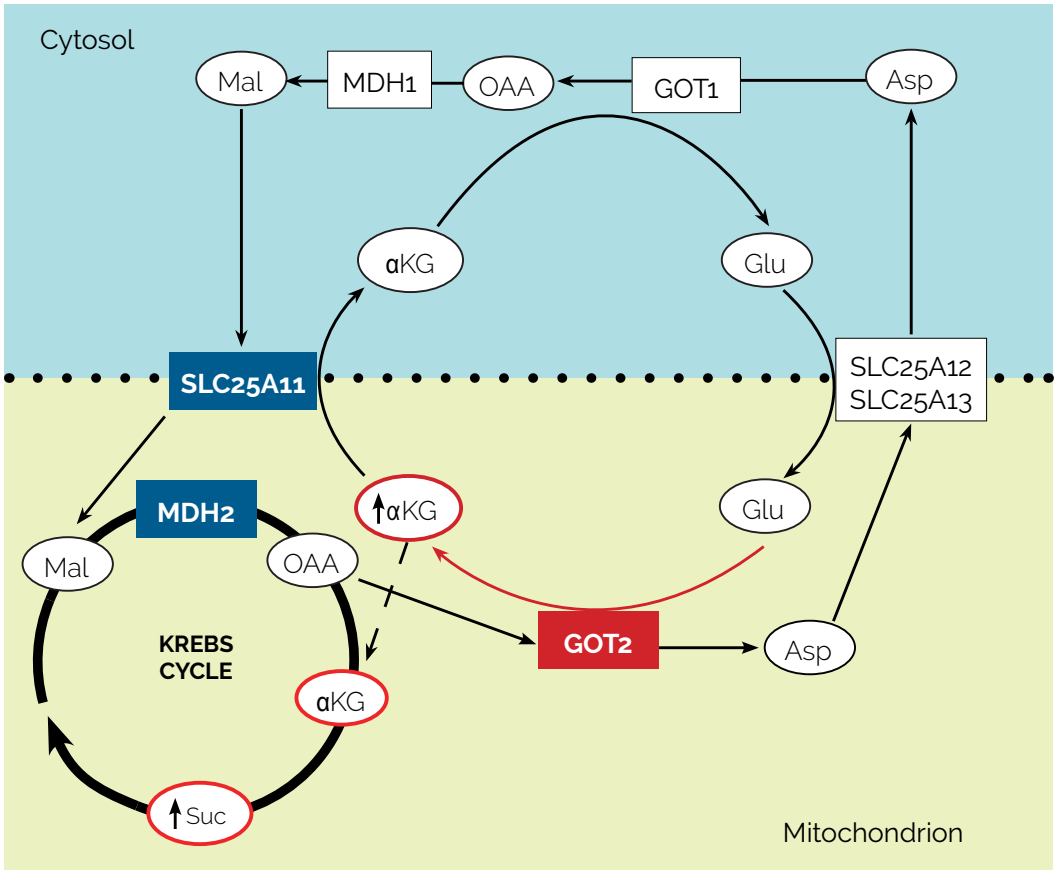

Figure 4. The malate-aspartate shuttle. PPGL susceptibility genes found activated are denoted in red (*GOT2*) while those inactivated are represented in blue (*SLC25A11* and *MDH2*). Red arrows indicate altered pathways due to mutated genes and metabolite accumulation is denoted by red circles.

Upon extension of the series analysed, a novel truncating germline mutation in the gene *IDH3B* (c.128_138delTGAGGGTGGAG) was detected in a patient with a single PGL. *IDH3B*-mutated tumour exhibited a CIMP-like profile in concordance with a negative 5-hmC IHC as well as an altered αKG/isocitrate ratio, thus suggesting a driver role of the variant in the tumorigenesis. IDH3B plays a structural role facilitating the assembly of the heterodimer and ensuring the full activity of the enzyme that catalyses the decarboxylation of isocitrate into αKG in the TCA cycle. Although extremely rare, somatic mutations in the gene *IDH3B* have been recently found in acute myeloid leukaemia (AML) tumours with a FLT3 internal tandem duplication[174], and homozygous loss-of-function mutations have been identified in two families with retinitis pigmentosa[175]. Despite the prevalence in PPGL is very low, the oncogenic role of *IDH1* and *IDH2* mutations in many cancers is well known for more than ten years[176–178]. As previously mentioned, *IDH1/2* mutations lead to a neomorphic activity and the concomitant loss of the enzyme's normal catalytic activity. Therefore, our finding of an inactivating mutation in *IDH3B*, with the consequent loss of the activity of IDH3, is in agreement with the relevant role of isocitrate dehydrogenase alterations in tumour development.

In summary, taking advantage of a selection of PPGL cases based on the expression of a methylation marker, we were able to identify different candidate mutations affecting TCA cycle-related genes (*IDH1*, *IDH3B* and *SDHC*), thus highlighting the relevance of this metabolic pathway in PPGL pathogenesis. In addition, we have also found altered an enzyme involved in metabolite exchange across the mitochondria (GOT2) which, as occurs with the finding of *SLC25A11* mutations in PPGL patients, points towards the involvement of mitochondrial shuttles in disease development.

- **ARTICLE 2: Identification of gain-of-function mutations in an epigenetic regulator.**

Among the PPGL patients with a CIMP profile that were included for the analysis with the TCA cycle panel (Article 1), there was a very interesting case: a young woman (22 yr.) with multiple PGLs (>7), but without family history of the disease, who tested negative not only for the canonical PPGL susceptibility genes, but also for any of the candidate genes included in our TCA cycle panel. For this particular patient there were different genetic scenarios accounting for the disease, being the main ones the presence of a *de novo* mutation, following a recessive model of inheritance, or an autosomal dominant model with incomplete penetrance.

Following a trio-based approach, WES was applied to germline samples from the two parents and the proband, identifying a single *de novo* missense variant in the gene *DNMT3A* (c.896A>T; p.Lys299Ile). *De novo* highly deleterious mutations play a prominent role in neurodevelopmental diseases. These mutations are individually rare with a rate of one *de novo* mutation per exome[179], so our trio-based strategy allowed us to probably find the only coding *de novo* variant and the causal mutation of the patient.

DNMT3A is a DNA methyltransferase that, together with DNMT3B, is in charge of the establishment of methylation patterns early in mammal embryogenesis through *de novo* methylation of unmethylated CpG sites[180,181] (Figure 5A). The p.Lys299Ile variant affects a highly conserved residue within the PWWP domain of DNMT3A that binds to the DNA and targets the protein to trimethyl lysines in histone H3[182,183] (Figure 5B). *In silico* predictors classified the variant as deleterious and it was found neither in public databases such as gnomAD and the database of Epigenetic Modifiers nor in more than 570 Spanish exomes from the CIBERER Spanish Variant Server.

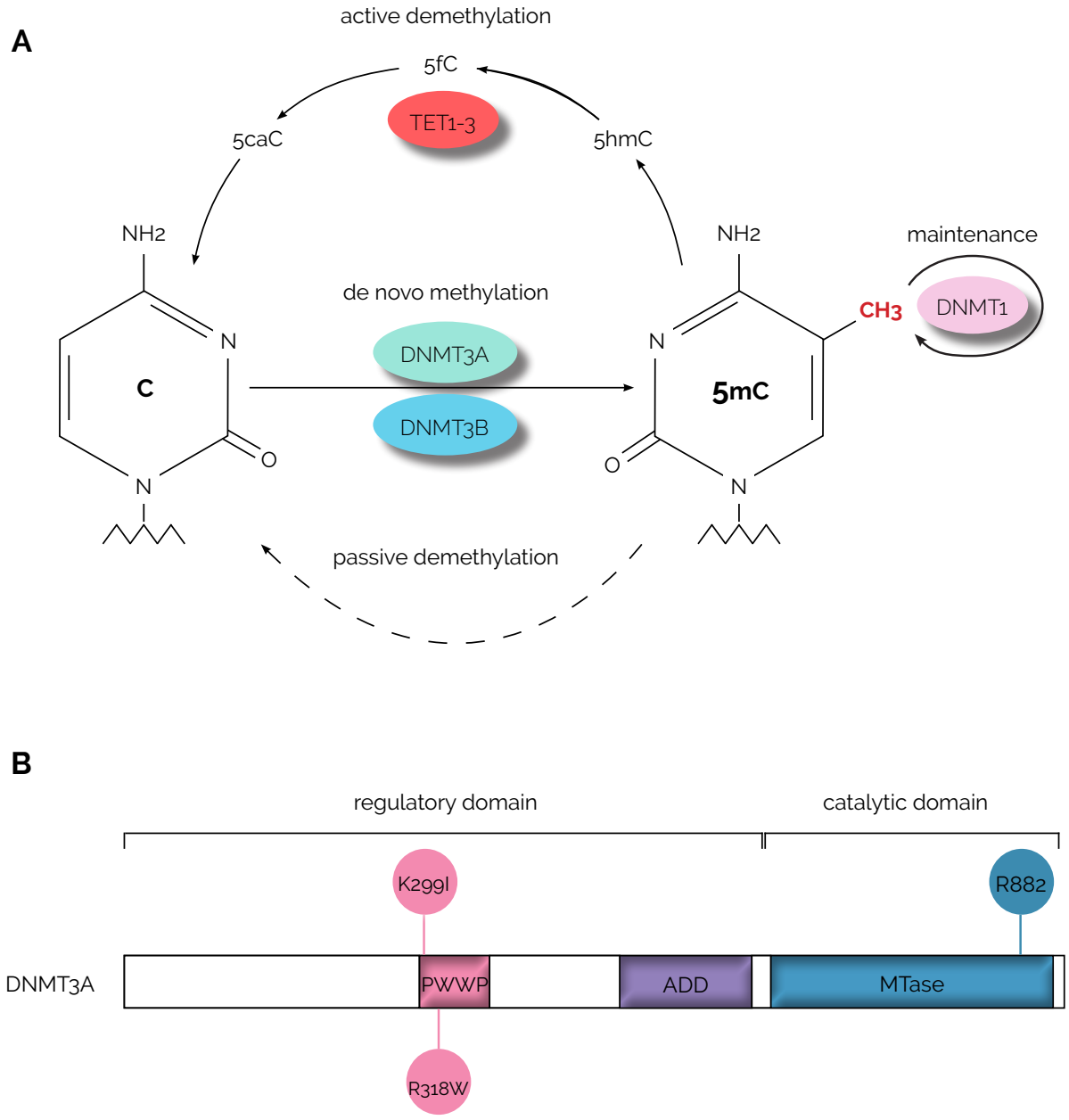

Figure 5. DNMT3A role and structure. (A) Role of the different DNA methyltransferases (DNMT1, DNMT3A, and DNMT3B) in the DNA methylation process. **(B)** Structural domains of the DNMT3A protein: a proline-tryptophan-tryptophan-proline (PWWP) domain, an ATRX, DNMT3, and DNMT3L-type zinc finger (ADD) domain, and the methyltransferase (MTase) domain. The *DNMT3A* mutations (Lys299Ile; K299I and p.Arg318Trp; R318W) as well as the hotspot R882 appear indicated in the different domains.

A characteristic hypermethylation of several Hox genes and other homeobox-containing genes, all targets for DNMT3A-dependent methylation, was observed in p.Lys299Ile-DNMT3A tissues, meaning both tumours available and lymphocytes extracted from patient's blood. This finding suggested that the p.Lys299Ile variant is associated with a transcriptional repression role due to a gain-of-function of DNMT3A, rather than an inactivation of the protein. Hypermethylation of homeobox-containing genes and specifically Hox genes with a tumour suppressor role has been widely reported in different cancer types including neuroblastoma and PPGL[184,185]. In fact, aberrant expression of many members of this transcription factors superfamily has been related to tumorigenesis and loss-of-function *DNMT3A* mutations[186]. Of note, the effect on global DNA methylation caused by the introduction of the p.Lys299Ile mutation in our CRISPR/Cas9 model of HeLa cells supports the gain-of-function role of this mutation, being consistent with the hypermethylated profile observed in the tumours. A high immunostaining of H3K9me3 was observed in all *DNMT3A*-mutated tumours available, something also found in *SDH*- and *FH*-mutated PPGLs[187], thus providing further evidence for the gain-of-function role of the *DNMT3A* mutations.

Somatic loss-of-function mutations in *DNMT3A* are highly recurrent in patients with AML and many other haematological malignancies[188,189]; with a hotspot for variants affecting the arginine 882 (Figure 5B). In the same way, germline *de novo* inactivating genetic alterations in *DNMT3A* have been commonly reported for overgrowth syndrome patients[190,191]. So far, the index patient carrying the p.Lys299Ile mutation is free of AML or any haematological malignancy and overgrowth syndrome. In addition, the p.Lys299Ile DNMT3A variant was not found in AML or overgrowth syndrome patients. Somatic mutations in other epigenetic modifying genes involved in chromatin-remodelling have been also reported not only in overgrowth syndromes (*EZH2*[192], *NSD1*[193] and *SETD2*) but also in many solid tumours including PPGL cases[79]. In addition, overexpression of *DNMT3A* has been related to tumorigenesis and progression of different tumours[194,195], supporting an oncogenic role for the DNMT family proteins. Although not curative, the success of DNA hypomethylating agents, including azacitidine and decitabine, in the treatment of multiple hematologic malignancies further supports the oncogenic role of *DNMT3A*[181,196]. Despite there is a well-reported existence of a crosstalk between genomic alterations and deregulation of epigenetics as a cause of different cancer types, the case reported herein would be the first example of a mutation in an epigenetic regulator causing a hereditary cancer.

Considering the recurrence of activating mutations affecting oncogenes, a screening of the PWWP domain of DNMT3A in a series of additional PPGL patients was performed. This way, we were able to identify a second germline *DNMT3A* mutation (c.952C>T; p.Arg318Trp) in a woman with multiple HN-PGLs and family history of the disease. The p.Arg318Trp substitution was also affecting a highly conserved residue within the PWWP domain of DNMT3A. In the same manner, we were able to identify the mutation p.Lys299Ile with a subclonal somatic character in six HN-PGLs (6.4% of PPGLs studied). However, we consider that the *DNMT3A* mutation is not the cancer driver event in these sporadic patients due to the low allele frequencies observed.

To summarize, in this second study *DNMT3A* appears as a new PGL related gene. Despite altered DNA methylation is one of the most common epigenetic changes in human cancers, this would be the first example of a gain-of-function mutation affecting *DNMT3A*. Additionally, *DNMT3A* sub-clonal somatic mutations seems to be relatively frequent in HN-PGLs although the biological meaning of these non-driver alterations remains unknown.

- **ARTICLE 3: Identification of a recurrent germline mutation in a TCA cycle gene in patients with multiple PPGLs.**

The TCA cycle has become one of the most relevant pathways in PPGL development since more than ten different genes (including *GOT2* and *IDH3B*) directly or indirectly involved in this key metabolic pathway have been found altered. In this third study, upon extension of the series of samples analysed through the TCA cycle-related genes panel (Article 1), we could identify five germline variants affecting *DLST* in seven unrelated patients (~7% of the patients included in the analysis) without mutations in any of the known susceptibility genes.

The *DLST* gene encodes one of the three subunits of the mitochondrial oxoglutarate dehydrogenase (OGDH) complex in charge of the conversion of αKG to succinyl-CoA, CO2 and NADH (Figure 6).

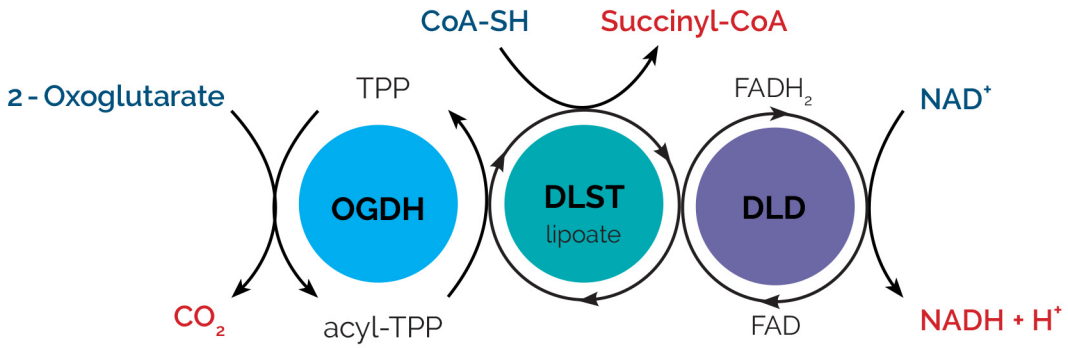

Figure 6. OGDH complex structure. E1: OGDH (2-oxoglutarate dehydrogenase), E2: DLST (dihydrolipoamide S-succinyltransferase), E3: DLD (dihydrolipoamide dehydrogenase). The E1 subunit contains tightly bound TPP (thiamine pyrophosphate) and catalyses the decarboxylation of 2-oxoglutarate and the formation of TPP-hydroxysuccinate, followed by the conversion of oxidized lipoate (covalently linked to the E2 subunits) into succinate dihydrolipoate. The E2 subunit induces the formation of succinyl-CoA by transesterification as well as the E3 subunit catalyses the transference of H^+ (from $FADH_2$) to NAD^+ to form NADH and the regeneration of oxidized lipoate.

As it happens with the SDH complex, depletion of any of the OGDH complex subunits leads to impaired enzymatic activity and αKG accumulation. Among the *DLST* variants identified, c.1121G>A; p.Gly374Glu

appeared as a recurrent mutation in four unrelated PPGL patients (three individuals identified with the panel and an additional one by WES). The Gly374 residue locates within the pocket of the enzyme that is also a region of monomers interaction, so the Glu-containing substitution may interfere not only with the binding to the succinyl group, but also in the oligomerization of the protein.

Upon disruption of the OGDH complex activity, high levels of accumulated αKG may be converted to the L enantiomer of 2HG by promiscuous enzymatic activity of both malate dehydrogenase enzymes (MDH1 and MDH2), and especially by lactate dehydrogenase A in hypoxic cells[197]. This production has been seen enhanced by acidic pH even under normoxic conditions[198]. Therefore, the increased αKG to fumarate, and 2HG to fumarate ratios observed in p.Gly374Glu-DLST tumours, as well as the accumulation of significant levels of L-2HG in DLST-KO cells reconstituted with the mutant protein, suggests that this mutation is leading to a DLST functional impairment.

Six available tumours carrying the recurrent p.Gly374Glu variant showed LOH by paternal UPD, suggesting a tumour suppressor role for DLST. This unusual second hit mechanism was already reported for the PPGL susceptibility gene *MAX*[199] which is also located in chromosome 14q, therefore underscoring the relevance of this mechanism for PPGL pathogenesis. A detailed omics study showed a homogeneous expression profile within p.Gly374Glu-DLST tumours, and alike to the one exhibited by *MAX*-mutated tumours, being a presumably consequence of the 14q chromosomal loss. However, absence of gross deletions, alterations in the promotor, and deep intronic mutations in *MAX* ruled out this gene as the disease-causing and confirmed the main driver role of *DLST*.

When we analysed the expression data from a large series of PPGLs carrying known mutations using a previously reported list of 451 genes differentially expressed in PPGLs with different genetic backgrounds[128], the p.Gly374Glu-DLST cases were grouped in Cluster 1 together with all, except one, tumours carrying mutations in *EPAS1*. This result confirmed the homogeneous profile of the p.Gly374Glu-DLST tumours, as well as it suggested a link between DLST disruption and pseudohypoxia, and further supported the differences between these tumours and tumours carrying mutations in *MAX*. Among the significant differentially expressed genes, the hypoxic transcriptional factor *HIF3A* appeared overexpressed in *DLST*-mutated tumours. Although the functional implications of the overexpression of this hypoxic factor is unknown, it is though that HIF3A acts as a dominant-negative regulator of the hypoxia-inducible gene expression[200].

Moreover, p.Gly374Glu-DLST tumours also exhibited characteristic homogeneous methylation profiles, that although not hypermethylated as occurred in SDHx-mutated tumours, indicate that a similar mutational status account for all of them, therefore pointing to a *DLST* driver role in the pathogenesis of these tumours. To note, the absence of a CIMP profile in p.Gly374Glu-DLST tumours explains why these samples were not selected in the first study presented in this thesis focused on hypermethylated PPGLs.

Regarding the clinical features of mutation carriers, there was a predominance of multiple tumours within the *DLST*-mutated patients (six out of seven, p<0.001), which was especially relevant in the thoracic-abdominal region (p<0.0003). This multiplicity supports the pathogenic role of DLST in PPGL development, as it is a common feature among hereditary cancer syndromes. In addition, the lack of family history of the disease in mutation carriers points towards *de novo* or low penetrant mutations, being both mechanisms already reported for PPGL[118,201,202].

Concerning the remaining *DLST* substitutions (c.692G>A, p.Arg231Gln; c.910G>A, p.Asp304Asn; and c.1265A>G, p.Tyr422Cys), although two of them affect highly conserved residues within the protein and were predicted as deleterious, displayed a similar behaviour to WT-DLST in our cellular model. Similarly, it was not possible to determine a pathogenic role for the *DLST* intronic splice site variant (c.1060-3T>A) since there was not enough tissue to work with.

Finally, we observed a highly positive DLST immunostaining not only in *DLST*-mutated tumours but also in any other PPGL with mutations in TCA cycle-associated genes, as well as in *EPAS1*-mutated PPGLs, highlighting once more, the possible association between *DLST* mutations and a pseudo-hypoxic profile. This observation may suggest that, as occurs with *SDHD* and the SDH complex[203], the presence of disrupting mutations in TCA cycle genes or *DLST* itself obstructs OGDH complex assembly making the DLST epitope more accessible. Although still unexplained, DLST IHC may be helpful in the classification of VUS in genes from the pseudohypoxic Cluster 1, either in TCA cycle-related genes or in *EPAS1*.

To the best of our knowledge, this is the first example of OGDH complex mutations leading to cancer. However, mutations in the OGDH complex and related genes, as well as alterations in enzyme functionality have been linked to neurodegeneration[204–206], something also frequently observed in other TCA cycle–related PPGL susceptibility genes[207–211].

In summary, this third study highlights *DLST* as a new candidate PPGL susceptibility gene. Four unrelated patients were found carrying a recurrent germline mutation (p.Gly374Glu) that functionally compromises DLST function. Tumours and cells harbouring this mutation display elevated αKG and 2HG to fumarate ratios and consequently altered and characteristic methylation and transcriptional profiles.

- **GENERAL DISCUSSION**

Advances in sequencing technologies within the past few years led a majority of genetics laboratories to embrace NGS as the new gold standard not only for routine diagnosis but also for identification of new susceptibility genes, due to that NGS is especially pertinent for disorders such as hereditary PPGLs with

a highly genetic heterogeneity[37].

In this thesis, we have developed three projects with the aim of identify new PPGL susceptibility genes employing NGS. Taking into consideration the relevance of TCA cycle in PPGL pathogenesis, we applied a targeted sequencing panel of genes related to this key metabolic pathway to PPGL samples without mutations in any of the already known predisposing genes. Selection of samples was key as we could just focus on genetically undiagnosed PPGL patients with similar molecular features, such as a CIMP profile. This strategy let us to discover mutations in genes that so far had not been implicated in disease development such as *GOT2* and *IDH3B*, and to select for WES another patient the finally carried a mutation in the epigenetic modifier *DNMT3A*. Additionally, we could identify extremely rare mutations in already known PPGL susceptibility genes such as *IDH1* and an epimutation in *SDHC*. Finally, upon extension of the PPGL samples series to be analysed for alterations in the TCA cycle, a potentially pathogenic variant in the *DLST* gene was unravelled, appearing it as a new candidate PPGL driver gene.

These three studies add invaluable data to a growing list of potential susceptibility genes for PPGL. However, segregation analyses and testing of large populations of PPGL patients will be required in future studies in order to uncover the prevalence of mutations in these genes, as well as a complete understanding of the variants' penetrance. Moreover, clinicians must act cautiously when rare variants are identified in PPGL patients since clinical action is only recommended for truly established pathogenic genes and variants[212].

Despite all genetic discoveries achieved during the past years, therapeutics development against M-PPGL has been very unsuccessful for three main reasons: difficulty of patient enrolment in large clinical trials, paucity of preclinical animal models, and lack of efficiency of molecular targeted drugs[41]. Therefore, identification of clinically effective treatments for M-PPGL is for sure the most important unmet clinical need nowadays. Although the patients carrying TCA cycle-related mutations identified in this thesis have not developed metastases so far, the association of alterations in this metabolic pathway and metastases is well known in PPGL. The results gathered in our studies uncover new possible druggable targets which can be used in the near future for the development of novel personalized PPGL targeted therapies.

CONCLUSIONES/CONCLUSIONS

CONCLUSIONES

1. El hallazgo de diversas variantes candidatas en genes relacionados con el ciclo de los ácidos tricarboxílicos (TCA), apoya la relevancia de esta vía metabólica central en la patogénesis del PPGL. También pone de manifiesto el éxito de una estrategia de selección de muestras basada en marcadores, para evitar problemas de interpretación relacionados con la presencia de heterogeneidad genética.

2. La mutación c.357A>T *GOT2*, asociada a una mayor expresión y actividad de la proteína, así como a ratios de metabolitos alterados, tiene un papel directo en el desarrollo de PPGL, lo que incrementa el número de genes de susceptibilidad involucrados en la enfermedad. Pese a que la prevalencia de mutaciones en *GOT2* parece ser baja en pacientes con PPGL, este hallazgo apunta hacia la implicación de la lanzadera de malato-aspartato en la enfermedad, como ya se ha visto para otras enzimas relacionadas con el intercambio metabólico a través de la mitocondria.

3. El empleo de paneles de genes para la secuenciación masiva, combinado con perfiles de metilación, permitió la identificación de alteraciones patológicas raras en genes de susceptibilidad a desarrollar PPGL ya conocidos (*IDH1* y *SDHC*) e identificó a *IDH3B* como un nuevo gen candidato responsable de la enfermedad.

4. Mutaciones germinales en el dominio PWWP del gen *DNMT3A* causan un fenotipo metilado en aquellos tejidos mutados y confiere susceptibilidad hereditaria a desarrollar PPGL. Hasta ahora, este es el primer ejemplo de mutaciones activadoras en un gen con actividad ADN metiltransferasa involucrado en una predisposición a desarrollar cáncer. Además, las mutaciones somáticas subclonales en *DNMT3A* son relativamente frecuentes en PPGLs de cabeza y cuello, lo que subraya por tanto la importancia de las alteraciones en *DNMT3A* en el desarrollo de PPGL.

5. *DLST*, otro gen que codifica una enzima crucial del ciclo TCA, aparece mutado hasta en un 7% de los pacientes con PPGL que no presentaban alteraciones en ninguno de los principales genes de susceptibilidad de la enfermedad. En presencia de la variante germinal recurrente p.Gly374Glu-DLST, y después de una pérdida de heterocigosidad por disomía uniparental, se produce una interrupción de la actividad del complejo OGDH dando lugar a una acumulación de αKG así como a una producción de 2HG.

6. Los tumores portadores de la variante recurrente p.Gly374Glu-DLST exhiben un perfil de metilación homogéneo, pero no hipermetilado, y una marca de expresión pseudohipóxica, como ocurre en los tumores con mutación en *EPAS1*, en la cual parece estar involucrado HIF3A.

7. La inmunohistoquímica de DLST se vislumbra como una nueva herramienta que podría ayudar a discernir entre mutaciones y variantes de significado desconocido (VUS), no sólo en el gen *DLST* sino también en *EPAS1* y en los genes pseudohipóxicos del Cluster 1A.

CONCLUSIONS

1. The finding of several candidate variants affecting TCA cycle-related genes further attests the relevance of this key metabolic pathway in PPGL pathogenesis, as well as it highlights the success of an appropriate marker-based sample selection strategy in order to avoid the interpretation problems related to the presence of genetic heterogeneity.

2. The c.357A>T *GOT2* mutation, that is associated with a higher expression and activity of the protein, and with altered metabolite ratios, has a driver role in PPGL development, which increases the number of susceptibility genes involved in the disease. Although the prevalence of *GOT2* mutations seems to be low across PPGL patients, this finding points towards the involvement of the malate-aspartate shuttle in the disease, as it has already been seen for other enzymes related to metabolite exchange across the mitochondria.

3. The use of targeted gene panel sequencing, combined with methylation profiling, allowed the identification of rare pathological alterations in known PPGL susceptibility genes (*IDH1* and *SDHC*), as well as uncovered *IDH3B* as a new candidate gene responsible for the disease.

4. Germline mutations in the PWWP domain of the *DNMT3A* gene cause a methylated phenotype in mutated tissues, and confer hereditary susceptibility to develop PGLs. This is the first example of gain-of-function mutations in a DNA methyltransferase gene involved in cancer predisposition reported so far. Moreover, *DNMT3A* subclonal somatic mutations are relatively frequent in HN-PGLs highlighting the importance of *DNMT3A* alterations in PGL development.

5. *DLST*, another gene encoding a pivotal enzyme of the TCA cycle, is found mutated in up to 7% of the PPGL patients without alterations in the main PPGL susceptibility genes. Upon the presence of the recurrent p.Gly374Glu-DLST germline variant, and after LOH caused by UPD, there is a disruption of OGDH complex activity leading to accumulation of αKG and production of 2HG.

6. Tumours carrying the recurrent p.Gly374Glu-DLST variant exhibit a homogeneous but not hypermethylated profile, and a pseudohypoxic expression signature, close to *EPAS1*-mutated tumours, in which HIF3A seems to play a role.

7. DLST IHC appears as a new tool that may be useful in order to discern between mutations and VUS not only in the *DLST* gene, but also in *EPAS1* and pseudohypoxic Cluster 1A genes.

REFERENCES

1. Dahia, P. L. M. Pheochromocytoma and paraganglioma pathogenesis: Learning from genetic heterogeneity. *Nat. Rev. Cancer* **14**, 108–119 (2014).

2. Castro-Vega, L. J., Lepoutre-Lussey, C., Gimenez-Roqueplo, a. P. & Favier, J. Rethinking pheochromocytomas and paragangliomas from a genomic perspective. *Oncogene* **35**, 1080–1089 (2016).

3. Crona, J., Taïeb, D. & Pacak, K. New perspectives on pheochromocytoma and paraganglioma: Toward a molecular classification. *Endocrine Reviews* **38**, 489–515 (2017).

4. Barontini, M., Levin, G., Sanso, G. & Guti, R. Characteristics of Pheochromocytoma in a 4- to 20-Year-Old Population. *Ann. N. Y. Acad. Sci.* **1073**, 30–37 (2006).

5. Aron, D., Terzolo, M. & Cawood, T. J. Adrenal incidentalomas. *Best Pract. Res. Clin. Endocrinol. Metab.* **26**, 69–82 (2012).

6. McNeil, a. R., Blok, B. H., Koelmeyer, T. D., Burke, M. P. & Hilton, J. M. Phaeochromocytomas discovered during coronial autopsies in Sydney, Melbourne and Auckland. *Aust. N. Z. J. Med.* **30**, 648–652 (2000).

7. Lenders, J. W. M. *et al.* Pheochromocytoma and Paraganglioma: An Endocrine Society Clinical Practice Guideline. *J. Clin. Endocrinol. Metab.* **99**, 1915–1942 (2014).

8. Kantorovich, V. & Pacak, K. Pheochromocytoma and paraganglioma. *Prog. Brain Res.* **182**, 343–73 (2010).

9. Peitzsch, M. *et al.* Analysis of plasma 3-methoxytyramine, normetanephrine and metanephrine by ultraperformance liquid chromatography-tandem mass spectrometry: utility for diagnosis of dopamine-producing metastatic phaeochromocytoma. *Ann. Clin. Biochem.* **50**, 147–155 (2013).

10. Därr, R. *et al.* Pheochromocytoma - update on disease management. *Ther. Adv. Endocrinol. Metab.* **3**, 11–26 (2012).

11. Lussey-Lepoutre, C., Buffet, A., Gimenez-Roqueplo, A. P. & Favier, J. Mitochondrial deficiencies in the predisposition to paraganglioma. *Metabolites* **7**, 1–13 (2017).

12. Fishbein, L. & Nathanson, K. L. Pheochromocytoma and paraganglioma: Understanding the complexities of the genetic background. *Cancer Genet.* **205**, 1–11 (2012).

13. Zhang, R., Gupta, D. & Albert, S. G. Pheochromocytoma as a reversible cause of cardiomyopathy: Analysis and review of the literature. *Int. J. Cardiol.* **249**, 319–323 (2017).

14. Roman-Gonzalez, A. & Jimenez, C. Malignant pheochromocytoma–paraganglioma. *Curr. Opin. Endocrinol. Diabetes Obes.* **24**, 174–183 (2017).

15. Björklund, P., Pacak, K. & Crona, J. Precision medicine in pheochromocytoma and paraganglioma:

current and future concepts. *J. Intern. Med.* **280**, 559–573 (2016).

16. Baudin, E. *et al.* Therapy of endocrine disease: Treatment of malignant pheochromocytoma and paraganglioma. *Eur. J. Endocrinol.* **171**, R111–R122 (2014).

17. Goffredo, P., Sosa, J. A. & Roman, S. A. Malignant pheochromocytoma and paraganglioma: A population level analysis of long-term survival over two decades. *J. Surg. Oncol.* **107**, 659–664 (2013).

18. Turkova, H. *et al.* CHARACTERISTICS AND OUTCOMES OF METASTATIC SDHB AND SPORADIC PHEOCHROMOCYTOMA/PARAGANGLIOMA: AN NATIONAL INSTITUTES OF HEALTH STUDY. *Endocr. Pract.* **22**, 302–314 (2016).

19. Eisenhofer, G. *et al.* Plasma methoxytyramine: A novel biomarker of metastatic pheochromocytoma and paraganglioma in relation to established risk factors of tumour size, location and SDHB mutation status. *Eur. J. Cancer* **48**, 1739–1749 (2012).

20. Nicolas, M. & Dahia, P. Predictors of outcome in phaeochromocytomas and paragangliomas. *F1000Research* **6**, 2160 (2017).

21. Gimenez-Roqueplo, A. P. *et al.* Mutations in the SDHB Gene Are Associated with Extra-adrenal and / or Malignant Phaeochromocytomas. *Cancer Res.* **63**, 5615–5621 (2003).

22. Jimenez, C. Treatment for Patients With Malignant Pheochromocytomas and Paragangliomas: A Perspective From the Hallmarks of Cancer. *Front. Endocrinol. (Lausanne).* **9**, 277 (2018).

23. Timmers, H. J. L. M. *et al.* Biochemically Silent Abdominal Paragangliomas in Patients with Mutations in the Succinate Dehydrogenase Subunit B Gene. *J. Clin. Endocrinol. Metab.* **93**, 4826–4832 (2008).

24. Timmers, H. J. L. M., Taieb, D. & Pacak, K. Current and Future Anatomical and Functional Imaging Approaches to Pheochromocytoma and Paraganglioma. *Horm. Metab. Res.* **44**, 367–372 (2012).

25. Lenders, J. W. M. & Eisenhofer, G. Update on Modern Management of Pheochromocytoma and Paraganglioma. *Endocrinol. Metab.* **32**, 152 (2017).

26. Taïeb, D. *et al.* EANM 2012 guidelines for radionuclide imaging of phaeochromocytoma and paraganglioma. *Eur. J. Nucl. Med. Mol. Imaging* **39**, 1977–1995 (2012).

27. Elston, M. S. *et al.* Increased SSTR2A and SSTR3 expression in succinate dehydrogenase–deficient pheochromocytomas and paragangliomas. *Hum. Pathol.* **46**, 390–396 (2015).

28. Leung, K., Stamm, M., Raja, A. & Low, G. Pheochromocytoma: The range of appearances on ultrasound, CT, MRI, and functional imaging. *Am. J. Roentgenol.* **200**, 370–378 (2013).

29. Janssen, I. *et al.* Superiority of [68Ga]-DOTATATE PET/CT to Other Functional Imaging

Modalities in the Localization of SDHB-Associated Metastatic Pheochromocytoma and Paraganglioma. *Clin. Cancer Res.* **21**, 3888–3895 (2015).

30. Janssen, I. *et al.* PET/CT comparing 68Ga-DOTATATE and other radiopharmaceuticals and in comparison with CT/MRI for the localization of sporadic metastatic pheochromocytoma and paraganglioma. *Eur. J. Nucl. Med. Mol. Imaging* **43**, 1784–1791 (2016).

31. Janssen, I. *et al.* 68Ga-DOTATATE PET/CT in the Localization of Head and Neck Paragangliomas Compared with Other Functional Imaging Modalities and CT/MRI. *J. Nucl. Med.* **57**, 186–191 (2016).

32. van Nederveen, F. H. *et al.* An immunohistochemical procedure to detect patients with paraganglioma and phaeochromocytoma with germline SDHB, SDHC, or SDHD gene mutations: a retrospective and prospective analysis. *Lancet Oncol.* **10**, 764–771 (2009).

33. Hoekstra, A. S., Graaff, M. A. De, Bruijn, I. H. B. & Ras, C. Inactivation of SDH and FH cause loss of 5hmC and increased H3K9me3 in paraganglioma / pheochromocytoma and smooth muscle tumors. *Oncotarget* **6**, 38777–38788 (2015).

34. Mannelli, M. *et al.* Clinically guided genetic screening in a large cohort of Italian patients with pheochromocytomas and/or functional or nonfunctional paragangliomas. *J. Clin. Endocrinol. Metab.* **94**, 1541–1547 (2009).

35. Erlic, Z. *et al.* Clinical predictors and algorithm for the genetic diagnosis of pheochromocytoma patients. *Clin. Cancer Res.* **15**, 6378–6385 (2009).

36. Favier, J., Amar, L. & Gimenez-Roqueplo, A. P. Paraganglioma and phaeochromocytoma: From genetics to personalized medicine. *Nat. Rev. Endocrinol.* **11**, 101–111 (2015).

37. Toledo, R. A. *et al.* Consensus Statement on next-generation-sequencing-based diagnostic testing of hereditary phaeochromocytomas and paragangliomas. *Nat. Rev. Endocrinol.* **13**, 233–247 (2017).

38. Richter, S. *et al.* Metabolome-guided genomics to identify pathogenic variants in isocitrate dehydrogenase, fumarate hydratase, and succinate dehydrogenase genes in pheochromocytoma and paraganglioma. *Genet. Med.* (2018).

39. Toledo, R. A. & Dahia, P. L. M. Next-generation sequencing for the diagnosis of hereditary pheochromocytoma and paraganglioma syndromes. *Curr. Opin. Endocrinol. Diabetes Obes.* **22**, 169–179 (2015).

40. Mazza, A. *et al.* Anti-hypertensive treatment in pheochromocytoma and paraganglioma: Current management and therapeutic features. *Endocrine* **45**, 469–478 (2014).

41. Toledo, R. & Jimenez, C. Recent advances in the management of malignant pheochromocytoma and paraganglioma: focus on tyrosine kinase and hypoxia-inducible factor inhibitors. *F1000Research* **7**, 1148 (2018).

42. Conzo, G. *et al.* Laparoscopic adrenalectomy, a safe procedure for pheochromocytoma. A retrospective review of clinical series. *Int. J. Surg.* **11**, 152–156 (2013).

43. Jimenez, C. *et al.* Current and Future Treatments for Malignant Pheochromocytoma and Sympathetic Paraganglioma. *Curr. Oncol. Rep.* **15**, 356–371 (2013).

44. Castinetti, F. *et al.* Outcomes of adrenal-sparing surgery or total adrenalectomy in phaeochromocytoma associated with multiple endocrine neoplasia type 2: An international retrospective population-based study. *Lancet Oncol.* **15**, 648–655 (2014).

45. Bacciu, A. *et al.* Lower cranial nerves function after surgical treatment of Fisch Class C and D tympanojugular paragangliomas. *Eur. Arch. Oto-Rhino-Laryngology* **272**, 311–319 (2015).

46. Lenders, J. W. M. & Eisenhofer, G. Update on Modern Management of Pheochromocytoma and Paraganglioma. *Endocrinol. Metab.* **32**, 152 (2017).

47. Yu, R. Proteasome Inhibitors: A Potential Medical Therapy for Malignant Pheochromocytoma. *Endocrinology* **158**, 3083–3085 (2017).

48. Niemeijer, N. D., Alblas, G., Van Hulsteijn, L. T., Dekkers, O. M. & Corssmit, E. P. M. Chemotherapy with cyclophosphamide, vincristine and dacarbazine for malignant paraganglioma and pheochromocytoma: Systematic review and meta-analysis. *Clin. Endocrinol. (Oxf).* **81**, 642–651 (2014).

49. Kulke, M. H. *et al.* Phase II study of temozolomide and thalidomide in patients with metastatic neuroendocrine tumors. *J. Clin. Oncol.* **24**, 401–406 (2006).

50. Hadoux, J. *et al.* SDHB mutations are associated with response to temozolomide in patients with metastatic pheochromocytoma or paraganglioma. *Int. J. Cancer* **135**, 2711–2720 (2014).

51. 51.Plouin, P.-F. *et al.* Metastatic Pheochromocytoma and Paraganglioma: Focus on Therapeutics. *Horm. Metab. Res.* **44**, 390–399 (2012).

52. van Hulsteijn, L. T., Niemeijer, N. D., Dekkers, O. M. & Corssmit, E. P. M. 131 I-MIBG therapy for malignant paraganglioma and phaeochromocytoma: systematic review and meta-analysis. *Clin. Endocrinol. (Oxf).* **80**, 487–501 (2014).

53. Martiniova, L. *et al.* Increased uptake of [123I]meta-iodobenzylguanidine, [18F]fluorodopamine, and [3H]norepinephrine in mouse pheochromocytoma cells and tumors after treatment with the histone deacetylase inhibitors. *Endocr. Relat. Cancer* **18**, 143–157 (2011).

54. Barrett, J. A. *et al.* Comparison of High-Specific-Activity Ultratrace 123/131 I-MIBG and Carrier-Added 123/131 I-MIBG on Efficacy, Pharmacokinetics, and Tissue Distribution. *Cancer Biother. Radiopharm.* **25**, 299–308 (2010).

55. Forrer, F., Riedweg, I., Maecke, H. R. & Mueller-Brand, J. Radiolabeled DOTATOC in patients with

advanced paraganglioma and pheochromocytoma. *Q. J. Nucl. Med. Mol. Imaging* **52**, 334–40 (2008).

56. Zovato, S. *et al.* Peptide receptor radionuclide therapy (PRRT) with 177Lu-DOTATATE in individuals with neck or mediastinal paraganglioma (PGL). *Horm. Metab. Res.* **44**, 411–414 (2012).

57. Ayala-Ramirez, M. *et al.* Treatment with sunitinib for patients with progressive metastatic pheochromocytomas and sympathetic paragangliomas. *J. Clin. Endocrinol. Metab.* **97**, 4040–4050 (2012).

58. Oh, D. Y. *et al.* Phase 2 study of everolimus monotherapy in patients with nonfunctioning neuroendocrine tumors or pheochromocytomas/paragangliomas. *Cancer* **118**, 6162–6170 (2012).

59. Giubellino, A. *et al.* Combined inhibition of mTORC1 and mTORC2 signaling pathways is a promising therapeutic option in inhibiting pheochromocytoma tumor growth: In vitro and in vivo studies in female athymic nude mice. *Endocrinology* **154**, 646–655 (2013).

60. Schovanek, J. *et al.* Inhibitory Effect of the Noncamptothecin Topoisomerase I Inhibitor LMP-400 on Female Mice Models and Human Pheochromocytoma Cells. *Endocrinology* **156**, 4094–4104 (2015).

61. McCormack, P. L. Pazopanib: A Review of Its Use in the Management of Advanced Renal Cell Carcinoma. *Drugs* **74**, 1111–1125 (2014).

62. Hao, Z. & Sadek, I. Sunitinib: the antiangiogenic effects and beyond. *Onco. Targets. Ther.* **9**, 5495–5505 (2016).

63. Al-Salama, Z. T. & Keating, G. M. Cabozantinib: A Review in Advanced Renal Cell Carcinoma. *Drugs* **76**, 1771–1778 (2016).

64. Jasim, S. *et al.* Phase II trial of pazopanib in advanced/progressive malignant pheochromocytoma and paraganglioma. *Endocrine* **57**, 220–225 (2017).

65. Gross, D. J. The role of imatinib mesylate (Glivec) for treatment of patients with malignant endocrine tumors positive for c-kit or PDGF-R. *Endocr. Relat. Cancer* **13**, 535–540 (2006).

66. Bullova, P., Cougnoux, A., Marzouca, G., Kopacek, J. & Pacak, K. Bortezomib Alone and in Combination With Salinosporamid A Induces Apoptosis and Promotes Pheochromocytoma Cell Death In Vitro and in Female Nude Mice. *Endocrinology* **158**, 3097–3108 (2017).

67. Chouaib, S., Noman, M. Z., Kosmatopoulos, K. & Curran, M. A. Hypoxic stress: obstacles and opportunities for innovative immunotherapy of cancer. *Oncogene* **36**, 439–445 (2017).

68. Dillman, R. O. Cancer Immunotherapy. *Cancer Biother. Radiopharm.* **26**, 1–64 (2011).

69. Hadoux, J. *et al.* Interferon-alpha Treatment for Disease Control in Metastatic Pheochromocytoma/Paraganglioma Patients. *Horm. Cancer* **8**, 330–337 (2017).

70. Chen, W. *et al.* Targeting renal cell carcinoma with a HIF-2 antagonist. *Nature* **539**, 112–117 (2016).

71. Toledo, R. A. New HIF2α inhibitors: potential implications as therapeutics for advanced pheochromocytomas and paragangliomas. *Endocr. Relat. Cancer* **24**, C9–C19 (2017).

72. Kwok, M. *et al.* ATR inhibition induces synthetic lethality and overcomes chemoresistance in TP53 or ATM defective chronic lymphocytic leukemia cells. *Blood* **127**, 582–95 (2016).

73. Sulkowski, P. L. *et al.* Krebs-cycle-deficient hereditary cancer syndromes are defined by defects in homologous-recombination DNA repair. *Nat. Genet.* **50**, 1086–1092 (2018).

74. Dahia, P. L. M. Pheochromocytomas and Paragangliomas, Genetically Diverse and Minimalist, All at Once! *Cancer Cell* **31**, 159–161 (2017).

75. Buffet, A. *et al.* Germline mutations in the mitochondrial 2-oxoglutarate/malate carrier SLC25A11 gene confer a predisposition to metastatic paragangliomas. *Cancer Res.* **78**, 1914–1922 (2018).

76. Fishbein, L. *et al.* Comprehensive Molecular Characterization of Pheochromocytoma and Paraganglioma. *Cancer Cell* **31**, 181–193 (2017).

77. Fishbein, L. *et al.* Whole-exome sequencing identifies somatic ATRX mutations in pheochromocytomas and paragangliomas. *Nat. Commun.* **6**, 6140 (2015).

78. Buffet, A. *et al.* Mosaicism in HIF2A-related polycythemia-paraganglioma syndrome. *J. Clin. Endocrinol. Metab.* **99**, 369–373 (2014).

79. Toledo, R. a. *et al.* Recurrent Mutations of Chromatin-Remodeling Genes and Kinase Receptors in Pheochromocytomas and Paragangliomas. *Clin. Cancer Res.* **22**, 2301–2310 (2016).

80. Pacak, K. & Wimalawansa, S. J. Pheochromocytoma and paraganglioma. *Endocr. Pract.* **21**, 406–412 (2015).

81. Dahia, P. L. M. *et al.* A HIF1alpha regulatory loop links hypoxia and mitochondrial signals in pheochromocytomas. *PLoS Genet.* **1**, 72–80 (2005).

82. López-Jiménez, E. *et al.* Research Resource: Transcriptional Profiling Reveals Different Pseudohypoxic Signatures in SDHB and VHL-Related Pheochromocytomas. *Mol. Endocrinol.* **24**, 2382–2391 (2010).

83. Fishbein, L. *et al.* Comprehensive Molecular Characterization of Pheochromocytoma and Paraganglioma. *Cancer Cell* **31**, 181–193 (2017).

84. Gordan, J. D. & Simon, M. C. Hypoxia-inducible factors: central regulators of the tumor phenotype. *Curr. Opin. Genet. Dev.* **17**, 71–77 (2007).

85. Favier, J. *et al.* The Warburg effect is genetically determined in inherited pheochromocytomas. *PLoS One* **4**, e7094 (2009).

86. Maher, E. R., Neumann, H. P. H. & Richard, S. Von Hippel-Lindau disease: A clinical and scientific review. *Eur. J. Hum. Genet.* **19**, 617–623 (2011).

87. Astrom, K., Cohen, J. E., Willett-Brozick, J. E., Aston, C. E. & Baysal, B. E. Altitude is a phenotypic modifier in hereditary paraganglioma type 1: Evidence for an oxygen-sensing defect. *Hum. Genet.* **113**, 228–237 (2003).

88. Vaidya, A. *et al.* EPAS1 Mutations and Paragangliomas in Cyanotic Congenital Heart Disease. *N. Engl. J. Med.* **378**, 1259–1261 (2018).

89. Aresta, C. *et al.* Pheochromocytoma in Congenital Cyanotic Heart Disease. *Case Rep. Endocrinol.* **2018**, 1–4 (2018).

90. He, W. *et al.* Citric acid cycle intermediates as ligands for orphan G-protein-coupled receptors. *Nature* **429**, 188–193 (2004).

91. Xiao, M. *et al.* Inhibition of -KG-dependent histone and DNA demethylases by fumarate and succinate that are accumulated in mutations of FH and SDH tumor suppressors. *Genes Dev.* **26**, 1326–1338 (2012).

92. Letouzé, E. *et al.* SDH Mutations Establish a Hypermethylator Phenotype in Paraganglioma. *Cancer Cell* **23**, 739–752 (2013).

93. Turcan, S. *et al.* IDH1 mutation is sufficient to establish the glioma hypermethylator phenotype. *Nature* **483**, 479–483 (2012).

94. Ricketts, C. *et al.* Abstract 2660: A renal CpG island methylator phenotype (R-CIMP) in kidney tumors associated with germline mutations of FH and SDHB. *Cancer Res.* **76**, 2660-2660(2016).

95. Andrews, K. A. *et al.* Tumour risks and genotype–phenotype correlations associated with germline variants in succinate dehydrogenase subunit genes SDHB , SDHC and SDHD. *J. Med. Genet.* **55**, 384–394 (2018).

96. Hederstedt, L. Structural biology: Complex II is complex too. *Science* **299**, 671–672 (2003).

97. Selak, M. A. *et al.* Succinate links TCA cycle dysfunction to oncogenesis by inhibiting HIF-α prolyl hydroxylase. *Cancer Cell* **7**, 77–85 (2005).

98. Pollard, P. J. *et al.* Accumulation of Krebs cycle intermediates and over-expression of HIF1α in tumours which result from germline FH and SDH mutations. *Hum. Mol. Genet.* **14**, 2231–2239 (2005).

99. Burnichon, N. *et al.* SDHA is a tumor suppressor gene causing paraganglioma. *Hum. Mol. Genet.*

19, 3011–3020 (2010).

100. Hao, H. *et al.* SDH5, a gene required for flavination of succinate dehydrogenase, is mutated in paraganglioma. *Science* **325**, 1139–1142 (2009).

101. Astuti, D. *et al.* Gene Mutations in the Succinate Dehydrogenase Subunit SDHB Cause Susceptibility to Familial Pheochromocytoma and to Familial Paraganglioma. *Am. J. Hum. Genet.* **69**, 49–54 (2001).

102. Niemann, S. & Muller, U. Mutations in SDHC cause autosomal dominant paraganglioma, type 3. *Nat. Genet.* **26**, 268–270 (2000).

103. Baysal, B. E. *et al.* Mutation in SDHD, a mitochondrial complex II gene, in hereditary paraganglioma. *Science* **287**, 848–851 (2000).

104. McWhinney, S. Familial gastrointestinal stromal tumors and germ-line mutations. *N. Engl. J. Med.* **357**, 1054–1056 (2007).

105. Vanharanta, S. *et al.* Early-Onset Renal Cell Carcinoma as a Novel Extraparaganglial Component of SDHB-Associated Heritable Paraganglioma. *Am. J. Hum. Genet.* **74**, 153–159 (2004).

106. Xekouki, P. *et al.* Succinate dehydrogenase (SDH) D subunit (SDHD) inactivation in a growth-hormone-producing pituitary tumor: A new association for SDH? *J. Clin. Endocrinol. Metab.* **97**, 357–366 (2012).

107. Mannelli, M. *et al.* DIAGNOSIS of ENDOCRINE DISEASE: SDHx mutations: Beyond pheochromocytomas and paragangliomas. *Eur. J. Endocrinol.* **178**, R11–R17 (2018).

108. Kavinga Gunawardane, P. T. & Grossman, A. The clinical genetics of phaeochromocytoma and paraganglioma. *Arch. Endocrinol. Metab.* **61**, 490–500 (2017).

109. Amar, L. *et al.* Succinate dehydrogenase B gene mutations predict survival in patients with malignant pheochromocytomas or paragangliomas. *J. Clin. Endocrinol. Metab.* **92**, 3822–3828 (2007).

110. Richter, S. *et al.* Epigenetic mutation of the succinate dehydrogenase c promoter in a patient with two paragangliomas. *J. Clin. Endocrinol. Metab.* **101**, 359–363 (2016).

111. Haller, F. *et al.* Aberrant DNA hypermethylation of SDHC: a novel mechanism of tumor development in Carney triad. *Endocr. Relat. Cancer* **21**, 567–577 (2014).

112. Remacha, L. *et al.* Targeted Exome Sequencing of Krebs Cycle Genes Reveals Candidate Cancer–Predisposing Mutations in Pheochromocytomas and Paragangliomas. *Clin. Cancer Res.* **23**, 6315–6324 (2017).

113. Bausch, B. *et al.* Clinical characterization of the pheochromocytoma and paraganglioma susceptibility genes SDHA, TMEM127, MAX, and SDHAF2 for gene-informed prevention. *JAMA Oncol.*

3, 1204–1212 (2017).

114. Kunst, H. P. M. *et al.* SDHAF2 (PGL2-SDH5) and hereditary head and neck paraganglioma. *Clin. Cancer Res.* **17**, 247–254 (2011).

115. Sullivan, L. B. *et al.* The Proto-oncometabolite Fumarate Binds Glutathione to Amplify ROS-dependent signaling. *Mol. Cell* **51**, 236–248 (2013).

116. Castro-Vega, L. J. *et al.* Germline mutations in FH confer predisposition to malignant pheochromocytomas and paragangliomas. *Hum. Mol. Genet.* **23**, 2440–2446 (2014).

117. Tomlinson, I. P. M. *et al.* Germline mutations in FH predispose to dominantly inherited uterine fibroids, skin leiomyomata and papillary renal cell cancer the multiple leiomyoma consortium. *Nat. Genet.* **30**, 406–410 (2002).

118. Cascón, A. *et al.* Whole-exome sequencing identifies MDH2 as a new familial paraganglioma gene. *J. Natl. Cancer Inst.* **107**, 1–5 (2015).

119. Calsina, B. *et al.* Role of MDH2 pathogenic variant in pheochromocytoma and paraganglioma patients. Genet. Med. (2018).

120. Yan, H. *et al.* IDH1 and IDH2 Mutations in Gliomas. *N. Engl. J. Med.* **360**, 765–773 (2009).

121. Gaal, J. *et al.* Isocitrate dehydrogenase mutations are rare in pheochromocytomas and paragangliomas. *J. Clin. Endocrinol. Metab.* **95**, 1274–1278 (2010).

122. Pollard, P. J. *et al.* Expression of HIF-1α, HIF-2α (EPAS1), and Their Target Genes in Paraganglioma and Pheochromocytoma with VHL and SDH Mutations. *J. Clin. Endocrinol. Metab.* **91**, 4593–4598 (2006).

123. Kaelin Jr, W. G. The von Hippel–Lindau tumour suppressor protein: O2 sensing and cancer. *Nat. Rev. Cancer* **8**, 865–873 (2008).

124. Kim, W. Y. & Kaelin, W. G. Role of VHL gene mutation in human cancer. *J. Clin. Oncol.* **22**, 4991–5004 (2004).

125. Latif, F. *et al.* Identification of the von Hippel-Lindau disease tumor suppressor gene. *Science* **260**, 1317–1320 (1993).

126. Varshney, N. *et al.* A Review of Von Hippel-Lindau Syndrome. *J. Kidney Cancer VHL* **4**, 20-29 (2017).

127. Shanbhogue, K. P., Hoch, M., Fatterpaker, G. & Chandarana, H. von Hippel-Lindau Disease. *Radiol. Clin. North Am.* **54**, 409–422 (2016).

128. Burnichon, N. *et al.* Integrative genomic analysis reveals somatic mutations in pheochromocytoma and paraganglioma. *Hum. Mol. Genet.* **20**, 3974–3985 (2011).

129. Comino-Méndez, I. *et al.* Tumoral EPAS1 (HIF2A) mutations explain sporadic pheochromocytoma and paraganglioma in the absence of erythrocytosis. *Hum. Mol. Genet.* **22**, 2169–2176 (2013).

130. Welander, J. *et al.* Frequent EPAS1/HIF2α exons 9 and 12 mutations in non-familial pheochromocytoma. *Endocr. Relat. Cancer* **21**, 495–504 (2014).

131. Gordan, J. D., Bertout, J. a., Hu, C. J., Diehl, J. A. & Simon, M. C. HIF-2α Promotes Hypoxic Cell Proliferation by Enhancing c-Myc Transcriptional Activity. *Cancer Cell* **11**, 335–347 (2007).

132. Zhuang, Z. *et al.* Somatic HIF2A Gain-of-Function Mutations in Paraganglioma with Polycythemia. *N. Engl. J. Med.* **367**, 922–930 (2012).

133. Yang, C. *et al.* Somatic mosaicism of EPAS1 mutations in the syndrome of paraganglioma and somatostatinoma associated with polycythemia. *Hum. Genome Var.* **2**, 15053 (2015).

134. Ladroue, C. *et al.* PHD2 Mutation and Congenital Erythrocytosis with Paraganglioma. *N. Engl. J. Med.* **359**, 2685–2692 (2008).

135. Yang, C. *et al.* Germ-line PHD1 and PHD2 mutations detected in patients with pheochromocytoma/paraganglioma-polycythemia. *J. Mol. Med.* **93**, 93–104 (2015).

136. Welander, J., Söderkvist, P. & Gimm, O. Genetics and clinical characteristics of hereditary pheochromocytomas and paragangliomas. *Endocr. Relat. Cancer* **18**, 253–276 (2011).

137. Schuchardt, A., D'Agati, V., Larsson-Blomberg, L., Costantini, F. & Pachnis, V. Defects in the kidney and enteric nervous system of mice lacking the tyrosine kinase receptor Ret. *Nature* **367**, 380–383 (1994).

138. Mulligan, L. M. *et al.* Germ-line mutations of the RET proto-oncogene in multiple endocrine neoplasia type 2A. *Nature* **363**, 458–460 (1993).

139. Brandi, M. L. *et al.* CONSENSUS: Guidelines for Diagnosis and Therapy of MEN Type 1 and Type 2. *J. Clin. Endocrinol. Metab.* **86**, 5658–5671 (2001).

140. Currás-Freixes, M. *et al.* PheoSeq: A Targeted Next-Generation Sequencing Assay for Pheochromocytoma and Paraganglioma Diagnostics. *J. Mol. Diagnostics* **19**, 575–588 (2017).

141. Mulligan, L. M. RET revisited: Expanding the oncogenic portfolio. *Nat. Rev. Cancer* **14**, 173–186 (2014).

142. Wallace, M. *et al.* Type 1 neurofibromatosis gene: identification of a large transcript disrupted in three NF1 patients. *Science* **249**, 181–186 (1990).

143. Ferner, R. E. Neurofibromatosis 1. *Eur. J. Hum. Genet.* **15**, 131–138 (2007).

144. Gutmann, D. H. *et al.* Diagnostic Evaluation and Multidisciplinary Management of Neurofibromatosis 1. *J. Am. Med. Assoc.* **278**, 52 (1997).

145. Welander, J. *et al.* Integrative genomics reveals frequent somatic NF1 mutations in sporadic pheochromocytomas. *Hum. Mol. Genet.* **21**, 5406–5416 (2012).

146. Qin, Y. *et al.* Germline mutations in TMEM127 confer susceptibility to pheochromocytoma. *Nat. Genet.* **42**, 229–233 (2010).

147. Qin, Y. *et al.* The tumorsusceptibilitygene TMEM127 is mutated in renal cell carcinomas and modulates endolysosomal function. *Hum. Mol. Genet.* **23**, 2428–2439 (2014).

148. Comino-Méndez, I. *et al.* Exome sequencing identifies MAX mutations as a cause of hereditary pheochromocytoma. *Nat. Genet.* **43**, 663–667 (2011).

149. Blackwood, E. M., Luscher, B. & Eisenman, R. N. Myc and Max associate in vivo. *Genes Dev.* **6**, 71–80 (1992).

150. Cascoń, A. & Robledo, M. MAX and MYC: A heritable breakup. *Cancer Res.* **72**, 3119–3124 (2012).

151. Romero, O. A. *et al.* MAX Inactivation in Small Cell Lung Cancer Disrupts MYC-SWI/SNF Programs and Is Synthetic Lethal with BRG1. *Cancer Discov.* **4**, 292–303 (2014).

152. Schaefer, I.-M. *et al.* MAX inactivation is an early event in GIST development that regulates p16 and cell proliferation. *Nat. Commun.* **8**, 14674 (2017).

153. Walker, C. J. *et al.* MAX Mutations in Endometrial Cancer: Clinicopathologic Associations and Recurrent MAX p.His28Arg Functional Characterization. *J. Natl. Cancer Inst.* **110**, 517–526 (2018).

154. Wang, D. *et al.* MAX is an epigenetic sensor of 5-carboxylcytosine and is altered in multiple myeloma. *Nucleic Acids Res.* **45**, 2396–2407 (2017).

155. Korpershoek, E. *et al.* Complex MAX Rearrangement in a Family With Malignant Pheochromocytoma, Renal Oncocytoma, and Erythrocytosis. *J. Clin. Endocrinol. Metab.* **101**, 453–460 (2016).

156. Burnichon, N. *et al.* MAX mutations cause hereditary and sporadic pheochromocytoma and paraganglioma. *Clin. Cancer Res.* **18**, 2828–2837 (2012).

157. Stenman, A. *et al.* HRAS mutation prevalence and associated expression patterns in pheochromocytoma. *Genes, Chromosom. Cancer* **55**, 452–459 (2016).

158. Crona, J. *et al.* Somatic Mutations in H-RAS in Sporadic Pheochromocytoma and Paraganglioma Identified by Exome Sequencing. *J. Clin. Endocrinol. Metab.* **98**, 1266–1271 (2013).

159. Oudijk, L. *et al.* H-RAS Mutations Are Restricted to Sporadic Pheochromocytomas Lacking Specific Clinical or Pathological Features : Data From a Multi-Institutional Series. *J. Clin. Endocrinol. Metab.* **99**, 1376–1380 (2018).

160. Schlisio, S. *et al.* The kinesin KIF1Bβ acts downstream from EglN3 to induce apoptosis and is a potential 1p36 tumor suppressor. *Genes Dev.* **22**, 884–893 (2008).

161. Yeh, I. T. *et al.* A germline mutation of the KIF1Bβ gene on 1p36 in a family with neural and nonneural tumors. *Hum. Genet.* **124**, 279–285 (2008).

162. Brugarolas, J. & Kaelin, W. G. Dysregulation of HIF and VEGF is a unifying feature of the familial hamartoma syndromes. *Cancer Cell* **6**, 7–10 (2004).

163. Gordan, J. D. *et al.* HIF-α Effects on c-Myc Distinguish Two Subtypes of Sporadic VHL-Deficient Clear Cell Renal Carcinoma. *Cancer Cell* **14**, 435–446 (2008).

164. Comino-Méndez, I. *et al.* ATRX driver mutation in a composite malignant pheochromocytoma. *Cancer Genet.* **209**, 272–277 (2016).

165. Toledo, R. A. Genetics of Pheochromocytomas and Paragangliomas. *Endocrinol. Metab. Clin. North Am.* **46**, 459–489 (2017).

166. Papathomas, T. G. *et al.* Telomerase reverse transcriptase promoter mutations in tumors originating from the adrenal gland and extra-adrenal paraganglia. *Endocr. Relat. Cancer* **21**, 653–661 (2014).

167. Burnichon, N. *et al.* Somatic NF1 inactivation is a frequent event in sporadic pheochromocytoma. *Hum. Mol. Genet.* **21**, 5397–5405 (2012).

168. Welander, J. *et al.* Rare germline mutations identified by targeted next-generation sequencing of susceptibility genes in pheochromocytoma and paraganglioma. *J. Clin. Endocrinol. Metab.* **99**, 1352–1360 (2014).

169. Chou, A. P. *et al.* Identification of retinol binding protein 1 promoter hypermethylation in isocitrate dehydrogenase 1 and 2 mutant gliomas. *J. Natl. Cancer Inst.* **104**, 1458–1469 (2012).

170. Jochmanova, I. & Pacak, K. Pheochromocytoma: The First Metabolic Endocrine Cancer. *Clin. Cancer Res.* **22**, 5001–5011 (2016).

171. Killian, J. K. *et al.* Recurrent epimutation of SDHC in gastrointestinal stromal tumors. *Sci. Transl. Med.* **6**, 268ra177-268ra177 (2014).

172. Lussey-Lepoutre, C. *et al.* Loss of succinate dehydrogenase activity results in dependency on pyruvate carboxylation for cellular anabolism. *Nat. Commun.* **6**, 8784 (2015).

173. Buffet, A. *et al.* Germline mutations in the mitochondrial 2-oxoglutarate/malate carrier SLC25A11

gene confer a predisposition to metastatic paragangliomas. *Cancer Res.* **78**, 1914–1922 (2018).

174. Garg, M. *et al.* Pro fi ling of somatic mutations in acute myeloid leukemia with FLT3 -ITD at diagnosis and relapse. *Blood* **126**, 2491–2502 (2015).

175. Hartong, D. T. *et al.* Insights from retinitis pigmentosa into the roles of isocitrate dehydrogenases in the Krebs cycle. *Nat. Genet.* **40**, 1230–1234 (2008).

176. Yan, H. *et al.* IDH1and IDH2Mutations in Gliomas. *N. Engl. J. Med.* **360**, 765–773 (2009).

177. Mardis, E. R. *et al.* Recurring Mutations Found by Sequencing an Acute Myeloid Leukemia Genome. *N. Engl. J. Med.* **361**, 1058–1066 (2009).

178. Williams Parsons, D. *et al.* An Integrated Genomic Analysis of Human Glioblastoma Multiforme I An Integrated Genomic Analysis of Human Glioblastoma Multiforme. *Source Sci. New Ser.* **321**, 1807–1812 (2008).

179. Veltman, J. A. & Brunner, H. G. De novo mutations in human genetic disease. *Nat. Rev. Genet.* **13**, 565–575 (2012).

180. Bestor, T. H. The DNA methyltransferases of mammals. *Hum. Mol. Genet.* **9**, 2395–2402 (2000).

181. Brunetti, L., Gundry, M. C. & Goodell, M. A. DNMT3A in Leukemia. *Cold Spring Harb. Perspect. Med.* **7**, a030320 (2017).

182. Rondelet, G., Dal Maso, T., Willems, L. & Wouters, J. Structural basis for recognition of histone H3K36me3 nucleosome by human de novo DNA methyltransferases 3A and 3B. *J. Struct. Biol.* **194**, 357–367 (2016).

183. Wu, H. *et al.* Structural and histone binding ability characterizations of human PWWP domains. *PLoS One* **6**, e18919 (2011).

184. Margetts, C. D. E. *et al.* Evaluation of a functional epigenetic approach to identify promoter region methylation in phaeochromocytoma and neuroblastoma. *Endocr. Relat. Cancer* **15**, 777–786 (2008).

185. Yap, L. F. *et al.* HOPX functions as a tumour suppressor in head and neck cancer. *Sci. Rep.* **6**, 38758 (2016).

186. Meyer, S. E. *et al.* DNMT3A haploinsufficiency transforms FLT3ITDmyeloproliferative disease into a rapid, spontaneous, and fully penetrant acute myeloid leukemia. *Cancer Discov.* **6**, 501–515 (2016).

187. Hoekstra, A. S. *et al.* Inactivation of SDH and FH cause loss of 5hmC and increased H3K9me3 in paraganglioma/pheochromocytoma and smooth muscle tumors. *Oncotarget* **6**, 38777–38788 (2015).

188. Ley, T. J. *et al.* DNMT3A Mutations in Acute Myeloid Leukemia. *N. Engl. J. Med.* **363**, 2424–2433

(2010).

189. Yang, L., Rau, R. & Goodell, M. A. DNMT3A in haematological malignancies. *Nat. Rev. Cancer* **15**, 152–165 (2015).

190. Tatton-Brown, K. *et al.* Mutations in the DNA methyltransferase gene DNMT3A cause an overgrowth syndrome with intellectual disability. *Nat. Genet.* **46**, 385–388 (2014).

191. Tlemsani, C. *et al.* SETD2 and DNMT3A screen in the Sotos-like syndrome French cohort. *J. Med. Genet.* **53**, 743–751 (2016).

192. Tatton-Brown, K. *et al.* Germline mutations in the oncogene EZH2 cause Weaver syndrome and increased human height. *Oncotarget* **2**, 1127–33 (2011).

193. Baujat, G. *et al.* Paradoxical NSD1 Mutations in Beckwith-Wiedemann Syndrome and 11p15 Anomalies in Sotos Syndrome. *Am. J. Hum. Genet.* **74**, 715–720 (2004).

194. Oh, B. *et al.* DNA methyltransferase expression and DNA methylation in human hepatocellular carcinoma and their clinicopathological correlation. *Int. J. Mol. Med.* **20**, 65–73 (2007).

195. Rahman, M. M. *et al.* DNA methyltransferases 1, 3a, and 3b overexpression and clinical significance in gastroenteropancreatic neuroendocrine tumors. *Hum. Pathol.* **41**, 1069–1078 (2010).

196. Santini, V. Novel therapeutic strategies: hypomethylating agents and beyond. *Hematol. Am. Soc. Hematol. Educ. Progr.* **2012**, 65–73 (2012).

197. Intlekofer, A. M. *et al.* Hypoxia Induces Production of L-2-Hydroxyglutarate. *Cell Metab.* **22**, 304–311 (2015).

198. Intlekofer, A. M. *et al.* L-2-Hydroxyglutarate production arises from noncanonical enzyme function at acidic pH. *Nat. Chem. Biol.* **13**, 494–500 (2017).

199. Comino-Méndez, I. *et al.* Exome sequencing identifies MAX mutations as a cause of hereditary pheochromocytoma. *Nat. Genet.* **43**, 663–667 (2011).

200. Maynard, M. A. *et al.* Human HIF-3α4 is a dominant-negative regulator of HIF-1 and is down-regulated in renal cell carcinoma. *FASEB J.* **19**, 1396–1406 (2005).

201. Remacha, L. *et al.* Gain-of-function mutations in DNMT3A in patients with paraganglioma. *Genet. Med.* **20**, 1644-1651 (2018).

202. Schiavi, F. *et al.* Are we overestimating the penetrance of mutations in SDHB? *Hum. Mutat.* **31**, 761–762 (2010).

203. Menara, M. *et al.* SDHD immunohistochemistry: A new tool to validate SDHx mutations in

pheochromocytoma/paraganglioma. *J. Clin. Endocrinol. Metab.* **100**, E287–E291 (2015).

204. Yoon, W. H. *et al.* Loss of Nardilysin, a Mitochondrial Co-chaperone for α-Ketoglutarate Dehydrogenase, Promotes mTORC1 Activation and Neurodegeneration. *Neuron* **93**, 115–131 (2017).

205. Danhauser, K. *et al.* DHTKD1 mutations cause 2-aminoadipic and 2-oxoadipic aciduria. *Am. J. Hum. Genet.* **91**, 1082–1087 (2012).

206. Gibson, G. E. *et al.* Abnormal thiamine-dependent processes in Alzheimer's Disease. Lessons from diabetes. *Mol. Cell. Neurosci.* **55**, 17–25 (2013).

207. Bourgeron, T. *et al.* Mutation of the fumarase gene in two siblings with progressive encephalopathy and fumarase deficiency. *J. Clin. Invest.* **93**, 2514–2518 (1994).

208. Bourgeron, T. *et al.* Mutation of a nuclear succinate dehydrogenase gene results in mitochondrial respiratory chain deficiency. *Nat. Genet.* **11**, 144–149 (1995).

209. Fattal-Valevski, A. *et al.* Homozygous mutation, p.Pro304His, in IDH3A, encoding isocitrate dehydrogenase subunit is associated with severe encephalopathy in infancy. *Neurogenetics* **18**, 57–61 (2017).

210. Spiegel, R. *et al.* Infantile cerebellar-retinal degeneration associated with a mutation in mitochondrial aconitase, ACO2. *Am. J. Hum. Genet.* **90**, 518–523 (2012).

211. Punzi, G. *et al.* SLC25A10 biallelic mutations in intractable epileptic encephalopathy with complex I deficiency. *Hum. Mol. Genet.* **27**, 499–504 (2018).

212. Else, T. & Fishbein, L. Discovery of new susceptibility genes: proceed cautiously. *Genet. Med.* **20**, 1512-1514 (2018).

APPENDIX: Other publications

1. *ATRX* driver mutation in a composite malignant phaeochromocytoma

Comino-Méndez I, Tejera ÁM, Currás-Freixes M, Remacha L, Gonzalvo P, Tonda R, Letón R, Blasco MA, Robledo M, Cascón A.

Published in *Cancer Genetics*, 2016 Jun;209(6):272-7.

Pheochromocytomas (PCCs) and paragangliomas (PGLs) are tumors arising from the adrenal medulla and sympathetic/parasympathetic paraganglia, respectively. Approximately 40% of PCCs/PGLs are due to germline mutations in one of 16 susceptibility genes, and a further 30% are due to somatic alterations in 5 main genes. Recently, somatic *ATRX* mutations have been found in succinate dehydrogenase (SDH)-associated hereditary PCCs/PGLs. In the present study we applied whole-exome sequencing to the germline and tumor DNA of a patient with metastatic composite PCC and no alterations in known PCC/PGL susceptibility genes. A somatic loss-of-function mutation affecting *ATRX* was identified in tumor DNA. Transcriptional profiling analysis classified the tumor within cluster 2 of PCCs/PGLs (without SDH gene mutations) and identified downregulation of genes involved in neuronal development and homeostasis (*NLGN4*, *CD99* and *CSF2RA*) as well as upregulation of *Drosha*, an important gene involved in miRNA and rRNA processing. CpG island methylator phenotype typical of SDH gene-mutated tumors was ruled out, and SNP array data revealed a unique profile of gains and losses. Finally, we demonstrated the presence of alternative lengthening of telomeres in the tumor, probably associated with the failure of ATRX functions. In conclusion, somatic variants affecting *ATRX* may play a driver role in sporadic PCC/PGL.

2. PheoSeq: A Targeted Next-Generation Sequencing Assay for Pheochromocytoma and Paraganglioma Diagnostics

Currás-Freixes M, Piñeiro-Yañez E, Montero-Conde C, Apellániz-Ruiz M, Calsina B, Mancikova V, Remacha L, Richter S, Ercolino T, Rogowski-Lehmann N, Deutschbein T, Calatayud M, Guadalix S, Álvarez-Escolá C, Lamas C, Aller J, Sastre-Marcos J, Lázaro C, Galofré JC, Patiño-García A, Meoro-Avilés A, Balmaña-Gelpi J, De Miguel-Novoa P, Balbín M, Matías-Guiu X, Letón R, Inglada-Pérez L, Torres-Pérez R, Roldán-Romero JM, Rodríguez-Antona C, Fliedner SMJ, Opocher G, Pacak K, Korpershoek E, de Krijger RR, Vroonen L, Mannelli M, Fassnacht M, Beuschlein F, Eisenhofer G, Cascón A, Al-Shahrour F, Robledo M.

Published in the *Journal of Molecular Diagnostics*, 2017 Jul;19(4):575-588.

Genetic diagnosis is recommended for all pheochromocytoma and paraganglioma (PPGL) cases, as driver mutations are identified in approximately 80% of the cases. As the list of related genes expands, genetic diagnosis becomes more time-consuming, and targeted next-generation sequencing (NGS) has emerged as a cost-effective tool. This study aimed to optimize targeted NGS in PPGL genetic diagnostics. A workflow based on two customized targeted NGS assays was validated to study the 18 main PPGL genes in germline and frozen tumor DNA, with one of them specifically directed toward formalin-fixed paraffin-embedded tissue. The series involved 453 unrelated PPGL patients, of whom 30 had known mutations and were used as controls. Partial screening using Sanger had been performed in 275 patients. NGS results were complemented with the study of gross deletions. NGS assay showed a sensitivity ≥99.4%, regardless of DNA source. We identified 45 variants of unknown significance and 89 pathogenic mutations, the latter being germline in 29 (7.2%) and somatic in 58 (31.7%) of the 183 tumors studied. In 37 patients previously studied by Sanger sequencing, the causal mutation could be identified. We demonstrated that both assays are an efficient and accurate alternative to conventional sequencing. Their application facilitates the study of minor PPGL genes, and enables genetic diagnoses in patients with incongruent or missing clinical data, who would otherwise be missed.

3. Role of *MDH2* pathogenic variant in phaeochromocytoma and paraganglioma patients

Calsina B, Currás-Freixes M, Buffet A, Pons T, Contreras L, Letón R, Comino-Méndez I, Remacha L, Calatayud M, Obispo B, Martin A, Cohen R, Richter S, Balmaña J, Korpershoek E, Rapizzi E, Deutschbein T, Vroonen L, Favier J, de Krijger RR, Fassnacht M, Beuschlein F, Timmers HJ, Eisenhofer G, Mannelli M, Pacak K, Satrústegui J, Rodríguez-Antona C, Amar L, Cascón A, Dölker N, Gimenez-Roqueplo AP, Robledo M.

Published in *Genetics in Medicine*, 2018 Dec;20(12):1652-1662.

Purpose: *MDH2* (malate dehydrogenase 2) has recently been proposed as a novel potential pheochromocytoma/paraganglioma (PPGL) susceptibility gene, but its role in the disease has not been addressed. This study aimed to determine the prevalence of *MDH2* pathogenic variants among PPGL patients and determine the associated phenotype.

Methods: Eight hundred thirty patients with PPGLs, negative for the main PPGL driver genes, were included in the study. Interpretation of variants of unknown significance (VUS) was performed using an algorithm based on 20 computational predictions, by implementing cell-based enzymatic and immunofluorescence assays, and/or by using a molecular dynamics simulation approach.

Results: Five variants with potential involvement in pathogenicity were identified: three missense (p.Arg104Gly, p.Val160Met and p.Ala256Thr), one in-frame deletion (p.Lys314del), and a splice-site variant (c.429+1G>T). All were germline and those with available biochemical data, corresponded to noradrenergic PPGL.

Conclusion: This study suggests that *MDH2* pathogenic variants may play a role in PPGL susceptibility and that they might be responsible for less than 1% of PPGLs in patients without pathogenic variants in other major PPGL driver genes, a prevalence similar to the one recently described for other PPGL genes. However, more epidemiological data are needed to recommend *MDH2* testing in patients negative for other major PPGL genes.

4. Concomitant Medications and Risk of Chemotherapy-Induced Peripheral Neuropathy

Sánchez-Barroso L, Apellaniz-Ruiz M, Gutiérrez-Gutiérrez G, Santos M, Roldán-Romero JM, Curras M, Remacha L, Calsina B, Calvo I, Sereno M, Merino M, García-Donas J, Castelo B, Guerra E, Letón R, Montero-Conde C, Cascón A, Inglada-Pérez L, Robledo M, Rodríguez-Antona C.

Published in *The Oncologist*, 2018 Nov 23. doi: 10.1634/theoncologist.2018-0418.

Background. Peripheral neuropathy is the dose-limiting toxicity of many oncology drugs, including paclitaxel. There is large interindividual variability in the neuropathy, and several risk factors have been proposed; however, many have not been replicated. Here we present a comprehensive study aimed at identifying treatment and physiopathology-related paclitaxel-induced neuropathy risk factors in a large cohort of well-characterized patients.

Patients and Methods. Analyses included 503 patients with breast or ovarian cancer who received paclitaxel treatment. Paclitaxel dose modifications caused by the neuropathy were extracted from medical records and patients self-reported neuropathy symptoms were collected. Multivariate logistic regression analyses were performed to identify concomitant medications and comorbidities associated with paclitaxel-induced neuropathy.

Results. Older patients had higher neuropathy: for each increase of 1 year of age, the risk of dose modifications and grade 3 neuropathy increased 4% and 5%, respectively. Cardiovascular drugs increased the risk of paclitaxel dose reductions (odds ratio [OR], 2.51; $p = .006$), with a stronger association for beta-adrenergic antagonists. The total number of concomitant medications also showed an association with dose modifications (OR, 1.25; $p = .012$ for each concomitant drug increase). A dose modification predictive model that included the new identified factors gave an area under the curve of 0.74 ($p = 1.07 \times 10\text{-}10$). Preexisting nerve compression syndromes seemed to increase neuropathy risk.

Conclusion. Baseline characteristics of the patients, including age and concomitant medications, could be used to identify individuals at high risk of neuropathy, personalizing chemotherapy treatment and reducing the risk of severe neuropathy.